

PL-TR-95-2042(II)
Environmental Research Papers, No. 1168



**PROCEEDINGS OF THE 16TH ANNUAL
CONFERENCE ON ATMOSPHERIC
TRANSMISSION MODELS,
8-9 JUNE 1993**

Editors:

Gail P. Anderson
James H. Chetwynd

7 April 1995

APPROVED FOR PUBLIC RELEASE; DISTRIBUTION UNLIMITED


DTIC QUALITY INSPECTED &

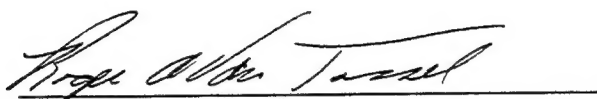


PHILLIPS LABORATORY
Directorate of Geophysics
AIR FORCE MATERIEL COMMAND
HANSCOM AIR FORCE BASE, MA 01731-3010

19950501 005

"This technical report has been reviewed and is approved for publication"


WILLIAM A.M. BLUMBERG, Chief
Simulation Branch
Optical Environment Division


ROGER A. VAN TASSEL, Director
Optical Environment Division

This report has been reviewed by the ESC Public Affairs Office (PA) and is releasable to the National Technical Information Service (NTIS).

Qualified requestors may obtain additional copies from the Defense Technical Information Center (DTIC). All others should apply to the National Technical Information Service (NTIS).

If your address has changed, or if you wish to be removed from the mailing list, or if the addressee is no longer employed by your organization, please notify PL/IM, 29 Randolph Road, Hanscom AFB, MA 01731-3010. This will assist us in maintaining a current mailing list.

Do not return copies of this report unless contractual obligations or notices on a specific document requires that it be returned.

REPORT DOCUMENTATION PAGE

Form Approved
OMB No. 0704-0188

Public reporting burden for this collection of information is estimated to average 1 hour per response, including the time for reviewing instructions, searching existing data sources, gathering and maintaining the data needed, and completing and reviewing the collection of information. Send comments regarding this burden estimate or any other aspect of this collection of information, including suggestions for reducing this burden, to Washington Headquarters Services, Directorate for Information Operations and Reports, 1215 Jefferson Davis Highway, Suite 1204, Arlington, VA 22202-4302, and to the Office of Management and Budget, Paperwork Reduction Project (0704-0188), Washington, DC 20503.

1. AGENCY USE ONLY (Leave blank)	2. REPORT DATE 7 April 1995	3. REPORT TYPE AND DATES COVERED Scientific
----------------------------------	--------------------------------	--

4. TITLE AND SUBTITLE Proceedings of the 16th Annual Conference on Atmospheric Transmission Models, 8-9 June 1993	5. FUNDING NUMBERS PE: 62101F PR 3054 TA GD WU 01
--	---

6. AUTHOR(S) Editors: Gail P. Anderson James H. Chetwynd

7. PERFORMING ORGANIZATION NAME(S) AND ADDRESS(ES) Phillips Laboratory/GPOS 29 Randolph Road Hanscom AFB, MA 01731-3010	8. PERFORMING ORGANIZATION REPORT NUMBER PL-TR-95-2042 (II) ERP, No. 1168
--	---

9. SPONSORING/MONITORING AGENCY NAME(S) AND ADDRESS(ES)	10. SPONSORING/MONITORING AGENCY REPORT NUMBER
---	--

11. SUPPLEMENTARY NOTES
Volume I consists of pages 1 - 379; Volume II consists of pages 380 - 778

12a. DISTRIBUTION/AVAILABILITY STATEMENT Approved for public release; distribution unlimited	12b. DISTRIBUTION CODE
---	------------------------

13. ABSTRACT (Maximum 200 words)
This report contains the viewgraphs and other materials for the 37 papers presented at the 16th Annual Review Conference on Atmospheric Transmission Models held at the Geophysics Directorate, Phillips Laboratory (AFMC), Hanscom AFB, MA On 8-9 June 1993.

DTIC QUALITY INSPECTED 3

14. SUBJECT TERMS Atmospheric transmittance Radiance Propagation		Clouds Radiative transfer Remote sensing	15. NUMBER OF PAGES 410
			16. PRICE CODE
17. SECURITY CLASSIFICATION OF REPORT Unclassified	18. SECURITY CLASSIFICATION OF THIS PAGE Unclassified	19. SECURITY CLASSIFICATION OF ABSTRACT Unclassified	20. LIMITATION OF ABSTRACT SAR

CONTENTS

SESSION A: REMOTE SENSING AND APPLICATIONS

Chairs: Gail Anderson, PL/GPOS; David Robertson, SSI

(Invited) Jean I.F. King	3
PL/Geophysics Directorate	
<i>Dependence of Remote Temperature Retrieval on Atmospheric Transmittance Accuracy</i>	
(Invited) Robert O. Green, James E. Conel and Thomas G. Chrien	5
Jet Propulsion Lab	
<i>Mapping Atmospheric Water Vapor and the Inversion of Spectral Radiance to Apparent Reflectance with MODTRAN2 and Data Measured by the Airborne Visible-Infrared Imaging Spectrometer (AVIRIS)</i>	
Bo-Cai Gao	37
NASA/GSFC	
<i>The Presence of Earth Atmospheric Bands in the LOWTRAN 7 Solar Irradiance Curve</i>	
William M. Cornette and Joseph G. Shanks	48
Photon Research Associates	
<i>The Impact of Thin Cirrus Clouds on Terrain Remote Sensing</i>	
T. Schmugge, P. Bougarel, M. Sugita, W. Brutsaert	69
USDA Hydrology Lab	
<i>Application of LOWTRAN 7 to AVHRR Thermal Data in FIFE</i>	
Zhengming Wan and Jeff Dozier	86
UC Santa Barbara	
<i>An Urgent Need of Validating Water Vapor Absorption Coefficients for the Development of EOS's Earth Surface Temperature Algorithms</i>	
Kelly V Chance and Akihiko Kuze	102
Smithsonian Astrophysical Observatory	
<i>Analysis of Cloud-Top Height and Related Cloud Parameters from Satellites Using the O₂ A and B Bands</i>	
Peter Ashcroft	116
Carnegie Mellon Univ.	
<i>The Use of Space Based Remote Sensing for Estimation of the Methane Mixing Ratio in the Mixing Layer</i>	
A.S. Grossman, K.E. Grant	132
Lawrence Livermore National Laboratory	
<i>A Correlated K-Distribution Model of the Atmospheric Heating Rates for Overlapping Spectra of CO₂/H₂O and CH₄/N₂O</i>	

ion For

CRA&I
TAB

Unannounced
Justification

By
Distribution /

Availability C

Dist Avail and
Special

A-1

CONTENTS

SESSION B: RADIATIVE TRANSFER CODE DEVELOPMENT

Chair: William A.M. Blumberg, PL/GPOS	156
G. Anderson, J. Chetwynd, F. Kneizys, A. Berk, L. Bernstein, D. Robertson, P. Acharya, J.-M. Theriault, L. Abreu, S.A. Clough, J.-L. Moncet	157
PL/Geophysics Directorate, SSI, DREV, ONTAR, AER	
<i>FASCODE/MODTRAN: Validation and Applications</i>	
J.-M. Theriault, G.P. Anderson, J.H. Chetwynd, E. Murphy, V. Turner, M. Cloutier, A. Smith, J.-L. Moncet	192
DREV (Valcartier), PL/Geophysics Directorate, ONTAR, Univ. of Wisc., AER	
<i>Retrieval of Tropospheric Profiles from IR Emission Spectra: Preliminary Results With DBIS</i>	
L.W. Abreu, J. Schroeder, A. McCann, J. Kristl, S. Harvey, and M. Voltaire	199
ONTAR Corp	
<i>PcModTRAN 2: ONTAR'S PC Compatible MODTRAN 2 Software</i>	
A. Berk, D.C. Robertson, L.S. Bernstein, R.L. Sundberg, R.J. Healey R.D. Sharma, G.P. Anderson, J.H. Chetwynd, M.L. Hoke	214
Spectral Sciences, Inc., Yap Analytics, PL/Geophysics Directorate	
<i>SAMM: SHARC and MODTRAN Merged</i>	
William M. Cornette and David C. Robertson	234
Photon Research Assoc., and Spectral Sciences Inc.	
<i>The Moderate Spectral Atmospheric Radiance and Transmittance (MOSART) Program</i>	
K. Stamnes, S. Tsay, and M. Yeh	291
Univ. of Alaska and Calem Research Corp	
<i>Inclusion of Accurate Multiple Scattering in MODTRAN</i>	
Donald E. Anderson, Robert De Majistre and Scott Evans	305
John Hopkins/APL and Computational Physics Inc.	
<i>Rayleigh and Aerosol Scattering in the Troposphere and Stratosphere in the Spectral Range 175-850nm: An Interactive Model</i>	
P.C. Ip, S.B. Downer, M. Noah, K. Radermacher, J.P. Kennealy and D. Einstein, F.O. Clark	318
Mission Research and PL/Geophysics Directorate	
<i>PLEXUS: Expert System and Expert-Assisted User Software</i>	
Susan McKenzie	340
Mission Research Corp.	
<i>Earthlimb Backgrounds in the Strategic Scene Generator Model</i>	
Larrene K. Harada & Daniel H. Leslie	353/391
W.J. Schafer Associates	
<i>Atmospheric Extinction Analysis for the Air Force Airborne Laser Program</i>	

SESSION C: SPECTROSCOPY APPLICATIONS

Chair: Laila Jeong, PL/GPOS	354
Shinji Kadokura and Akio Shimota	355
Komae Research Lab, Japan <i>A Fast Scheme for Line-by-Line Forward Model</i>	
Nobuo Takeuchi	357
Chiba University, Japan <i>Application of FASCODE Program to a High Temperature Gas Monitoring</i>	
K. Yoshino, J.R. Esmond, J.E. Murray, Y. Sun, A. Dalgarno, W.H. Parkinson, A.P. Thorne	380
Smithsonian Center for Astrophysics and Blackett Laboratory <i>VUV Fourier Transform Spectroscopy of the $\delta(0,0)$ Band of NO</i>	

SESSION D: Non-LTE SPECTROSCOPY APPLICATIONS

Chair: Richard H. Picard, PL/GPOS	440
David Robertson, Robert Sundberg, James Duff, John Gruninger, Steve Adler-Golden, and Ramesh Sharma	441
Spectral Sciences Inc. and PL/Geophysics Directorate <i>SHARC: A Model for Calculating Atmospheric Radiation Under Non-Equilibrium Conditions</i>	
David P. Edwards, Manuel Lopez-Puertas, Miguel Lopez-Valverde	462
National Center for Atmospheric Research and Institute for Astrophysics, Andalucia <i>Non-LTE Studies of the 15 μm Bands of CO₂ for Atmospheric Remote Sensing</i>	
R.H. Picard, J.R. Winick, U. Makhlof, A. J. Paboojian, A. J. Ratkowski, K.U. Grossmann, D. Homann, and J.C. Ulwick	464
PL/Geophysics Directorate, Stewart Radiance Lab, ARCON, and Univ. of Wuppertal <i>Critical Tests of Non-LTE Radiative Models Against High Latitude Rocket Data</i>	

SESSION E: STRUCTURE ALGORITHMS

Chair: Edmond M. Dewan, PL/GPOS	490
James H. Brown	491
PL/Geophysics Directorate <i>Atmospheric Structure Simulation: An Autoregressive Model for Smooth Geophysical Power Spectra with Known Autocorrelation Function</i>	
Edmond M. Dewan	512
PL/Geophysics Directorate <i>An Update on the AFGL Optical Turbulence Radiosonde Model</i>	
James H. Brown	530
PL/Geophysics Directorate <i>A Nighttime Structure Model of Atmospheric Optical Turbulence, C^2_n, Derived from Thermosonde and High Resolution Rawinsonde Measurements</i>	

SESSION F: CLIMATOLOGIES

Chair: James H. Chetwynd, PL/GPOS	557
William M. Cornette	558
Photon Research Assoc. <i>The MOSART Global Climatological and Terrain Data Bases</i>	
S. Adler-Golden, J. Gruninger and M. Matthew	662
Spectral Science Inc. <i>SHARC/SAMM/MODTRAN Calculations Using a Climatology Model Atmosphere Generator</i>	

SESSION G: LIDAR APPLICATIONS

Chair: E.P. Shettle, Naval Research Lab	643
M.G. Cheifetz, D.R. Longtin, and J.R. Hummel	644
SPARTA <i>Development of a Signal-to-Noise Performance Model with Backscat Version 4.0</i>	
Neal H. Kilmer and Henry Rachele	659
Physcial Science Laboratory and Army Research Laboratory <i>An Optical Profile Function for Modeling Extinction and Backscatter Coefficients in Very Low Stratus Clouds and Subcloud Regions</i>	
Richard Garner	677
PhotoMetrics Inc. <i>Time and Polarization Dependent Double Scattering Calculations of Lidar Returns from Water Clouds</i>	
Gertrude Kornfeld	711
Army Research Laboratory <i>Sky Radiance and Ray Bending Calculation</i>	
S.A. Wood and G.D. Emmit	725
Simpson Weather Associates, Inc <i>Integration of LOWTRAN into Global Circulation Models for Observing System Simulation Experiments</i>	
Mireille Tanguy, Michel Autric, Bernard Salles	743
DGA FRANCE <i>Aerosol Distribution and IR Broadband Transmittance in the Marine Boundary Layer in the Mediterranean Environment</i>	
Carl R. Zeisse	756
Naval Command Control and Ocean Surveillance Center <i>Maritime Modifications to LOWTRAN Radiance</i>	

ATMOSPHERIC TRANSMISSION MODELS MEETING

8-9 JUNE 1993

ATTENDANCE LIST

NAME	AFFILIATION	PHONE NUMBER
ROBERT O. GREEN	JPL	818-354-9136
PAUL E. LEWIS	NPIC	202-863-3422
DANIEL E. CRAUN	NRAA	619-553-4598
BROOKE KOFFEND	AEROSPACE	319-336-7412
KURT STAMMES	UNIV OF ALASKA	907-474-7368
STACY L. ANGLE	LORAL	617-863-3918
ISABELLE LE NAOUR	ENSSAT BPHH7	33 96465030
WILLIAM M. CORNETTE	PRA	619-455-9741
LARRY BERNSTEIN	SSI	617-273-4770
TATSUYA YOKOTA	NIFS	81 298-51-6111
SHINUI KADOTURA	CRIEPE	81-3-3480-2111
ROBERT L. HAWKINS	PL/GPOS	617-377-8664
DOUGLAS YOUMANS	W J SCHAFER	508-256-2070
ROBERT WATERLAND	DUPONT	302-695-1511
JEAN RENE JEVAIS	CEA	33 56685083
YONG HAN	WPL	303-497-7109
ALLEN S. GROSSMAN	LLNL	510-423-6371
KEN PATTEN	LLNL	510-423-9418
RICHARD SHIRKEY	ARL/BE	505-678-5470
TOM SCHMUGGE	USDA/HYDROLOGY	301-504-8554
DAN LESLIE	W J SCHAFER	703-558-7900
JOHN SCHROEDER	ONTAR	617-739-6607
JEAN-MARIE FLAUD	LPMA, CNRS	33 144273161
NOBUO TAKEUCHI	RSIRC, CHIBA UNIV	81 43-251-1111
STEVE MAZUK	AEROSPACE	310-336-5614
MELANIE GOUVEIA	HUGHES STX	617-862-0715
STEVEN J. LIPSON	PL/GPOS	617-377-3626
JON MURRAY	SMITHSONIAN OBSER	617-496-7614
SAM MAKHLOUF	STEWART RADIANCE LAB	617-377-4203
VINCE DILEONE	MIT-LINCOLN LAB	617-981-2333
STEVEN ADLER-GOLDEN	SSI	617-273-4770
SEAN P. McGOWAN	MISSION RESEARCH	603-891-0070
LAILA S. JEONG	PL/GPOS	617-377-3671
RUTH LIEBOWITZ	PL/HO	617-377-3643
K. DIERER KLAES	EUMETSAT	49 6151 950 211
RICHARD TIPPING	UNIV OF ALABAMA	205-348-3799

JAMES H. CHETWYND	PL/GPOS	617-377-2613
LEONARD W. ABREU	ONTAR	508-689-9622
GERTRUDE KORNFELD	ARL/MSB	703-704-3201
RICHARD E. DAVIS	NASA-LANGLEY RES CTR	804-864-1647
KEN JUCKS	SMITHSONIAN AST OBSV	617-496-7580
RON RODNEY	WL/DOWA WPAFB	513-255-1978
OLGA LADO-BORDOWSKY	ENSSAT	33 96466613
JOHN BALLARD	RUTHERFORD LAB, UK	44 235 44 5132
LEX BERK	SSI	617-273-4770
AKIHIKO KUZE	SMITHSONIAN AST OBSV	617-496-7614
PETER ASHCROFT	CARNEGIE MELLON UNIV	412-268-2670
ANGELA PHILLIPS	HUGHES AIRCRAFT	310-616-0124
DAVID ROBERTSON	SSI	617-273-4770
C. MULER	BELG INST SPACE AER	32 2 3730372
J MESGENTHCLER	LOCKHEED	415-424-2483
ERIC SHETTLE	NRL	202-404-8604
TESS HOFFMAN	PL/EDWARDS	805-275-5419
ALAN WETMORE	ARL-BED, WSMR, NM	505-678-5563
C R ZEISSE	NCWSC RDT&E	619-553-3602
ZHENGMING WAN	UNIV OF CA	805-893-4541
SHERMAN NESTE	MARTIN MARIETTA	215-531-6360
RICHARD GARNER	PHOTOMETRICS	617-935-6500
GEORG ECHLE	METEOROLOGIE INSTITUT	49 7247822847
JOHN KEREKES	MIT LINCOLN LAB	617-981-0805
ROLANDO RIZZI	ECMWF, UK	44 734 499080
CHARLES HUMPHREY	VISIDYNE	617-273-2820
REBECCA HEALEY	YAP ANALYTICS	617-863-1599
KOICHI YOSHINU	CTR FOR ASTROPHYSICS	617-495-2796
GIL DAVIDSON	PHOTO METRICS	617-935-6500
EARL CURTIS	ROCKETDYNE	818-586-3121
MIREILLE TANGUY	DGA/PCN	33 94162190
ROBERT DEMAJISTRE	CPI/APL	301-953-6000
NEAL KILMER	PS LAB, NMSU	505-522-9495
ED NIPLE	ARI	508-663-9500
PIERRE SIMONEAU	ONERA, FRANCE	33 46936850
PAUL EITNER	MARTIN MARIETTA	215-531-1195
ELEANOR WALTHER	SANDIA NATIONAL LABS	505-844-4728
MARK CANN	YORK UNIV	416-736-2100
IAN S. ROBINSON	AEROSPACE	310-336-6142
MARC R. HAMMOND	MISSION RESEARCH CORP	603-891-0070
RONALD E. ALLEY	JET PROPULSION LAB	818-354-0751
AL ZACHOR	ARC	508-263-1931
ROBERT R. O'NEIL	PL/GPOS	617-377-4775
MARIE-ANNIDE GIRAUD	DGA/DCN	33 94162140
SHEPARD A. CLOUGH	AER	617-349-2282
WILLIAM A.M. BLUMBERG	PL/GPOS	617-377-3688

QUANCHENG MA	GISS, NASA	212-678-5574
OINAS VALDAR	HUGHES HTX	212-678-5528
RICHARD H. PICARD	PL/GPOS	617-377-2222
SUSAN MCKENZIE	MRC	603-891-0070
CHAN TOUART	HSTX	617-863-0677
STUART GATHMAN	NCCOSC-NKAD	619-554-1417
DAVID EDWARDS	NCAR, BOULDER, CO	303-497-1857
HARRY FINKLE	MIT/LL	617-981-4905
HANK REVERCOMB	UNIV OF WISCONSIN	608-263-6758
BERNARD SALLES	DGA/DCN	33 94162281
TERRY E. BATTALINO	NAWC	805-989-8383
ROBERT WILSON	BOSTON COLLEGE	617-552-8765
MARGARET GARDNER	VISIDYNE	617-273-2820
JAMES H. BROWN	PL/GPOS	617-377-4412
LARRY S. ROTHMAN	PL/GPOS	617-377-2336
JOHN EOLL	GRC	508-777-6323
JAMES WALLACE	FAR FIELD, INC	508-443-9214
JOHN O. WISE	PL/GPOB	617-377-5993
NICOLE HUSSON	LMD/CNRS	33 69334802
AGNES BAUER	LSH-UNIV LILLE	33 20434789
SUSAN DOWNER	MRC	603-891-0070
ROGER A. VAN TASSEL	PL/GPO	617-377-2951
WILLIAM GALLERY	AER	617-349-2284
RAFAEL QUIROGA	ITT-FED SERV	805-734-8232
MEG NOAH	MRC	613-891-0070
JAMES J. GIBSON	PL/GPOS	617-377-4171
JAMES J. KLEESPIES	PL/GPAS	617-377-3136
KELLY CHANCE	SMITHSONIAN/HARVARD	617-495-7389
ALBERT BOEHM	HUGHES STX	617-377-2971
DON GRANTHAM	PL/GPA	617-377-2982
DAVE LONGTIN	SPARTA	617-863-1060
RICHARD ENG	MIT/LINCOLN LAB	617-981-3695
JEREMY R. WINICK	PL/GPOS	617-377-3619
JULIA VAIL	YAP ANALYTICS	617-377-3654
G. DAVID EMMITT	SWA	804-979-3571
ROBERT A. JOSEPH	ARCON	617-890-3330
VINCENT FALCONE	PL/GPAS	617-377-4029
PRECILA IP	MRC	603-891-0070
PETER P. WINTERSTEINER	ARCON	617-890-3330
PAUL HILTON	HUGHES STX	617-863-0388
ROBERT SUNDBERG	SPECTRAL SCIENCES	617-377-4770
PHAN DAO	PL/GPIM	617-377-4944
EDMOND M. DEWAN	PL/GPOS	617-377-4401
ROBERT HUFFMAN	PL/GPIM	617-377-3311
ARMAND PABOOJIAN	ARCON	617-377-2262
PIALI DE	SPECTRAL SCIENCES	617-273-4770

GABRIEL VAZQUEZ
MICHAEL CHEIFETZ
JAN HERRMANN
JOHN HUMMEL
ROY WALTERS
DAVID EDWARDS

NCAR
SPARTA
MIT/LINCOLN LAB
SPARTA
GENERAL RESEARCH
NCAR

303-497-1605
617-863-1060
617-981-3780
617-863-1060
508-777-6323
303-497-1857

AUTHOR INDEX

L.W. Abreu	199	J.I.F. King	3
P. Acharya	157	F.X. Kneizys	157
S. Adler-Golden	441,662	G. Kornfeld	711
G. P. Anderson	157,192,214	J. Kristl	199
D.E. Anderson	305	A. Kuze	102
P. Ashcroft	116	D.H. Leslie	353/391
M. Autric	743	D.R. Longtin	644
A. Berk	157,214	M. Lopez-Puertas	462
L.S. Bernstein	157,214	M. Lopez-Valverde	462
P. Bougarel	69	U. Makhlouf	464
J.H. Brown	491,530	M. Matthew	662
W. Brutsaert	69	A. McCann	199
Kelly V Chance	102	S. McKenzie	340
M.G. Cheifetz	644	J.-L. Moncet	157,192
J.H. Chetwynd	157,192,214	E. Murphy	192
T. G. Chrien	5	J.E. Murray	380
F.O. Clark	318	M. Noah	318
S.A. Clough	157	A. J. Paboojian	464
M. Cloutier	192	W.H. Parkinson	380
J.E. Conel	5	R.H. Picard	464
W.M. Cornette	48,234,558	Henry Rachele	659
A. Dalgarno	380	K. Radermacher	318
R. DeMajistre	305	A. J. Ratkowski	464
E.M. Dewan	512	D. Robertson	157,214,234,441
S.B. Downer	318	B. Salles	743
J. Dozier	86	T. Schmugge	69
J. Duff	441	J. Schroeder	199
D.P. Edwards	462	J. G. Shanks	48
D. Einstein	318	R.D. Sharma	214,441
G.D. Emmit	725	A. Shimota	355
J.R. Esmond	380	A. Smith	192
S. Evans	305	K. Stamnes	291
B.-C. Gao	37	M. Sugita	69
R. Garner	677	Y. Sun	380
K.E. Grant	132	R.L. Sundberg	214,441
R.O. Green	5	N. Takeuchi	357
A.S. Grossman	132	M. Tanguy	743
K.U. Grossmann	464	J.-M. Theriault	157,192
J. Gruninger	441,662	A.P. Thorne	380
L.K. Harada	353/391	S. Tsay	291
S. Harvey	199	V. Turner	192
R.J. Healey	214	J.C. Ulwick	464
M.L. Hoke	214	M. Voltaire	199
D. Homann	464	Z. Wan	86
J.R. Hummel	644	J.R. Winick	464
P.C. Ip	318	S.A. Wood	725
S. Kadokura	355	M. Yeh	291
J.P. Kennealy	318	K. Yoshino	380
N.H. Kilmer	659	Carl R. Zeisse	756

VUV FOURIER TRANSFORM SPECTROSCOPY OF THE (O,O) BAND OF NO

K. Yoshino, J.R. Esmond, J.E. Murray
Y. Sun, A. Dalgarno, W.H. Parkinson

A.P. Thorne

Harvard-Smithsonian Center for
Astrophysics
Cambridge, MA 02138

Blackett Laboratory
Imperial College
London SW7 2BZ, UK

Using the VUV Fourier transform spectrometer (FTS) at Imperial College we have observed the (O,O) and (1,O) bands of NO, at 191 nm and 183 nm respectively, in absorption. A high current hydrogen lamp was used as the background continuum source with a 0.3 m grating spectrometer as a bandpass filter. The absorption spectrum was observed at various pressures of NO ranging from 0.004 to 0.089 torr, and temperatures of 295 K and 78 K. To fully resolve the sharp NO lines (Doppler width 0.11 cm^{-1} at 295 K) we chose an FTS resolution of 0.06 cm^{-1} (2 mÅ). We report here on the first, absolute, cross section measurements made for the (0,0) band along with new improved energy precision for the low lying rotational levels (up to $J=20\frac{1}{2}$ for the $C^2\Pi$ and $J=8\frac{1}{2}$ for the $B^2\Pi$ electronic states). A deperturbation procedure to analyse the energy level structure will be presented.

This work is supported by NSF Division of Atmospheric Sciences grants ATM-91-16552 and ATM-90-19188 to Harvard College Observatory.

VUV Fourier Transform Spectroscopy of the $\delta(0,0)$ Band of NO

K. Yoshino, J.R. Esmond, J.E. Murray, Y. Sun, A. Dalgarno, W.H. Parkinson

Harvard-Smithsonian Center for Astrophysics, Cambridge, MA 02138

A.P. Thorne

Blackett Laboratory, Imperial College, London SW7 2BZ, UK

This work is supported by NSF Division of Atmospheric Sciences grants ATM-91-16552 and ATM-90-19188 to Harvard College Observatory.

Photo-destruction of NO is an important
stratospheric process

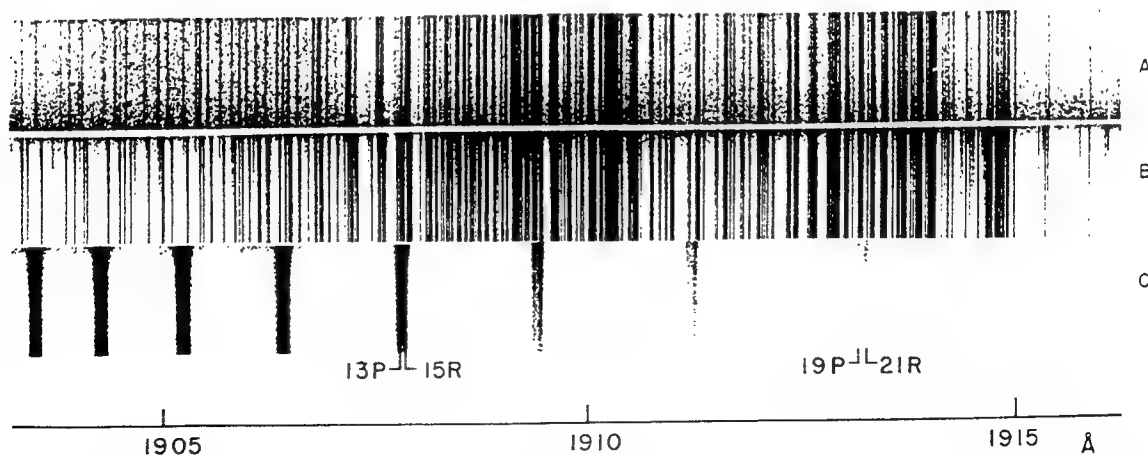
175 - 205 nm penetration controlled by O₂

Atmospheric model computations involving
O₂ and NO must be done on a line by
line basis

Such measurements have been completed for most
of the Schumann-Runge band

To fully resolve the linewidths of the NO band
we require resolving powers approaching 10⁶

$\delta(0,0)$ AND $\beta(7,0)$ BANDS OF NO
AND (5,0) S - R BAND OF O₂



Experimental setup

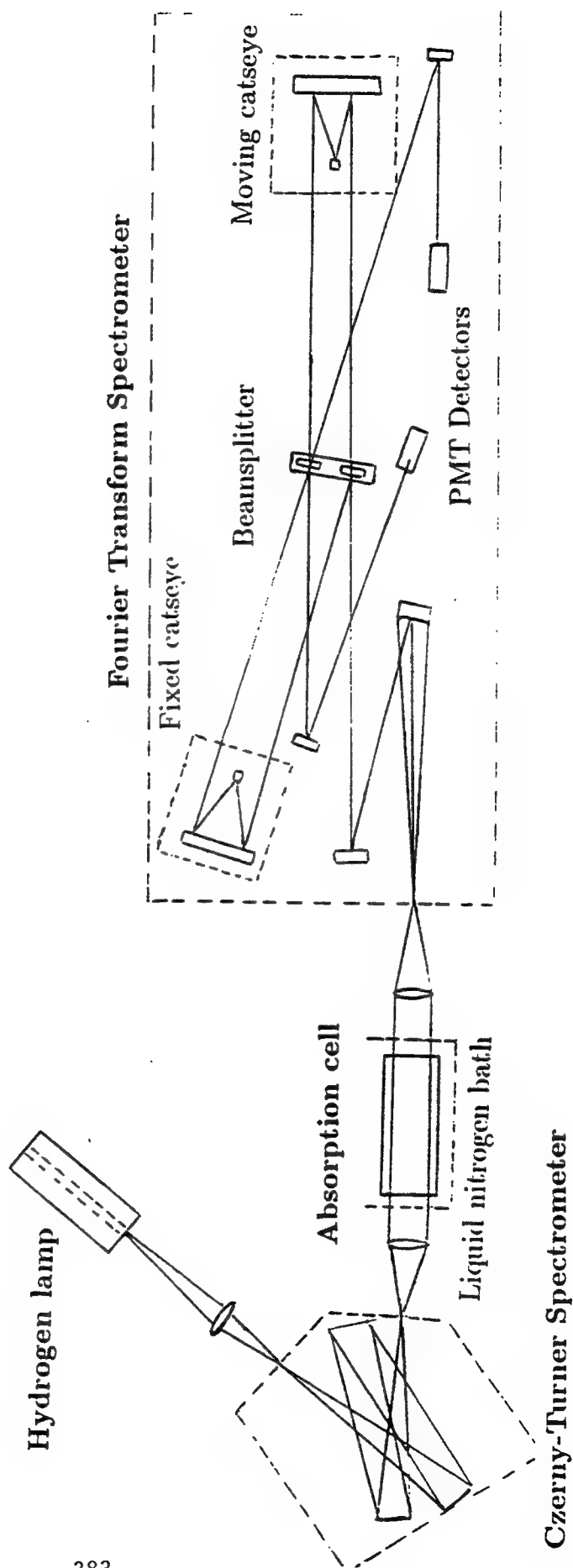


Fig 1

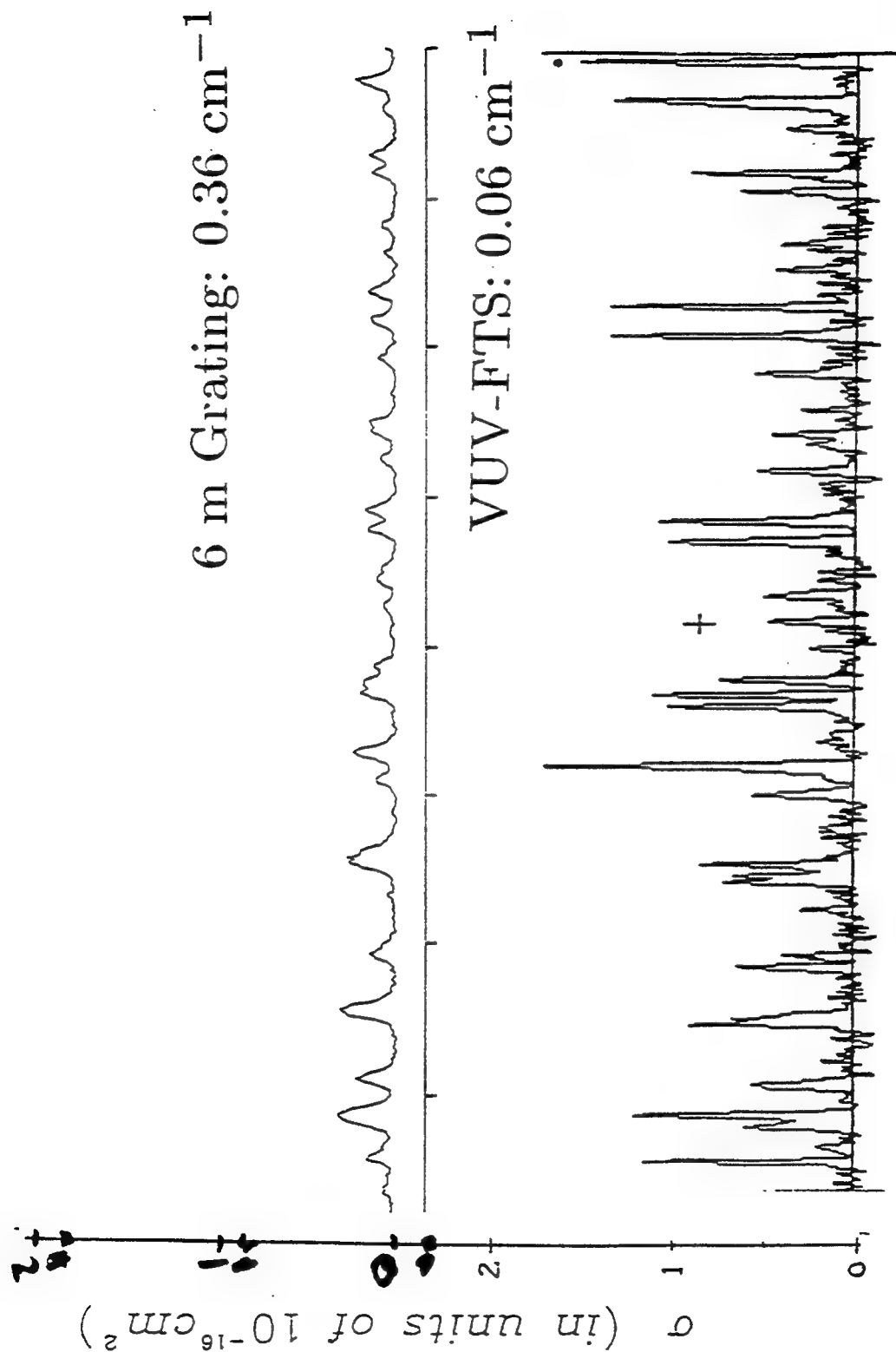
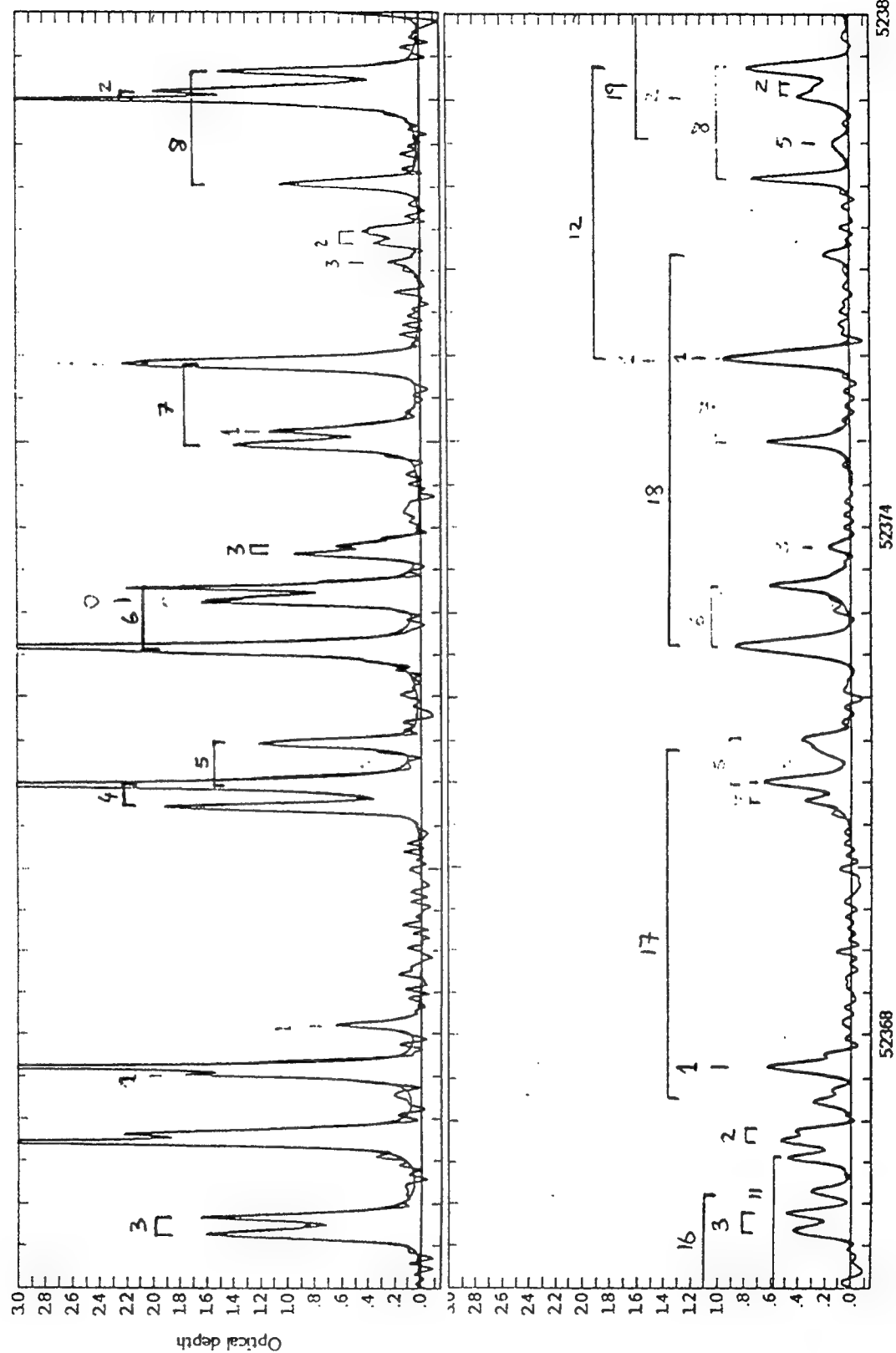
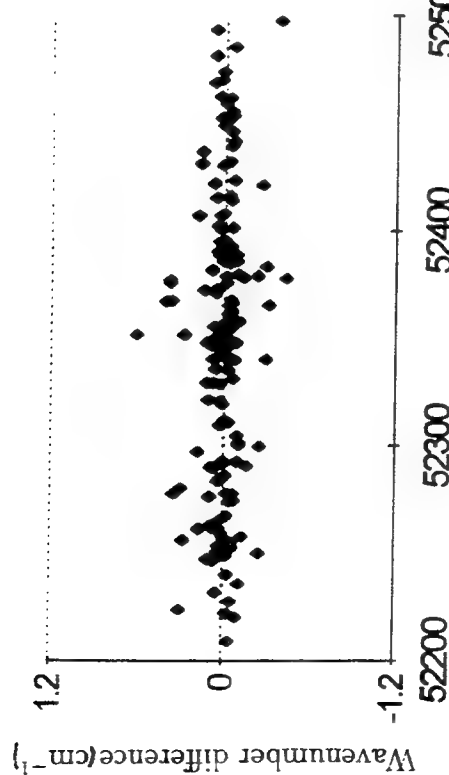


Fig. 2

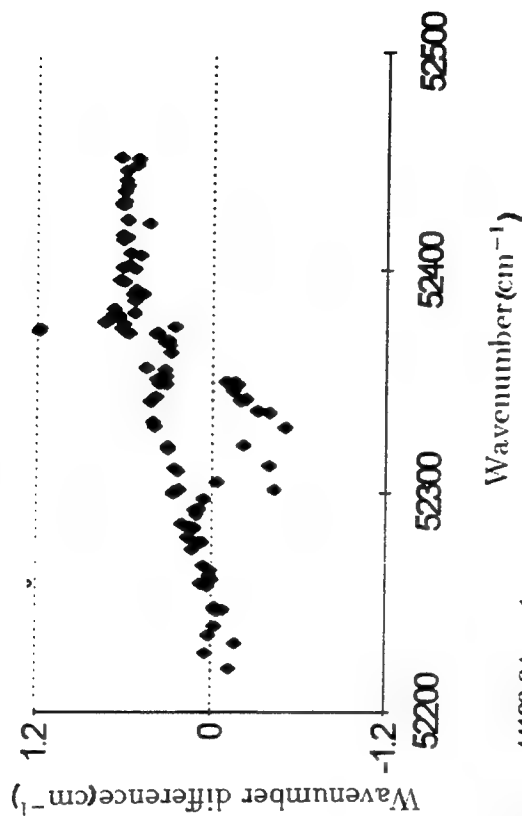


Wavenumber and term differences between this work and previous studies

a: Our work - Lagerqvist and Miescher
grating spectroscopy



b: Our work - Rotke and Zacharia
laser spectroscopy



Wavenumber (cm⁻¹)

Term value difference- 44199.04 cm⁻¹

C: This work - Aniot and Verges
FT spectroscopy

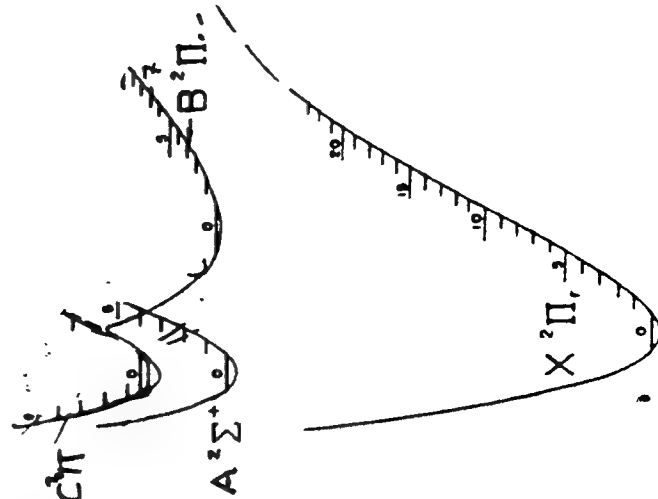
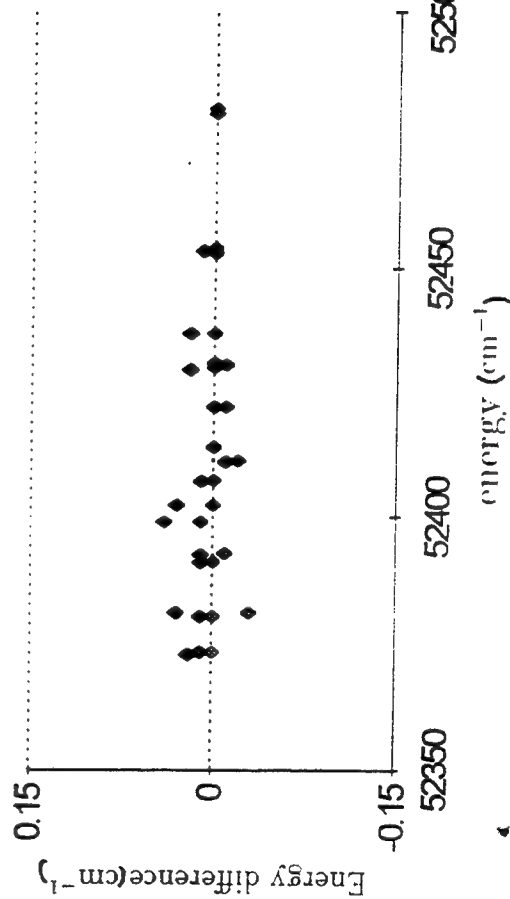


Table 1

Determination of the mixed $C^2\Pi$ and $B^2\Pi$ Tye terms
using rotational lines from different branches

J	R11	P11	R12	P12	Q11	Q12	Mean	std
0.5		52372.72			52372.69		52372.70	0.02
1.5	52380.29	52380.31		52380.32		52380.29	52380.30	0.01
2.5	52391.00	52390.99	52391.00	52390.99	52390.95	52391.02	52390.99	0.02
3.5	52402.34	52402.33			52402.27		52402.31	0.04
4.5	52414.02	52414.04					52414.03	0.02
5.5	52430.65	52430.65	52430.63	52430.64			52430.64	0.01
6.5	52453.45	52453.45	52453.45	52453.44			52453.45	0.00
7.5	52480.79		52480.80	52480.76			52480.78	0.02
8.5	52512.26	52512.26	52512.25	52512.25			52512.26	0.00
9.5	52547.75	52547.70	52547.76				52547.74	0.03
10.5	52587.19	52587.19	52587.24	52587.26			52587.22	0.03
11.5	52630.65	52630.63					52630.64	0.01
12.5	52678.06	52678.06	52678.04				52678.06	0.01
13.5	52729.40	52729.39					52729.40	0.01
14.5	52784.74	52784.72	52784.74				52784.73	0.02
15.5	52843.98	52844.02					52844.00	0.02
16.5	52907.15	52907.16					52907.16	0.00
17.5	52974.30	52974.35					52974.33	0.03
18.5	53045.38	53045.39					53045.38	0.01
19.5		53120.39					53120.39	

The eigenstates of the NO molecule are mixtures of four Hund's case (a) basis: $C^2\Pi_{1/2}(v=0, J)$, $C^2\Pi_{3/2}(v=0, J)$, $B^2\Pi_{1/2}(v=7, J)$, and $B^2\Pi_{3/2}(v=7, J)$. The corresponding 4×4 Hamiltonian is given in Table 2a. Least square nonlinear fitting of the observed energy values to the Hamiltonian results in the molecular constants (Table 2b). In the fitting, we fixed the D constant for the $B^2\Pi$ at 4.68×10^{-6} (calculated using the RKR potential of Gulluser and Dressler).

Table 2a: Hamiltonian for each $^2\Pi$ block

	$^2\Pi_{1/2}$	$^2\Pi_{3/2}$
$^2\Pi_{1/2}$	$T_v - A/2 + B(X+1) - D[(X+1)^2 + X]$ $+ p(1 \mp \sqrt{X+1})/2 + q(X+2 \mp 2\sqrt{X+1})/2$	symmetric
$^2\Pi_{3/2}$	$\sqrt{X}[-B + 2DX]$ $-p/4 + q(\pm\sqrt{X+1} - 1)/2]$	$T_v - A/2 + B(X-1)$ $-D[(X-1)^2 + X] - qX/2$

$X = (J - 1/2)(J + 3/2)$, upper (lower) signs are for e(f) parities.

$$\langle B^2\Pi_{\Omega} | H | C^2\Pi_{\Omega'} \rangle = H_{BC} \delta_{\Omega\Omega'}$$

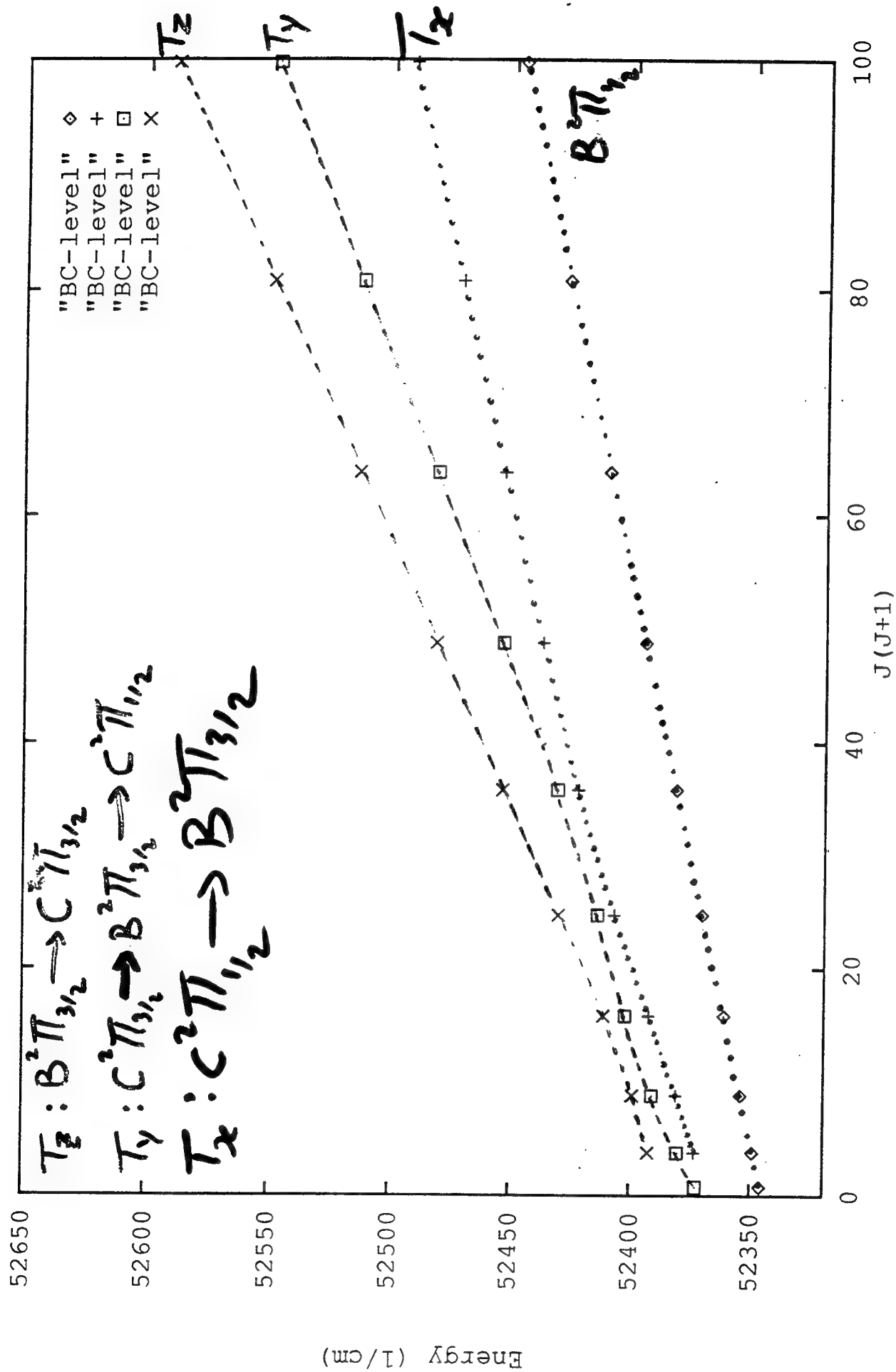
Table 2b: Molecular constants in cm^{-1} units

$C^2\Pi(v=0)$	T_v	A	B	D	p	q
this work	52371.26	3.21	1.9945	6.2×10^{-6}	-0.0059	-0.016
A&V		3.1957	1.994555	5.8694×10^{-6}	-0.0057	-0.0159484

$B^2\Pi(v=7)$	T_v	A	B	D	p	q
this work	52367.14	42.31	1.0320	4.68×10^{-6}	0.024	-0.0034

$$H_{BC} = 5.29, \text{rms} = 2.1 \times 10^{-3}.$$

The energy origin is the lowest $X^2\Pi$ level.



Band oscillator strengths of $\delta(0,0)$ and $\beta(7,0)$ bands of NO

	Band Oscillator strength	Resolution	Method
Bethke (1959)	0.00249	11 cm ⁻¹	Pressure-broadening: Ar
Callear & Pilling(1970)	0.0056		Curve of growth
Mandelman & Carrington(1974)	0.0022	82 cm ⁻¹	Extended to 0 pressure
Cieslik (1977)	0.0025		Extended to 0 pressure
Guest & Lee(1981)	0.00352	8 cm ⁻¹	Low pressure: 2 mtorr
Chan, Cooper & Brion(1993)	0.00266	300 cm ⁻¹	Dipole spectroscopy
6-m spectrometer	0.0013	0.35 cm ⁻¹	Direct integration
FTS at 78 K p=0.09 torr	0.0017	0.06 cm ⁻¹	Direct integration
FTS at 78 K p=0.033 torr	0.0021	0.06 cm ⁻¹	Direct integration
FTS at 295 K p=0.09 torr	0.0025	0.08 cm ⁻¹	Direct integration
FTS at 295 K p=0.078 torr	0.0036	0.06cm ⁻¹	Direct integration *

Table 3

Atmospheric Transmission Issues for the Air Force Airborne Laser (ABL)

Annual Review of Atmospheric Transmission Models
Air Force Phillips Laboratory
Geophysics Directorate
8 June 1993

Larrene Harada
Dan Leslie

WJSA

W. J. Schafer Associates Inc
1901 N. Fort Myer Dr.
Arlington, VA 22209
(703) 558-7900

Atmospheric Effects on ABL Performance

AGENDA

Introduction to the ABL

ABL Atmospheric Issues

LIDAR data

SAGE Satellite Data

Impact of Volcanic Aerosols on
ABL Performance

Future work

Purpose of This Briefing

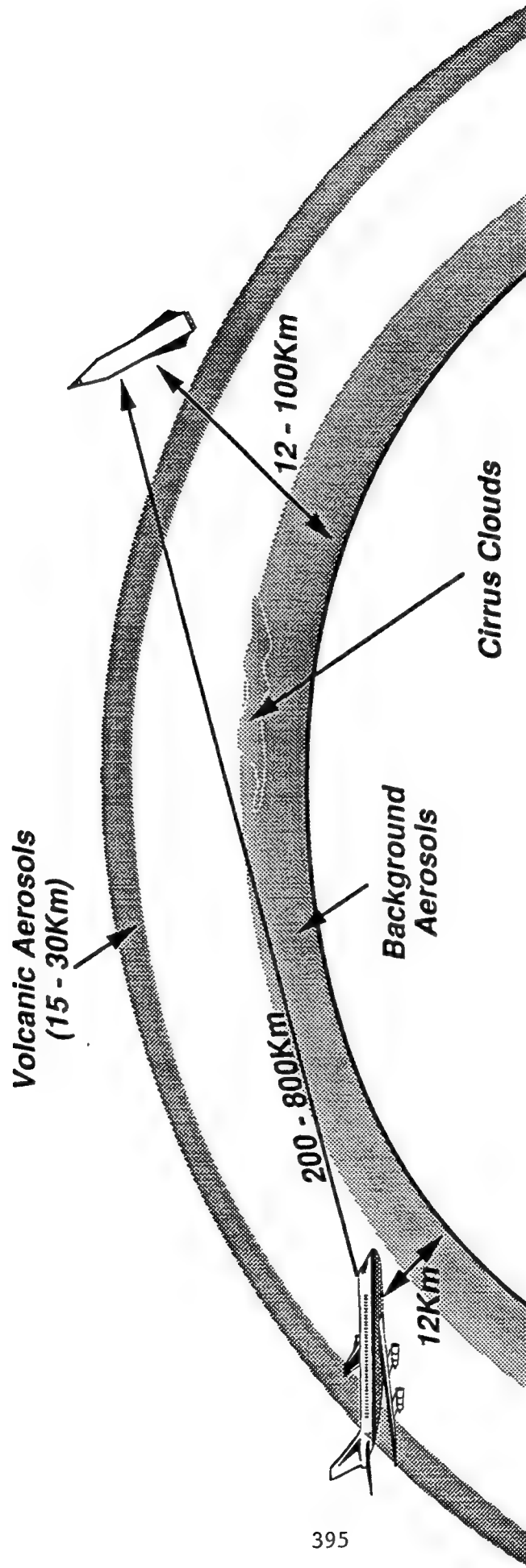
- Describe the atmospheric transmission issues and status for the ABL
 - molecular absorption
 - aerosol scattering
- Not discussed here
 - turbulence and compensation
 - specific program performance requirements



AIRBORNE LASER LABORATORY



ABL Propagation Geometry

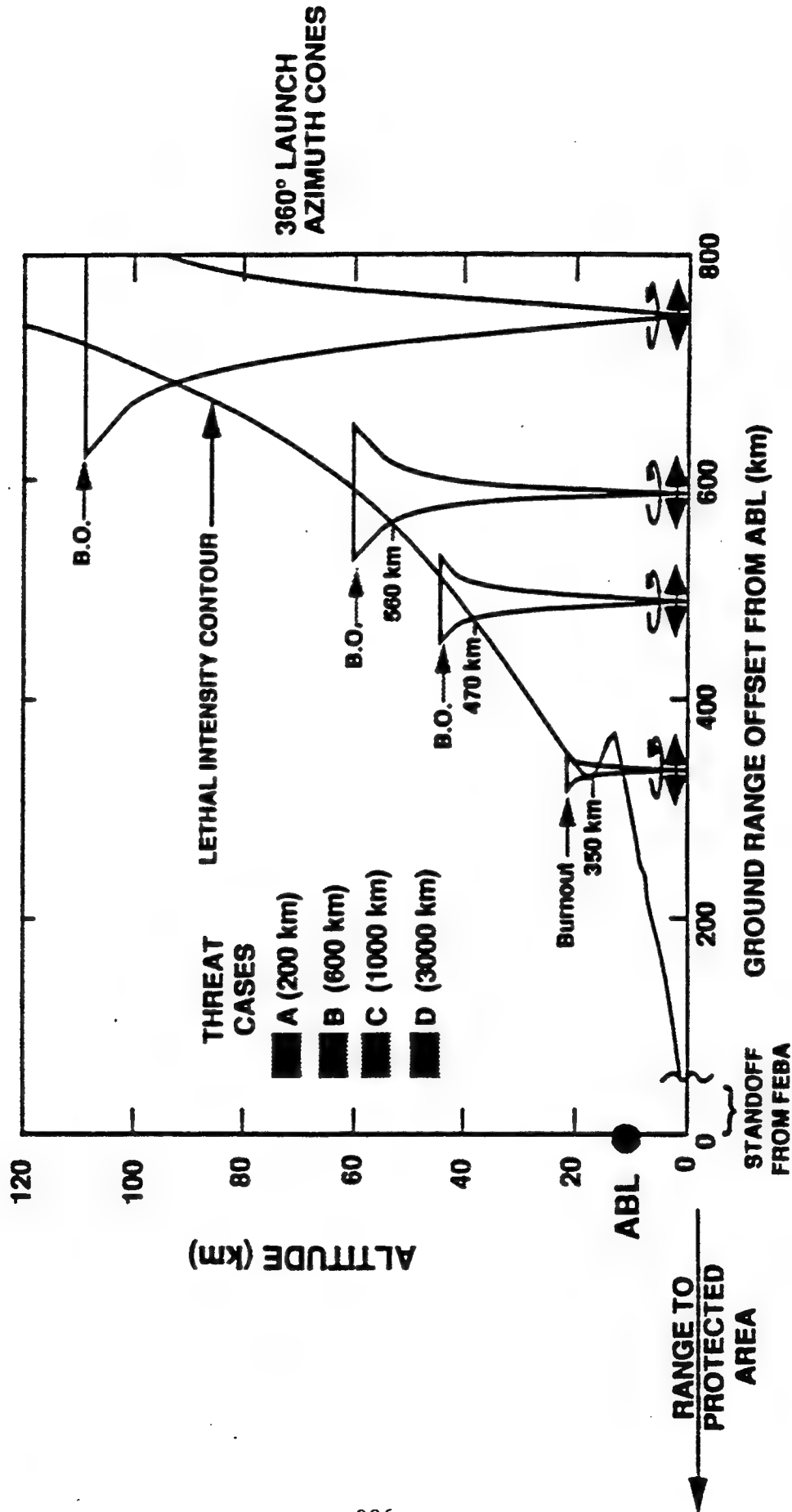


Optical Propagation

Acquisition Sensors	3 - 5	8 - 12 μ
Laser Tracker/Beacon	1.06	1.3
High Energy Laser	1.32	others

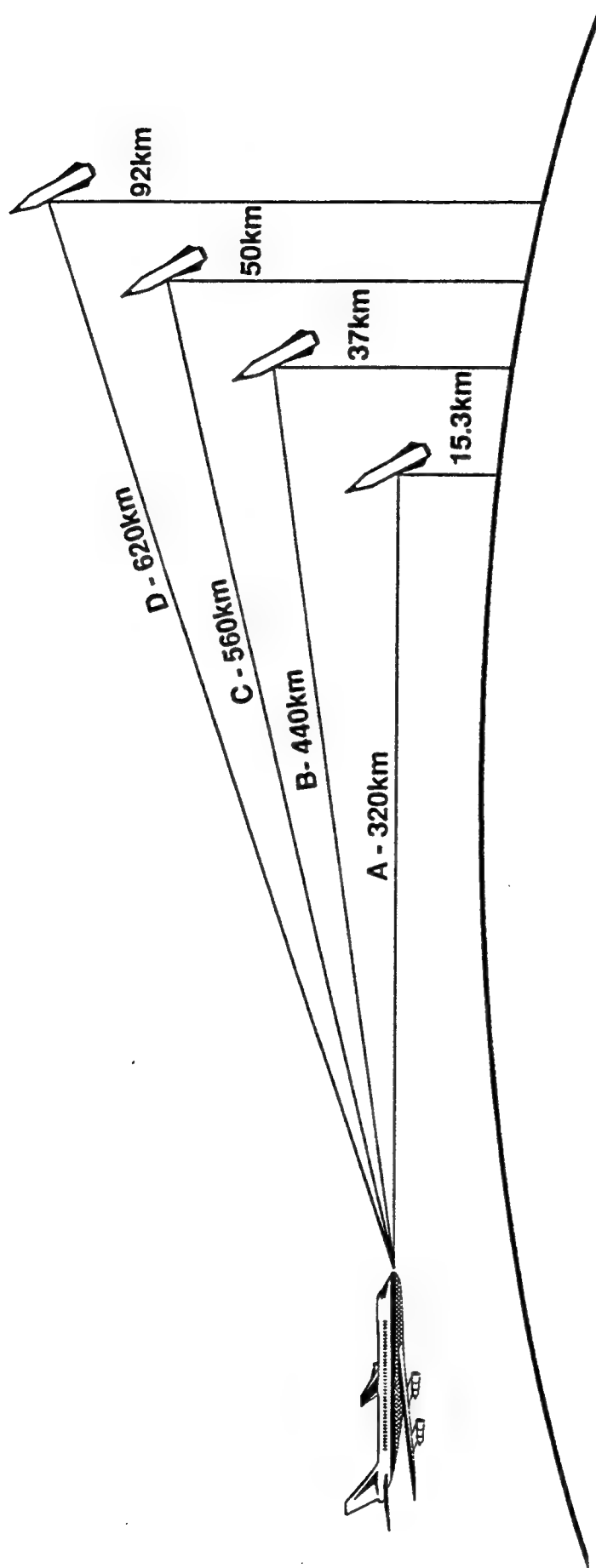


ABL RANGE VS. THREAT CASE



ABL LETHAL ENVELOPE EXPANDS WITH INCREASING RANGE OF TBM THREAT
(C560 = B470 = A350)

ABL Cases A, B, C, D



397

At maximum ranges, elevation angles vary from -0.8° (Case - A) to $+4^{\circ}$ (Case - D).

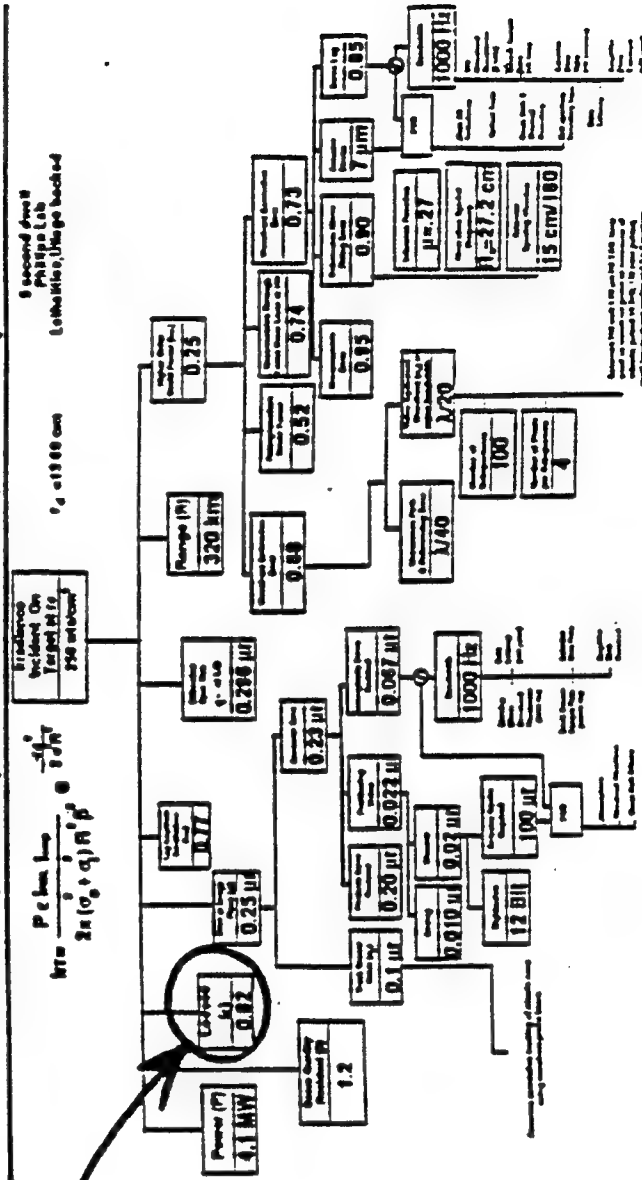
WJSA SDIO ABL Analysis

- Our work has concentrated on COLL (1.3 μ), but much analysis also has been done on DPSS (1.06 μ), HF-OT(1.32 μ), HF-Is(2.9 μ), DF(3.8 μ), and FEL(2.314 μ +...)
- Constructed performance code (ABL Engagement ABLE) to allow trade studies among system parameters including:
 - Adaptive Optics Complexity
 - Aperture Size
 - Turbulence Profile
 - Lethality
 - Jitter
 - Power
 - Target Trajectory
 - Aircraft Altitude
- Carefully tied turbulence scaling-laws to detailed wave-optics simulations (Russ Vernon SAIC) at selected points (Cases A, B, C, D) and compared with tOSC and MIT/LL w/o results
- Assessing the impact of excursions
 - Tilt-Only Compensation
 - Recent Volcanic Aerosols
 - SAGE Satellite Data
 - Higher Turbulence
 - Near-term Systems
 - Others

Atmospheric Transmission is One Loss Factor In ABL Power Requirement Budget



Performance Requirement Allocation For Operational Theater Missile Defense Oxygen Iodine Laser System -- 12.5 km Platform, 15.3 km Target, WSMR Clear 2 Night Turbulence, 2.0 M Aperture, 320 km Range



Case	Trans
A	0.82
B	0.88
C	0.88
D	0.95
MLS Atmosphere	
Bkg Strat/Mod	
Volc Aerosol	



INPUT ASSUMPTIONS DEVICES/AO

Device	Wavelength (μm)	Line	Wavenumber (cm^{-1})	% Power	Beam Quality
DPSS	1.064		9398.5		1.5
COIL	1.31524		7603.135		1.2
HF Overtone (Line Selected)	1.31260	$P_2^{(3)}$	7618.467	16	1.5
	1.32125	$P_2^{(4)}$	7568.577	84	
FEL (tunable)	2.31449		4320.59		1.2
HF (Line Selected)	2.865692	$P_1^{(10)}$	3489.559	30	1.5
	2.954009	$P_2^{(9)}$	3385.230	70	

System Jitter (1axis)	= 0.25 μrad	Boresight error	= 100 nrad
Mirror Diameter	= 2.0 m	Actuator Spacing	= 15.0 cm
Tracker Bandwidth	= 1000 Hz	DM Bandwidth	= 1000 Hz
Beam Shape	= Truncated Gaussian	Servo Delay	= 300 μsec
		Beacon Spot Diameter	= 1.4 m



INPUT ASSUMPTIONS TARGET/AIRPLANE/ATMOSPHERES/LETHALITY

Case	Range of Missile (km)	Ground Engagement Range (km)	6 sec before burnout		1 sec before burnout	
			Alt (km)	Speed (km/s)	Alt (km)	Speed (km/s)
A	200	320	15.3	0.97	19.3	1.18
B	600	440	37.1	1.79	43.7	2.11
C	1000	560	50.3	2.34	57.7	2.75
D	3000	620	92.1	3.90	104.8	4.49

AIRPLANE	ATMOSPHERES	LETHALITY
Airplane speed = 200 m/s ~ MACH 0.68 at 12.5 km altitude Turret a/speed at separation of flow = 250 m/s ~ MACH 0.85 at 12.5 km altitude (Azimuth = 100°) DK Model	FASCOD2 HITRAN '86 (will rerun when we get FASCOD3P and HITRAN '92) Midlatitude Summer Background Stratospheric / Moderate Volcanic Turbulence = Clear 2 night Wind = Clear 2 night	Ullage Backed 5 sec dwell Aspect Angle = 0°



POWER REQUIRED IN MEGAWATTS (ULLAGE-BACKED CATASTROPHIC KILL)

WAVELENGTH (μm)								
CASE	Target Engagement			1.06 (DPSS)	1.32 (COIL/HF-OT)	2.31 (FEL)**	2.9 (HF)	3.8 (DF)
	Altitude (km)	Range (km)	Speed (km/s)					
A	15.30	320	0.97	6.1	3.6	2.7	3.9	3.9
B	37.13	440	1.79	4.5	3.3	3.3	4.2	5.7
C	50.28	560	2.34	5.8	4.5	4.8	6.3	8.8
D*	92.11	620	3.90	2.7	2.6	4.3	5.9	9.1

Lethality set at a constant 1.1 kJ/cm²

1 kHz Adaptive Optics

1.2 Beam Quality

2 m aperture, 12.5 km plane altitude, 0.25 μrad jitter,

5 sec dwell, 200 m/s plane speed, Clear 2 night,

0° aspect angle, 100° azimuth angle

Mid-Latitude Summer Atmosphere

Background Stratospheric/Aged-Volcanic/Moderate Aerosol

* Class 1 Missile Lethality Used

** FEL Wavelength Selectable

Thermal Blooming not Included

Atmospheric Effects on ABL Performance

AGENDA

Introduction to the ABL



ABL Atmospheric Issues

LIDAR data

SAGE Satellite Data

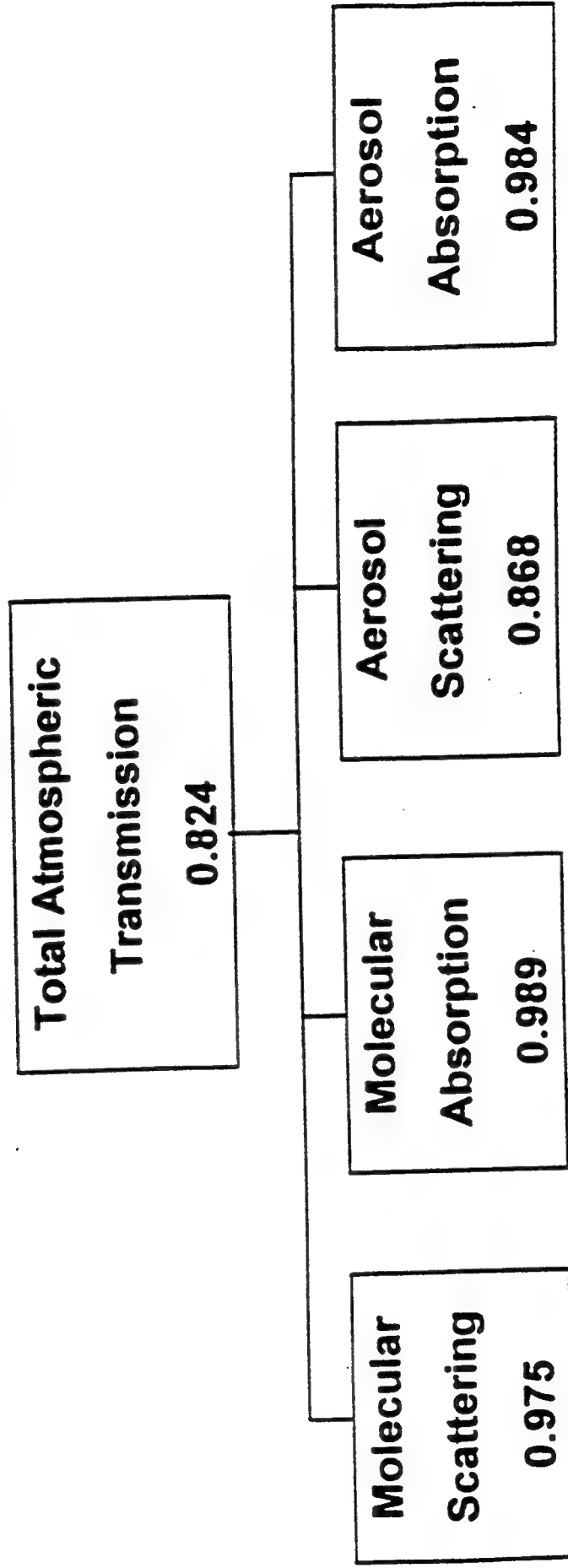
Impact of Volcanic Aerosols on
ABL Performance

Future work

Total Atmospheric Transmission

Is The Product of Four Factors

COIL (1.32 μ) Case-A Path Example (12.5/15.3/320)



- For COIL, Aerosol Scattering is the only factor of importance

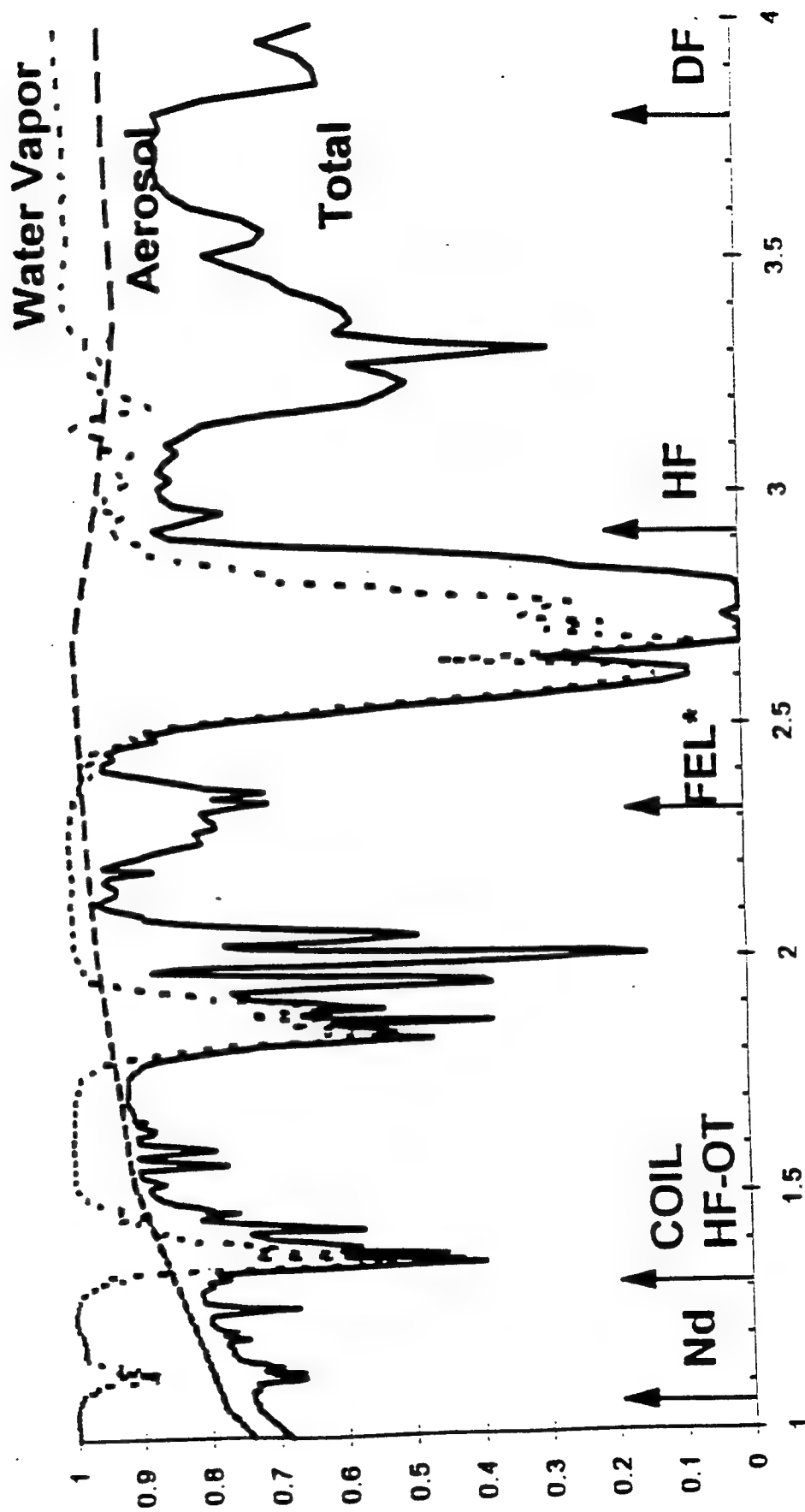
- Only factor significantly different from 100%

- Can vary widely - as bad as 0.2 shortly after volcanic activity

- Molecular Absorption effects can dominate for other laser frequencies

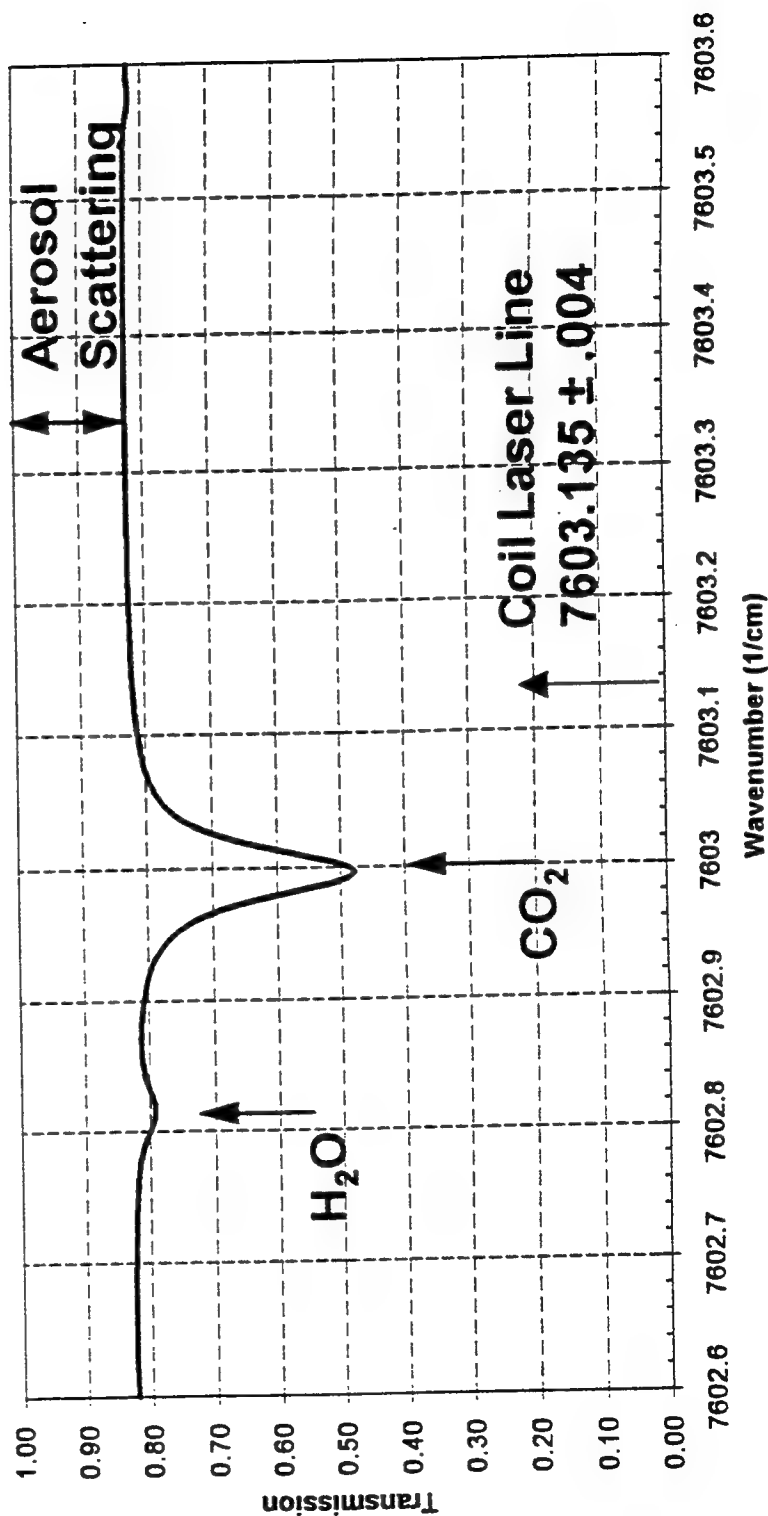
Low-Resolution (LOWTRAN) - Case-A

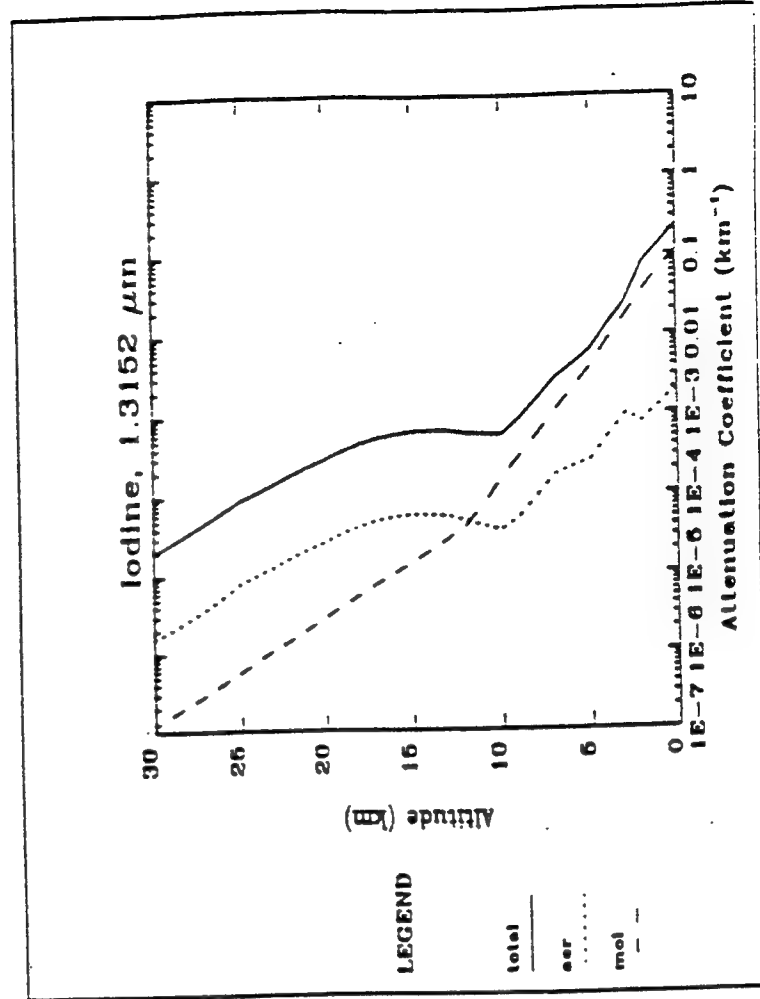
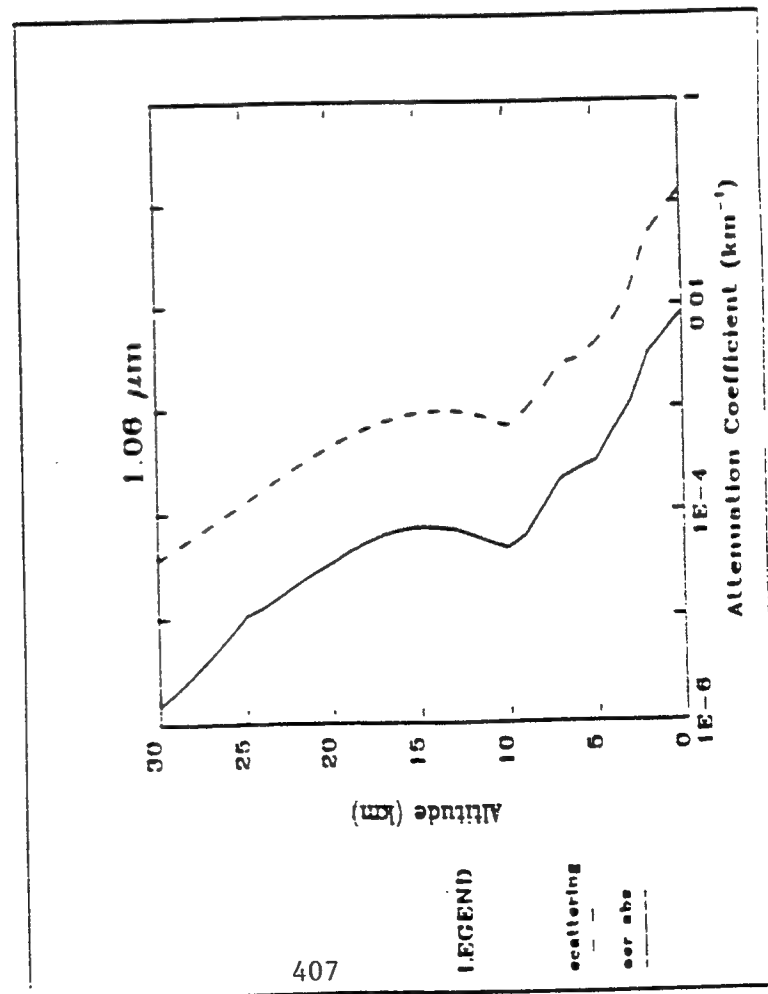
Bkg Strat/Mod Volc MLS 12.5/15.3/320 km



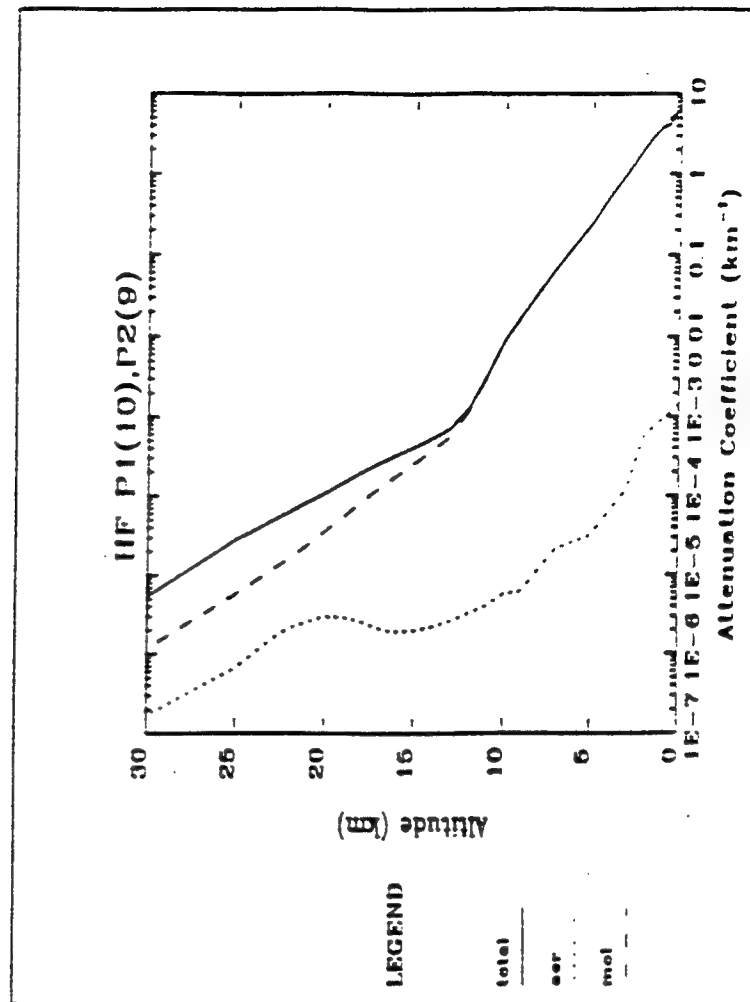
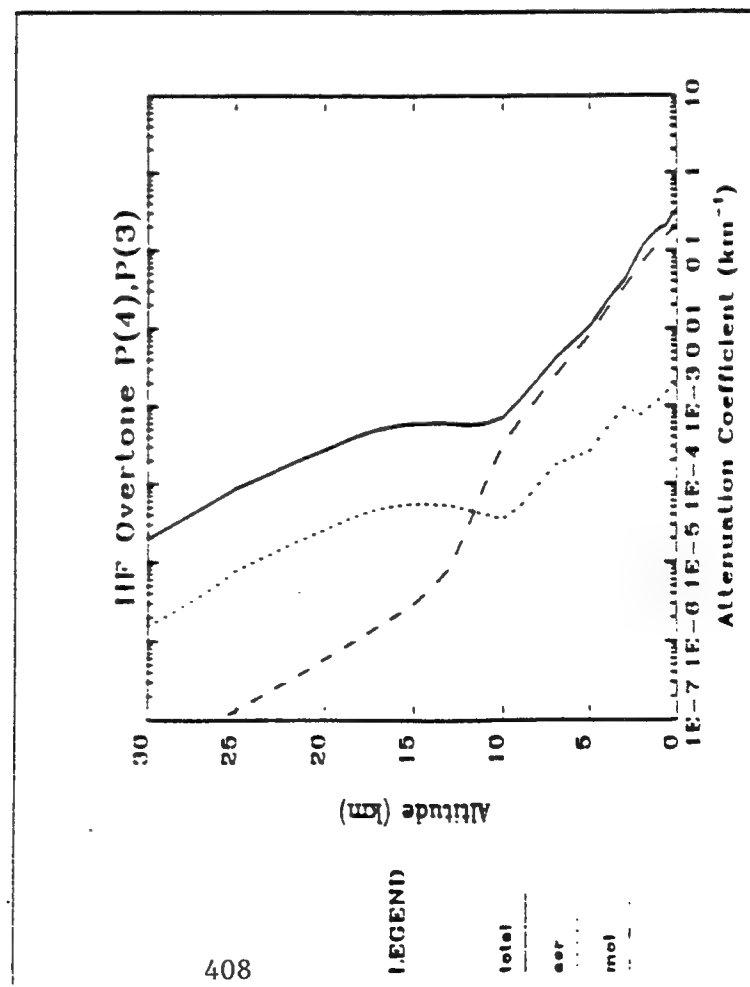
High-Resolution Atmospheric Absorption Spectra near the Iodine Laser Frequency

- FASCOD2, HITRAN92 Database
- Case-A geometry (12.5/15.3/320 km)
- laser frequency is well separated from absorption lines
- dominant extinction mechanism is aerosol scattering





WJSA Attenuation Coefficients Background Stratospheric, MLS



Sources of Aerosol Extinction

(Above Clouds)

- Background stratospheric aerosols
- Sub-visual cirrus clouds
- Volcanic dust, Sulfuric Acid droplets, ...

Stratospheric Aerosol Measurement Tools

	<u>Global</u>	<u>Optical</u>	<u>ABL-Path</u>	<u>High Alt</u>
LIDAR		X		X
Balloon Particulate Collection				X
Satellite Limb View	X	X	X	X

RECENT VOLCANOES

Date of Eruption	Volcano	Total Global Injection (10 ⁶ Metric Tons)
August 1883	Krakatoa	50
June 1912	Katmai	20
March 1963	Agung	16 - 30
October 1974	Fuego	3 - 6
1979	Background	0.57
November 1979	Sierra Negra	0.16
May 1980	St. Helens	0.55
October 1980	Ulawun	0.18
April 1981	Alaid	0.50
May 1981	Pagan	
January 1982	Mystery Volcano	0.85
April 1982	El Chichon	12.0
June 1991	Pinatubo	40+

**VOLCANIC AEROSOL TRANSMITTANCE
CASE A**

Stratospheric Aerosol Model	DPSS (1.06)	COIL (1.32)	FEL (2.31)	HF (2.9)*
Stratospheric Background	0.93	0.96	0.99	0.99
Aged Type/Moderate Profile	0.61	0.72	0.92	0.95
Fresh Type/High Profile	0.38	0.38	0.47	0.53
Aged Type/High Profile	0.58	0.69	0.91	0.94
Fresh Type/Moderate Profile	0.42	0.42	0.51	0.56
Background type/Moderate Profile	0.74	0.85	0.97	0.96
Background type/High Profile	0.71	0.83	0.97	0.96

* Absorption from these Aerosols could exacerbate thermal blooming.

A Brief Description of the Life of a (Volcanic) Stratospheric Aerosol

- Origin - Volcanic eruption launches megatons of SO_2 and other debris high enough to cross the tropopause into the relatively benign stratosphere.
- Dispersion - High altitude winds distribute the gas and particles.
- Growth - The SO_2 vapor combines with H_2O vapor to form liquid sulfuric acid H_2SO_4 droplets. Over time the droplets grow from sub-micron to several microns in diameter.
- Decay - As the droplets gain weight (over several years) they gradually fall to the tropopause.
- Death - Vertical mixing at the tropopause rapidly causes the droplets to fall to earth.

Atmospheric Effects on ABL Performance

AGENDA

Introduction to the ABL

ABL Atmospheric Issues

LIDAR data

SAGE Satellite Data

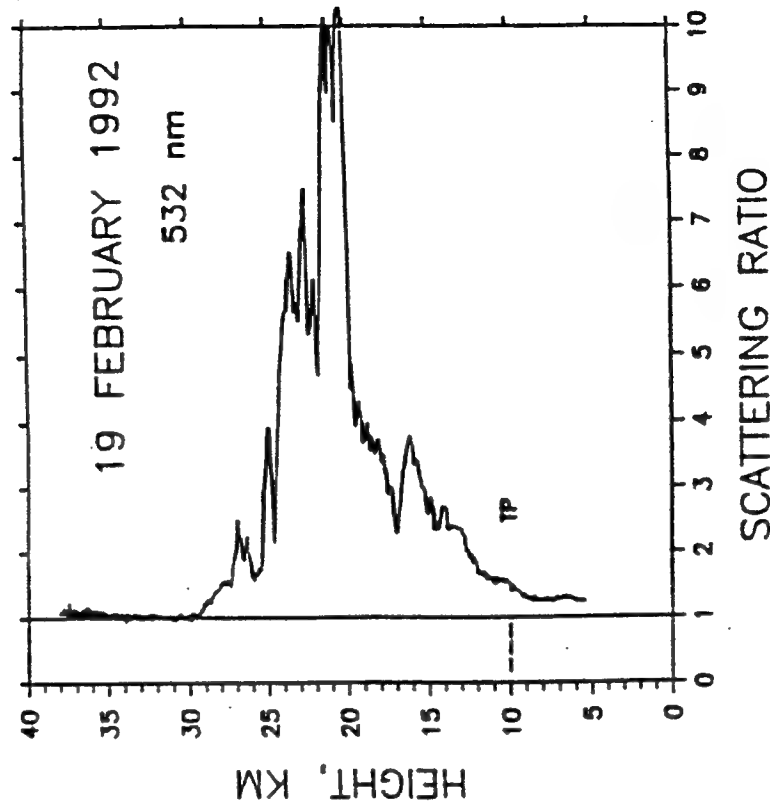
Impact of Volcanic Aerosols on
ABL Performance

Future work

Profile of the Scattering Ratio Taken at the Maximum - About 8 Months After Pinatubo

The LIDAR scattering ratio is the ratio of the total (aerosol + molecular) laser backscatter in each range bin relative to the Rayleigh (molecular only) backscatter.

Data taken at Garmisch-Germany (47 deg N)



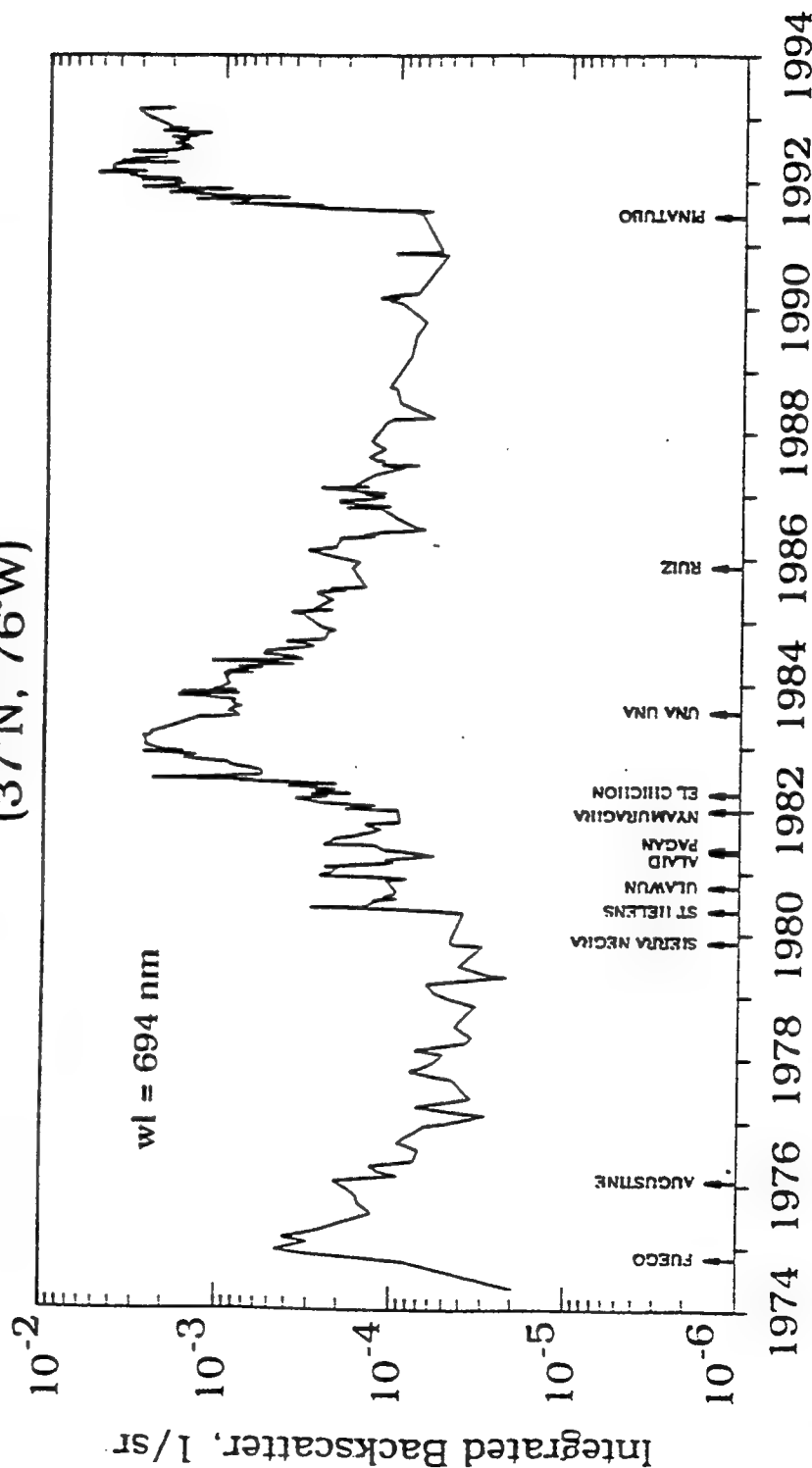
H. Jager, The Pinatubo Eruption in Relation to the El Chichon Event and the Stratospheric Background Load, QSA Topical Conference on Remote Sensing of the Atmosphere, March, 1993.

NASA LIDAR Backscatter Results

- 1/e recovery time of about 7.3 months after volcanic aerosol peak
- Peak is reached about 8 months after eruption
- Extinction varies with geographic location and specific volcano

STRATOSPHERIC INTEGRATED BACKSCATTER

Aerosol Lidar Measurements at LaRC
(37°N, 76°W)

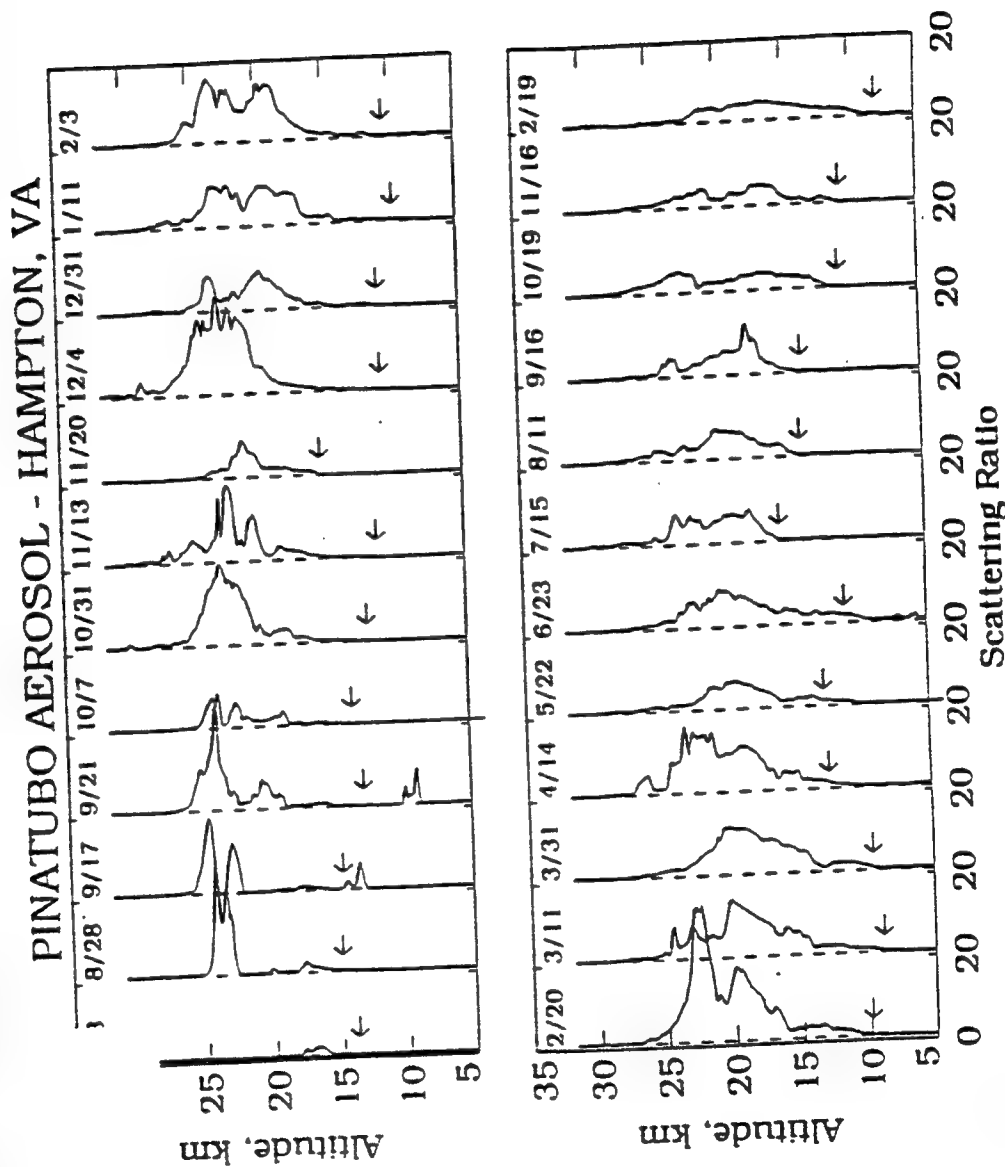


M. Osborn et al, Evolution of the Pinatubo Volcanic Cloud Over Hampton, VA, OSA Tropical Conference on Remote Sensing of the Atmosphere, March, 1993.

WJSA

NASA LIDAR Backscatter Results

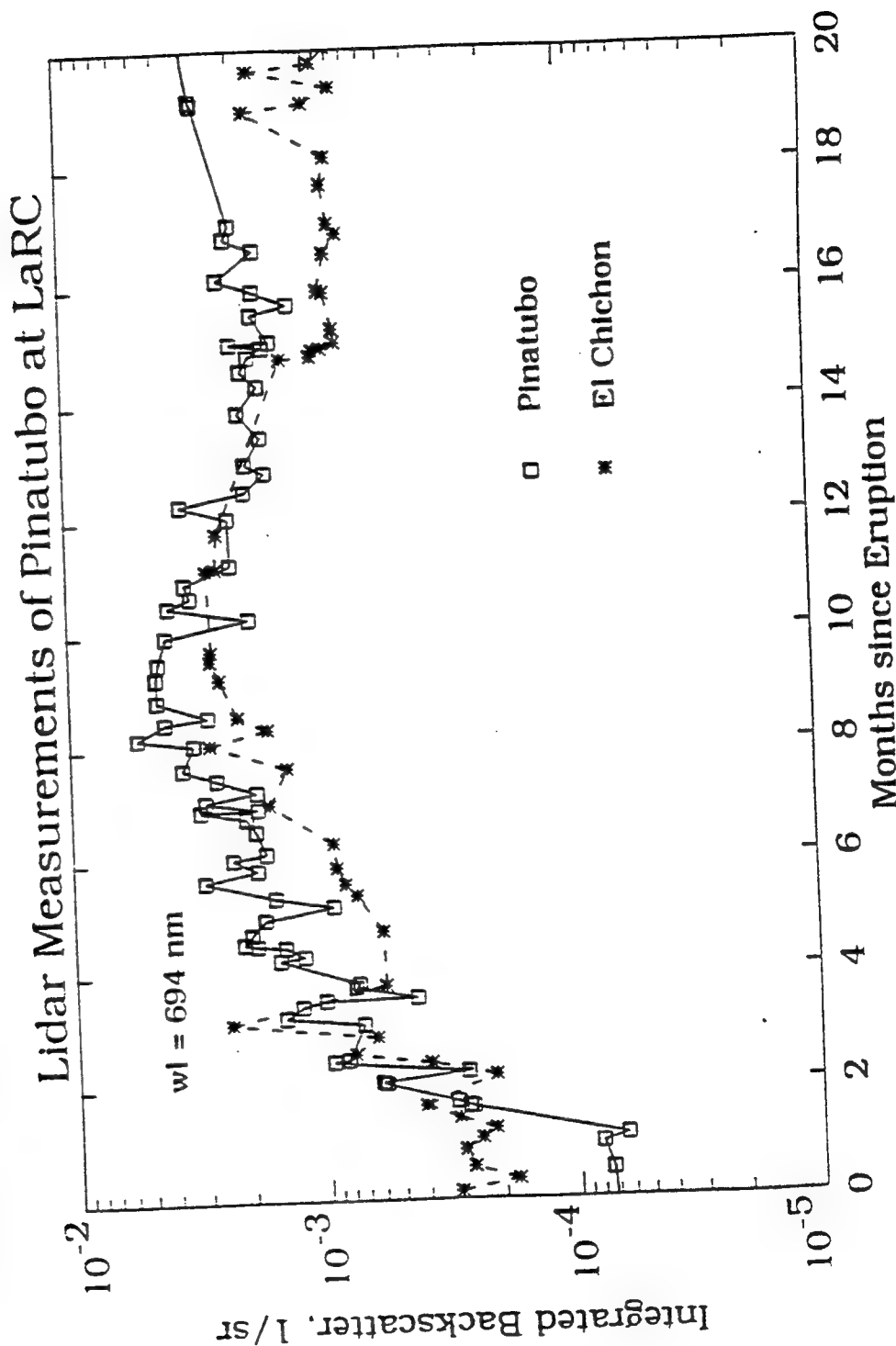
- 1/e recovery time of about 7.3 months after volcanic aerosol peak
- Peak is reached about 8 months after eruption



M. Osborn et al, Evolution of the Pinatubo Volcanic Cloud Over Hampton, VA, OSA Topical Conference on Remote Sensing of the Atmosphere, March, 1993.

NASA LIDAR Backscatter Results

- 1/e recovery time of about 7.3 months after volcanic aerosol peak
- Peak is reached about 8 months after eruption



Atmospheric Effects on ABL Performance

AGENDA

Introduction to the ABL

ABL Atmospheric Issues

LIDAR data

→ SAGE Satellite Data

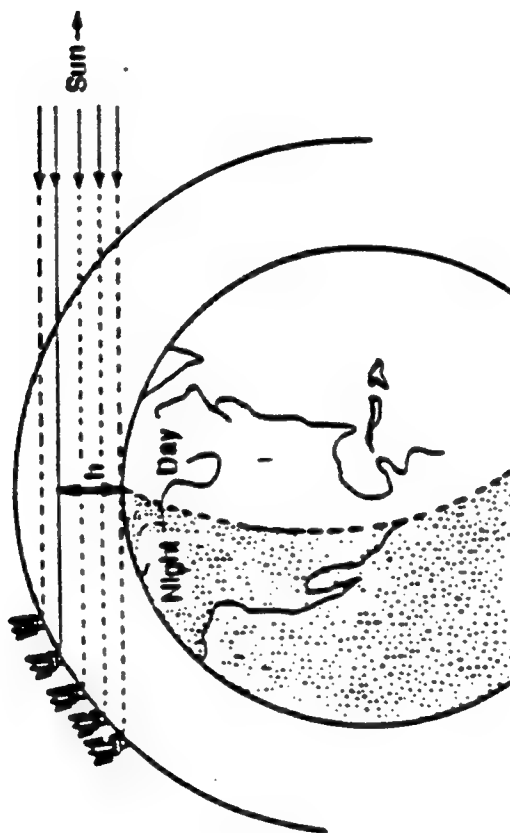
Impact of Volcanic Aerosols on
ABL Performance

Future work

SAGE SOLAR OCCULTATION MEASUREMENT GEOMETRY

Orbital Altitude = 600km

Angle of Inclination = 56°



Lattitudinal coverage from 79°S to 79°N . Provides 15 sunrise and 15 sunset measurements each day whose latitudes varied daily providing near global coverage in 3 - 4 weeks.

SAGE (STRATOSPHERIC AEROSOL AND GAS EXPERIMENT)

**SAGE I (February 1979 to November 1981)
SAGE II (October 1984 to present)**

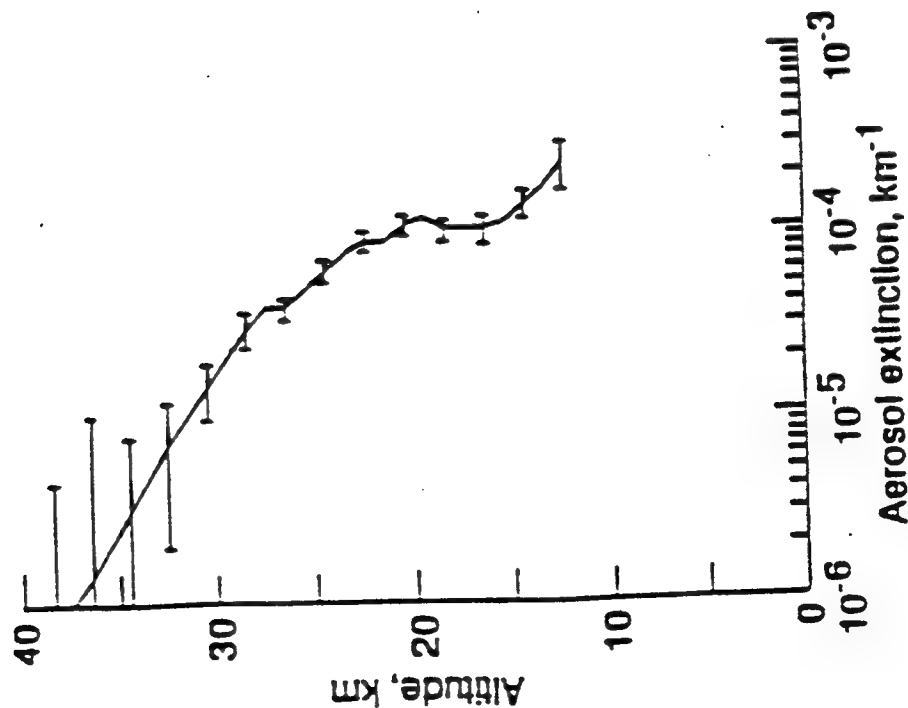
Objective: Develop a global stratospheric aerosol, ozone, and nitrogen dioxide data base that could be used for the investigation of the spatial and temporal variations of these species caused by seasonal and short-term meteorological variations, atmospheric chemistry and microphysics, and transient phenomena such as volcanic eruptions.

Measures: Aerosol extinction at 1,000nm and 450nm can be used to generate high altitude cloud climatology

Validated: Compared with correlative lidar and dustsonde measurements

Orbit: Tailored to maximize geographic coverage of solar occultation measurements.

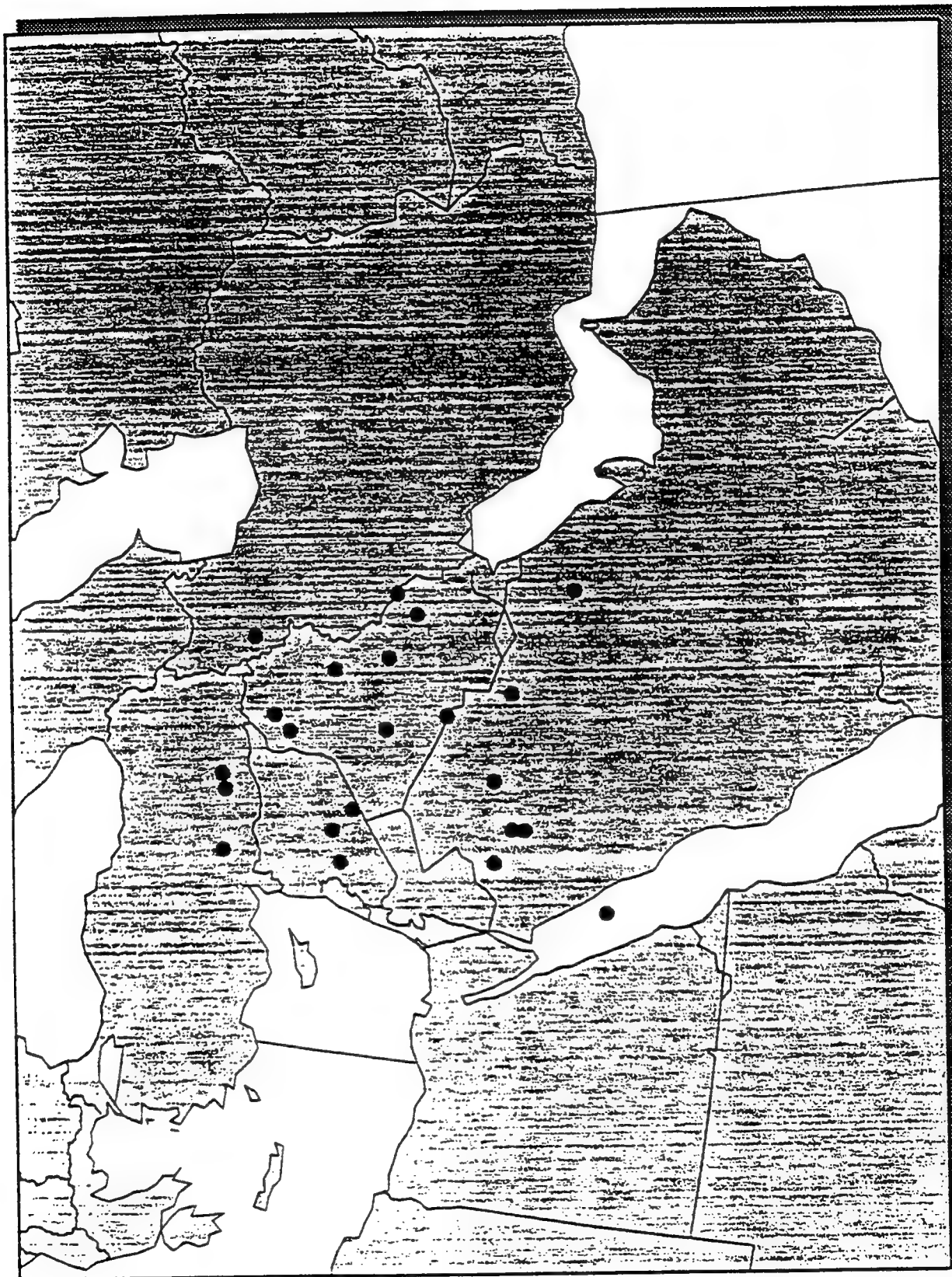
SAGE AEROSOL EXTINCTION SAMPLE

 $\lambda = 1000 \text{ nm}$ 

Background conditions. 0722
LCT; long 85.4° W, lat 19.8° N
Horizontal bars indicate 10
error. Below 25km aerosol
extinction exceeds molecular
extinction by 50%, yielding
errors typically less than 10%.

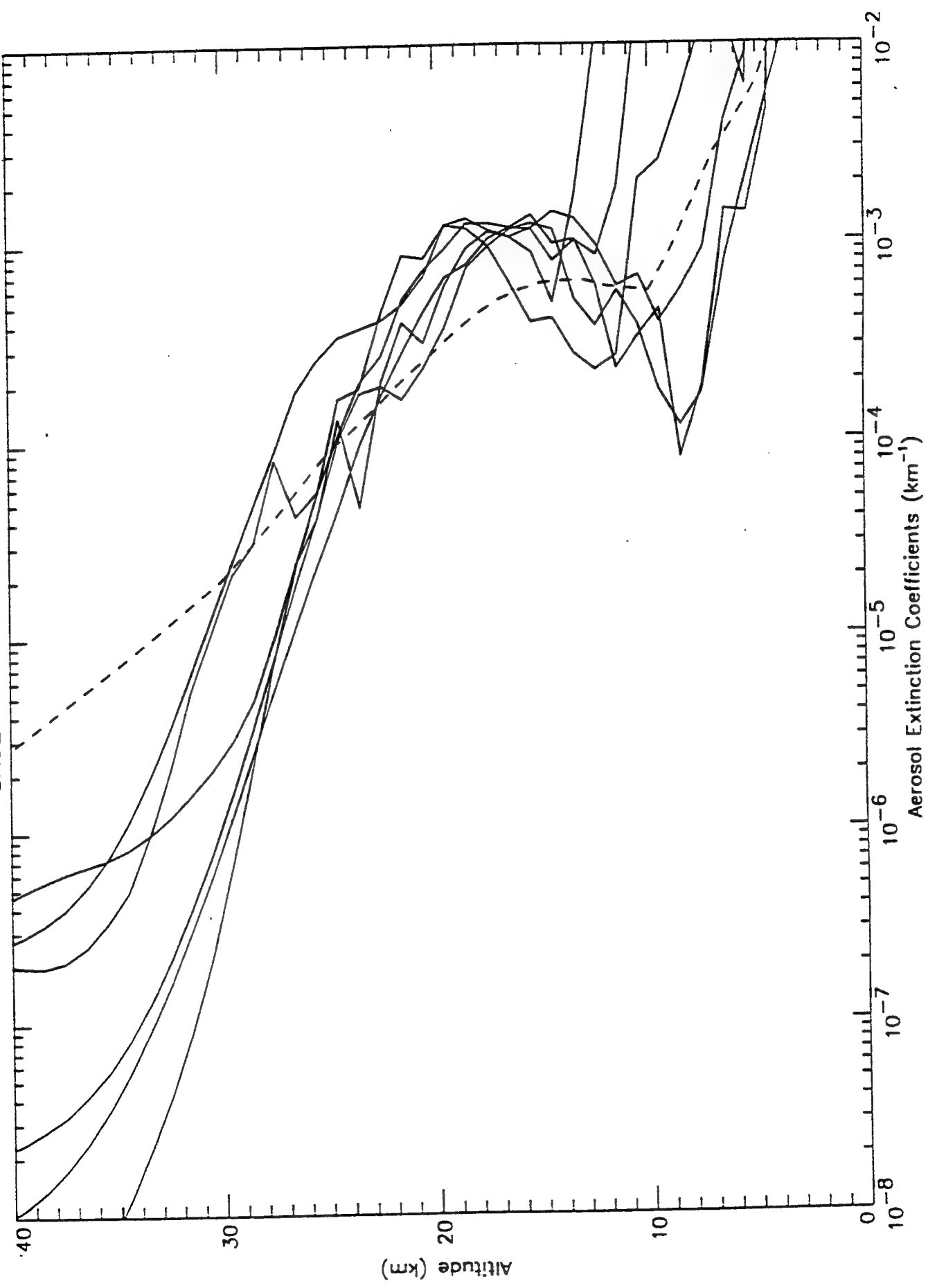
SAGE-Derived ABL Transmission Color Plots of Global Data

SAGE 1990 - 91 Middle East

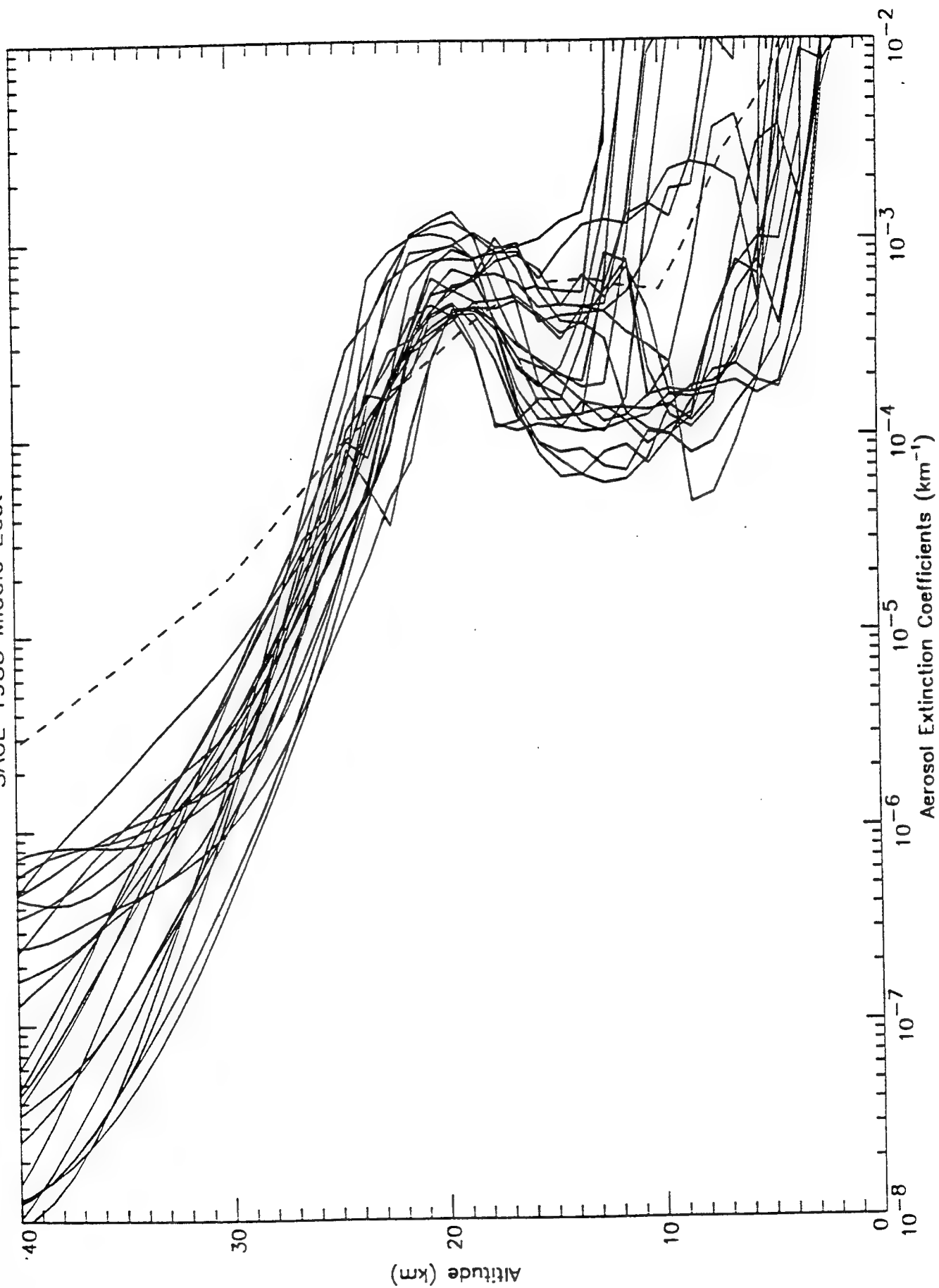


WJSA

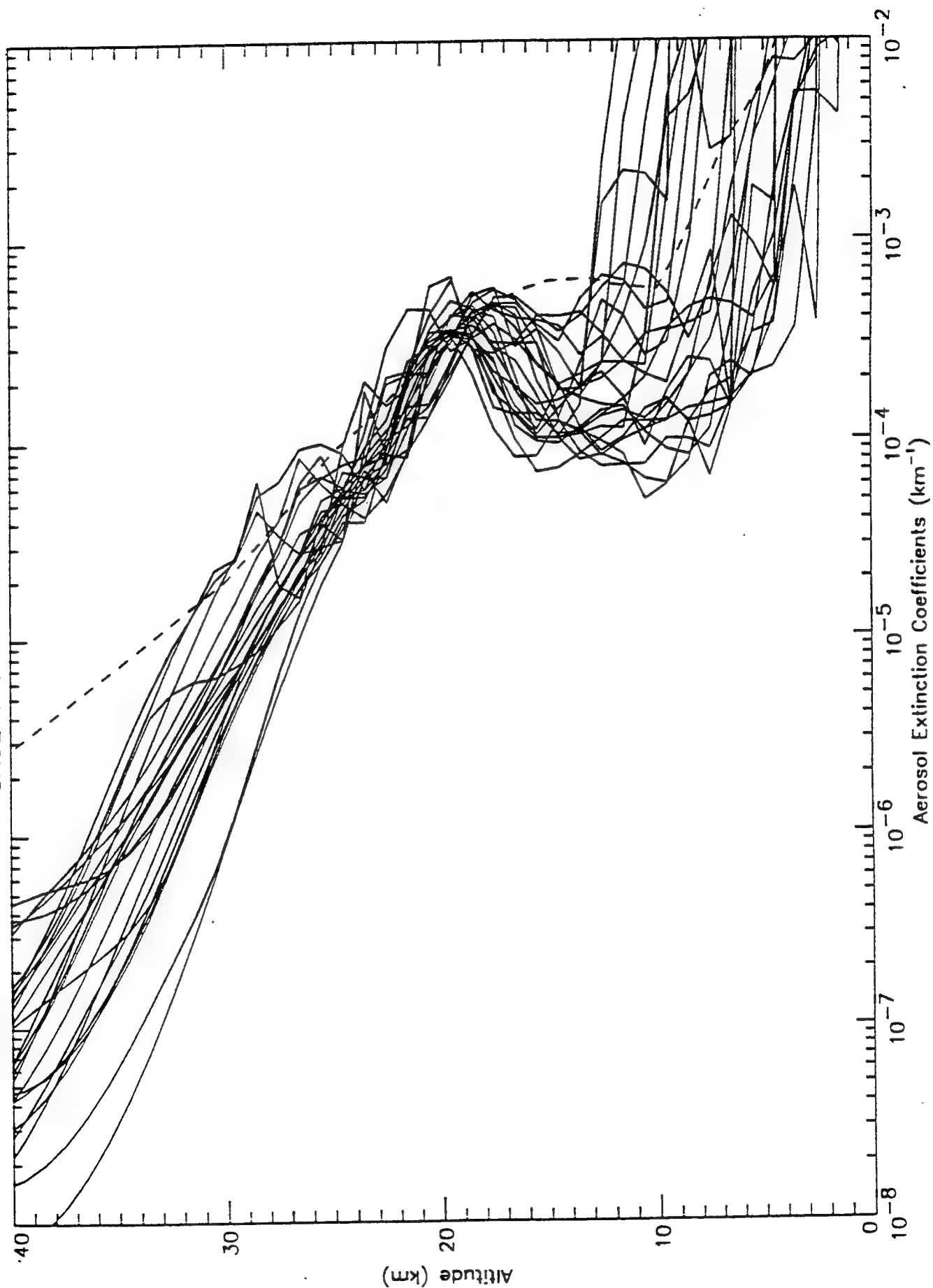
SAGE 1984 Middle East



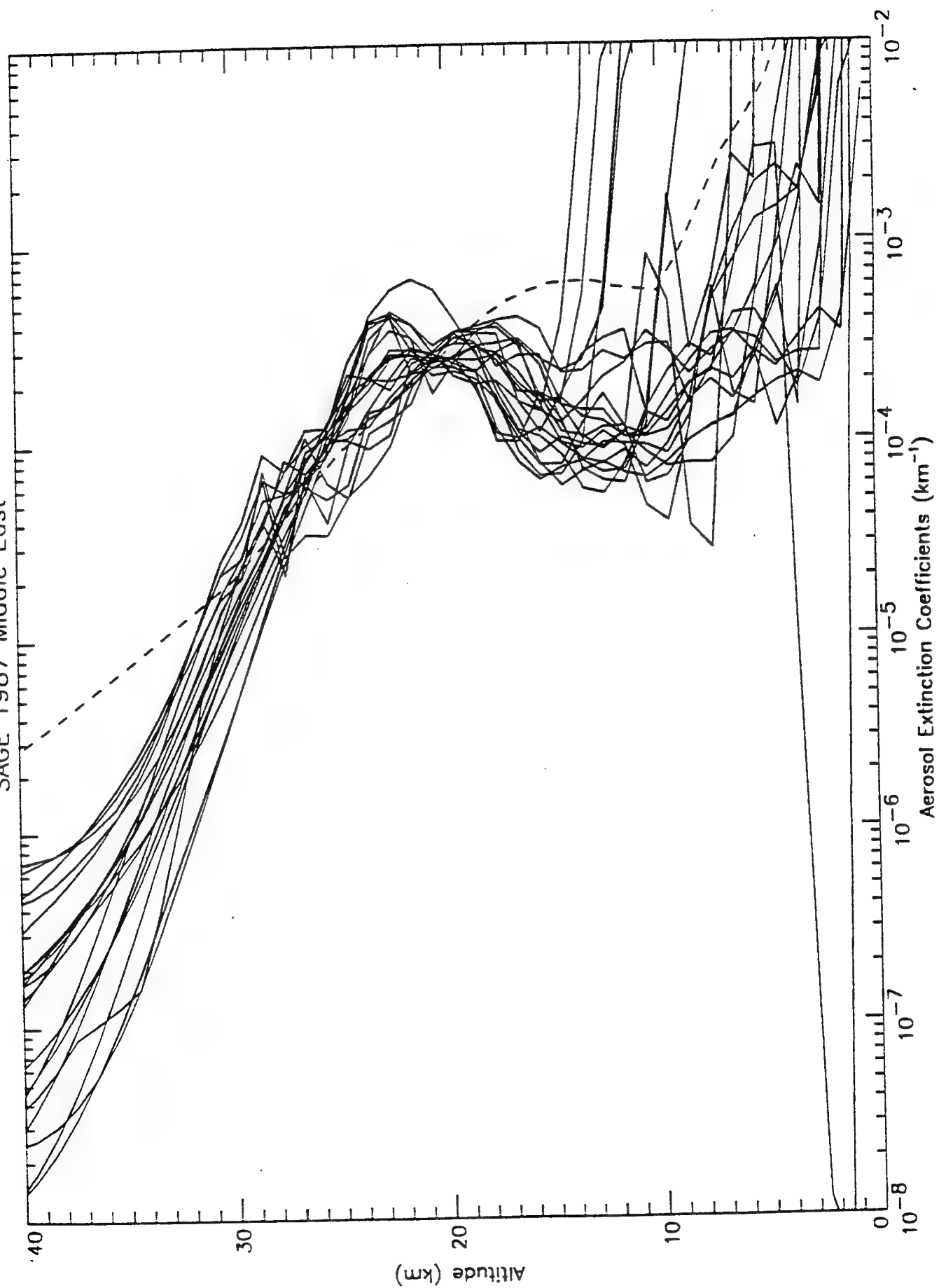
SAGE 1985 Middle East



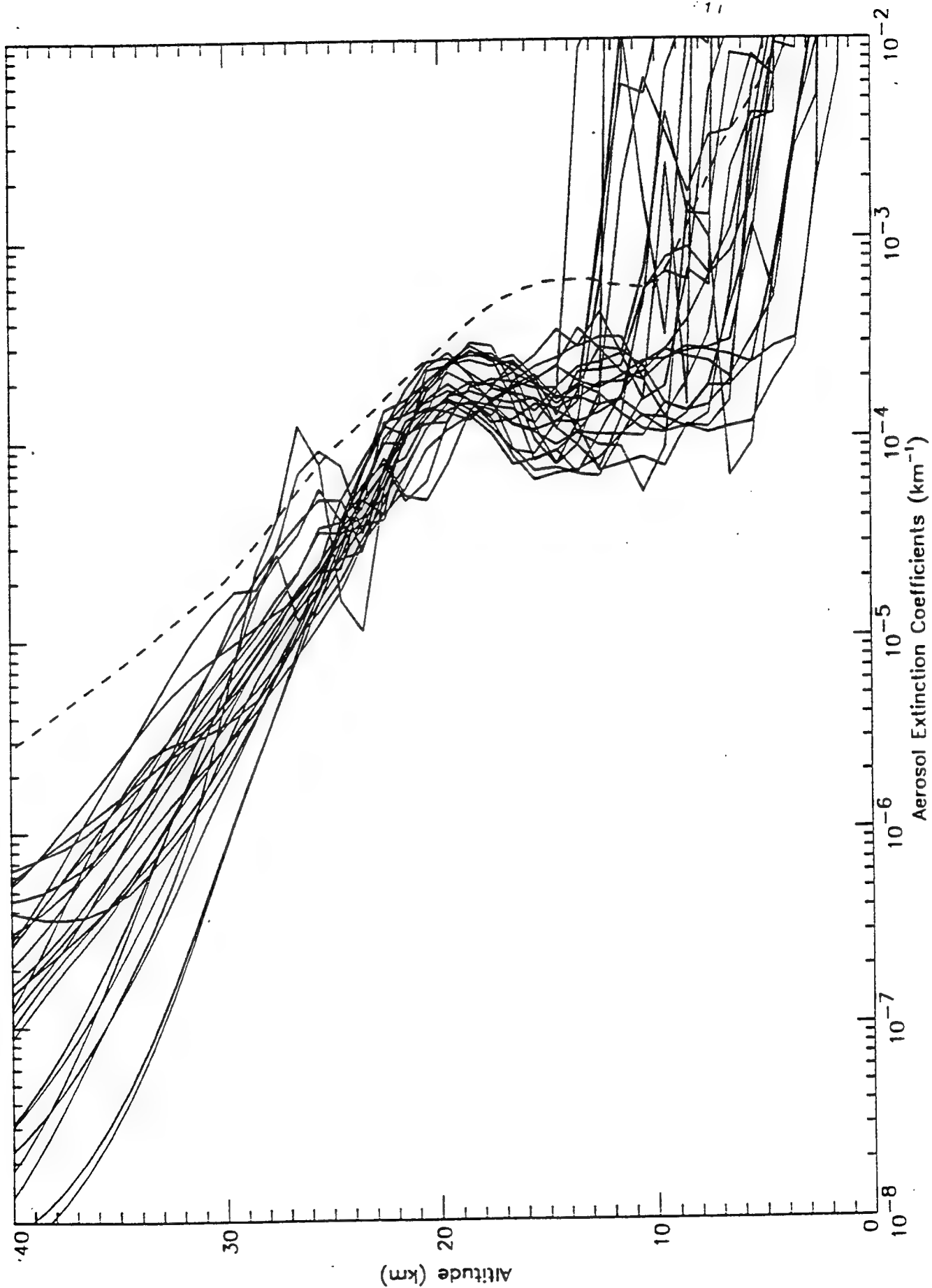
SAGE 1986 Middle East



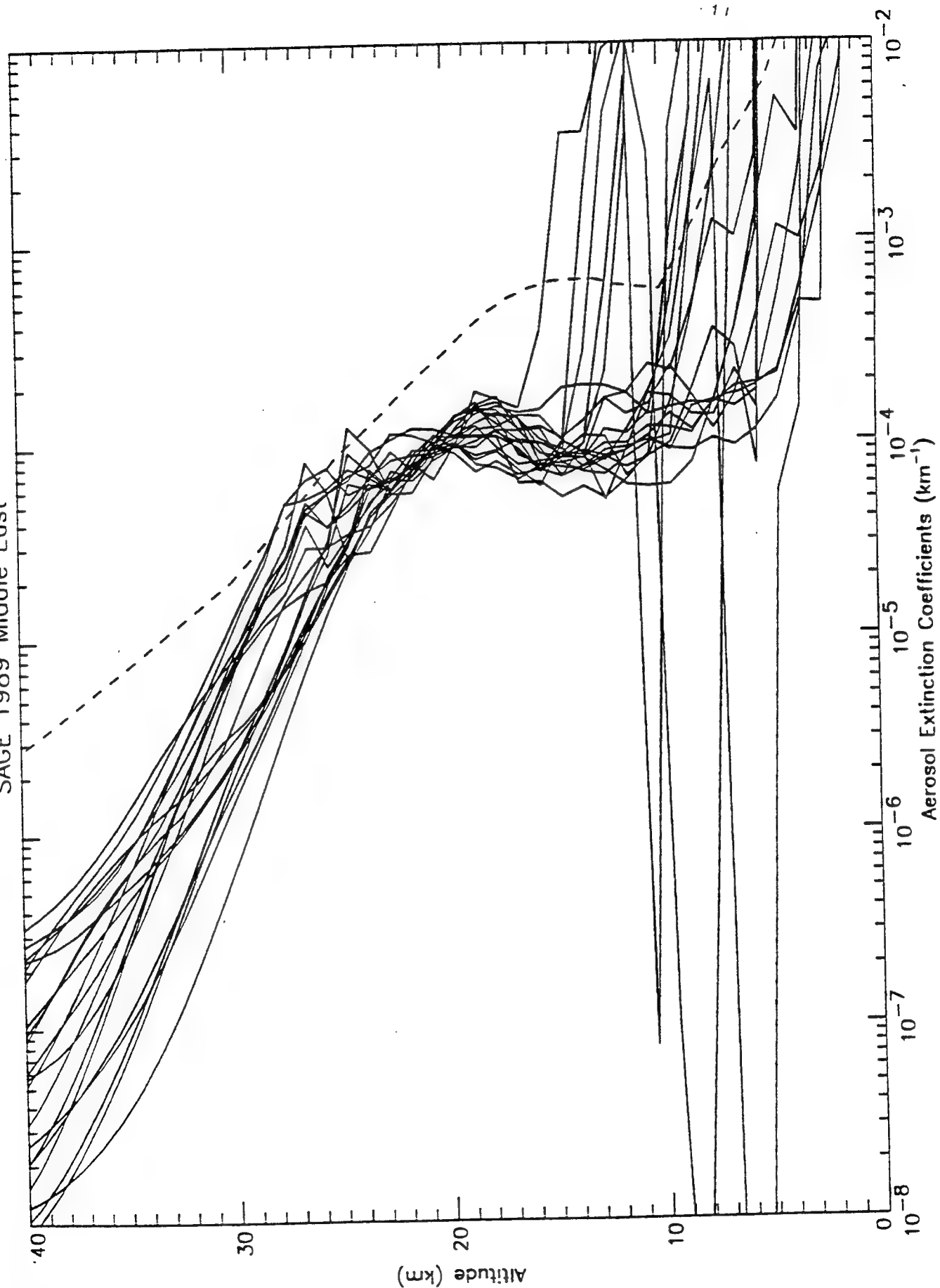
SAGE 1987 Middle East



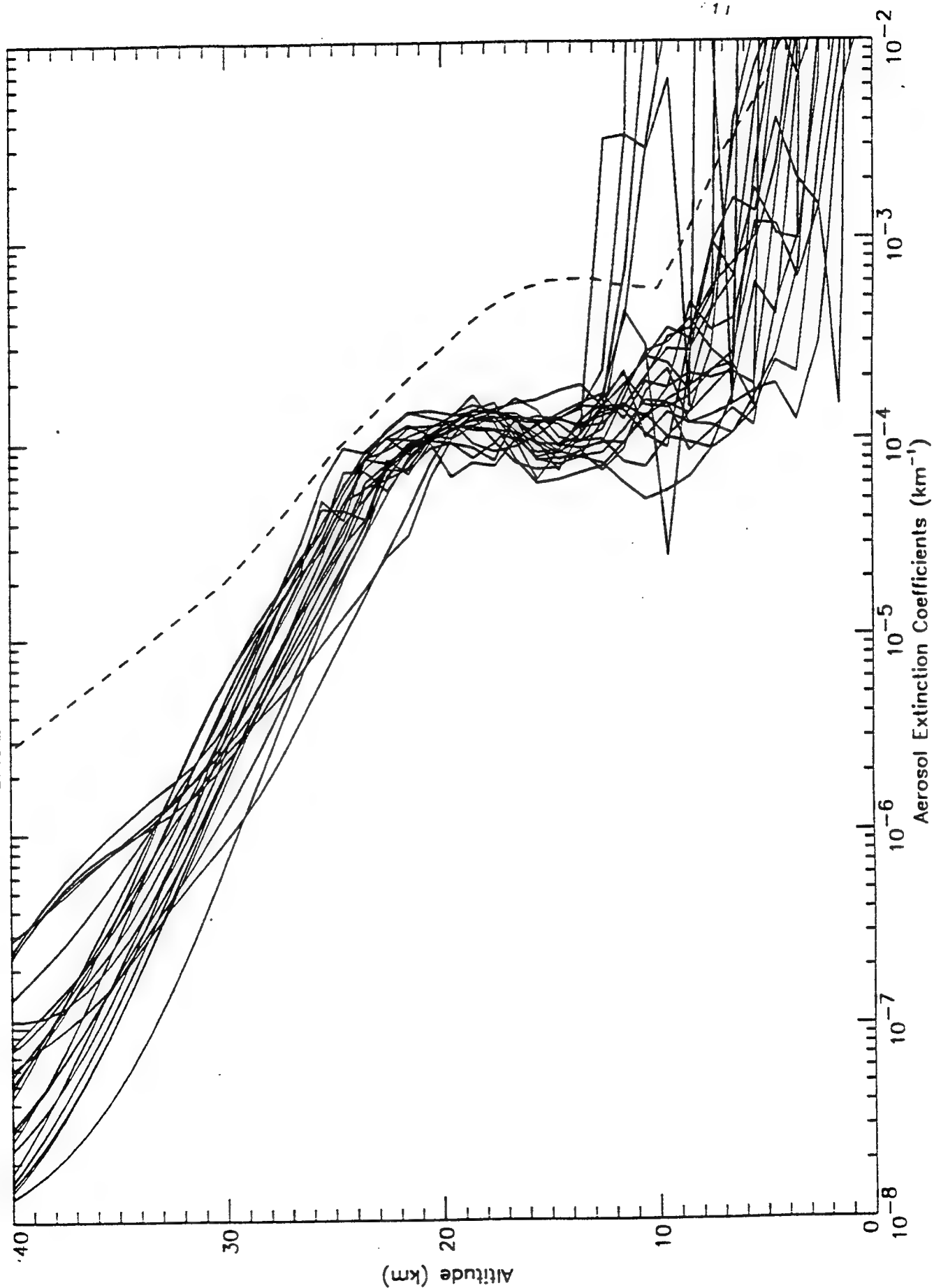
SAGE 1988 Middle East



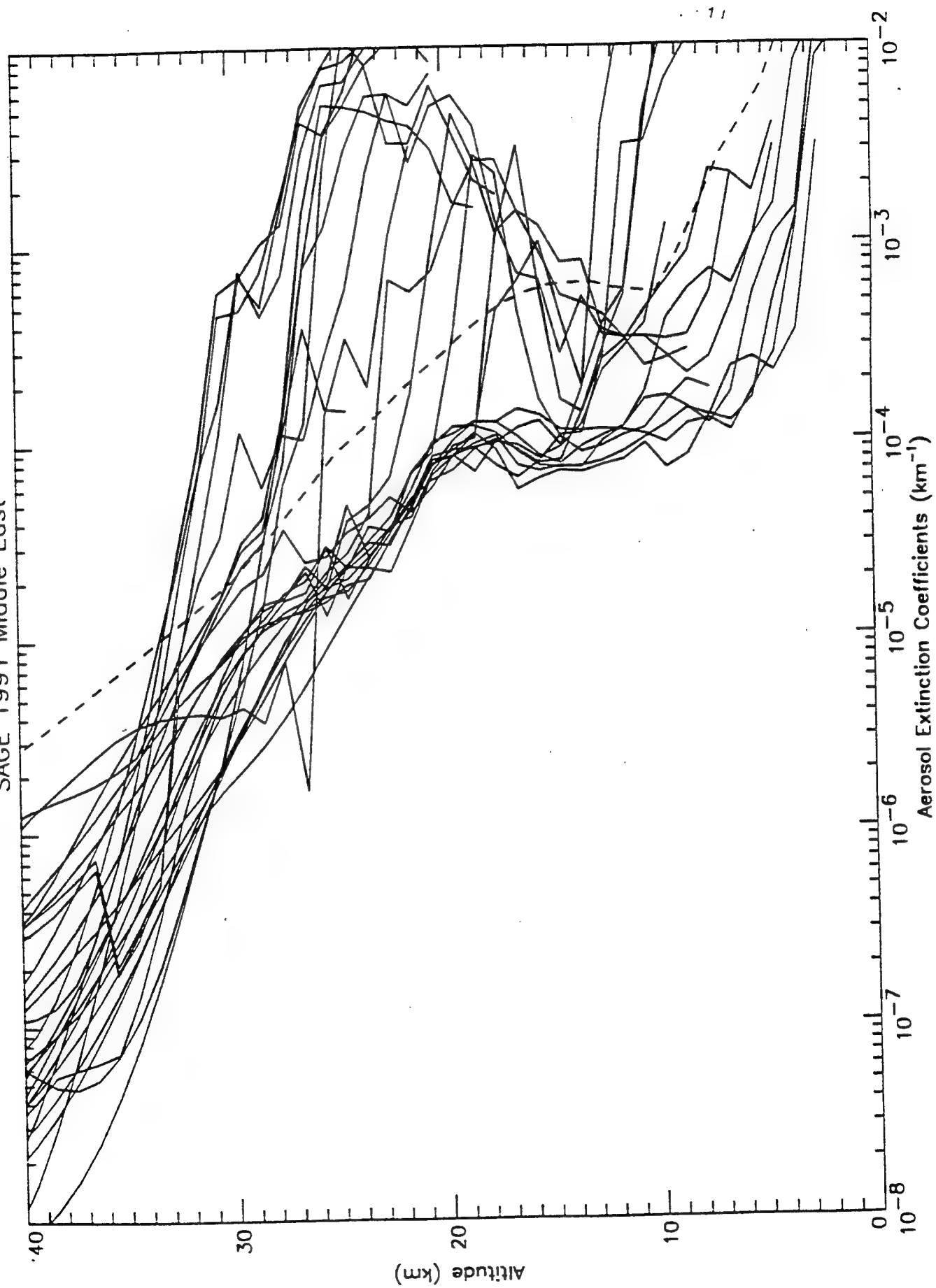
SAGE 1989 Middle East



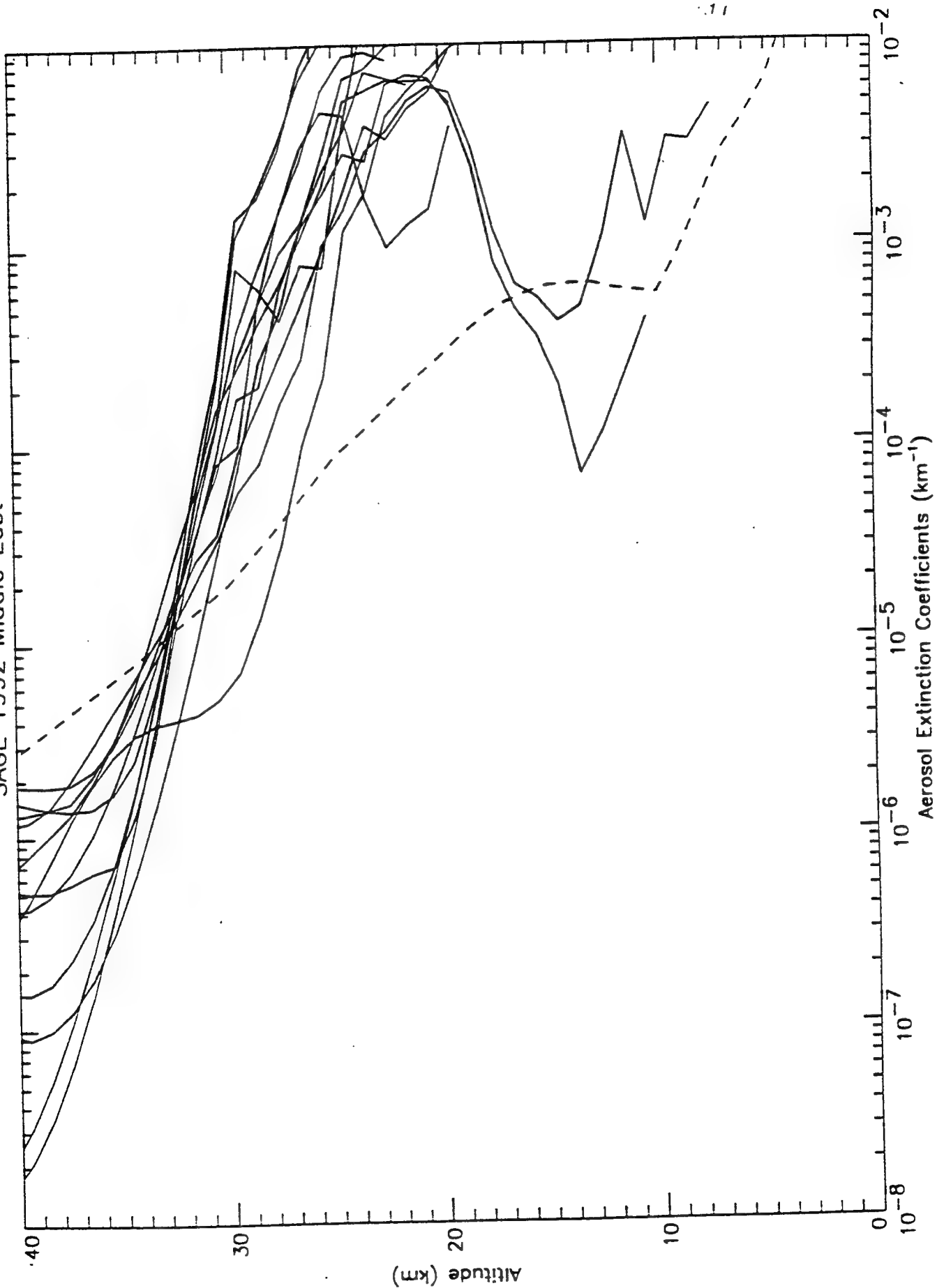
SAGE 1990 Middle East



SAGE 1991 Middle East



SAGE 1992 Middle East



Atmospheric Effects on ABL Performance

AGENDA

Introduction to the ABL

ABL Atmospheric Issues

LIDAR data

SAGE Satellite Data

→ Impact of Volcanic Aerosols on
ABL Performance

Future work

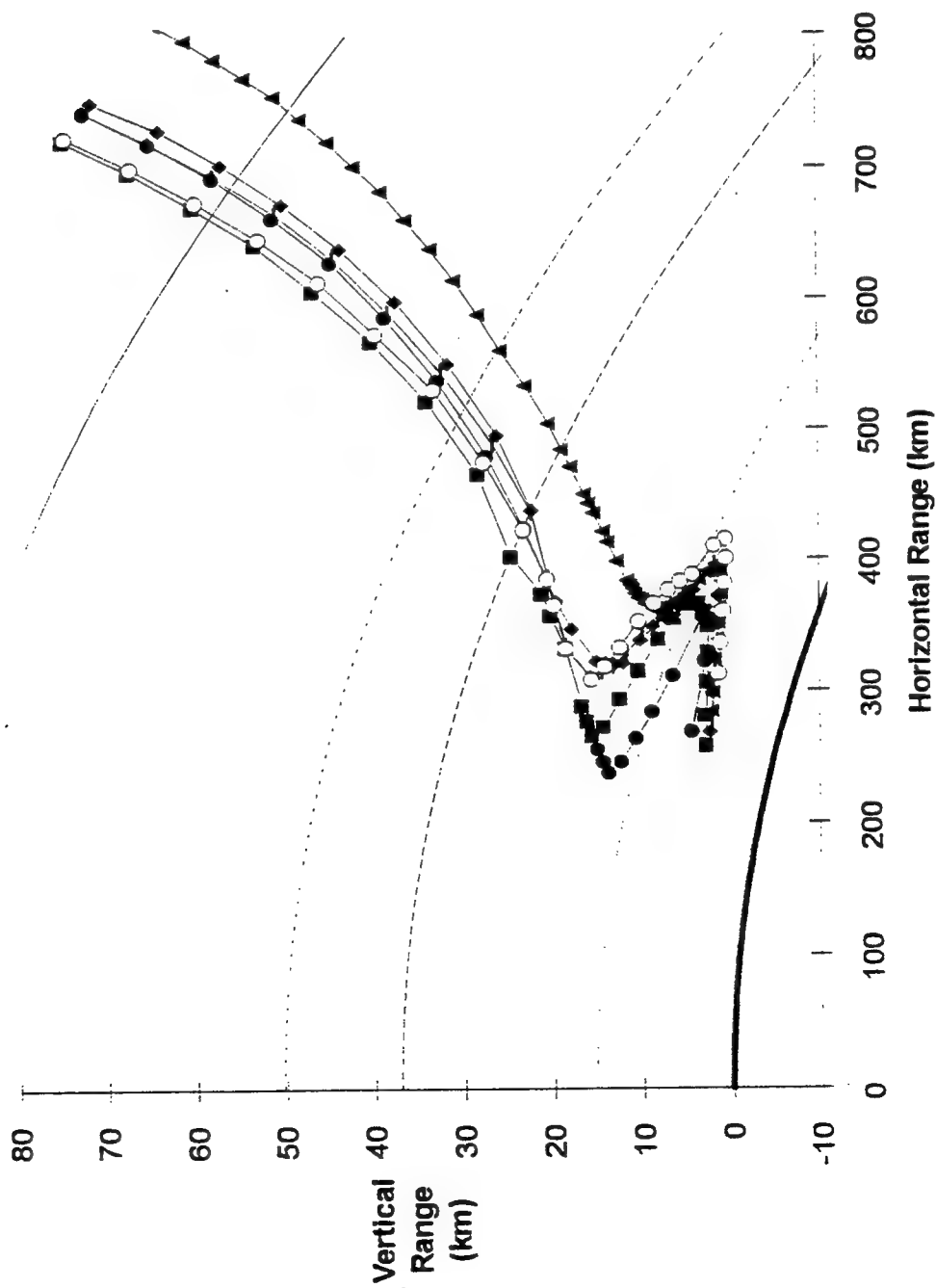
Volcanic Aerosol Analysis

Methodology

- Global SAGE database is scanned for all sunrise/sunset observations in the geographic region of interest.
- Measured extinction profiles in channel-7 ($1.02 \pm .02 \mu$) are converted to 1.32μ using LOWTRAN aerosol scaling factor.
- Unless we are examining cloud statistics, profiles with interfering clouds are thrown out.
- Individual extinction profiles (106 for mid-east, 11/84 - 6/92) are used in WJSA -ABLE code (AirBorne Laser Engagement) to calculate range performance for a fixed power, or power required for fixed geometry, using default values for dwell, turbulence model, etc.
- Also, we have two vertical extinction LIDAR profiles taken during maximum extinction in Japan and at JPL. The LIDAR-derived profiles are weaker than the SAGE data, leading to greater predicted range performance.

WJSA

ABL Performance Envelope Using LIDAR & Satellite Measured Aerosol Extinction Profiles

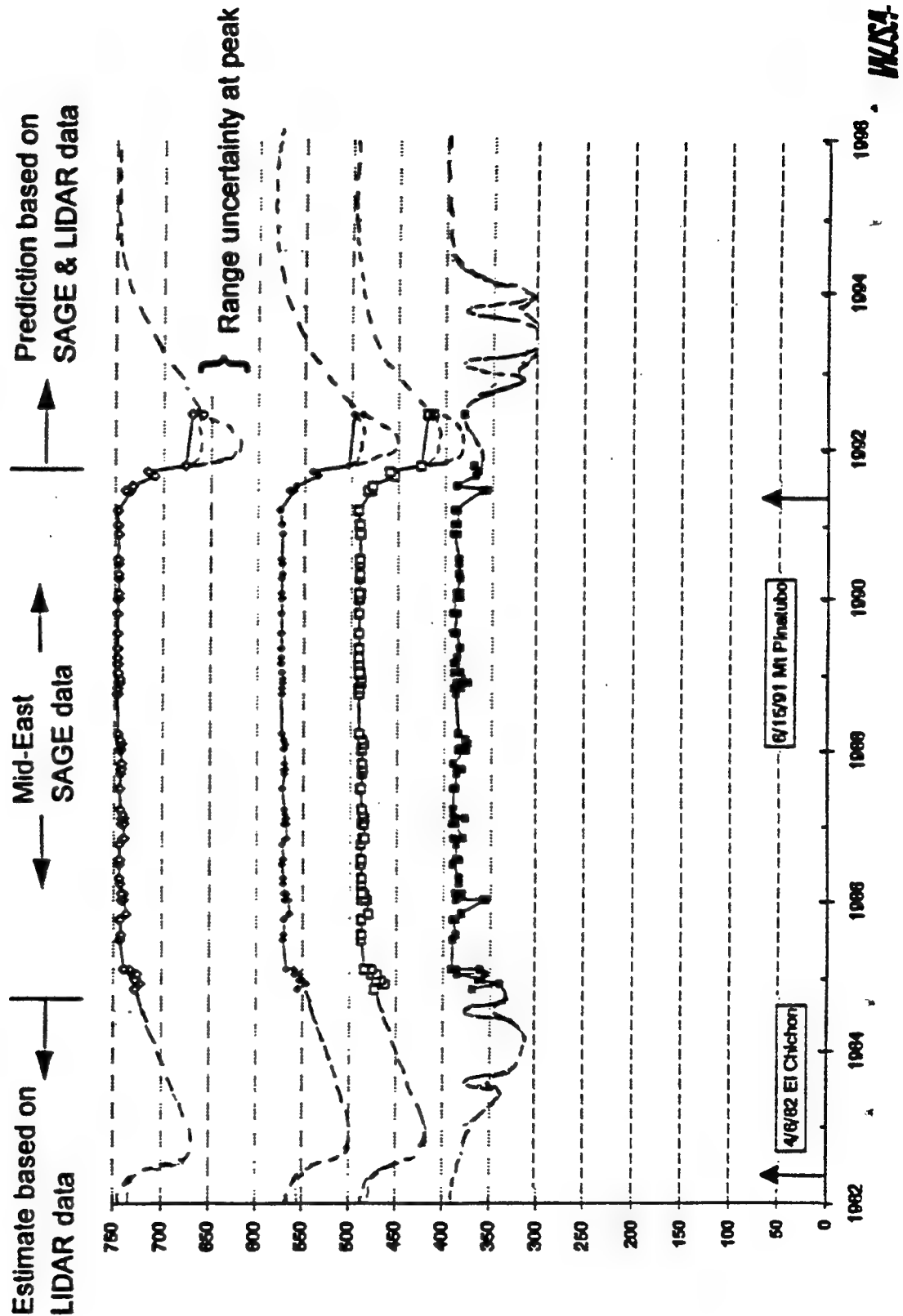


WJSA

ABL Range Performance (km) vs Time

Estimated Sensitivity to Volcanic Aerosols

- Case-A differences due to interaction of sinking aerosols with variable tropopause height
- Next satellite data release from NASA will add ~ 9 months data on recovery from Mt Pinatubo



Impact of Pinatubo Aerosols: BI Scenario

1 Baseline ABL in Loiter Orbit - 132 targets

<u>Aerosol Model</u>	<u>% Targets Negated</u>	<u>Mean Dwell Time (sec)</u>
Bkg Strat/Mod	85	3.4
ME-SAGE 10/29/91	84	3.7

Atmospheric Effects on ABL Performance

AGENDA

Introduction to the ABL

ABL Atmospheric Issues

LIDAR data

SAGE Satellite Data

Impact of Volcanic Aerosols on
ABL Performance

→ Future work

Volcanic Aerosols - Issues

- Clouds - need to account for high cirrus in SAGE data reduction
 - horizontal scale
 - opacity in ABL geometries
 - detailed regional statistics
- Horizontal variability of aerosols - SAGE resolution is 1 km in altitude, but > 100 km in range and cross-range. Ground-based LIDAR data could provide necessary resolution.
- Over time, case-A transmission becomes worse, and occurs later, as aerosols sink - How bad is this before recovery?
- 1992-1993 SAGE data (to be released by NASA this summer) will show more detail on recovery rates.
- Impact of backscatter on laser tracker and A/O beacon needs to be assessed.

WJSA

Wednesday 9 June 1993 a.m.

SESSION D: Non-LTE SPECTROSCOPY APPLICATIONS

Chair: Richard H. Picard, PL/GPOS

SHARC
A MODEL FOR CALCULATING ATMOSPHERIC RADIATION UNDER
NON-EQUILIBRIUM CONDITIONS

David Robertson,¹ Robert Sundberg,¹ James Duff,¹
John Gruninger,¹ Steve Adler-Golden,¹ Ramesh Sharma,²
and Rebecca Healey³

¹Spectral Sciences, Inc.
99 South Bedford Street, #7
Burlington, MA 01803-5169

²Phillips Laboratory/GPOS
29 Randolph Road
Hanscom AFB, MA 01731-3010

³Yap Analytics
594 Merrett Road
Lexington, MA 02173

SHARC was developed by the Air Force to provide both research and systems-level predictions for atmospheric IR radiance for arbitrary paths within the 50 to 300 km altitude regime and in the 2-30 μm spectral region. The code calculates LTE and NLTE emissions from the significant atmospheric IR radiators, CO_2 , NO , O_3 , H_2O , CO , OH , and CH_4 . Molecular excited state populations are calculated with a Monte Carlo model for layer-layer radiative excitation and energy transfer with a flexible chemical kinetics module derived from the CHEMKIN Code developed by Sandia, Livermore. Radiation transport calculations are based on an equivalent-width line-by-line (LBL) approach with a spectral resolution of about 0.5 cm^{-1} . The LBL algorithm uses the Roger-Williams and Curtis-Godson approximations for the equivalent widths of combined Doppler-Lorentz (Voigt) lineshapes. Spectroscopic data are taken from the HITRAN line atlas which has been augmented with additional O_3 , NO and NO^+ lines. SHARC also has an auroral module that describes electron dosing and solves the time/energy dependent rate equations to calculate secondary electron distributions and the resulting IR emissions from CO_2 , NO and NO^+ . This module is fully embedded in the ambient part of the code so that radiance calculations for paths passing through a finite auroral region are possible.

SHARC
A MODEL FOR CALCULATING ATMOSPHERIC RADIATION
UNDER NON-EQUILIBRIUM CONDITIONS

by
DAVID ROBERTSON, ROBERT SUNDBERG, JAMES DUFF,
JOHN GRUNINGER, STEVE ADLER-GOLDEN,
SPECTRAL SCIENCES, INC.

RAMESH SHARMA, JIM BROWN,
PHILLIPS LABORATORY/GPOS

REBECCA HEALEY,
YAP ANALYTICS, INC.

Presented at
THE ANNUAL REVIEW CONFERENCE
ON ATMOSPHERIC TRANSMISSION MODELS

9 JUNE 1993



ACKNOWLEDGEMENTS

- FUNDING

THIS WORK WAS SPONSORED BY SDIO, PMA-1105,
THE STRATEGIC DEFENSE INITIATIVE OFFICE

NOW

THE BALLISTIC MISSILE DEFENSE ORGANIZATION (BMDO)

- PREDECESSOR MODELS

HAIRM - HIGH ALTITUDE INFRARED RADIANCE MODEL (Tom Deggs)

ARC - ATMOSPHERIC RADIANCE CODE (PL)

AARC - AURORAL ATMOSPHERIC RADIANCE CODE (PL)



OUTLINE

- OBJECTIVES
- SHARC OVERVIEW
- MAJOR MODULES
 - NLTE EXCITATION (CHEMKIN & NEMESIS)
 - AURORAL MODULE
 - RADIATION TRANSPORT
- VALIDATION EXAMPLES
- FUTURE PLANS
- CONCLUDING REMARKS



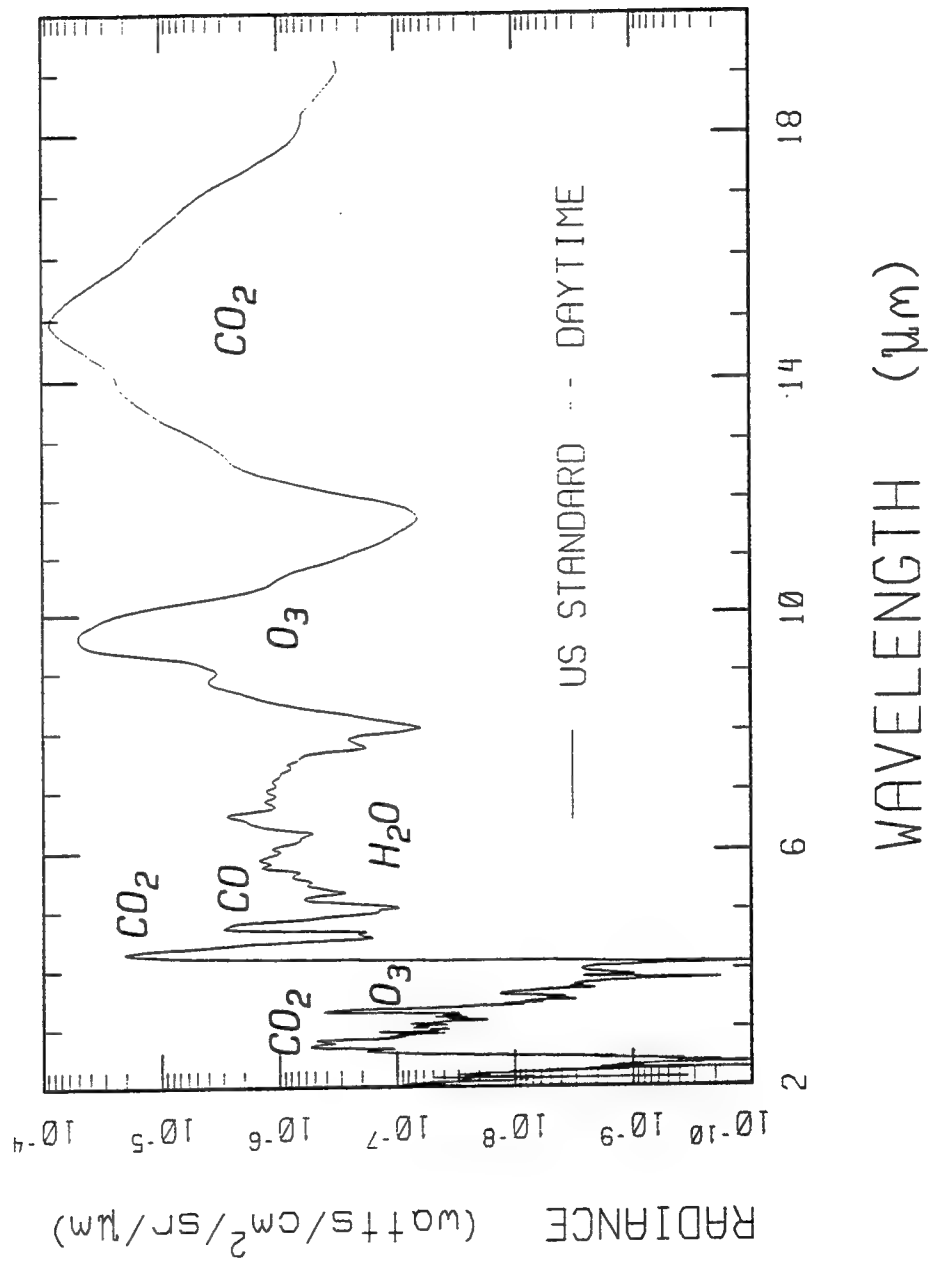
SHARC OBJECTIVES

- COMPUTER CODE TO CALCULATE HIGH-ALTITUDE BACKGROUNDS IN QUIESCENT AND AURORALLY DISTURBED ATMOSPHERES
 - SUITABLE FOR SYSTEMS STUDIES
- PROVIDE SPECTRAL PREDICTIONS FOR RADIANCE AND TRANSMITTANCE ALONG ARBITRARY PATHS THROUGH THE ATMOSPHERE
 - MODEL ATMOSPHERIC EMISSION PROCESSES
 - SUPPORT AF MEASUREMENTS PROGRAMS
CIRRIS 1A, SPIRIT II, MSX
 - VALIDATION WITH FIELD AND LAB DATA



ILLUSTRATIVE SHARC CALCULATION

- SPACE VIEWING THROUGH A 50km LIMB PATH



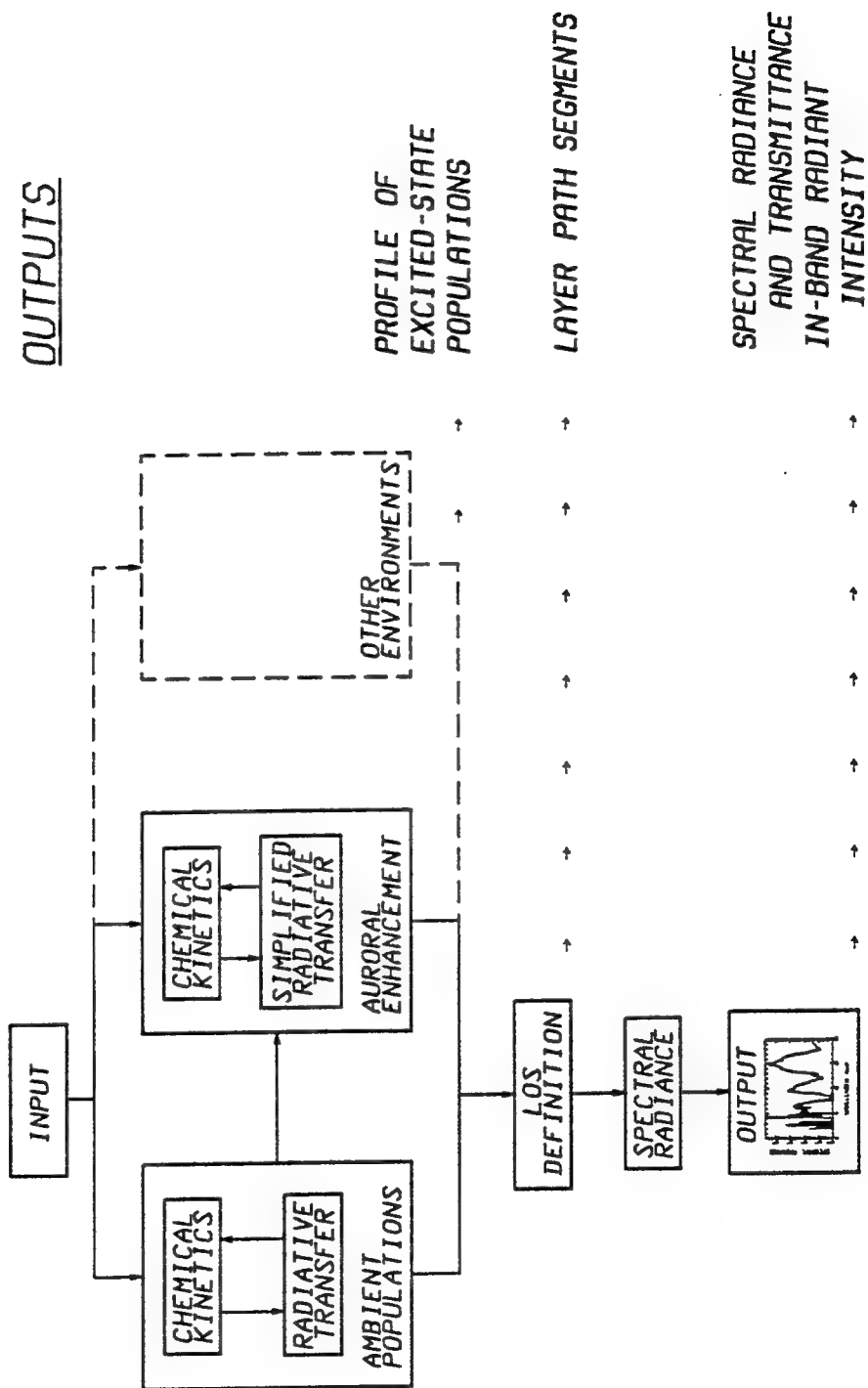


SHARC OVERVIEW

- SHARC CALCULATES NLTE RADIATION FROM AMBIENT AND AURORAL ATMOSPHERES
- SOME FEATURES:
 - 50-300 km ALTITUDE REGIME
 - 2-40 μm WITH A RESOLUTION OF 0.5 cm^{-1}
 - INTERACTIVE INPUT MODULE WITH ERROR CHECKING
 - ARBITRARY LOS PATHS
 - AUTOMATICALLY INCLUDES LTE & NLTE CONTRIBUTIONS
 - AMBIENT MOLECULES INCLUDE: H_2O , O_3 , CO , NO
 OH , CO_2 , CH_4 , and H_2O & CO_2 ISOTOPES
 - AURORAL MODULE WITH: NO^+ , NO , CO_2
 - EQUIVALENT-WIDTH LBL RADIANCE CALCULATIONS
 - MULTIPLE REGIONS (CHANGING ATMOSPHERIC CONDITIONS)
 - SOLAR TERMINATOR
 - AVAILABLE FOR WORKSTATION, MAIN FRAME AND PC



SHARC CALCULATIONAL FLOW





AMBIENT POPULATIONS MODULE

- SYMBOLIC DESCRIPTION OF CHEMICAL KINETICS MECHANISM
 - BASED ON WIDELY USED SANDIA CHEMKIN CODE
 - EXAMPLE: $M + O + O_2 \rightarrow M + O_3(000)$
 $M + O_3(001) \rightarrow M + O_3(000)$
 $O_3(001) \rightarrow O_3(000) + h\nu$
- RATE EQUATIONS SOLVED IN STEADY STATE
 - ASSUMES RATE EQUATIONS DEPEND LINEARLY ON VIBRATIONAL POPULATION
- MONTE CARLO CALCULATION FOR FIRST-ORDER RADIATIVE ENHANCEMENT
 - MULTIPLE APPLICATION YIELDS HIGHER ORDER ENHANCEMENTS



RADIATIVE EXCITATION MODULE (NEMESIS)

- RADIATIVE EXCITATION SIGNIFICANTLY ENHANCES THE EXCITED-STATE POPULATIONS OF STRONG BANDS AND HENCE THE STRENGTH OF THEIR EMISSIONS
- BASIC MODEL ASSUMPTIONS
 - SEMI-INFINITE PLANE-PARALLEL HOMOGENEOUS LAYERS
 - VOIGT LINESHAPE
 - TRANSLATIONAL-ROTATIONAL EQUILIBRIUM
 - COMPLETE LINE FREQUENCY REDISTRIBUTION
 - COMPLETE ROTATIONAL LEVEL REDISTRIBUTION
 - NO LINE OVERLAP



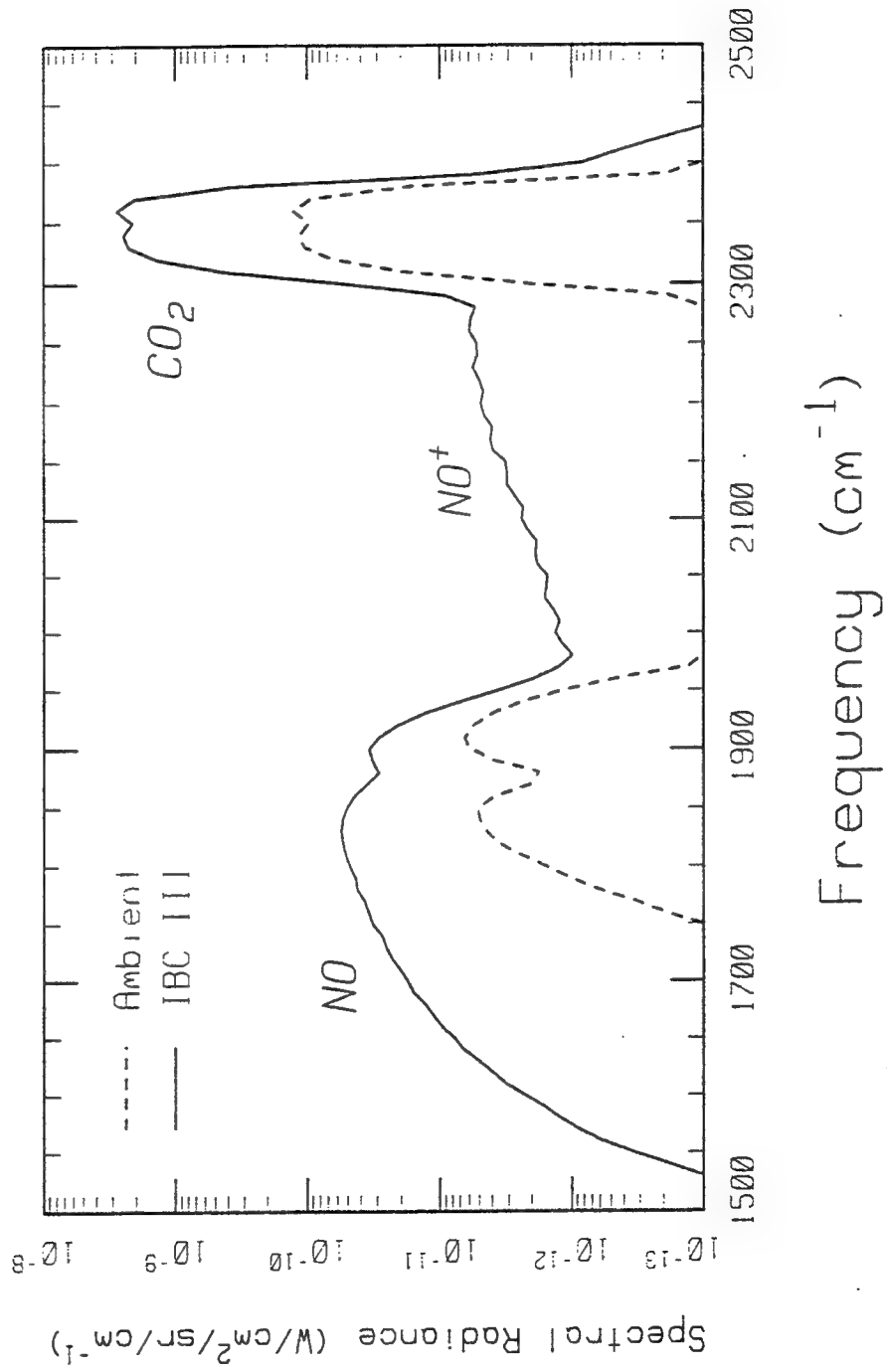
SHARC AURORAL MODULE

- AURORAL PHENOMENOLOGY
 - STARTING POINT IS PL AARC CODE
 - ELECTRON DEPOSITION MODELS FOR DIFFERENT STRENGTH AURORAS: CLASS II, III, III+
 - SOLVES TIME/ENERGY DEPENDENT RATE EQUATIONS TO CALCULATE BOTH SECONDARY ELECTRON DISTRIBUTIONS AND THE KINETICS FOR IR RADIATORS
 - PRESENT IR MOLECULES ARE: NO, NO⁺, CO₂
- SHARC AURORAL UPGRADE
 - GEAR'S STIFF ODE ALGORITHM USED AS REQUIRED
 - CAN ADD NEW RADIATORS VIA USER-DEFINED INPUT FILES
 - LOS CALCULATION FULLY COUPLES LOCALIZED AURORAL REGION EMBEDDED IN AN AMBIENT ATMOSPHERE
- GEOMETRY MODEL INSURES THAT LOS TRAJECTORIES INTERSECT AURORA AS DESIRED



ILLUSTRATIVE AURORAL ENHANCEMENT

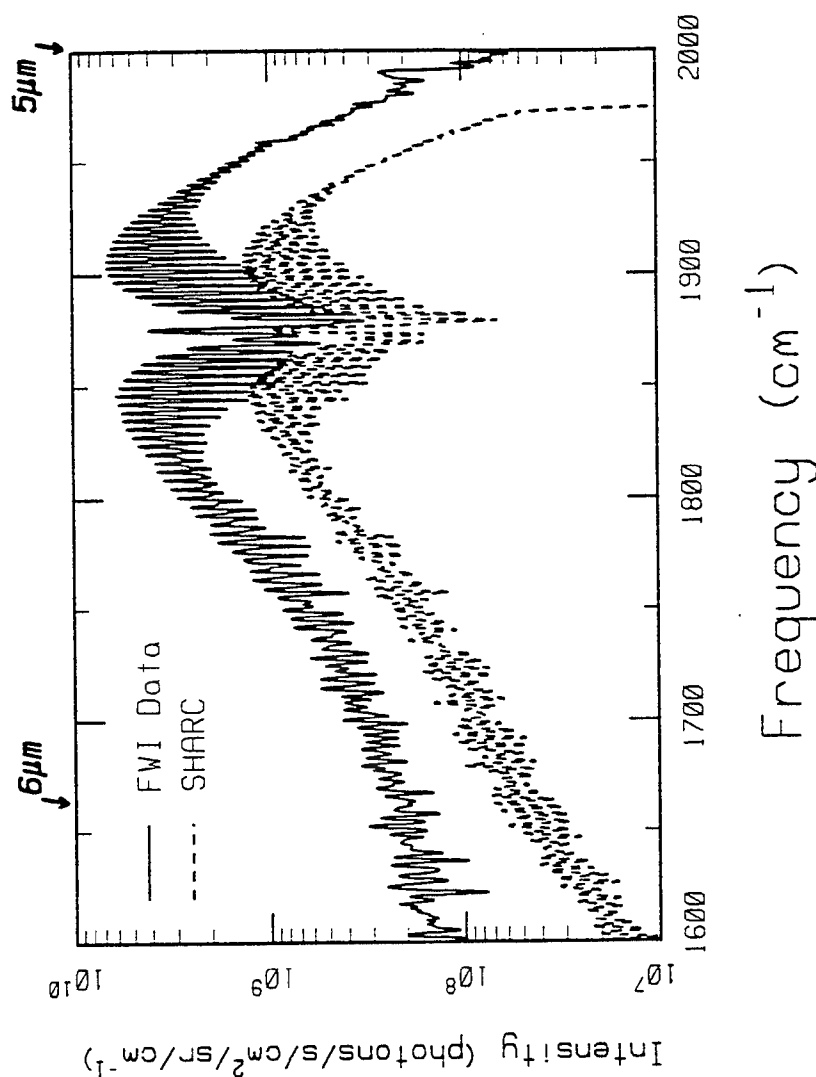
- RELATIVE STRENGTHS FOR PATH 90 km - SPACE





COMPARISON TO AURORAL FIELD DATA

- FWI DATA (FIELD WIDENED INTERFEROMETER)
- VERTICAL PATH TO SPACE FROM 90 KM
- CLASS II AURORA (~12 K RAYLEIGHS)
- SHARC CALCULATION FOR CLASS II (10 KR)
- MODEL CALCULATION USES A CONSTANT ELECTRON DOSE RATE
- BUT
- AURORA IS LIKELY STRONGLY PREDOSED





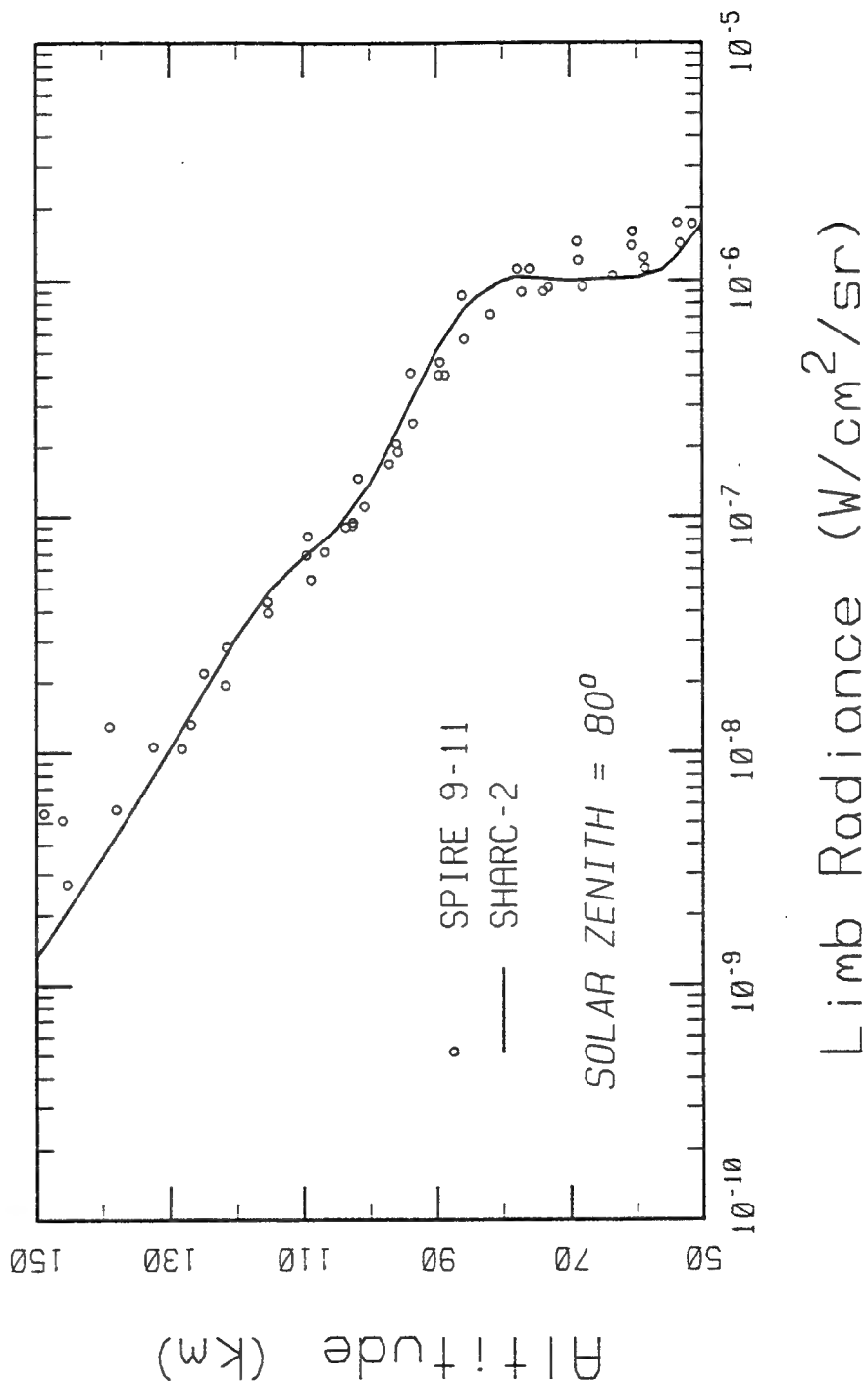
SPECTRAL RADIANCE MODULE

- RADIATION TRANSPORT CALCULATION PERFORMED FOR EACH MOLECULAR LINE
 - USES GL ATMOSPHERIC ABSORPTION LINE DATABASE (HITRAN)
- RODGERS-WILLIAMS APPROXIMATION FOR THE EQUIVALENT WIDTH (W) OF A SINGLE LINE WITH A VOIGT LINESHAPE
 - NASA HANDBOOK APPROXIMATION FOR W_D AND W_L
- LAYER-DEPENDENT LINE STRENGTHS
 - VIBRATIONAL AND ROTATIONAL TEMPERATURES
- CURTIS-GODSON APPROXIMATION
 - AVERAGING PROCEDURE FOR INHOMOGENEOUS PATHS
- LINE OVERLAP CORRECTION FOR DENSE REGIONS
- 50-70 TIMES FASTER THAN TRADITIONAL LBL APPROACH



SPIRE: DAYTIME CO₂ (4.3 μm)

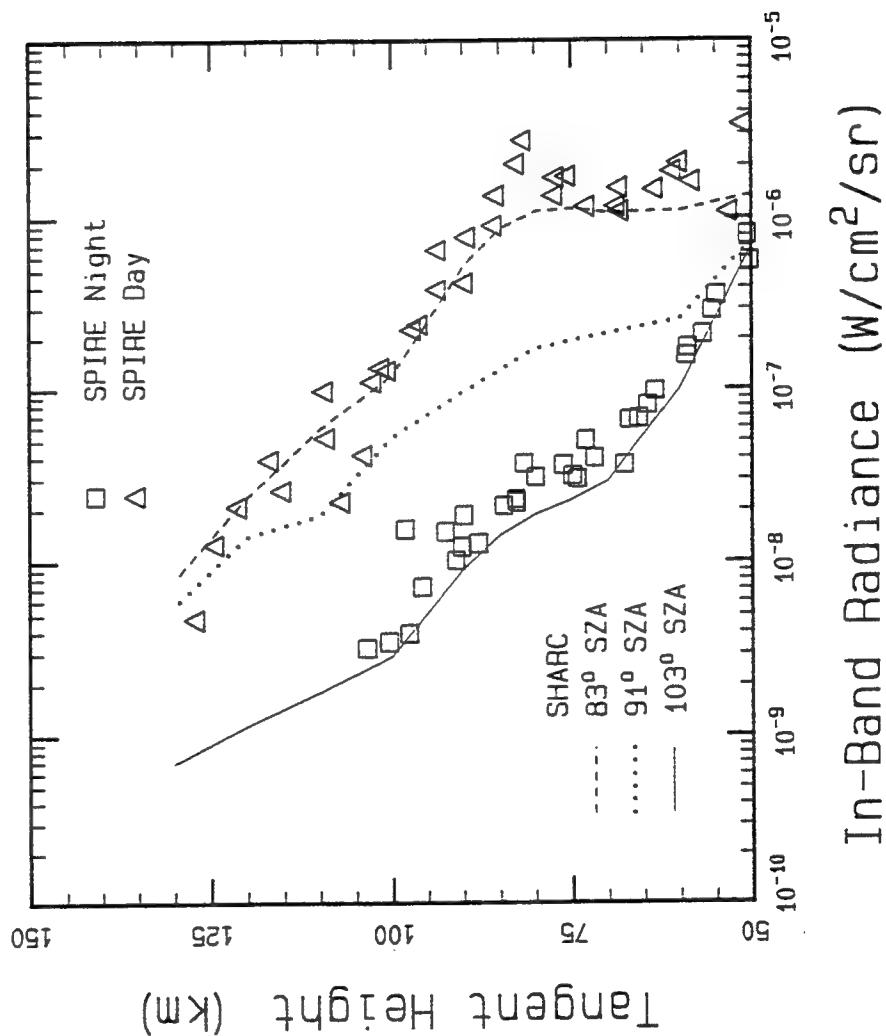
- SOLAR PUMPED VIA EXCITATION OF SHORT WAVE IR BANDS





SHARC-3 TERMINATOR

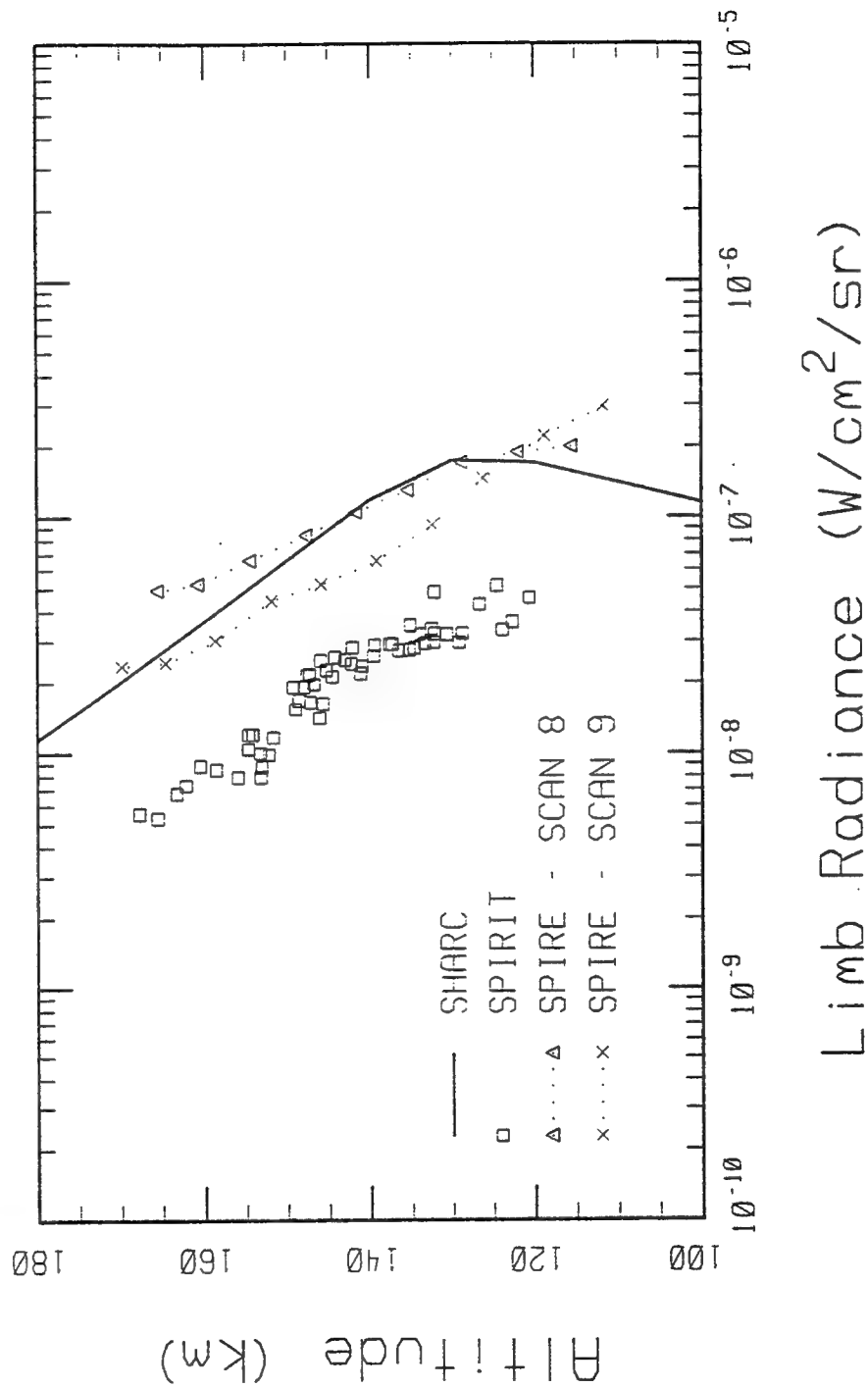
SPIRE SIMULATIONS 4.2-4.5 μM BANDPASS





COMPARISON TO NO (5.3 μm) DATA

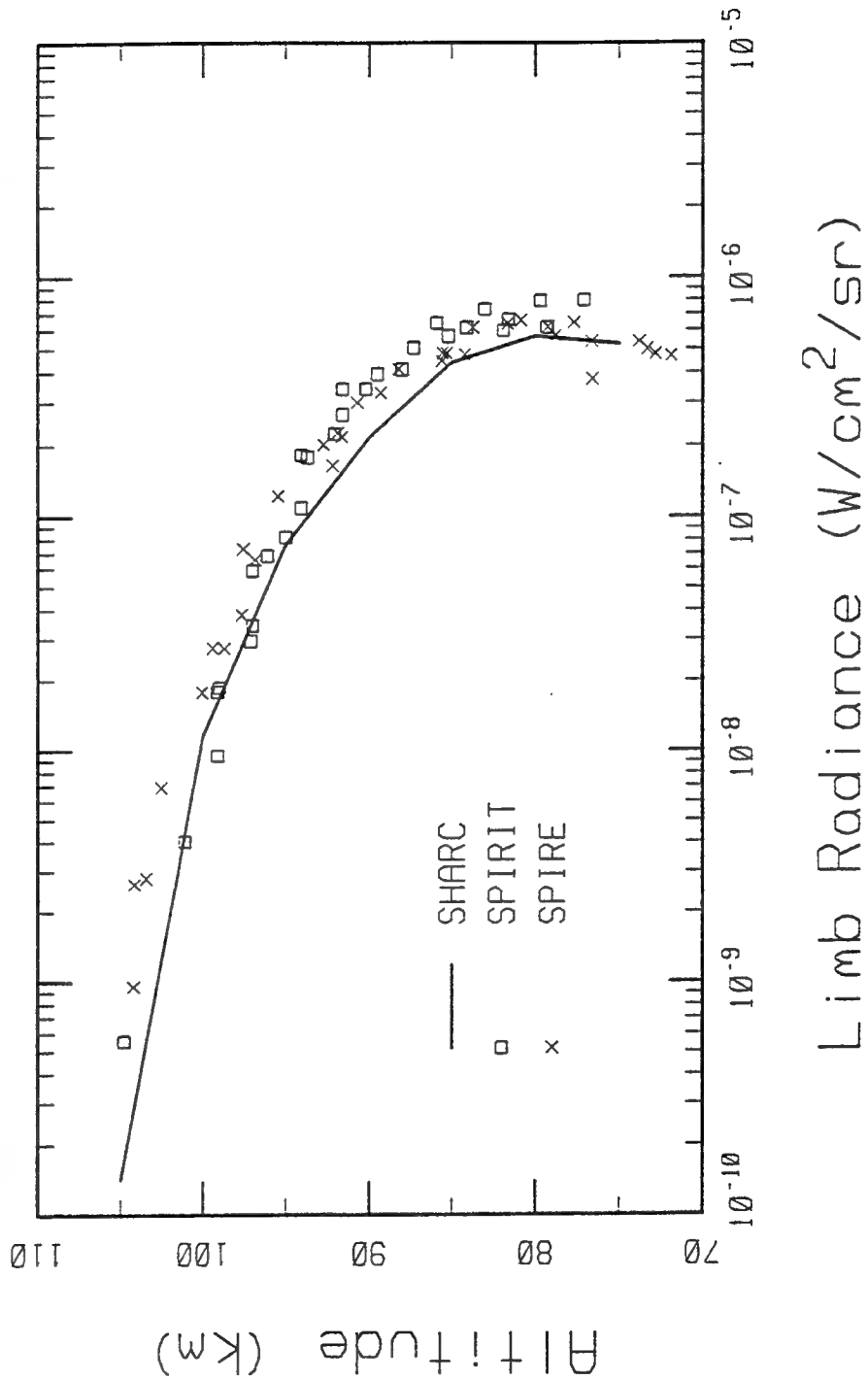
- SIGNIFICANT VARIABILITY IN OBSERVED NO RADIANCES





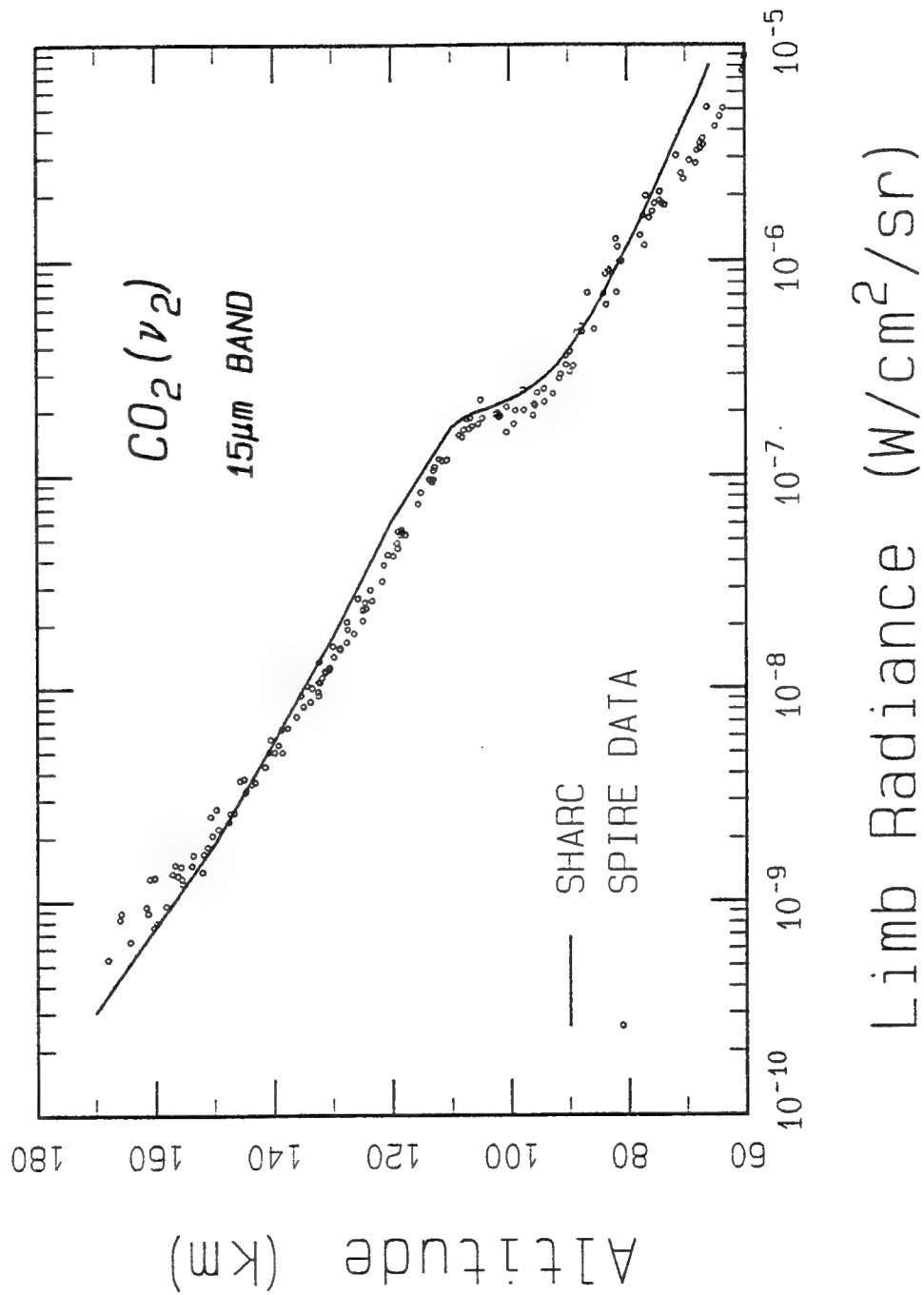
COMPARISON TO O₃ (9.6 μm) DATA

- SPIRIT 1 AND SPIRE DATA FOR NIGHTTIME CONDITIONS





SPIRE: LONG WAVE CO₂





FUTURE PLANS

- SHARC-3 WILL BE RELEASED THIS SUMMER BY PL/GPOS
 - MULTIPLE REGIONS WITH VARIABLE SOLAR ZENITHS
 - VARIATIONS ALONG LOS AROUND THE SOLAR TERMINATOR
- VALIDATION AND UPGRADES BY COMPARISON TO THE CIRRIIS-1A DATA BASE
- WORKING ON MODULE FOR ATMOSPHERIC STRUCTURES
 - BASED ON LOCKHEED CLUTTER MODEL (SEARS, et al.)
 - SHARC-4.1: AMBIENT CLUTTER
 - 4.2: AURORAL STRUCTURES
- EXTEND INTO THE NEAR INFRARED AND VISIBLE SPECTRAL REGIONS



SUMMARY

- SHARC IS A HIGH-ALTITUDE RADIANCE MODEL
FOR THE INFRARED SPECTRAL REGION
 - AUROREAL AND QUIESCENT ATMOSPHERES
 - SOLAR TERMINATOR MODULE
 - MODULARIZED STRUCTURE
 - ARBITRARY PATHS ABOVE 50 km
 - LINE-BY-LINE RADIANCE CALCULATIONS
 - FULLY INTEGRATED & LOCALIZED AURORAL REGION

- VALIDATED WITH FIELD DATA

- AVAILABLE FROM PL/GPOS - CONTACT
 - DR. RAMESH SHARMA (617) 377-4198

NON-LTE STUDIES OF THE 15- μ m BANDS OF CO₂ FOR ATMOSPHERIC REMOTE SENSING

David P. Edwards,¹ Manuel López-Puertas,² and
Miguel Angel López-Valverde²

¹National Center for
Atmospheric Research
Boulder, Colorado, USA

²Instituto de Astrofísica de
Andalucía
Granada, Spain

The new line-by-line non-LTE calculation capability of the GENLN2 radiative transfer code is described. Non-LTE model implementation and molecular state vibrational temperature input requirements are discussed for studies of the 15- μ m ν_2 bands of CO₂. Monochromatic and band-integrated radiance calculations have been performed for atmospheric limb view tangent heights between 50 and 120 km for non-LTE night and daytime conditions. Non-LTE radiance considerations are shown to be important for the 15- μ m CO₂ bands for tangent heights greater than 70 km, the magnitude of the divergence from LTE values and diurnal variation being dependent on the band and kinetic temperature profile. We show the importance of including Lorentzian line wings and overlapping lines. Calculations of synthetic radiance spectra are presented showing the non-LTE effect for two CO₂ temperature sounding channels of instruments aboard the Upper Atmosphere Research Satellite as a demonstration of the model capability.

VIEWGRAPHS UNAVAILABLE

CRITICAL TESTS OF NON-LTE RADIATIVE MODELS AGAINST HIGH-LATITUDE ROCKET DATA

R.H. Picard,¹ J.R. Winick,¹ U. Makhlof,² A.J. Paboojian,³
A.J. Ratkowski,¹ K.U. Grossmann,⁴ D. Homann,⁴ and J.C. Ulwick²

¹Phillips Laboratory/ Geophysics
Optical Environment Division
Hanscom AFB, MA 01731

²Stewart Radiance Laboratory
Utah State University
129 Great Road
Bedford, MA 01730

³ARCON Corporation
Waltham, MA 02154

⁴University of Wuppertal
Wuppertal, Germany

We have carried out tests of non-LTE radiation models against field data under conditions in which the state of the atmosphere was very well characterized and subject to extreme differences. The data were obtained during a series of rocket launches from northern Scandinavia, supported by ground-based observations. These included the series of SSSI flights, the first of which (6 Mar 1990) was part of the DYANA Campaign, and the MI-1 rocket launched 10 Feb 1984 during the MAP/WINE Campaign. The measured state of the atmosphere, including temperature and atomic-oxygen profiles, is input to the line-by-line ARC (Atmospheric Radiance Code) non-LTE code and associated models, and model predictions are compared with spectral data from a rocketborne Ebert-Fastie spectrometer, emphasizing the CO₂ 15 μ m data. We conclude that the models are able to predict non-LTE spectral radiance very well when provided good input data on the atmospheric state. We also show that very significant differences between model predictions and point measurements can occur when climatologies are used to generate inputs for the radiative models.

Critical Tests of Non-LTE Radiative Models Against High-Latitude Rocket Data

R.H. PICARD, J.R. WINICK,
A.J. RATKOWSKI
U. MAKHLOUF, J.C. ULWICK
A.J. PABOOJIAN
K.U. GROSSMANN, D. HOMANN

Phillips Lab / Geophysics

Stewart Radiance Lab, USU
ARCON Corp
Univ Wuppertal

Annual Review Conference on Atmospheric Transmission Models
Phillips Lab, Bedford, Mass., 8-9 Jun 1993

OUTLINE

- Experiment Design - SISSI and M-I1 Payloads
- ARC Non-LTE Radiative Model Testing
 - Model Description
 - Model Inputs - [O], T, [CO₂], [O₂], [N₂]
 - Results - CO₂ ν_2 (15 μ m)
- 1D Diurnal Photochemical Model Testing
 - Model Description
 - Results - OH Meinel $\Delta v=2$ (1.5 μ m)
- Summary/Conclusions

SISSI PROGRAM

Spectroscopic Infrared Structure Signature Investigation

Joint Investigation: Univ. of Wuppertal, Germany
Phillips Laboratory/Utah State

Four Rocket Flights: 2 in March (1990, 1991)
2 in Summer (July, Aug. 1990)

Location: Esrange, Kiruna, Sweden

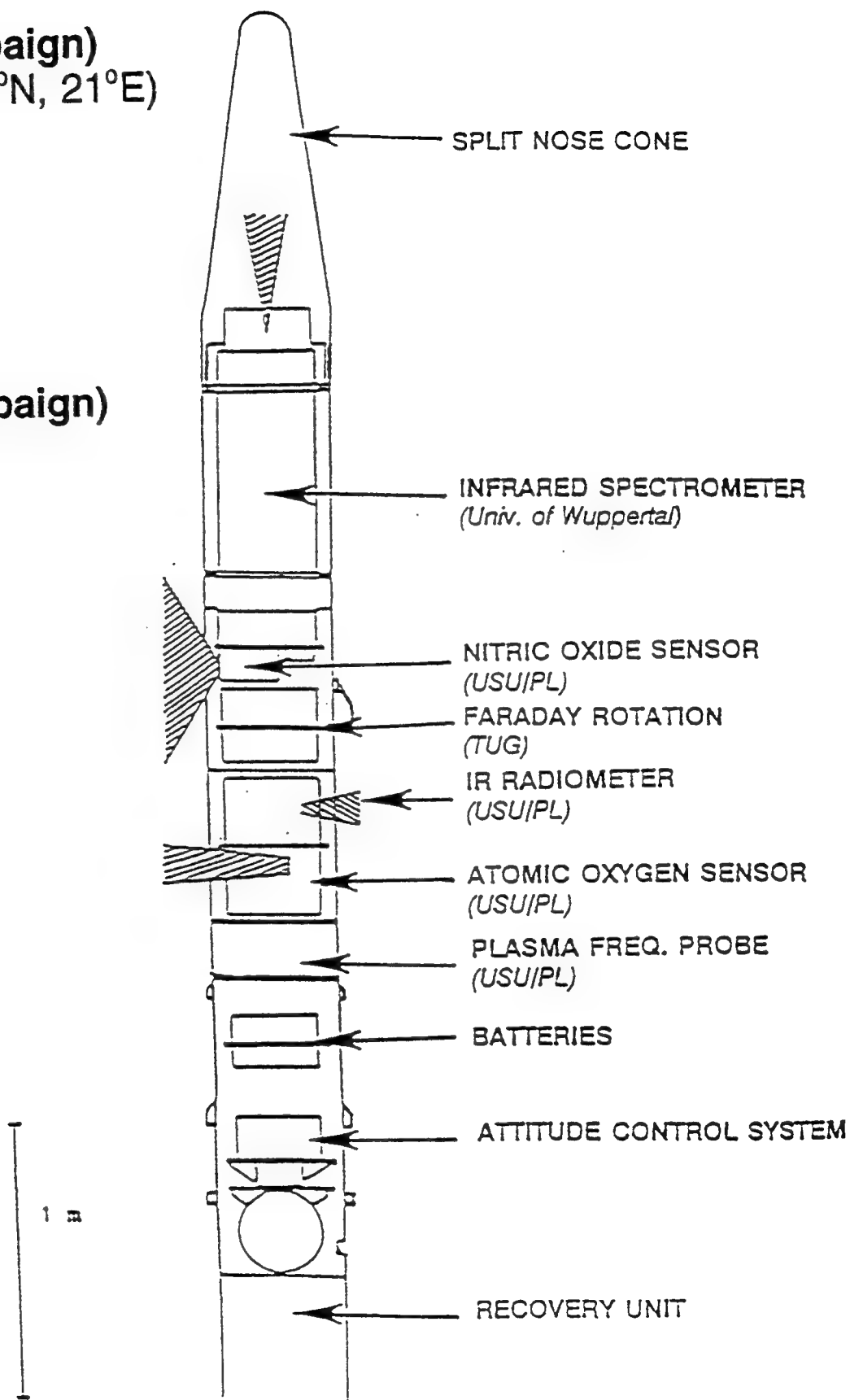
Solar Depression Angle near 5° all flights

SISSI PROGRAM

- Infrared spectra (Univ Wuppertal, Ebert-Fastie spectrometer)
 - + atmospheric measurements [Phillips Lab / Utah State Univ; [O], [NO], [e], OH and O₂(¹Δ_g) radiometers]
- Concentrate on SISSI-F1
 - Part of DYANA Campaign → Coordinated measurements (rocket salvos, ground-based measurements)
- Interesting contrast with M-I1 rocket data (MAP/WINE Campaign)
 - SISSI-F1: High [O] and mesopause temperature
 - M-I1: Very low [O] and mesopause temperature (minor stratospheric warming)
- Vertical probe - Comparison to limb scans
 - Well characterized atmosphere; crucial for testing IR model response to atmospheric variability

SISSI-1 (DYANA Campaign)
 ESRANGE, Sweden (68°N, 21°E)
 6 Mar 90, 0440 UT
 Rocket - Skylark VI
 Apogee: 200km
 SZA: $\approx 95^\circ$

M-I1 (MAP/WINE Campaign)
 ESRANGE, Sweden
 10 Feb 84, 0412 UT
 Rocket - Skylark VI
 Apogee: 179km
 SZA: 106°



ARC (Atmospheric Radiance Code)

- Line-by-line (LBL) non-LTE model:
 - Full temperature variation; Voigt lineshape
 - Full LBL for both *radiative excitation* & *line-of-sight radiance*
- Spectral range: 1.4 - 17 μm (5000 - 600 cm^{-1})
- Resolution: Unlimited
- Radiators: Selected
 - CO₂ ν_2 (15 μm), ν_3 (4.3 μm), $\nu_1+\nu_3$ (2.7 μm)
 - CO (4.7 μm)
 - NO (5.3 μm)
 - OH (2.7 μm , 1.5 μm , ...)
 - O₂($^1\Delta_g$) (1.27 μm , 1.5 μm)
- LBL auroral model AARC (Auroral ARC) included

ARC (Atmospheric Radiance Code) [cont.]

- 3 modules:
 - RAD: Production and loss processes for excited-state populations (radiation, collisions, photochemistry)
 - NLTE: Line-of-sight radiative transfer
 - CONV: Degraded spectra

CO₂ 15-μm RADIANCE MODEL (ARC)

- Production and loss processes

- Radiative

A

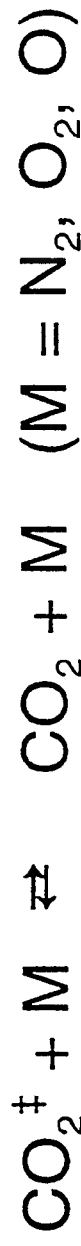


B_J

(Earthshine pumped; little diurnal variation)

- Collisional (V-T)

k



k'

- Atomic oxygen excitation / quenching especially important because of large value of rate constant: $k_{\text{O}} = 6.1 \times 10^{-12} \text{ cm}^3/\text{s}$ at $T = 300\text{K}$, varies as $T^{1/2}$ (Sharma & Wintersteiner, 1990; Wintersteiner *et al.*, 1992)

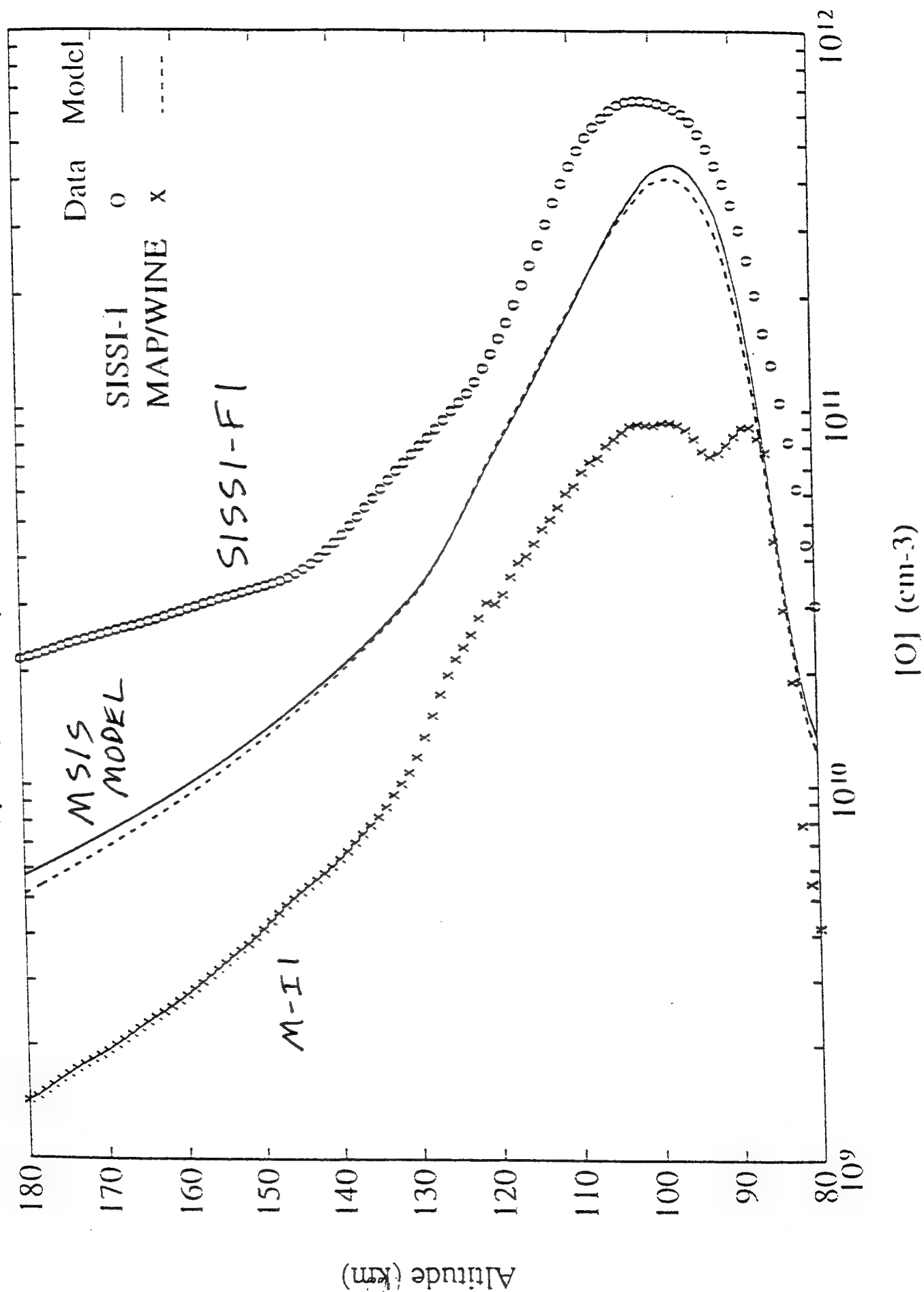
CO₂ 15-μm RADIANCE MODEL (ARC) [cont.]

- For application to SLSI / M-I1 cases:
 - 2 isotopes (626, 636)
 - 4 hot bands (10001, 10002, 02201, 03301)
 - Instrumental shape triangular with 1% FWHM

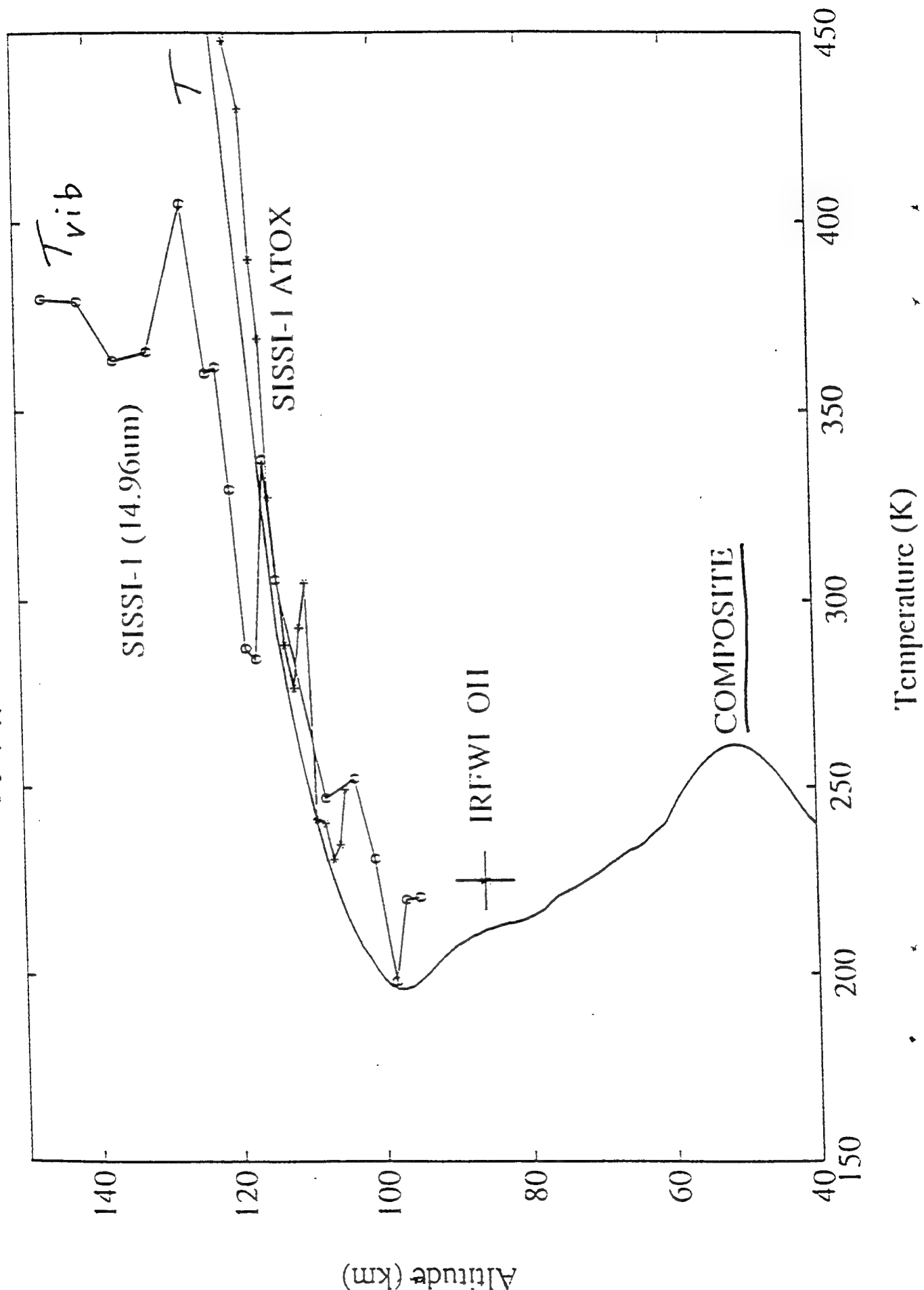
ARC MODEL INPUTS - SISSI / M-I1 SIMULATION

- Atomic oxygen profile measured onboard and smoothed
 - USU/PL 130.4nm resonance lamp and detector
- Temperature profile inferred from onboard measurements supported by measurements from ground and other rockets
- $[O_2]$, $[N_2]$ taken from merged CIRA 86 / MSIS 86 profiles
- $[CO_2]$ obtained by scaling SPIRE profile 'D' (Wintersteiner *et al.*, 1992) up to 350 ppmV below 90km

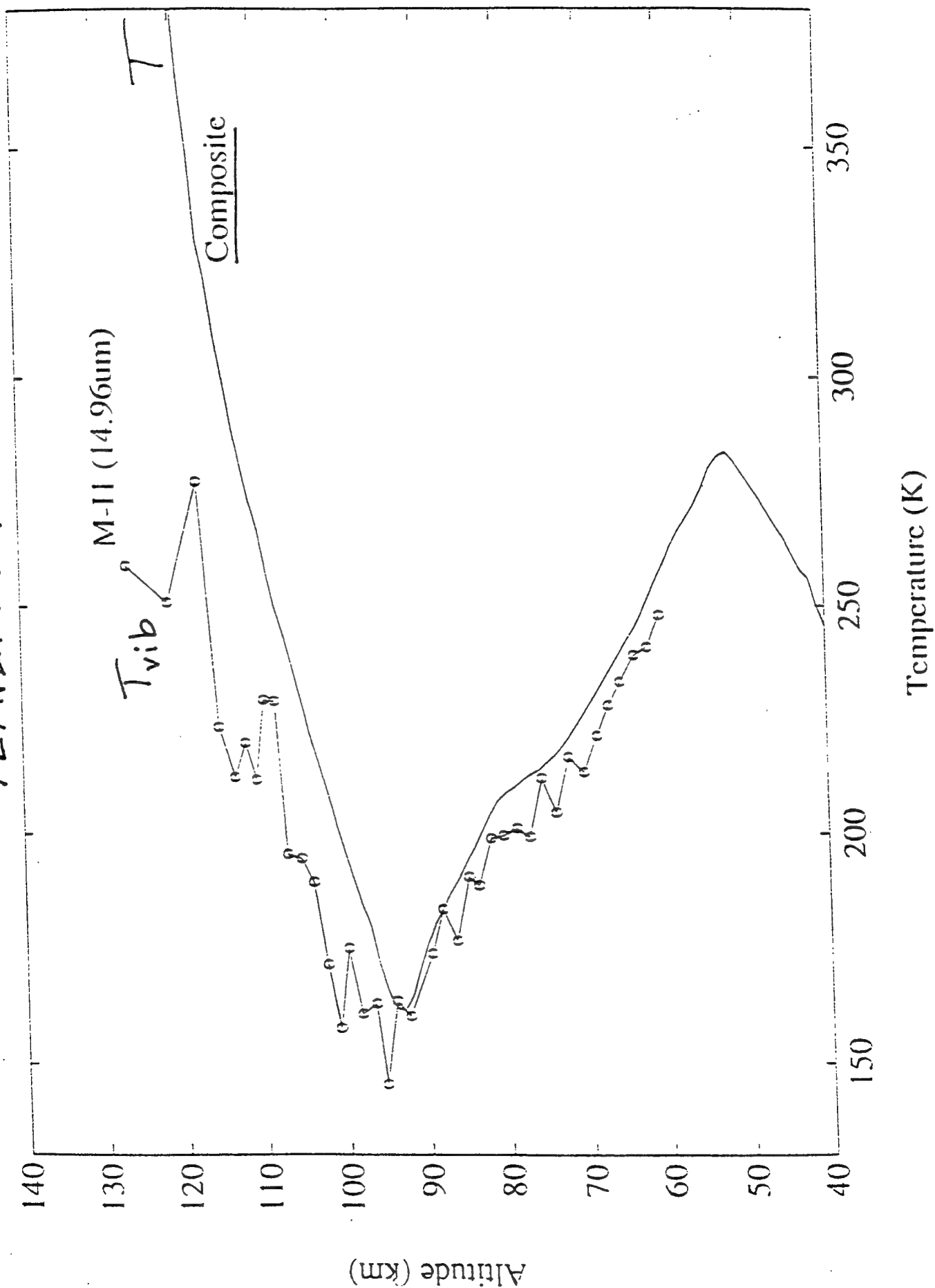
ATOMIC OXYGEN DENSITY



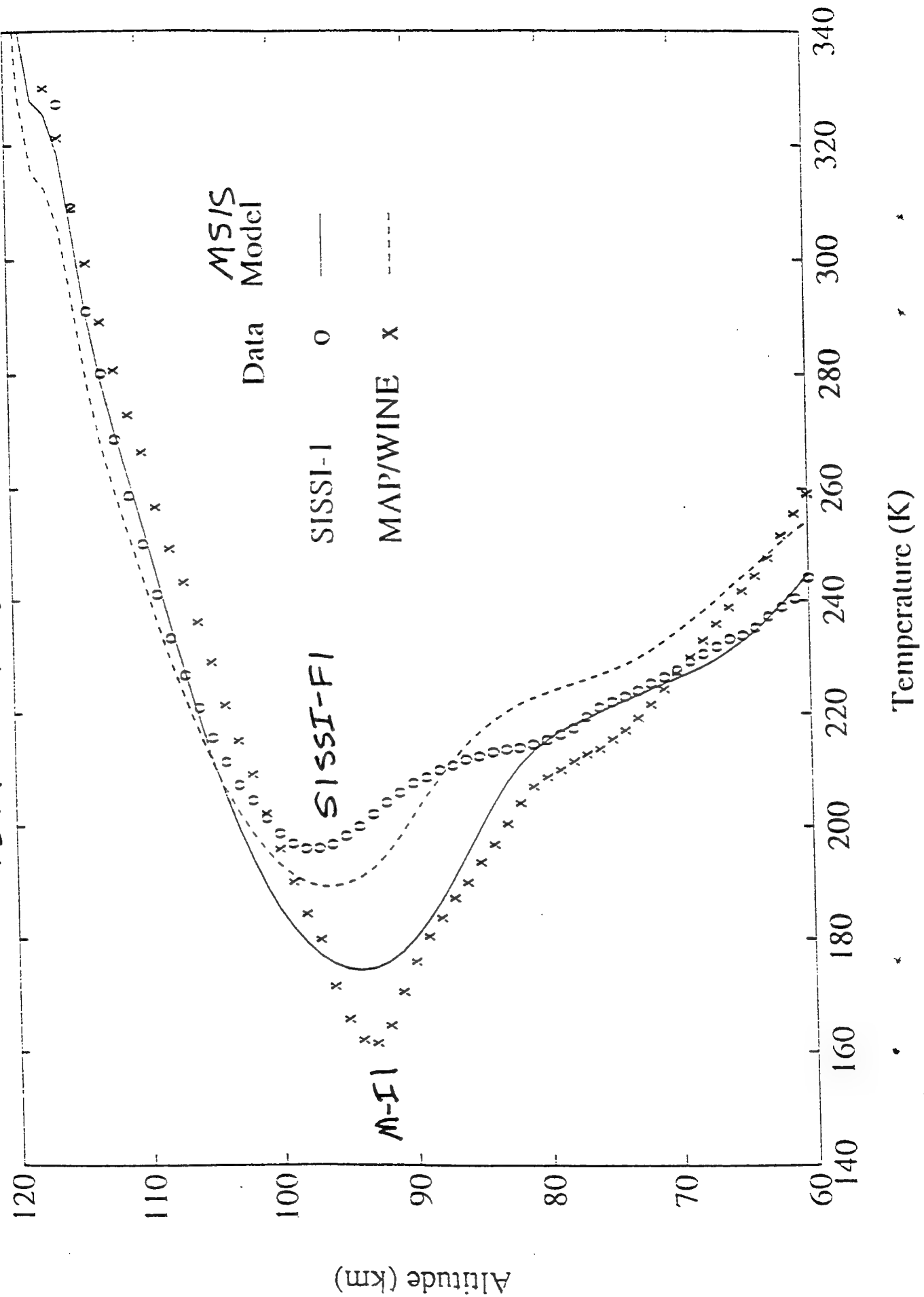
TEMPERATURE - SISSI-FI



TEMPERATURE - M-II



TEMPERATURE - MODEL VS. DATA



CONCEPT OF VIBRATIONAL TEMPERATURE T_{vib}

$$\begin{array}{c}
 E' \\
 \hline
 \uparrow \text{ } h\nu \\
 \hline
 E''
 \end{array}
 \begin{array}{c}
 n' \\
 \hline
 \hline
 n''
 \end{array}
 \quad \text{POPULATION RATIO} \quad = \frac{g'}{g''} e^{-\frac{E' - E''}{k_B T_{vib}}}$$

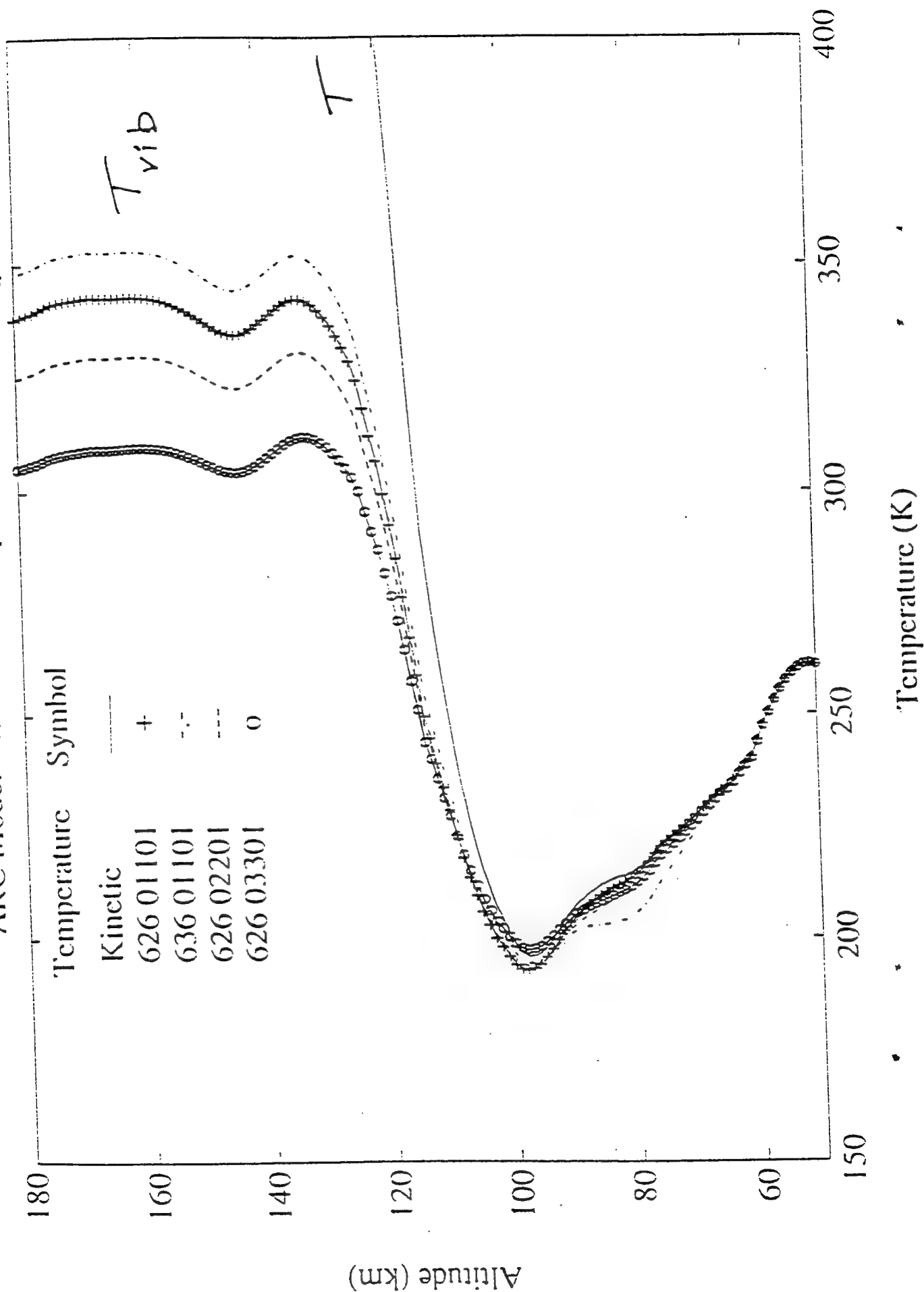
LTE : $T_{vib} = T$ COLLISIONS DOMINATE

Non-LTE : $T_{vib} \neq T$

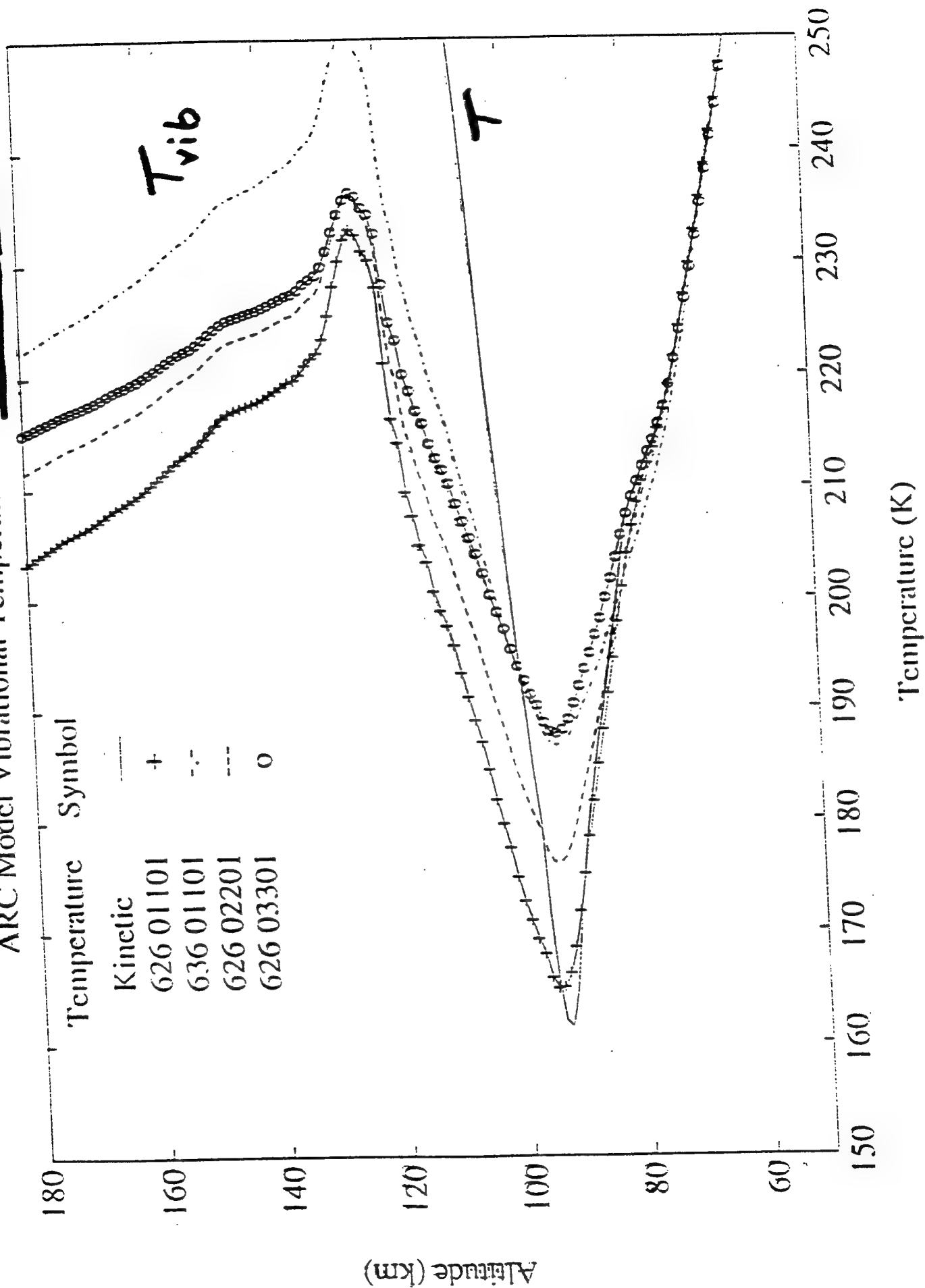
$T_{vib} < T \Rightarrow$ NON-COLLISIONAL LOSS

$T_{vib} > T \Rightarrow$ NON-COLLISIONAL PRODUCTION

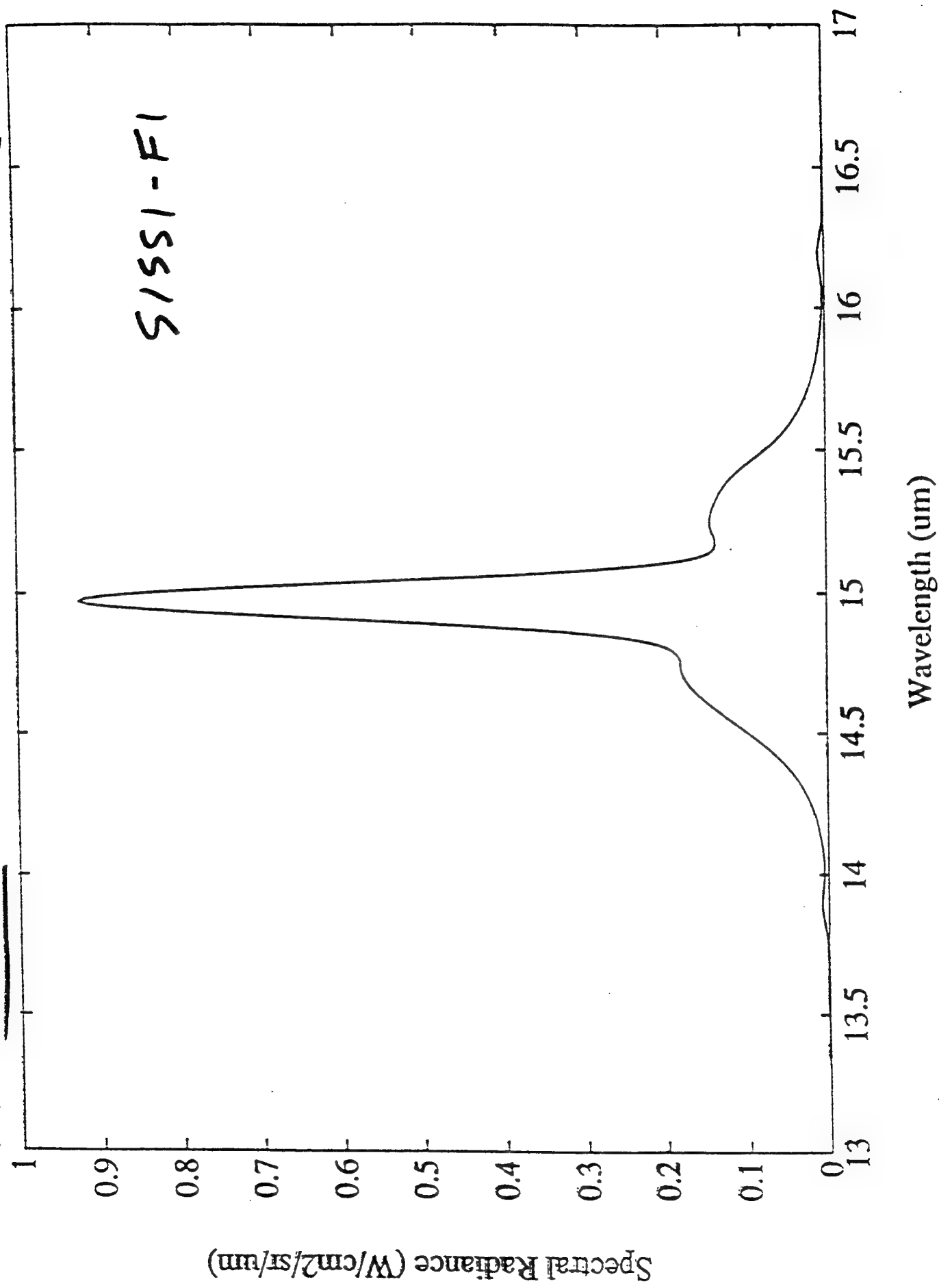
ARC Model Vibrational Temperatures - SISSI-1

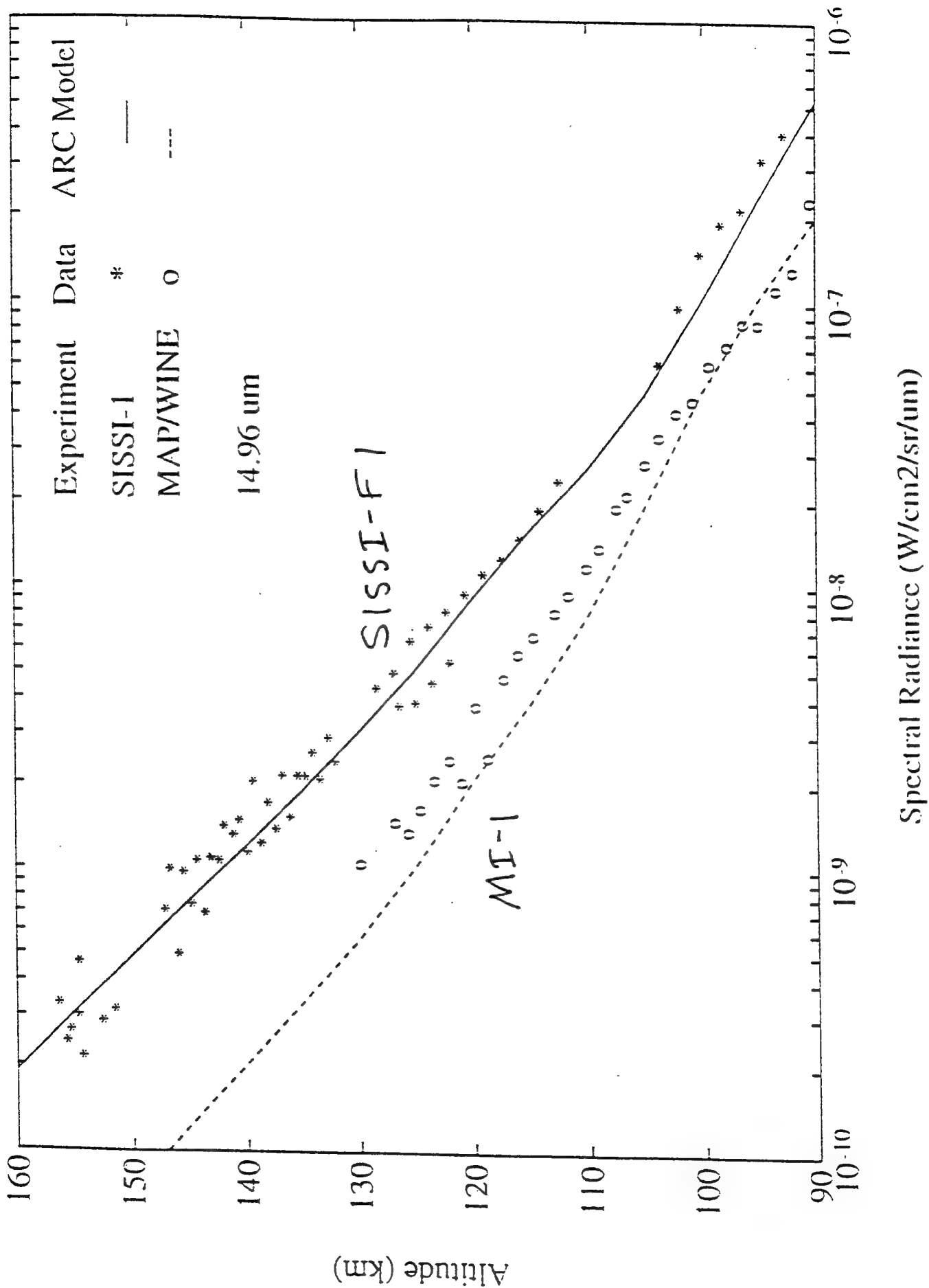


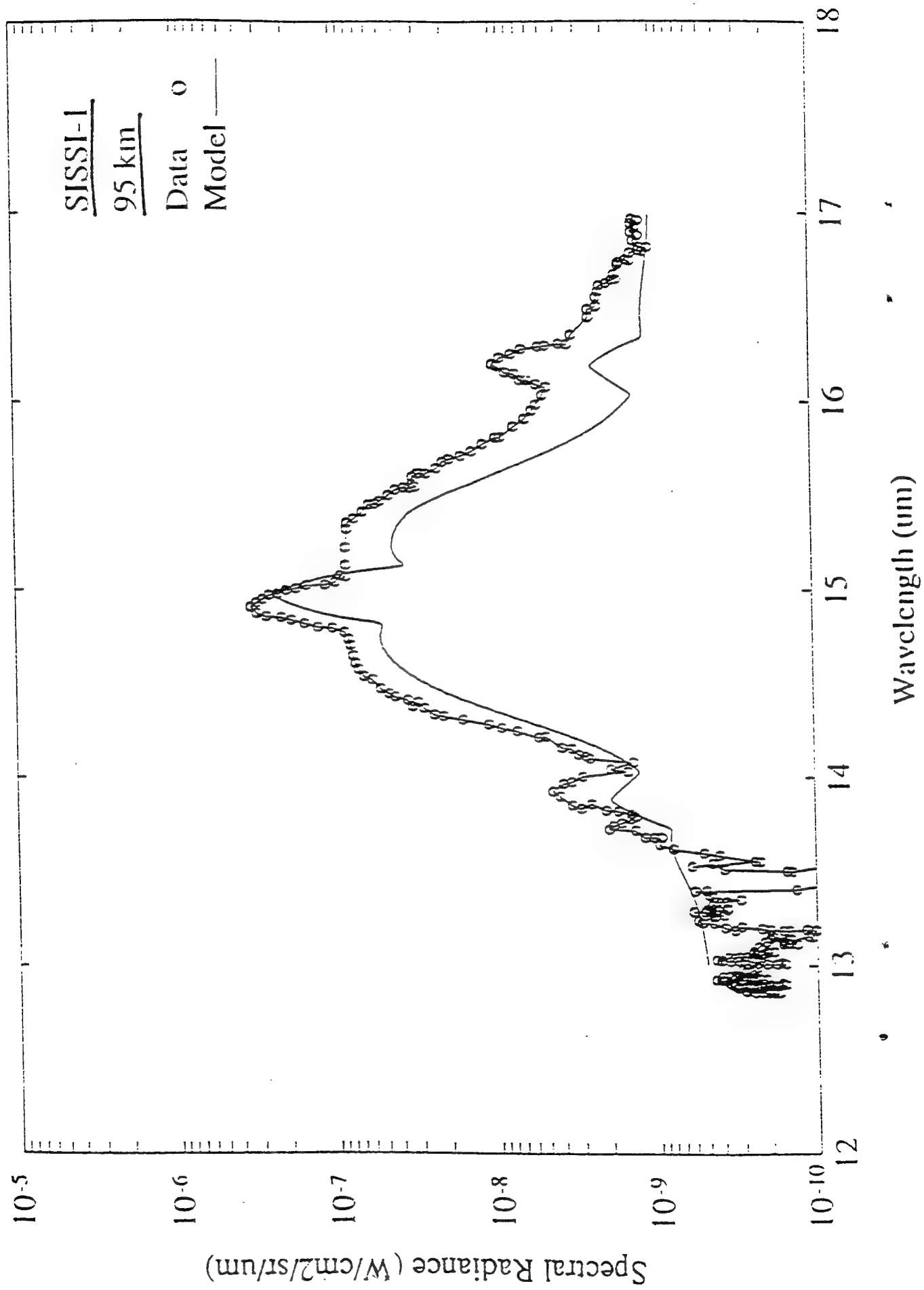
ARC Model Vibrational Temperatures - MAP/WINE MS-1

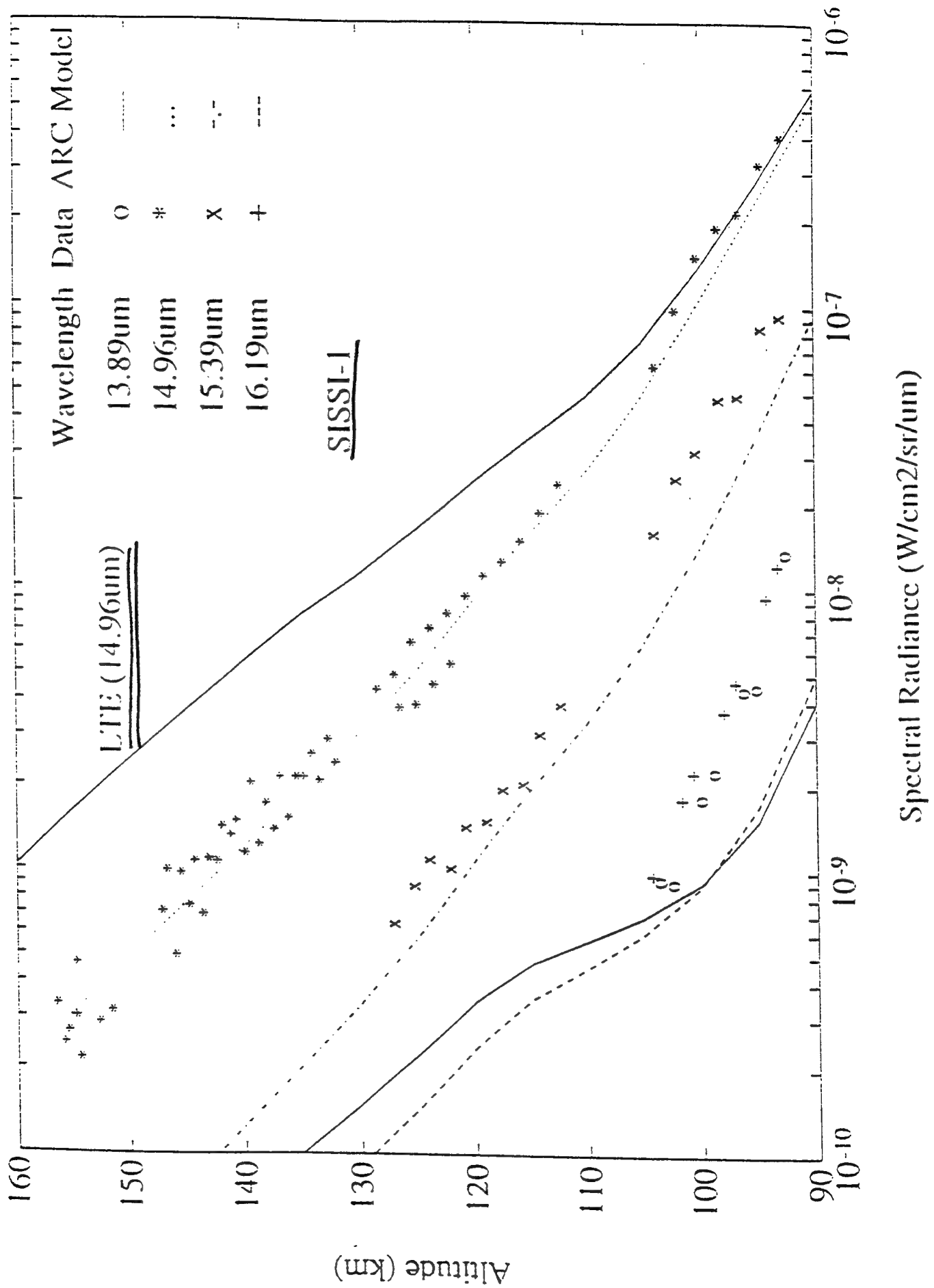


$\times 10^{-7}$ ARC Model 626 & 636 01101; 626 02201; 626 03301 100 km









Self-consistent One-dimensional Photochemical Model

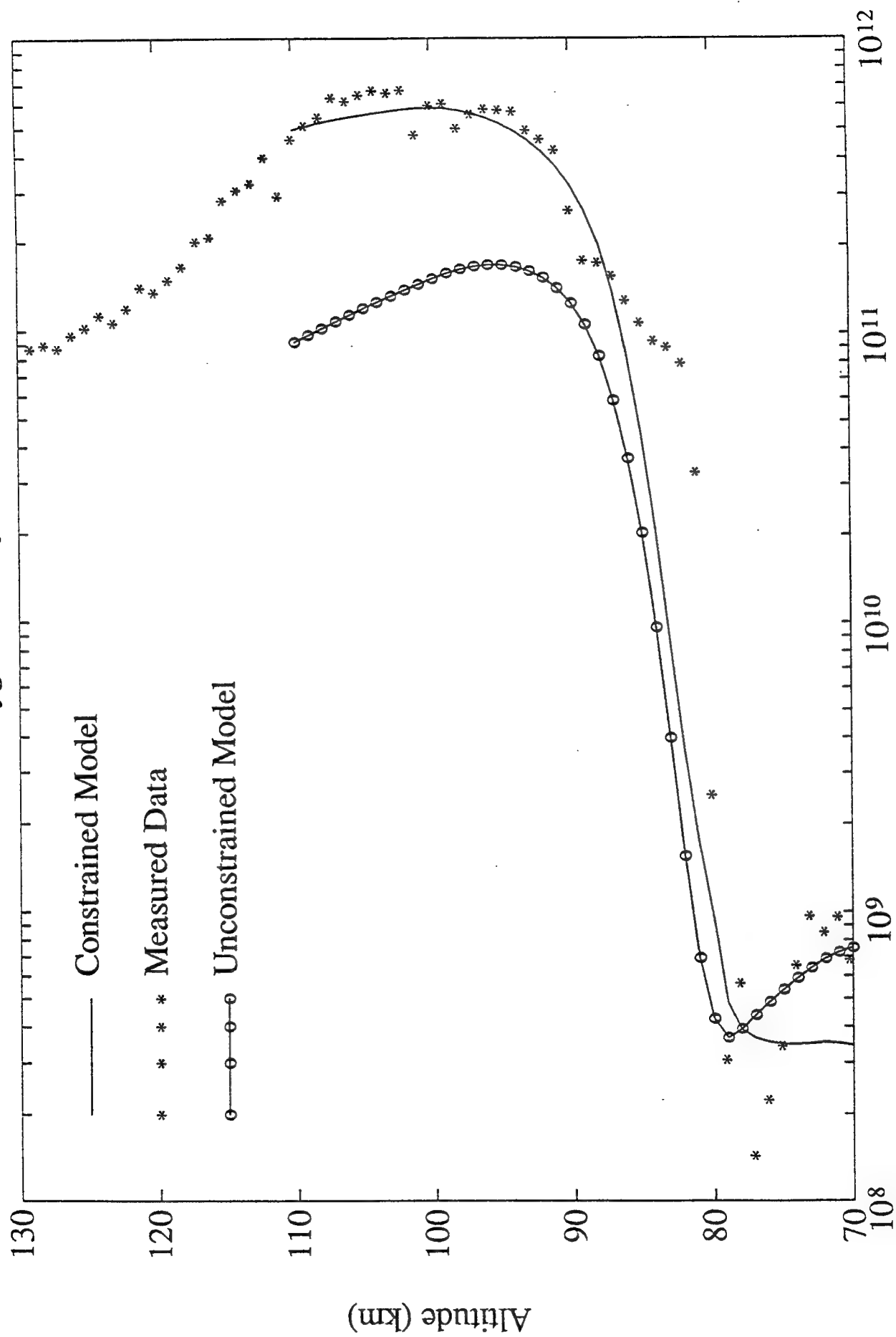
U. Makhoul¹, J. R. Winick² and R.H. Picard²

- General Description of Model
Model Features
 - 1-D diurnal photochemical model for self-consistent background profiles of reactive species (H, O₃, O, OH, HO₂, ...)
 - OH(v) vibrational-population model, including level-dependent quenching and expanded reaction set calculates steady-state [OH]₀ and brightness B_{ov}.
- Altitude range
 - 30-120 km
- Model atmosphere
 - Temperature T(z), [N₂(z)], [O₂(z)], [CO₂] and [H₂O(z)]:
 - z=0-120km: NRL climatologies, (Summers, Anderson *et al.*, 1990)
 - Scaled eddy diffusivities from Strobel *et al.* (1987).
- Chemical reactions and rates
 - Updated from latest JPL compilation (JPL 90-1, 1990), plus recent literature

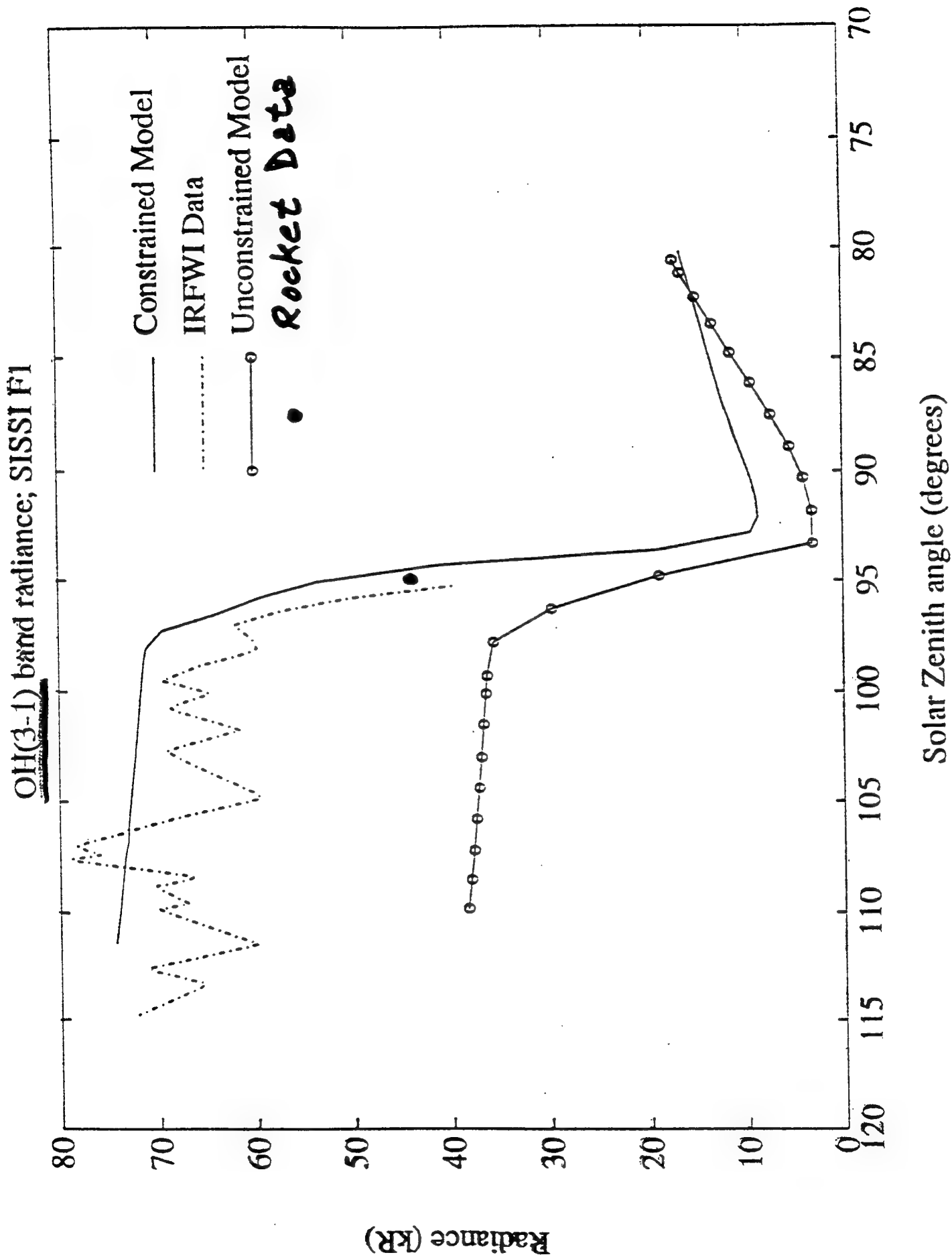
¹Stewart Radiance Laboratory, Bedford MA 01730

²Phillips Laboratory/GPOS, Hanscom AFB, MA 01731

Atomic Oxygen Density; SSSI F1



Atomic Oxygen Density (cm-3)



Summary/Conclusions

- SISSI/F1 payload measured both [O] and infrared emissions
- Elevated atomic oxygen profile (peak $> 6 \times 10^{11} \text{ cm}^{-3}$) resulted in enhanced CO_2 ν_2 radiance
- ARC model predicts well altitude profiles of SISSI/F1 CO_2 ν_2 data and differences with MAPWINE measurement
- Discrepancies on the weaker 1000x hot bands between 90 and 100 km can be caused by elevated mesopause temperature
- 1D PCHEM MODEL WITH MEASURED $\{\text{O}\}$ USED TO CONSTRAIN INPUT PARAMETERS AGREES WELL WITH MEASURED SZA-DEPENDENT OH MEINEL-BAND EMISSION

Wednesday 9 June 1993 a.m.

SESSION E: STRUCTURE ALGORITHMS

Chair: Edmond M. Dewan, PL/GPOS

**ATMOSPHERIC STRUCTURE SIMULATION: AN AUTOREGRESSIVE
MODEL FOR SMOOTH GEOPHYSICAL POWER SPECTRA WITH
KNOWN AUTOCORRELATION FUNCTION**

James H. Brown

Phillips Laboratory/ Geophysics
29 Randolph Road
Hanscom AFB, MA 01731-3010

Within a defined domain, geophysical phenomena often are characterized by smooth continuous power spectral densities having a negative power law slope. Frequently, Fourier transform analysis has been employed to generate synthetic scenes from pseudorandom arrays by passing the stochastic data through a Fourier filter having a desired correlation structure and power spectral dependency. This paper examines the possibility of producing synthetic structure by invoking autoregression analysis as contrasted with the Fourier method. Since computations that apply multidimensional fast Fourier transforms to large data arrays consume enormous resources and time, the goal of this study is to seek an alternative method to reduce the computational burden. Future editions of the Phillips Laboratory Strategic High Altitude Atmospheric Radiance Code (SHARC) will feature an ability to calculate structured radiance. The methods explored herein provide a process that can compliment or in some cases supplement methods presently being used.

**Atmospheric Structure Simulation: An
Autoregressive Model for Smooth
Geophysical Power Spectra with Known
Autocorrelation Function**

James H. Brown



Figure Captions

1. Expression for the linear difference equation. Future values of a time series predicted from past values and random data. So-called ARMA model.
2. Expression for power spectra given an ARMA linear predictor model. The a's and b's are the AR and MA predictor coefficients.
3. A theoretical model for power spectral density and autocorrelation function for constant power law slope.
4. Expression for the coherence length parameter . Function of power law slope and parameter "a".
5. Sample model PSD and autocorrelation function, Slope = -3., $\sigma^2 = 0.2$, $L_c = 5.0$ and $a = 0.05$. Upper left quadrant log-log PSD vs spatial frequency, upper right quadrant linear PSD plot, lower left quadrant autocorrelation function vs lag, lower right quadrant power curve.
6. White noise. Sample Gaussian random number sequence, mean = 0., standard deviation = 0.055, spacing 100m.
7. Histogram of sample Gaussian random number sequence. Theoretical mean = 0., theoretical S.D. = 0.055.
8. Left panel, theoretical PSD input (unmarked), autoregressive predictor PSD (marked by x), and simulated PSD (marked by small square). Right panel, corresponding autocorrelation functions. $L_c = 1.75$ Km, $S = -5/3$, $\sigma^2 = 1.02E-03$, spacing = 100m. Theoretical autocorrelation function modified at lag = 0. Six predictor coefficients.
9. Autoregressive simulated structure sequence. $L_c = 1.75$ Km, $S = -5/3$, $\sigma^2 = 1.02E-03$.
10. Histogram of autoregressive simulated structure sequence. $L_c = 1.75$ Km, $S = -5/3$, $\sigma^2 = 1.02E-03$.
11. Left panel, theoretical PSD input (unmarked), autoregressive predictor PSD (marked by x). Right panel, corresponding autocorrelation functions. $L_c = 1.75$ Km, $S = -5/3$, $\sigma^2 = 1.02E-03$, spacing = 100m. Modified theoretical autocorrelation function at lag = 0. One predictor coefficient.

12. Left panel, theoretical PSD input (unmarked), autoregressive predictor PSD (marked by x), and simulated PSD (marked by small square). Right panel, corresponding autocorrelation functions. $L_c = 10$ Km, $S = -5/3$, $\sigma^2 = 4.9E-03$, spacing = 100m. Theoretical autocorrelation function modified at lag = 0. Six predictor coefficients.
13. Autoregressive simulated structure sequence. $L_c = 10$ Km, $S = -5/3$, $\sigma^2 = 4.9E-03$.
14. Conclusions. Self-explanatory.
15. The auto-regression Yule-Walker Matrix equation for solving the AR coefficients.
16. The Levinson Recursion Algorithm. An iterative solution of the Yule-Walker equations.
17. A forward and backwards method for minimizing the error of an AR process power spectrum.

Linear Difference Equation

$$x(n) = - \sum_{k=1}^p a(k)x(n-k) + \sum_{k=0}^q b(k)\varepsilon(n-k)$$



Power Spectra Model



$$P_{\text{ARMA}}(f) = T \rho_w \left| \frac{B(f)}{A(f)} \right|^2$$

$$A(f) = 1 + \sum_{k=1}^p a(k) \exp(-2\pi i k T)$$

$$B(f) = 1 + \sum_{k=0}^q b(k) \exp(-2\pi i k T)$$

$$x(n) = - \sum_{k=1}^p a(k) x(n-k) + \varepsilon(n)$$

$$P_{\text{AR}}(f) = \frac{T \rho_w}{|A(f)|^2} = T \sum_{k=-\infty}^{\infty} r_{xx}(k) \exp(-2\pi i k T)$$

PSD and ACF Models

497

$$\text{PSD}(k) = \frac{\sigma^2 a^{2\nu} \Gamma\left(\nu + \frac{1}{2}\right)}{\sqrt{\pi} \Gamma(\nu) (a^2 + k^2)^{\nu + \frac{1}{2}}}$$

$$\text{ACF}(x) = \frac{\sigma^2 2^{(1-\nu)} (2\pi a x)^\nu K_\nu(2\pi a x)}{\Gamma(\nu)}$$

Coherence Length Parameter

$$L_c = \frac{\Gamma\left(\nu + \frac{1}{2}\right)}{2\sqrt{\pi}\Gamma(\nu)a}$$



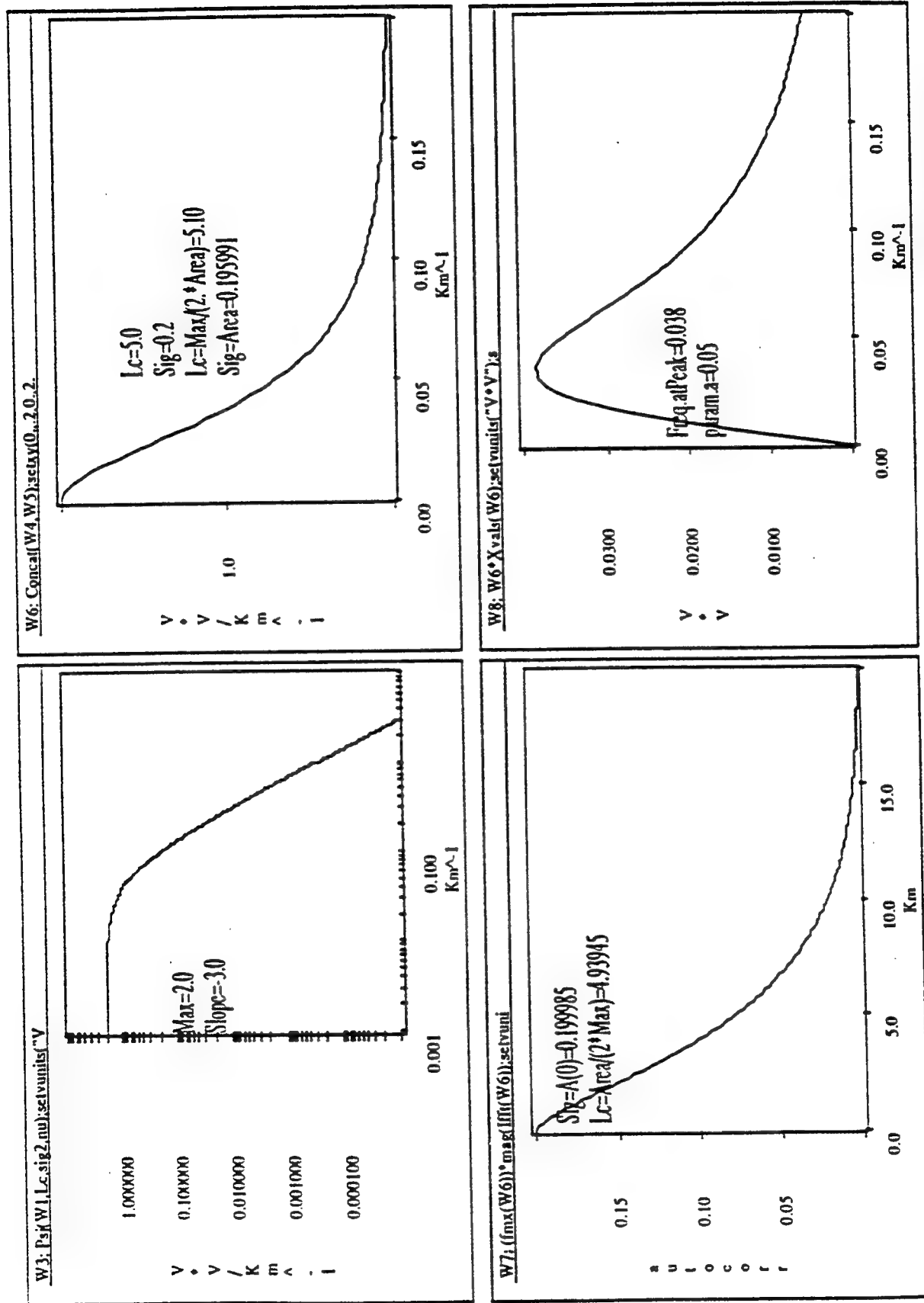


Figure 1. Sample model PSD and autocorrelation function, Slope = 3., $\sigma^2 = 0.2$, $L_c = 5.0$ and $a = 0.05$. Upper left quadrant log-log PSD vs spatial frequency, upper right quadrant linear PSD plot, lower left quadrant autocorrelation function vs lag, lower right quadrant, power curve

WHITE NOISE SIMULATED

SIMULATE DATA WITH SEED=3333 NUMBER OF POINTS SIMULATED=80000 NUMBER OF VALUES IN PSD=4096

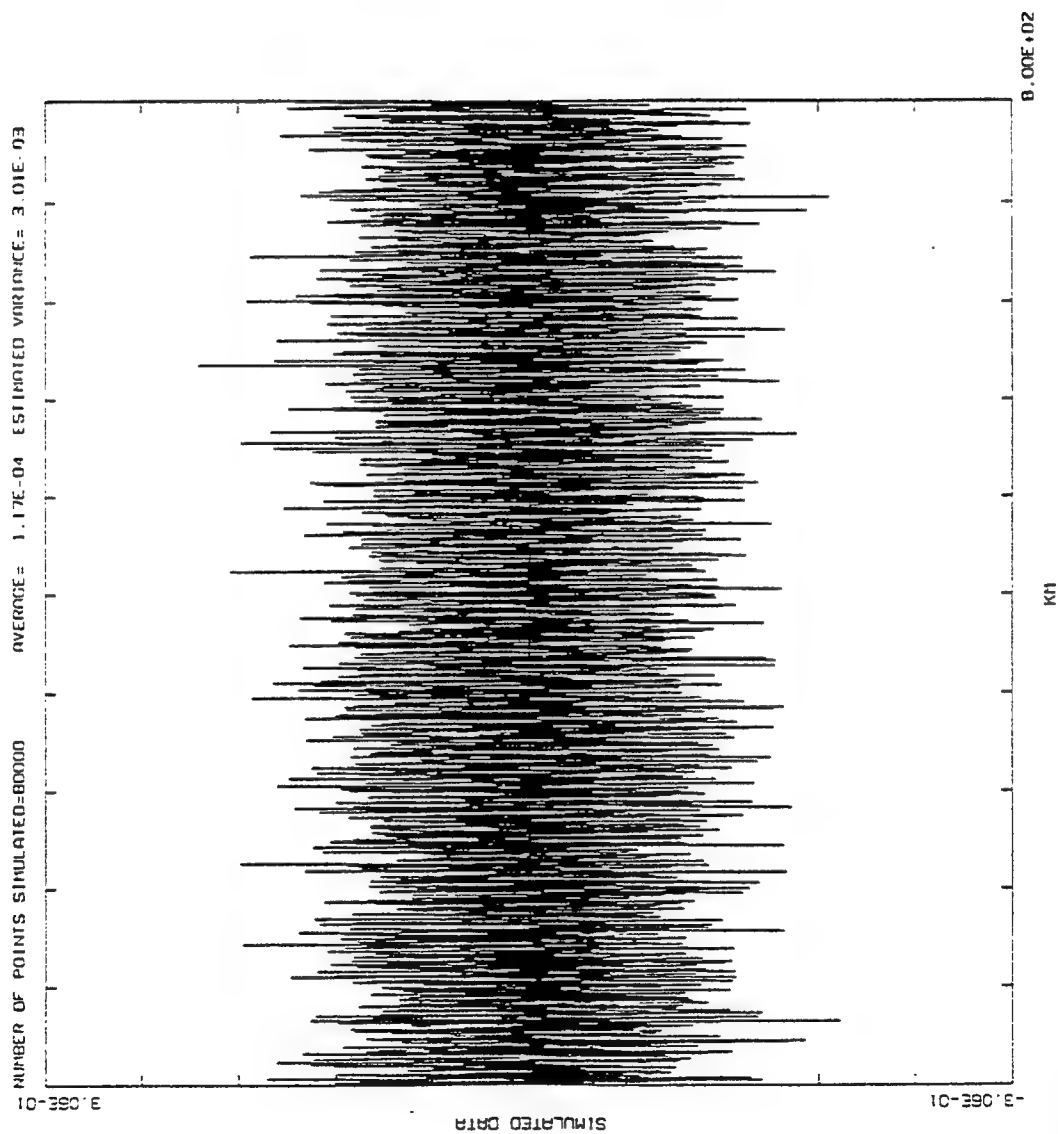
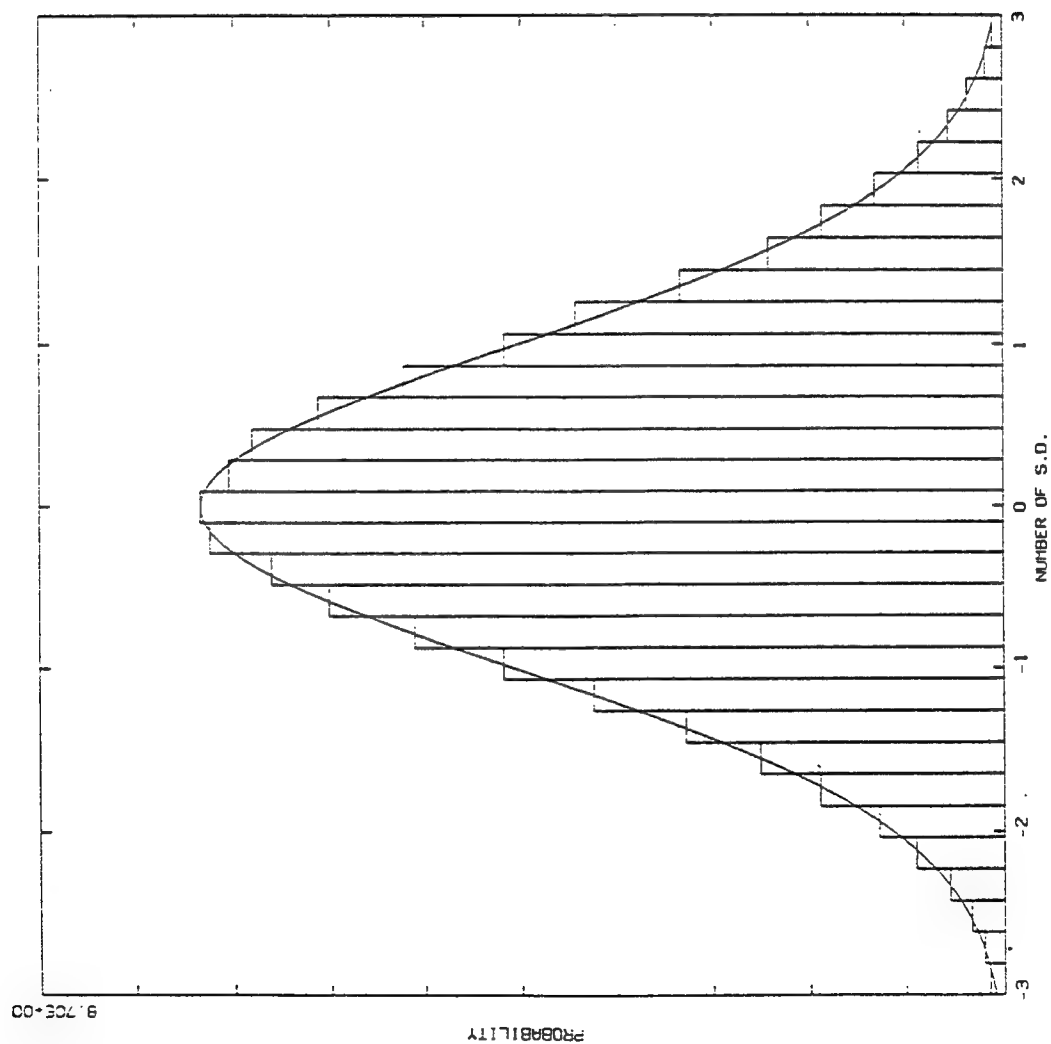


Figure 2. White noise. Sample Gaussian random number sequence, mean = 0., standard deviation = 0.055, spacing 100 m

THIS IS FILE SIMC 15-DEC-92 SIMULATE DATA WITH SEED=3333 NUMBER OF POINTS SIMULATED=80000 NUMBER OF VALUES IN PSD=4096
WHITE NOISE SIMULATED



SOLID=THEORETICAL
 BARS=SIMULATED
 MEAN(THEORETICAL)=0.
 VARIANCE(THEO)= 3.03E-03
 S.D.(THEO)= 5.50E-02
 AVERAGE(SIMULATED)= 1.17E-04
 VARIANCE(SIM)= 3.01E-03
 S.D.(SIM)= 5.49E-02
 NUMBER OF POINTS SIMULATED= 80000

Figure 8. Histogram of sample Gaussian random number sequence. Theoretical mean = 0., theoretical S.D. = 0.055.

THIS IS FILE SIM18 14-DEC-92 SIMULATE DATA WITH SEED=3333 NUMBER OF POINTS SIMULATED=80000 NUMBER OF VALUES IN PSD=4096
 OUTPUT FROM PROGRAM MODEL 1 14-DEC-92
 PREDICTOR WAS ESTIMATED FROM PSD MODEL LC= 1.75E+00 SIGNA=2 1.02E-03 SLOPE OF PSD=1.67 SPACING= 1.00E-01 A= 6.79E-02
 ALL AREA'S OF PSD ARE CORRECTED FOR VALUES ABOVE NYQUIST FREQUENCY OF 5.00E+00 IS 4.16E-05
 VALUES FROM ORIGINAL. AREA OF PSD= 1.02E-03 LC FROM PSD= 1.75E+00 AREA OF AUTOCORRELATION= 3.77E-03 LC FROM AUTOCORRELATION= 1.84E+00
 VALUES FROM PREDICTOR. AREA OF PSD= 1.07E-03 LC FROM PSD= 1.54E+00 AREA OF AUTOCORRELATION= 3.20E-03 LC FROM AUTOCORRELATION= 1.60E+00
 VALUES FROM SIMULATED AREA OF PSD= 1.05E-03 LC FROM PSD= 1.47E+00 AREA OF AUTOCORRELATION= 3.13E-03 LC FROM AUTOCORRELATION= 1.53E+00

PREDICTOR VALUES X
 USE 6 PREDICTOR COEFFICIENTS
 RM= 1.378470E-04

LINEAR PREDICTOR COEFFICIENTS
 1 -9.636805E-01
 2 8.958164E-02
 3 -3.511140E-02
 4 -6.827840E-03
 5 -5.614103E-03
 6 -1.353068E-02

SIMULATED VALUES □
 USE 12 PREDICTOR COEFFICIENTS
 RM= 1.372181E-04

LINEAR PREDICTOR COEFFICIENTS
 1 -9.672024E-01
 2 8.871353E-02
 3 -3.472552E-02
 4 -4.136733E-03
 5 -7.524158E-03
 6 -1.142308E-02
 7 3.375496E-03
 8 2.084824E-03
 9 -8.173436E-04
 10 -8.819729E-03
 11 8.115808E-03
 12 -1.27822E-03

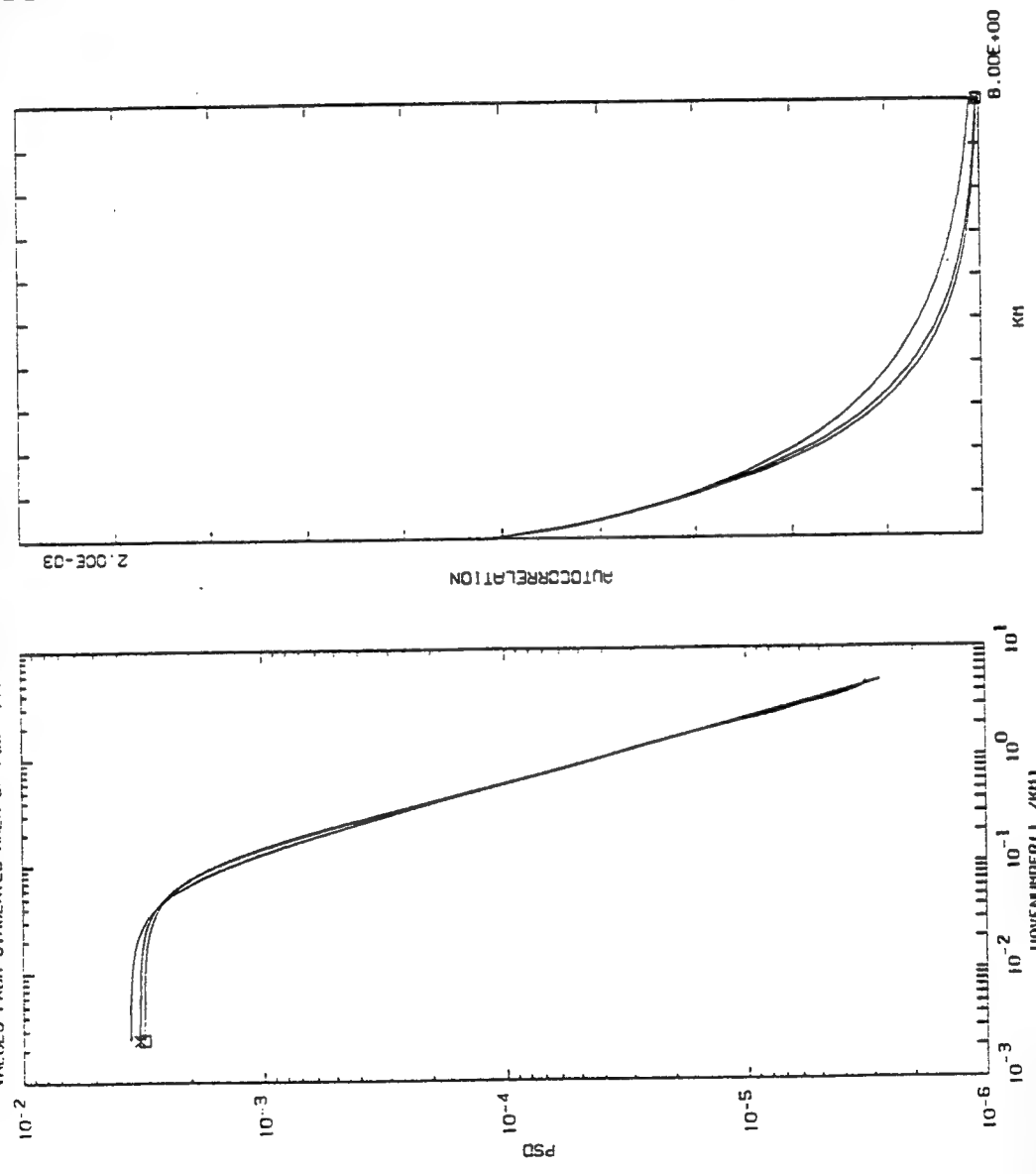


Figure 8. Left panel, theoretical PSD input (unmarked), autoregressive predictor PSD (marked by x), and simulated PSD (marked by small square). Right panel, corresponding autocorrelation functions. $L_c = 1.75$ km, $S = -5/3$, $\sigma^2 = 1.02E-03$, spacing = 100 m. Theoretical autocorrelation function modified at lag = 0. Six predictor coefficients

THIS IS FILE SIMIB 14-DEC-92 SIMULATE DATA WITH SEED=3333 NUMBER OF POINTS SIMULATED=80000 NUMBER OF VALUES IN PSD=4096
 OUTPUT FROM PROGRAM MODEL1 14-DEC-92
 PREDICTOR WAS ESTIMATED FROM PSD MODEL LC= 1.75E+00 SICHMAN=2 1.02E-03 SLOPE OF PSD=1.67 SPACING= 1.00E-01 σ = 6.79E-02
 ALL AREAS OF PSD ARE CORRECTED FOR VALUES ABOVE NYQUIST FREQUENCY IN 5.00E+00 IS 4.16E-05
 VALUES FROM ORIGINAL AREA OF PSD= 1.02E-03 LC FROM PSD= 1.75E+00 AREA OF AUTOCORRELATION= 3.77E-03 LC FROM AUTOCORRELATION= 1.04E+00
 VALUES FROM PREDICTOR AREA OF PSD= 1.07E-03 LC FROM PSD= 1.54E+00 AREA OF AUTOCORRELATION= 3.28E-03 LC FROM AUTOCORRELATION= 1.60E+00
 NUMBER OF POINTS SIMULATED=80000 AVERAGE= 3.96E-04 ESTIMATED VARIANCE= 1.02E-03

PREDICTOR VALUES
 USE 6 PREDICTOR COEFFICIENTS
 RM= 1.378470E-04

LINEAR PREDICTOR COEFFICIENTS
 1 -9.636005E-01
 2 8.958164E-02
 3 -3.511140E-02
 4 -6.827840E-03
 5 -5.614103E-03
 6 -1.353058E-02

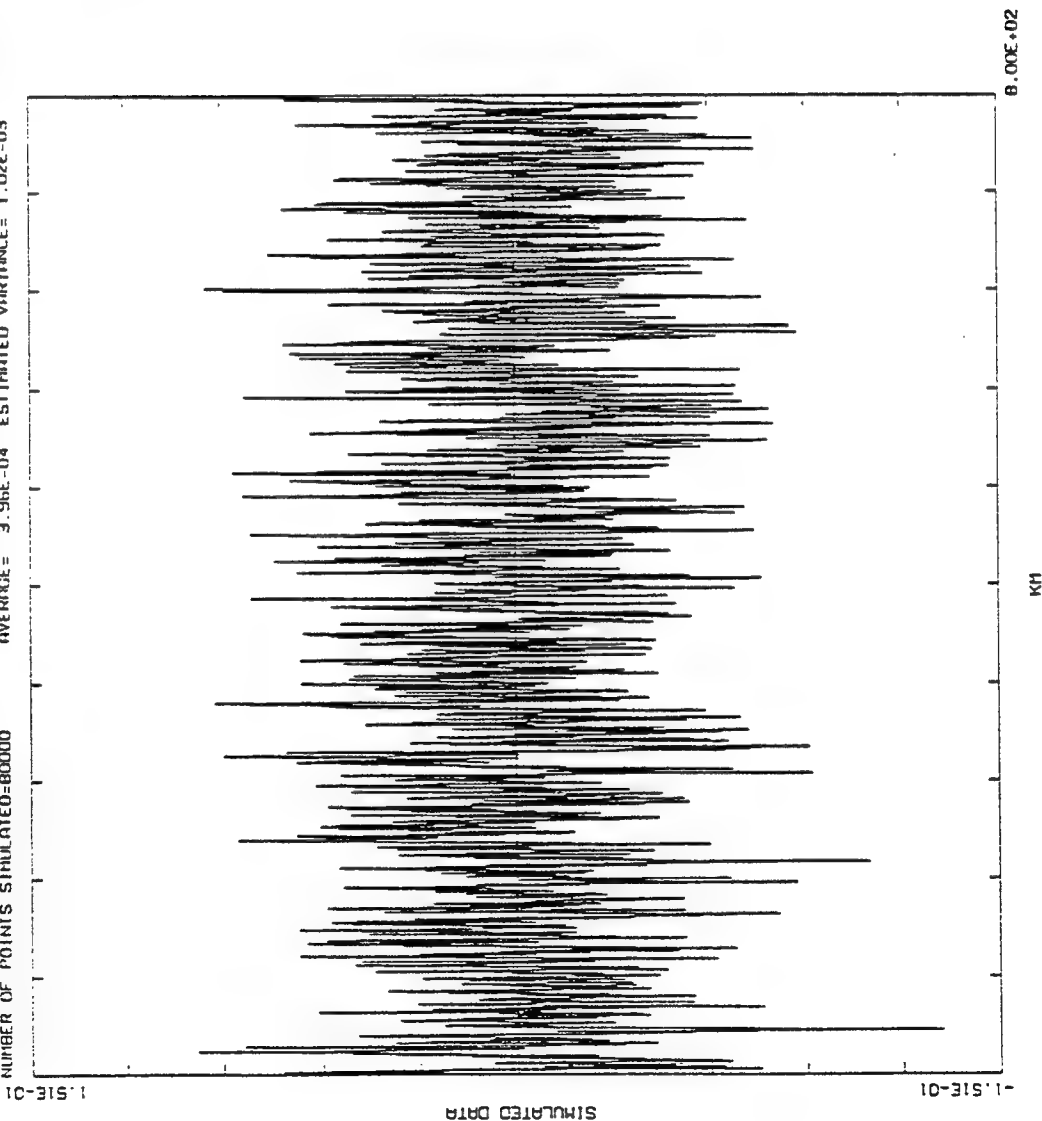


Figure 9. Autoregressive simulated structure sequence. $L_c = 1.75$ km, $S = -5/3$, $\sigma^2 = 1.02E-03$

THIS IS FILE SINIB 14-DEC-92 SIMULATE DATA WITH SEED=3333 NUMBER OF POINTS SIMULATED=80000 NUMBER OF VALUES IN PSD=4096
 OUTPUT FROM PROGRAM MODEL 14-DEC-92
 PREDICTOR WAS ESTIMATED FROM PSD MODEL LC= 1.75E+00 SIGMA=2 1.02E-03 SLOPE OF PSD=1.67 SPACING= 1.00E-01 α = 6.79E-02
 ALL AREAS OF PSD ARE CORRECTED FOR VALUES ABOVE NYQUIST FREQUENCY OF 5.00E+00 IS 4.16E-05
 VALUES FROM ORIGINAL AREA OF PSD= 1.02E-03 LC FROM PSD= 1.75E+00 AREA OF AUTOCORRELATION= 1.84E+00
 VALUES FROM PREDICTOR AREA OF PSD= 1.07E-03 LC FROM PSD= 1.54E+00 AREA OF AUTOCORRELATION= 1.60E+00

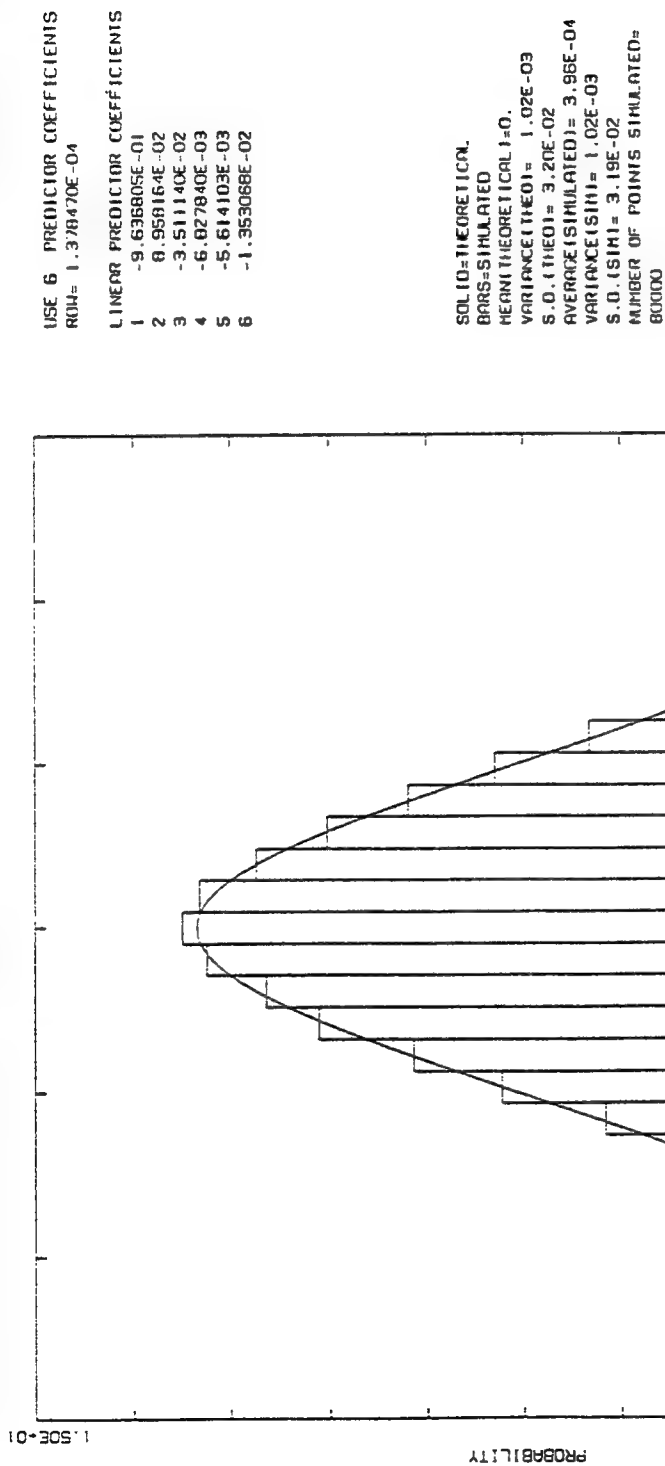


Figure 8. Histogram of autoregressive simulated structure sequence. $L_c = 1.75$ km, $S = -5/3$, $\sigma^2 = 1.02E-03$

THIS IS FILE PLOT11 2-DEC-92 OUTPUT FROM PROGRAM MODEL1 2-DEC-92 BESSEL FUNCTION USED IN CALCULATING AUTOCORRELATION
 LC= 1.75E+00 SIGMA=2 1.02E-03 SLOPE OF PSD=1.67 SPACING= 1.00E-01 A= 6.79E-02 LC FROM AUTOCORRELATION= 1.79E+00
 NUMBER OF VALUES IN FFT'S= 131072 MAXIMUM NUMBER OF LINEAR PREDICTOR COEFFICIENTS=20
 AREA OF PSD= 9.02E-04 APP CORR AREA= 4.16E-05 LC FROM PSD= 1.75E+00 AREA OF AUTOCORRELATION PREDICTOR= 2.82E-03 LC= 1.38E+00
 AREA OF P.S.D. PREDICTOR= 1.02E-03 LC= 1.38E+00
 USE 1 PREDICTOR COEFFICIENTS
 RM4= 1.385260E-04
 LINEAR PREDICTOR COEFFICIENTS
 1 -9.258511E-01
 AUTOCORRELATION VALUES
 0 1.024000E-03
 1 9.521700E-04
 2 8.803400E-04
 3 8.215800E-04
 4 7.705600E-04

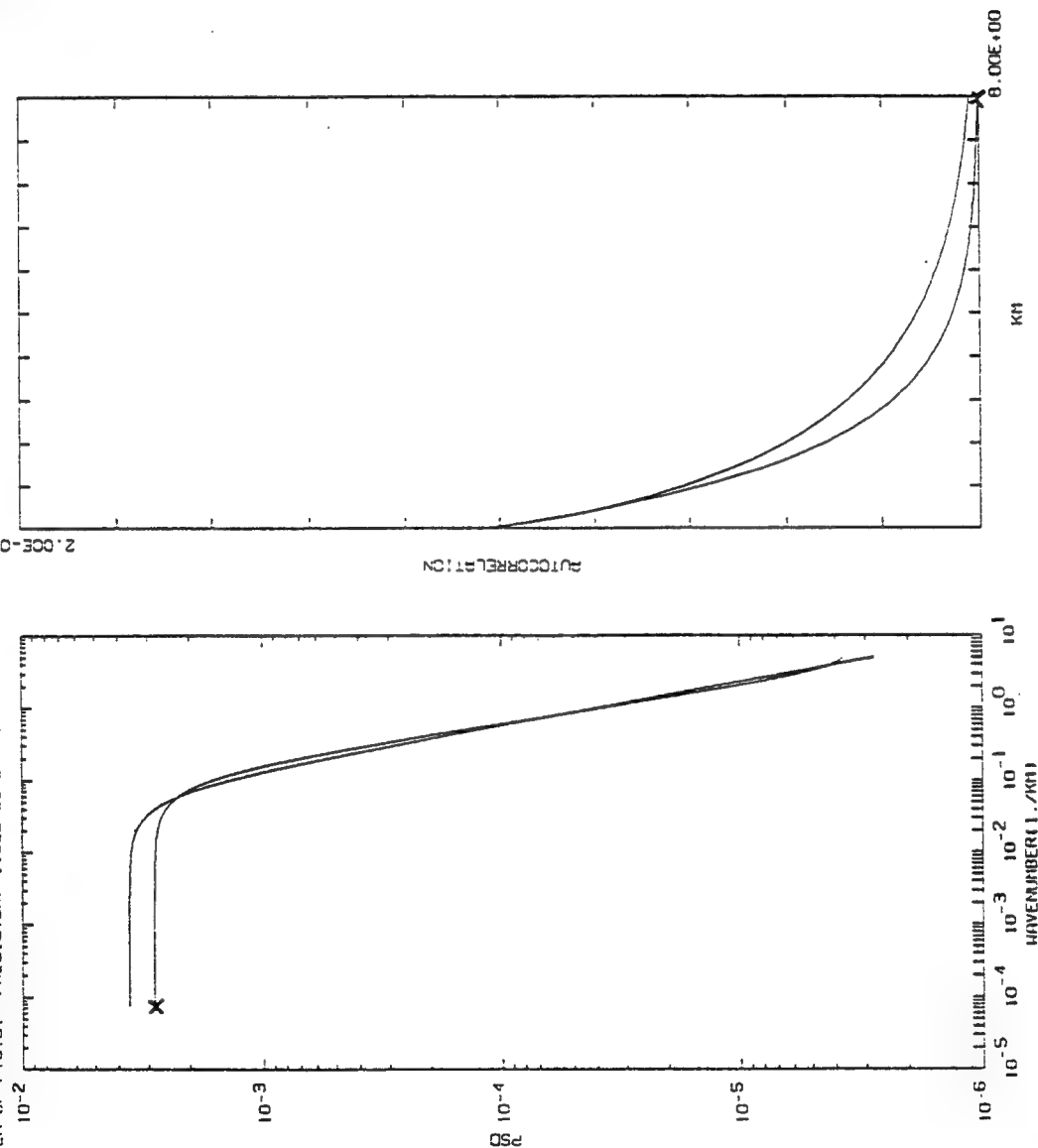


Figure 9. Left panel, theoretical PSD input (unmarked), autoregressive predictor PSD (marked by x). Right panel, corresponding autocorrelation functions. $L_c = 1.75$ km, $S = -5/3$, $\sigma^2 = 1.02E-03$, spacing = 100 m. Modified theoretical autocorrelation function at lag = 0. One predictor coefficient

```

USE MODIFIED AUTOCORRELATION
THIS IS FILE SIM18 15-DEC-92 SIMULATE DATA WITH SEED=3333 NUMBER OF POINTS SIMULATED=80000 NUMBER OF VALUES IN PSD=4096
OUTPUT FROM PROGRAM MODEL1 15-DEC-92
PREDICTOR WAS ESTIMATED FROM PSD MODEL LC= 1.00E+01 SICHM=2 4.90E-03 SLOPE OF PSD=1.67 SPACING= 1.00E-01 A= 1.19E-02
ALL AREA'S OF PSD ARE CORRECTED FOR VALUES ABOVE NYQUIST FREQUENCY OF 5.00E+00 IS 6.22E-05
VALUES FROM ORIGINAL . AREA OF PSD= 4.90E-03 LC FROM PSD= 1.00E+01 AREA OF AUTOCORRELATION= 9.95E-02 LC FROM AUTOCORRELATION= 1.02E+01
VALUES FROM PREDICTOR . AREA OF PSD= 4.96E-03 LC FROM PSD= 6.10E+00 AREA OF AUTOCORRELATION= 6.05E-02 LC FROM AUTOCORRELATION= 6.17E+00
VALUES FROM SIMULATED AREA OF PSD= 4.70E-03 LC FROM PSD= 5.69E+00 AREA OF AUTOCORRELATION= 5.44E-02 LC FROM AUTOCORRELATION= 5.76E+00
PREDICTOR VALUES X
USE 6 PREDICTOR COEFFICIENTS
ROW= 2.087145E-04

```

```

LINEAR PREDICTOR COEFFICIENTS
1 -9.853112E-01
2 7.993979E-02
3 -3.613644E-02
4 -9.537014E-03
5 -6.781318E-03
6 -2.359872E-02

```

```

SIMULATED VALUES Q
USE 12 PREDICTOR COEFFICIENTS
ROW= 2.077609E-04

```

```

LINEAR PREDICTOR COEFFICIENTS
1 -9.888303E-01
2 7.915045E-02
3 -3.562645E-02
4 -6.731728E-03
5 -8.639864E-03
6 -2.142172E-02
7 3.488553E-03
8 2.014051E-03
9 -9.337268E-04
10 -9.007721E-03
11 8.244855E-03
12 -2.117735E-03

```

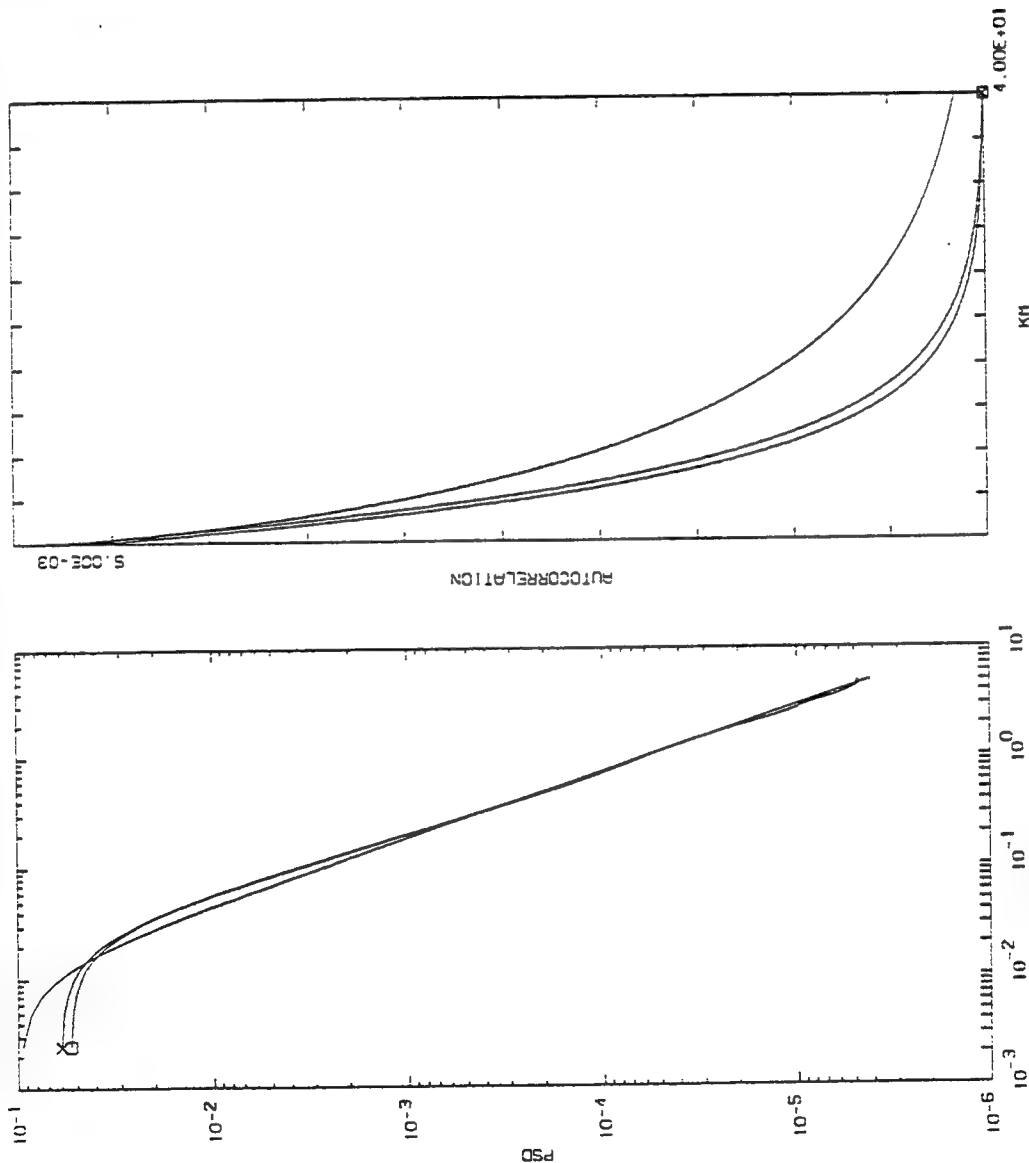


Figure 12. Left panel, theoretical PSD input (unmarked), autoregressive predictor PSD (marked by x), and simulated PSD (marked by small square). Right panel, corresponding autocorrelation functions. $L_c = 10$ km, $S = -5/3$, $\sigma = 4.9E-03$, spacing = 100 m. Theoretical autocorrelation function modified at lag = 0. Six predictor coefficients

USE MODIFIED AUTOCORRELATION
 THIS IS FILE SIM10 15-DEC-92 SIMULATE DATA WITH SEED=3333 NUMBER OF POINTS SIMULATED=80000 NUMBER OF VALUES IN PSD=4096
 OUTPUT FROM PROGRAM MODEL1 15-DEC-92
 PREDICTOR WAS ESTIMATED FROM PSD MODEL LC= 1.00E+01 SIGMA=2 4.90E-03 SLOPE OF PSD=1.67 SPACING= 1.00E-01 A= 1.19E-02
 ALL AREA'S OF PSD ARE CORRECTED FOR VALUES ABOVE NYQUIST FREQUENCY OF 5.00E+00 IS 6.22E-05
 VALUES FROM ORIGINAL AREA OF PSD= 4.90E-03 LC FROM PSD= 1.00E+01 AREA OF AUTOCORRELATION= 9.95E-02 LC FROM AUTOCORRELATION= 1.02E+01
 VALUES FROM PREDICTOR AREA OF PSD= 4.96E-03 LC FROM PSD= 6.10E+00 AREA OF AUTOCORRELATION= 6.05E-02 LC FROM AUTOCORRELATION= 6.17E+00
 NUMBER OF POINTS SIMULATED=80000 AVERAGE= 1.71E-03 ESTIMATED VARIANCE= 4.70E-03

PREDICTOR VALUES
 USE 6 PREDICTOR COEFFICIENTS
 ROH= 2.087145E-04

LINEAR PREDICTOR COEFFICIENTS

1	-9.853112E-01
2	7.993979E-02
3	-3.613644E-02
4	-9.537014E-03
5	-6.781318E-03
6	-2.359872E-04

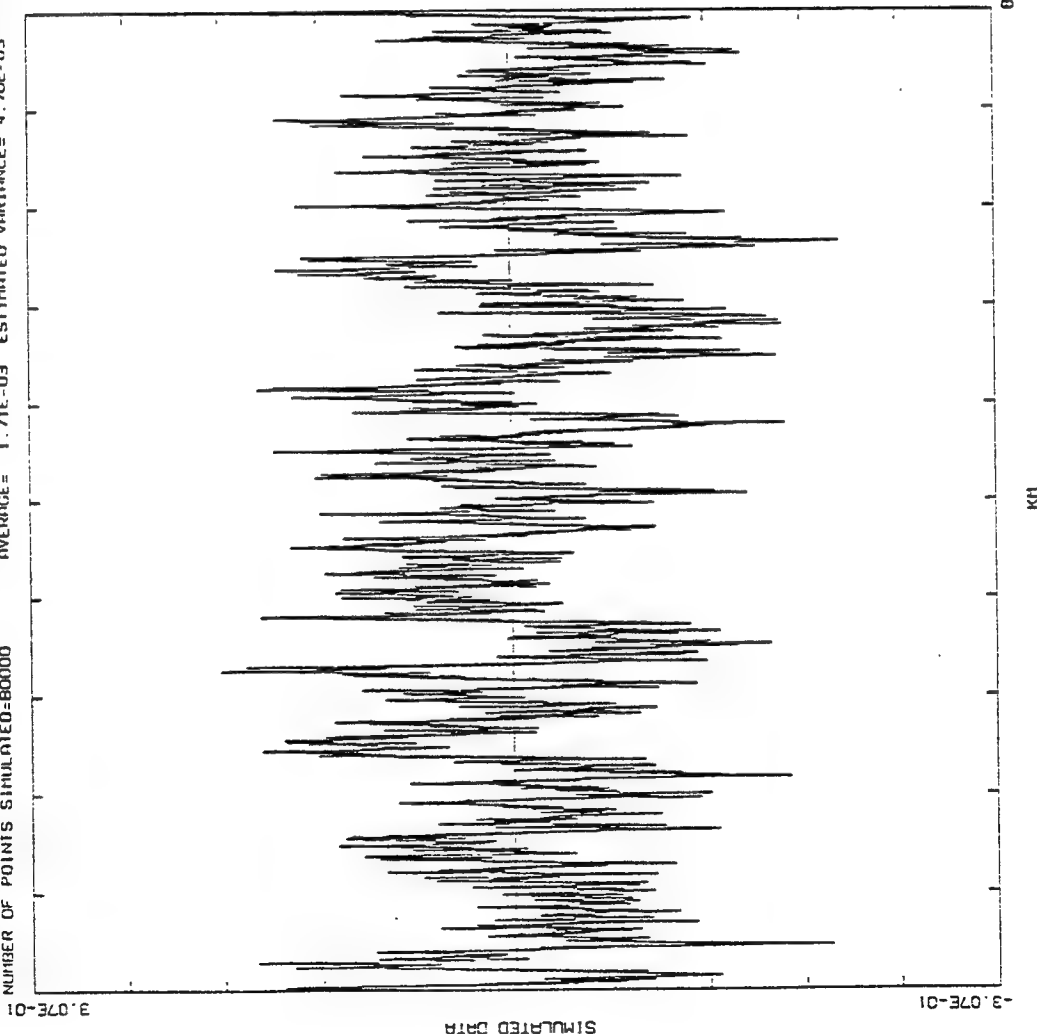


Figure 13. Autoregressive simulated structure sequence. $L_c = 10$ km, $S = -5/3$, $\sigma^2 = 4.9E-03$

Conclusions

- Autoregressive analysis accurately models common 1-D PSD's
- 6-20 coefficients are sufficient in most cases
- Spatial resolution good to 100m
- AR modelling preserves slope, coherence length, variance, and PDF
- AR requires less computer resources (15x)
- AR adaptable to non-stationary case and multidimensional simulation



Yule Walker Equations

$$r_{xx}(m) = \begin{cases} -\sum_{k=1}^p a(k)r_{xx}(m-k) & \text{for } m > 0 \\ -\sum_{k=1}^p a(k)r_{xx}(-k) + p_w & \text{for } m = 0 \\ r_{xx}^*(-m) & \text{for } m < 0 \end{cases}$$

$$\begin{pmatrix} r_{xx}(0) \\ r_{xx}(1) \\ \vdots \\ r_{xx}(p) \end{pmatrix} \begin{pmatrix} r_{xx}(-1) & \dots & r_{xx}(-p) \\ r_{xx}(0) & \dots & r_{xx}(-p+1) \\ \vdots & \ddots & \vdots \\ r_{xx}(p-1) & \dots & r_{xx}(0) \end{pmatrix} \begin{pmatrix} 1 \\ a(1) \\ \vdots \\ a(p) \end{pmatrix} = \begin{pmatrix} p_w \\ 0 \\ \vdots \\ 0 \end{pmatrix}$$

Levinson Recursion Algorithm

$$a_k[k] = - \frac{r_{xx}[k] + \sum_{\ell=1}^{k-1} a_{k-1}[\ell] r_{xx}[k-\ell]}{\rho_{k-1}}$$

$$a_k[i] = a_{k-1}[i] + a_k[k] a_{k-1}^*[k-i] \quad i = 1, 2, \dots, k-1$$

$$\rho_k = (1 - |a_k[k]|^2) \rho_{k-1}$$

with ,

$$a_1[1] = - \frac{r_{xx}[1]}{r_{xx}[0]}$$

$$\rho_1 = (1 - |a_1[1]|^2) r_{xx}[0]$$

3

PSD of Simulated Series

$$\text{PSD}(f) = \frac{2\sigma_c^2 \Delta x}{\left| 1 + \sum_{i=1}^{NN} b_i e^{j2\pi f \Delta x} \right|^2}$$

Minimize ERR,

$$\text{ERR} = \left(\sum_{j=NN+1}^M \left(Y(j) - \sum_{i=1}^{NN} b_i Y(j-i) \right)^2 \right) + \left(\sum_{j=1}^{M-NN} \left(Y(j) - \sum_{i=1}^{NN} b_i Y(j+i) \right)^2 \right)$$

$$\sigma_c^2 = \frac{\text{ERR}}{2(M-NN)}$$



AN UPDATE ON THE AFGL OPTICAL TURBULENCE RADIOSONDE MODEL

Edmond M. Dewan

Phillips Laboratory/ Geophysics
29 Randolph Road
Hanscom AFB, MA 01731-3010

Recently the AFGL C_N^2 model has been applied by Lt Col Roadcap of Phillips Lab (at Kirtland AFB) to radiosonde data for the purpose of estimating the effects of turbulence on an AF Airborne Laser Weapon System (ABL). This had the effect of bringing new attention to this model developed some years ago by Dewan, Good, Beland, and Brown*. While it is true that our model has been described in the open literature, these descriptions left out of account certain important items of interest. The purpose of this talk will be to make these available prior to their publication. (An in-house report is in press). These include (a) the basis of the model and how it was constructed, (b) the estimated uncertainty of its predictions, and (c) potential pitfalls in its use. An alternate (NOAA) model exists and comparisons will be made between it and the AFGL Model. Briefly, in contrast to the NOAA model, the AFGL model is (a) an order of magnitude simpler (i.e. faster), (b) has no "adjustable parameters" (site location dependence), and (c) it may possibly be more reliable in its application to the ABL program.

It has been indicated, with the help of this model, that jet streams may play an important role in how any future ABL system might be operated.

*In house report in press "A Model for C_N^2 (Optical Turbulence) Profiles Using Radiosonde Data".

**AN UPDATE ON THE AFGL
OPTICAL TURBULENCE RADIOSONDE MODEL***

**E.M. DEWAN, GPOS
SOAR/AFOSR**

*** DEWAN, GOOD, GROSSBARD, AND BROWN**

LASER BEAM PROBLEMS CAUSED BY TURBULENCE

- BEAM SPREADING
- BEAM STEERING
- COHERENCE DEGRADATION
- SCINTILLATIONS OF INTENSITY ("TWINKLING")
 - FLUCTUATIONS ACROSS BEAM WIDTH
 - FLUCTUATIONS IN TIME
- PHASE FLUCTUATIONS

SOLUTION: ADAPTIVE OPTICAL COMPENSATION SYSTEMS

ROLE OF C_N^2 IN OPTICAL TURBULENCE EFFECTS ON LASER BEAM PROPAGATION

- COHERENCE LENGTH, " r_o ":

"PLANE WAVE
APPROXIMATION"

$$r_o \sim \left[\int C_N^2(z) dz \right]^{-3/5}$$

- ISOPLANATIC ANGLE, " θ_o ":

$$\theta_o \sim \left[\int C_N^2(z) z^{5/3} dz \right]^{-3/5}$$

- SCINTILLATION PARAMETER:

$$\sigma_x^2 \equiv \left\langle \left[\ln \frac{A}{A_o} \right]^2 \right\rangle \sim \int C_N^2(z) z^{5/6} dz$$

KEY EQUATION*

$$C_N^2 = 2.8 M^2 L^{4/3}$$

$$M^2 = \left[\left(\frac{79 \times 10^{-6} P}{T^2} \right) \left(\frac{dI}{dz} + \gamma \right) \right]^2$$

$$P \text{ (mb)}, T \text{ (°K)}, \gamma = 9.8 \times 10^{-3} \text{ (°K/m)}$$

* [TATARSKI]

SEE "TUTORAL"

TURBULENT BREAKDOWN AND L

(MILES)

$$Ri \equiv \frac{N^2}{S^2} < 0.25$$

$$S \equiv \left[\left(\frac{dV_N}{dz} \right)^2 + \left(\frac{dV_E}{dz} \right)^2 \right]^{1/2}$$

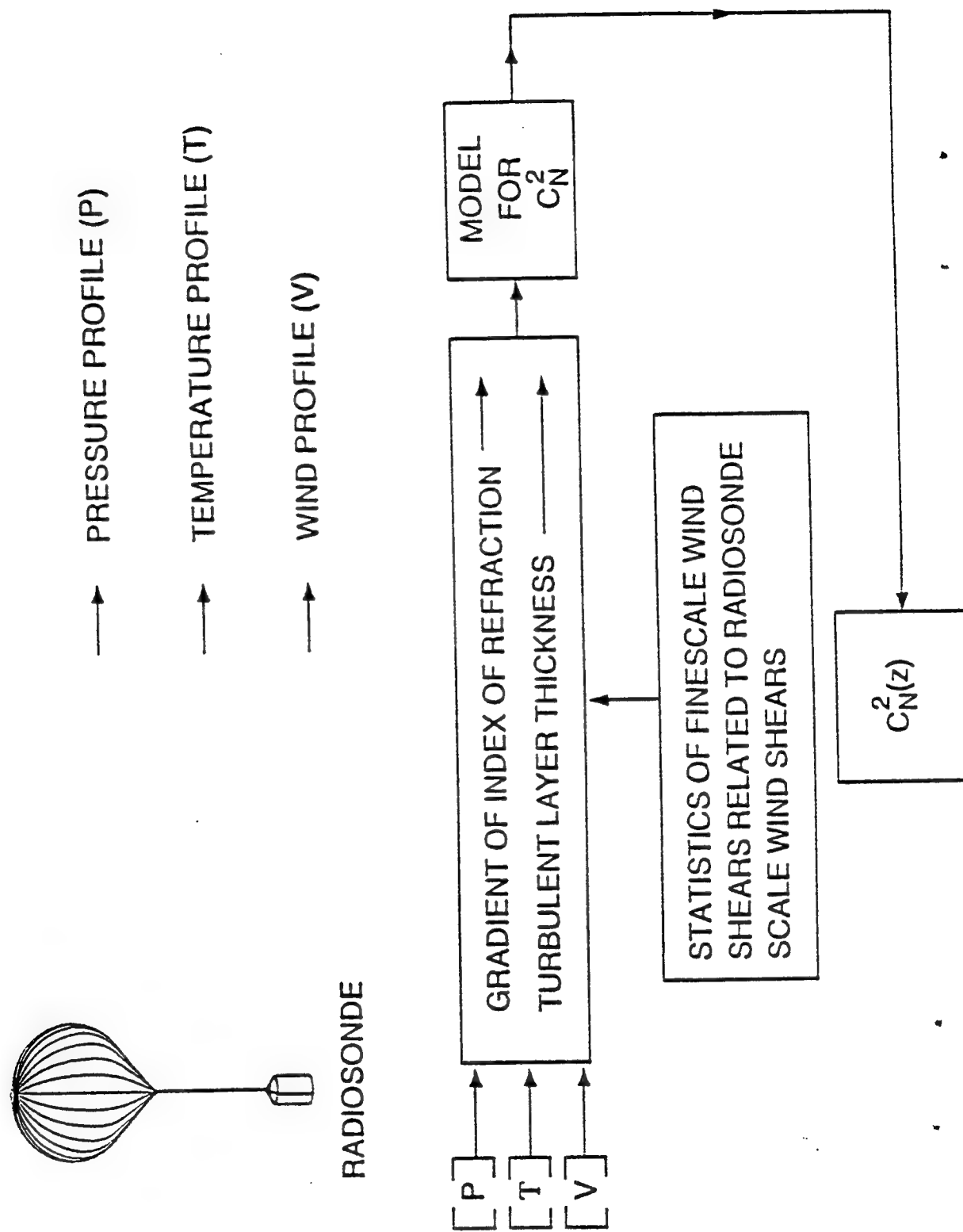
DEFINITION OF SHEAR, OR "S"

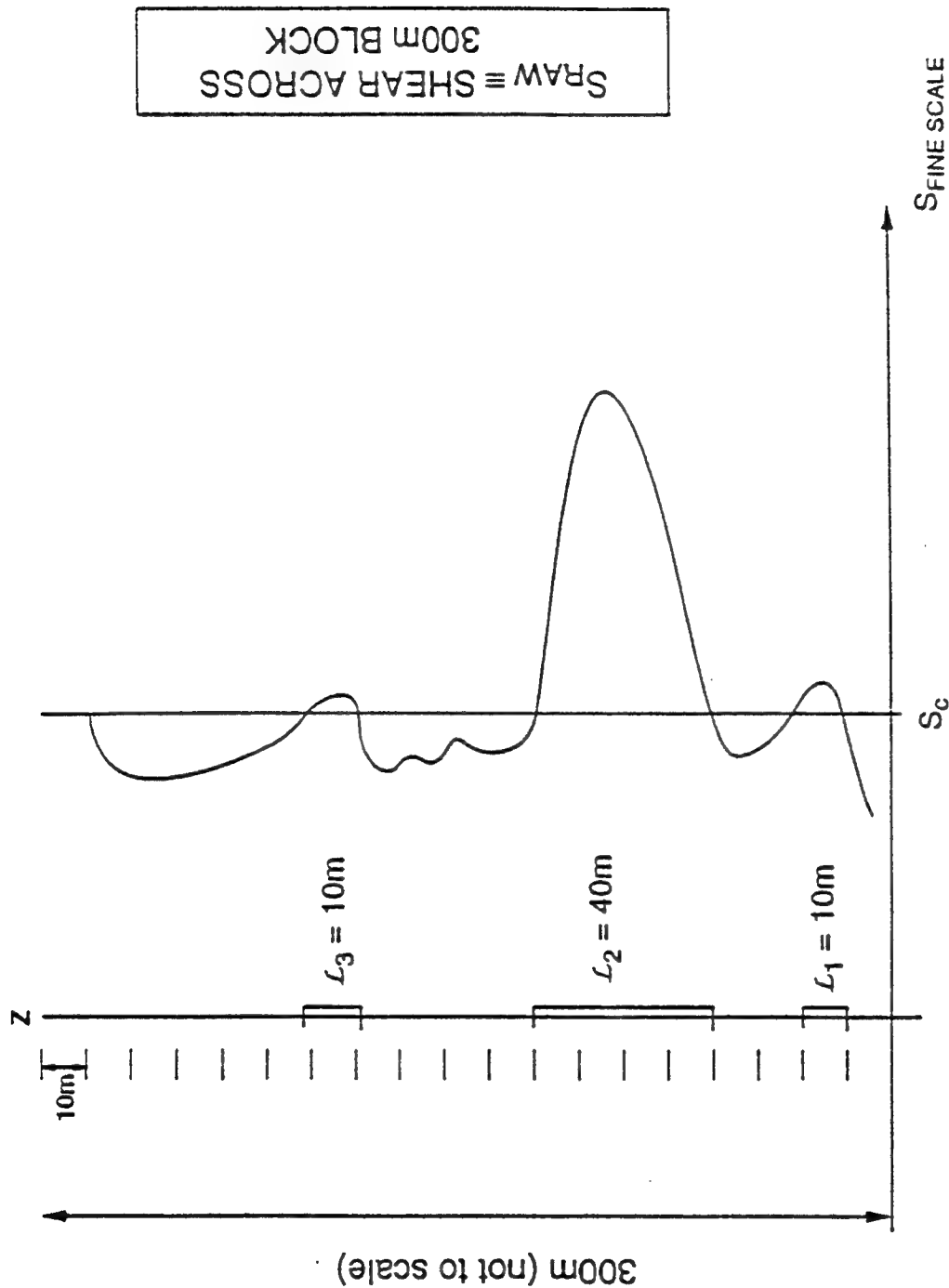
SHEAR ≥ 0.5 DEFINES
LAYER THICKNESS, L AND

$$L = \frac{1}{10} L$$

1 HOUR (LATER)

HOW TO DERIVE $C_N^2(z)$ (OPTICAL TURBULENCE PROFILES) FROM RADIOSONDES?



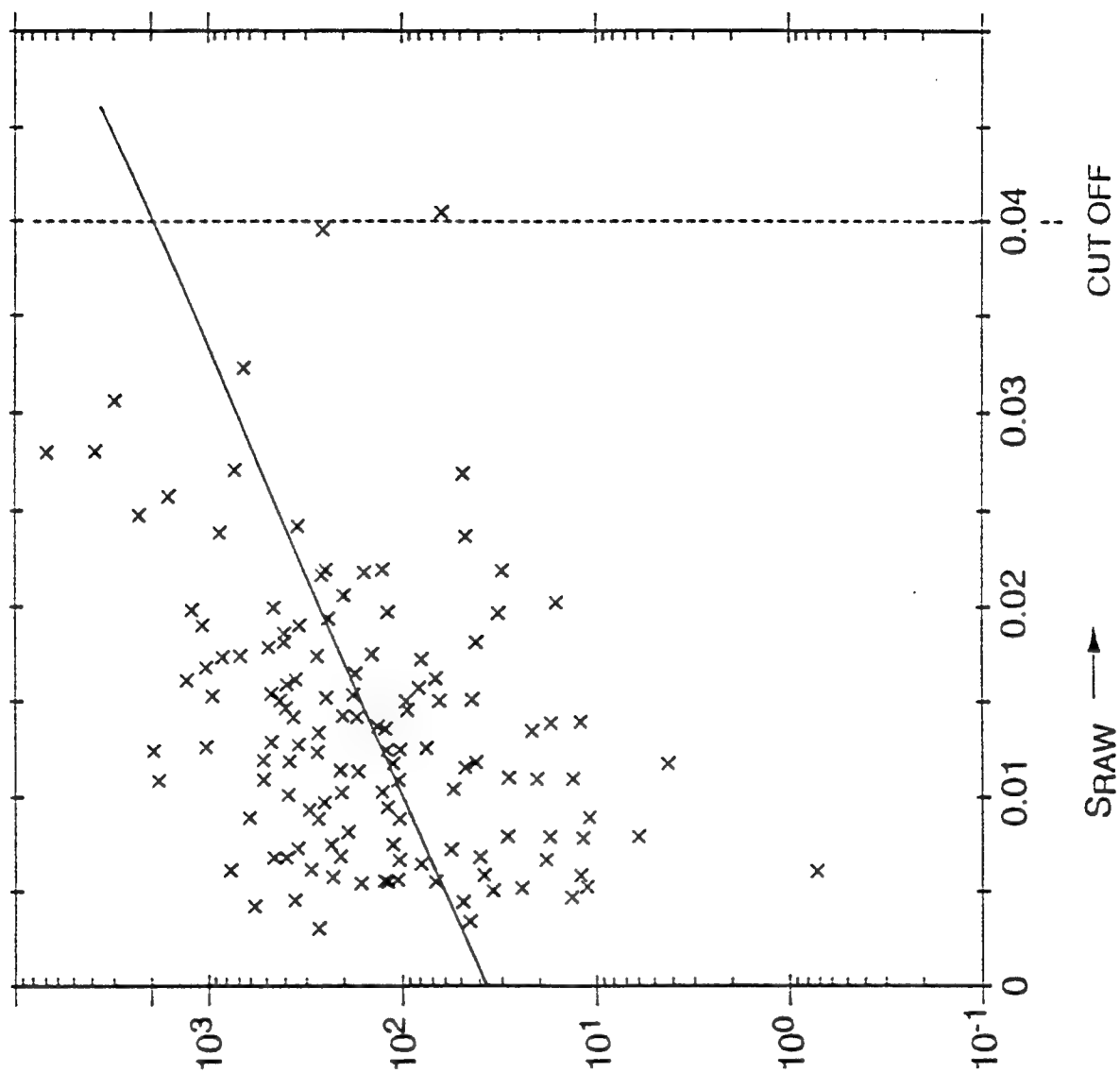


10 M
STRAT.
WINDS

$$\langle L_i^{4/3} \rangle \equiv \sum L_i^{4/3} \quad (L_i/290)$$

VS
SRAW

TROPOSPHERE



$$Y \equiv \text{Log} < (L_1)^{4/3} >$$

$$Y = \text{CONST.} + (\text{SLOPE}) S_{\text{RAW}}$$

MODELS USED

TROPOSPHERE:

$$Y = 1.57 + 40.0 S_{\text{RAW}}$$

STRATOSPHERE:

$$Y = 0.503 + 51.2 S_{\text{RAW}}$$

FINAL EQUATION

$$C_N^2 = 2.8 (0.1)^{4/3} M^2 10^Y$$

RADIOSONDE PROVIDES M^2 AND S_{RAW}

ERROR BARS ON C_N^2 MODEL

$$Y = 0.5 + 50 S_{\text{RAW}} \quad \text{AND} \quad \sigma_{\text{CONST.}} = 6 \times 10^{-2} \quad \sigma_{\text{SLOPE}} = 6.9$$

$$\therefore Y = 0.5 \pm (.06) + (50 \pm 7) S_{\text{RAW}}$$

$$\text{SET} \quad S_{\text{RAW}} = 0.025^{-1}$$

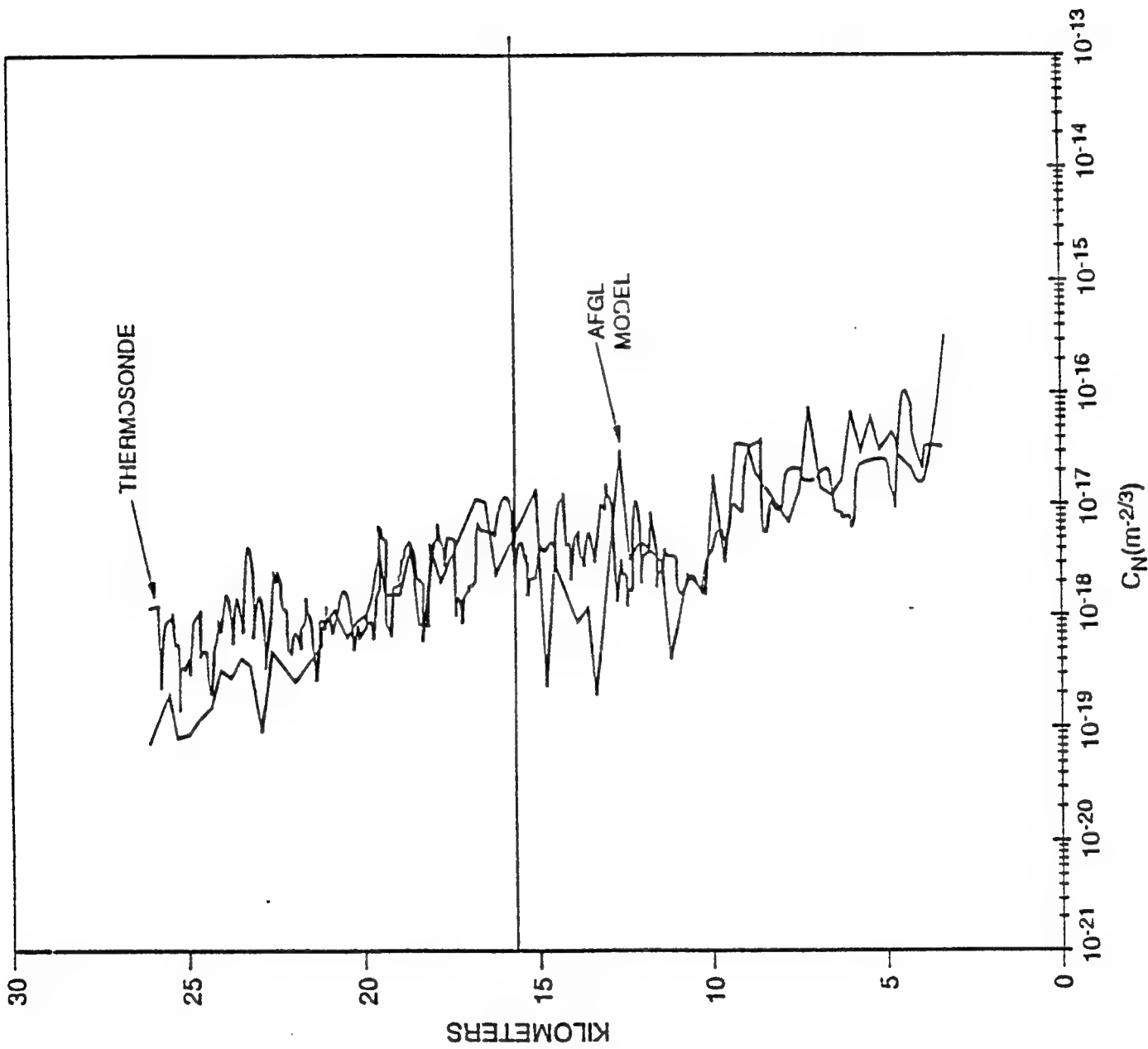
$$Y_{\text{MIN}} = 1.3, \quad Y_{\text{MEAN}} = 1.5, \quad Y_{\text{MAX}} = 1.7 \quad \text{ie} \quad Y = 1.5 \pm 0.2$$

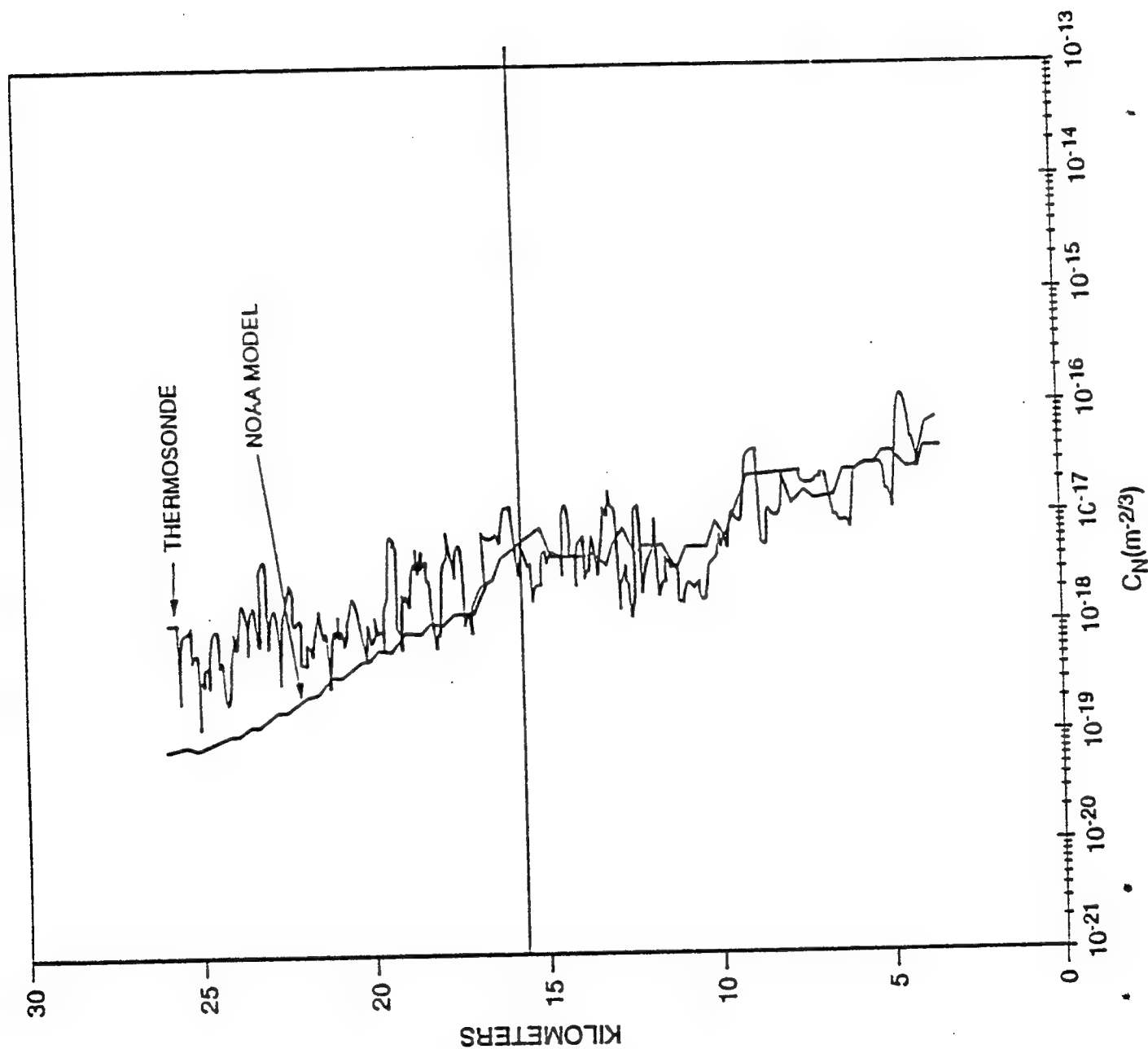
$$C_N^2 \sim 10^{Y_{\text{MEAN}}} X \div 10^{0.2}$$

$$C_N^2 \sim C_{N \text{ MEAN}}^2 X \div \underline{1.6}$$

SIMILARLY AT $S_{\text{RAW}} = 0.04 \text{ s}^{-1}$ (VERY RARE)

$$C_N^2 \sim C_{N \text{ (MEAN)}}^2 X \div \underline{2.2}$$





ROADCAP, VECTOR VIEW (1963) WL 6 #2, P.4.

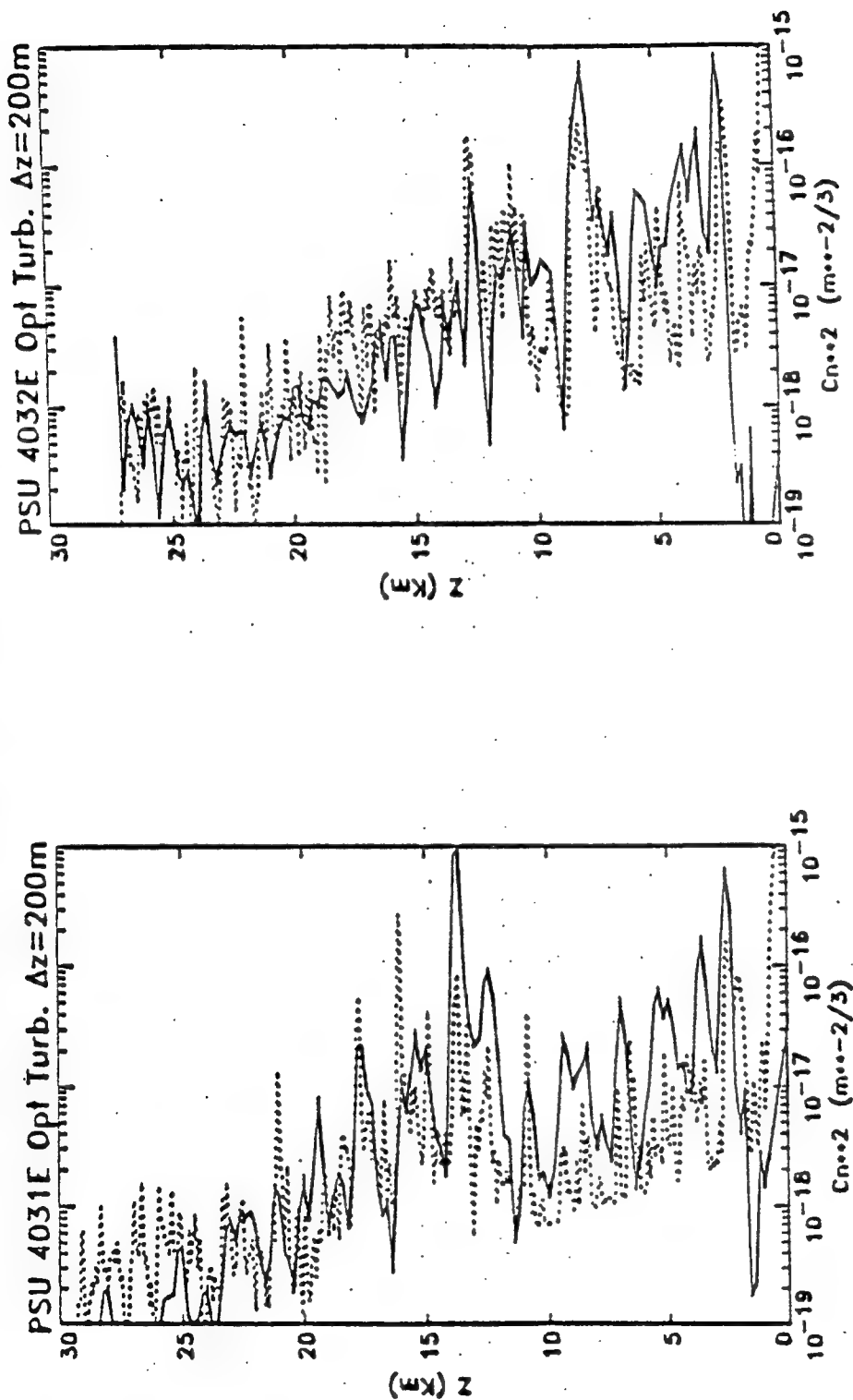


FIGURE 2: COMPARISONS OF OBSERVED C_n^{**2} (dashed line) vs. modeled C_n^{**2} (solid line) profiles in Pennsylvania using the Phillips Lab C_n^{**2} model developed by Dewan et. al of the Geophysics Directorate. Dewan's model needs only routinely-measured rawinsonde data such as pressure, temperature, and wind velocity and specification of tropopause height. This optical turbulence model shows promise for determining free atmospheric conditions affecting vertical laser propagation without using specialized instrumentation.

THE FIGURES OF MERIT ARE BASED ON:

- ISOPLANATIC ANGLE

$$\theta_{o_{\text{rad}}} \equiv \left\{ 2.91 k_{\text{op}}^2 \int_{z_1}^{z_2} C_N^2(z) z^{5/3} dz \right\}^{-3/5}$$

- SCINTILLATION VARIANCE

$$\sigma_{\chi}^2 \equiv \left\langle \ln \left(\frac{A}{A_o} \right)^2 \right\rangle \approx 0.56 k_{\text{op}}^{7/6} \int_{z_1}^{z_2} C_N^2(z) z^{5/6} dz$$

THEY ARE:

- $Z^{5/3} \equiv \int_{z_{\text{min}}}^{z_{\text{max}}} C_N^2(z) z^{5/3} dz$

- $Z^{5/6} \equiv \int C_N^2(z) z^{5/6} dz$

1. $A_{\text{FGL}} \approx \text{NOAA}$
2. UPDATE : DAYTIME STRATOSPHERIC THERMOSONDE DATA IS NOT VALID.

15

EFFECTS OF "BLINI" GEOMETRY OF ATMOSPHERIC TURBULENCE UPON HORIZONTAL LASER BEAM PROPAGATION

- LONG PATHS (10's OF km) THROUGH RELATIVELY HOMOGENIOUS LAYERS
OF TURBULENCE
- EFFECTS OF REFLECTIONS FROM HORIZONTAL DISCONTINUITIES
- EARTH CURVATURE EFFECTS

CONCLUSIONS

- USE OF AFGL MODEL FOR HORIZONTAL BEAM PROPAGATION MUST TAKE INTO ACCOUNT THE EFFECTS OF CHANGES IN GEOMETRY FROM THE ORIGINAL APPLICATION – VALIDATION (VERTICAL).
- THE AFGL MODEL IS ABOUT 10 TIMES FASTER THAN THE NOAA MODEL AND IS POTENTIALLY AS RELIABLE OR MORE RELIABLE FOR MODELING C_N^2 PROFILES. THIS SHOULD BE INVESTIGATED FURTHER.
- THIS MODEL IS DESIGNED FOR USE WITH STANDARD RADIOSONDE RESOLUTION (IN CONTRAST TO HIGH RESOLUTION RADIOSONDES). THEREFORE, GLOBAL ASSESSMENT OF ATMOSPHERIC TURBULENCE EFFECTS ON ABL SYSTEMS ARE ARE POSSIBLE FROM EXISTING PUBLISHED DATA.

REFERENCES

- "A MODEL FOR C_N^2 (OPTICAL TURBULENCE) PROFILES USING RADIOSONDE DATA" IN PRESS - PL REPT.) DEWAN, GOOD, GROSSBARD, BELAND, BROWN
- "STUDY OF POSSIBLE SOLAR HEATING EFFECTS ON THERMOSONDE PROBES..." BROWN, DEWAN, MURPHY, THOMAS GL-TR-89-0178 (1989)
- "OPTICAL TURBULENCE FORECASTING..." DEWAN, AFGL-TR-80-0030 (1980)

A NIGHTTIME STRUCTURE MODEL OF ATMOSPHERIC OPTICAL
TURBULENCE, C_N^2 DERIVED FROM THERMOSONDE AND
HIGH RESOLUTION RAWINSONDE MEASUREMENTS

James H. Brown

Phillips Laboratory/ Geophysics
29 Randolph Road
Hanscom AFB, MA 01731-3010

Data from fifteen thermosonde flights was used to develop a simple nighttime structure model of C_N^2 . High resolution rawinsondes provide fine scale estimates of atmospheric temperature gradients and variances of wind speed. Non-linear regression applied between the thermosonde and rawinsonde measurements provide the model C_N^2 estimator. This quasi-empirical model is based upon the theoretical description given by Tatarski and upon an exponentially scaled estimate of a theoretical model of the eddy dissipation rate given by Weinstock. A discussion of previous models and a comparison with the Dewan et.al. microshear model is presented. Model profiles computed for other sites and seasons is compared favorably to related thermosonde profiles.

A Nighttime Structure Model of Atmospheric Optical Turbulence C_n^2 , Derived from Thermosonde and High Resolution Rawinsonde Measurements

James H. Brown

Figure Captions

1. Turbulence Structure Constant equation. C_n^2 depends on temperature fluctuations C_t^2 .
2. C_n^2 Hufnagel model. C_n^2 expressed as a function of altitude and RMS wind speed only.
3. NOAA C_n^2 model. C_n^2 expressed as function of statistical distributions of Brunt-Vaisalla frequency, wind shear, and outer scale.
4. The Dewan et.al. model. C_n^2 expressed as function of outer scale where outer scale is modeled after high resolution wind shears.
5. Thermosonde model. C_n^2 expressed as function of Brundt-Vaisalla frequency and outer scale. Outer scale modeled after thermosonde measurements.
6. Thermosonde Model 1 and Model 2 expressions. Outer scale expressed as functions of RMS wind speed and Brundt-Vaisalla frequency.
7. Final Form of expression for outer scale model. Ratio of scaled wind speed variance and Brundt-Vaisalla frequency.
8. Thermosonde Profiles measured at Pennsylvania State University, Flight L4007, May 4, 1986, Temperature, Relative Humidity, C_n^2 , Wind Speed, Wind Direction.
9. Thermosonde C_t^2 measurement (raw and smoothed) profiles compared to model (1) C_t^2 profile. Flight L4007.
10. Binned scatter plot of data from entire Pennsylvania State University campaign. "L" for smoothed thermosonde measurements compared with "L" from model (1). A 45 degree slope represents perfect agreement. Error bars represent the standard deviation of the data in each bin. Numbers above the plots are the number of points falling outside three standard deviations. Left-hand plot is troposphere. Right-hand plot is stratosphere.
11. Regression constants for Model (1) and Model (2).

12. Thermosonde Profiles measured at Champaign, Illinois Flight L1014, June 1988.
13. Thermosonde C_t^2 measurement (raw and smoothed) profiles compared to model (1) C_t^2 profile. Flight L1014
14. Outer scale - smoothed thermosonde data compared to model.
15. Smoothed shear profile as determined by Dewan's application.
16. Thermosonde C_t^2 measurement (raw and smoothed) profiles compared to Dewan, et.al. C_t^2 model profile. Flight L4007.
17. $L(z)$ from smoothed thermosonde data compared to Dewan, et.al. $L(z)$ model profile. Flight L4007.
18. Brunt-Vaisala frequency and RMS wind speed profiles derived from smoothed measurement compared with Dewan et.al. model C_n^2 profile. Flight L4007.
19. Scatter plot of "L" for smoothed thermosonde measurements compared with "L" from Dewan, et.al. model. Flight L4007. Leftmost plot for troposphere. Rightmost plot for stratosphere.
20. Isoplanatic Angle expressed as function of C_n^2 and altitude.
21. Isoplanatic angle calculations for Pennsylvania State University Campaign. Comparison of measurement to model.
22. Dewan et. al. model. Isoplanatic angle calculations. Comparison of measurement to model.
23. Isoplanatic angle calculations for Pennsylvania State University Campaign, Champaign, Ill Campaign, and Desert Site Campaigns. Comparison of measurements to model.
24. Conclusions. Self-descriptive.

FIG. 1

Thermosonde Structure Constant Measurement

$$C_n^2 = \left(79.9 \times 10^{-6} \frac{P}{T^2} \right)^2 C_t^2$$



Hufnagel Model

$$C_n^2(\tilde{h}) = 8.2 \times 10^{-56} U^2 \tilde{h}^{10} e^{-\left(\frac{\tilde{h}}{1000}\right)} + 2.7 \times 10^{-16} e^{-\left(\frac{\tilde{h}}{1500}\right)}$$

$\tilde{h} \equiv$ meters above sea level

$U \equiv$ root-mean-square wind speed 5 to 20 Km

NOAA Model

$$\bar{C}_n^2(\text{dry}) = C_1 M_0^2 \int_{L_{\min}}^{L_{\max}} dL p_L L^{4/3} \int_0^\infty dS p_s \int_{-\infty}^{S^2 R_{ic}} dN^2 p_N (N^2)^2$$

$$C_1 = 2.8, \quad M_0 = C_2 \frac{P}{gT}, \quad C_2 = -77.6 \times 10^{-6}$$

P \equiv pressure T \equiv temperature

p_L, p_S, p_N \equiv prob dist of L, S, N

Dewan et. al. Model

$$C_n^2 = 2.8 M^2 L^{4/3}, \quad M = -79 \times 10^{-6} \frac{PN^2}{gT}$$

$$\text{Log}_{10} [L(z)] = -1 + \frac{3}{4} Y(z)$$

$$Y(z) = C_1 + C_2 S(z)$$

or

$$L(z) = 1.5 e^{51.15 S(z)}$$

troposphere

$$L(z) = .24 e^{63.92 S(z)}$$

stratosphere

Thermosonde Model

$$C_n^2 = 2.8 [M(z)]^2 [L(z)]^{4/3}$$

$$M(z) = -79 \times 10^{-6} \frac{P(z) \omega_B^2(z)}{g \Gamma(z)}$$

$$\omega_B^2 = \frac{g}{T(z)} \left(\frac{dT(z)}{dz} + \Gamma \right) \quad \Gamma = 0.0098$$

$$L_{\text{thermosonde}} = \left(\frac{C_1^2(\text{smooth})}{2.8 \times \left(\frac{T \omega_B^2}{g} \right)^2} \right)^{3/4}$$

FIG 5

Model 1

$$\text{Log}_{10}(\text{L}) = a_1 + a_2 \text{Log}_{10}(\sigma_v^2) + a_3 \text{Log}_{10}(\omega_B + a_4)$$

Model 2

$$\text{Log}_{10}(\text{L}) = b_1 + b_2 \text{Log}_{10}\left(\frac{\sigma_v^2}{\sigma_v^2}\right) + b_3 \text{Log}_{10}\left(\frac{\omega_B + b_4}{\omega_B}\right)$$

$$\sigma_{v,\text{est}}^2 = \frac{\sum (\text{v} - \bar{\text{v}}_{150})^2 \times \text{Weight}_{\text{triang}}}{\sum \text{Weight}_{\text{triang}} \text{ over } 150 \text{ m}}$$

Final Form

$$L = 10^{a_1} \frac{(\sigma_v^2)^{a_2}}{(\omega_B + a_3)^{a_4}}$$

540

$$L_0 \propto \varepsilon^2 \omega_B^{\frac{1}{2} - \frac{3}{2}} \propto \varepsilon^{1/2} \sqrt{v'^2} \omega_B^{1/2}$$

$$L_0 \propto \frac{\sqrt{v'^2}}{\omega_B}$$

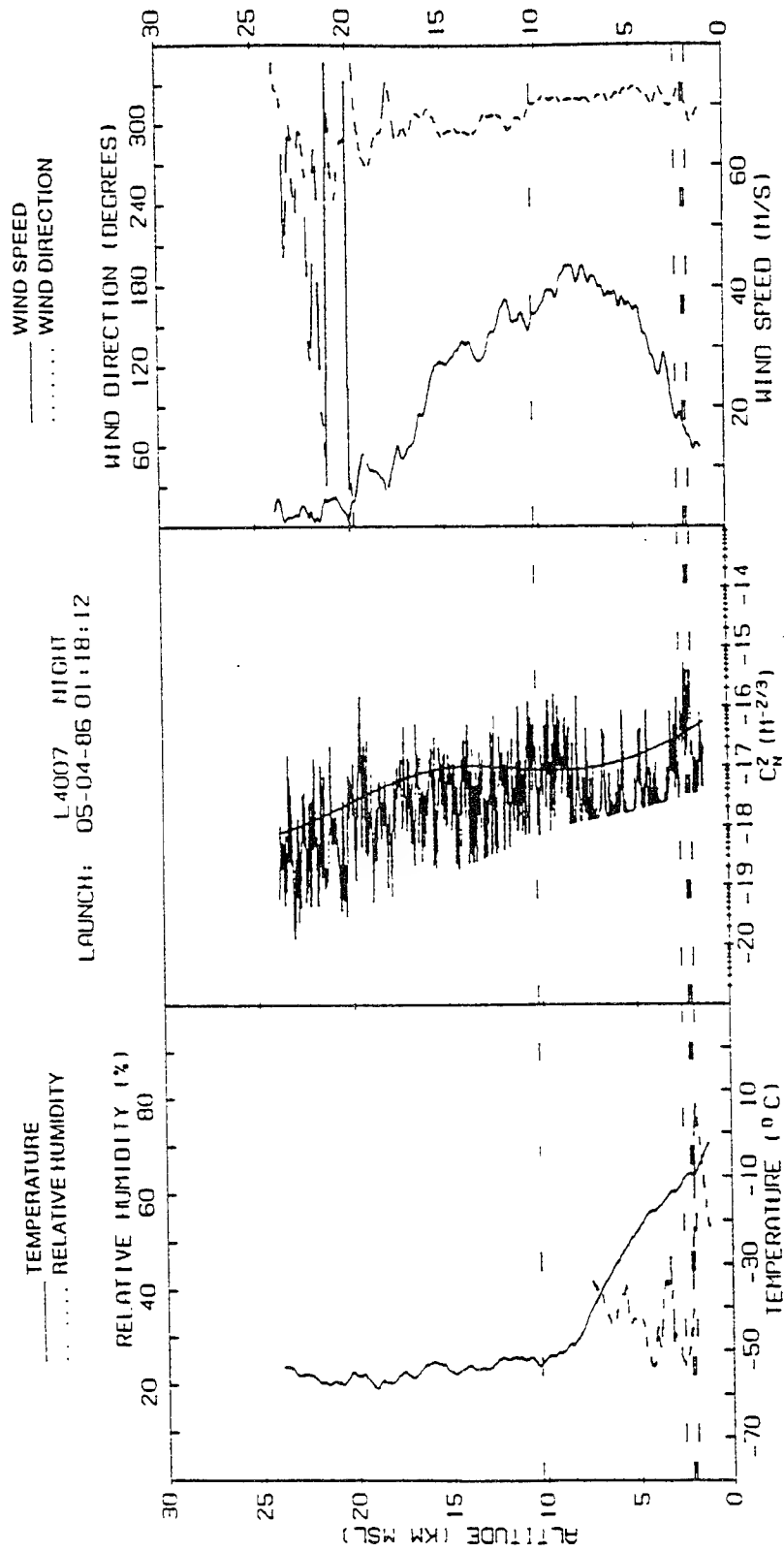


Figure 8 Thermosonde Profiles Measured at Pennsylvania State University, Flight L4007, 4 May, 1986, Temperature, Relative Humidity, C^2 , Wind Speed, Wind Direction

0₀ INT FOR ALT 2.62 THRU 23.78
 6.598E-06 DATA
 6.550E-06 SMOOTH DATA
 7.912E-06 MODEL

MODEL FOR TROPOSPHERE LOG10(1.0-5M(LI)-4.004E+00, 1.729E-01*LOG10(V, 0.000E+00),
 -2.001E+00*LOG10(HI)-5.391E-04)

MODEL FOR STRATOSPHERE LOG10(1.0-5M(LI)-2.680E+00, 2.285E-01*LOG10(V, 0.000E+00),
 -1.473E+00*LOG10(HI)-2.949E-03)

L4007 NIGHT
 LAUNCH: 05-04-86 01:18:12

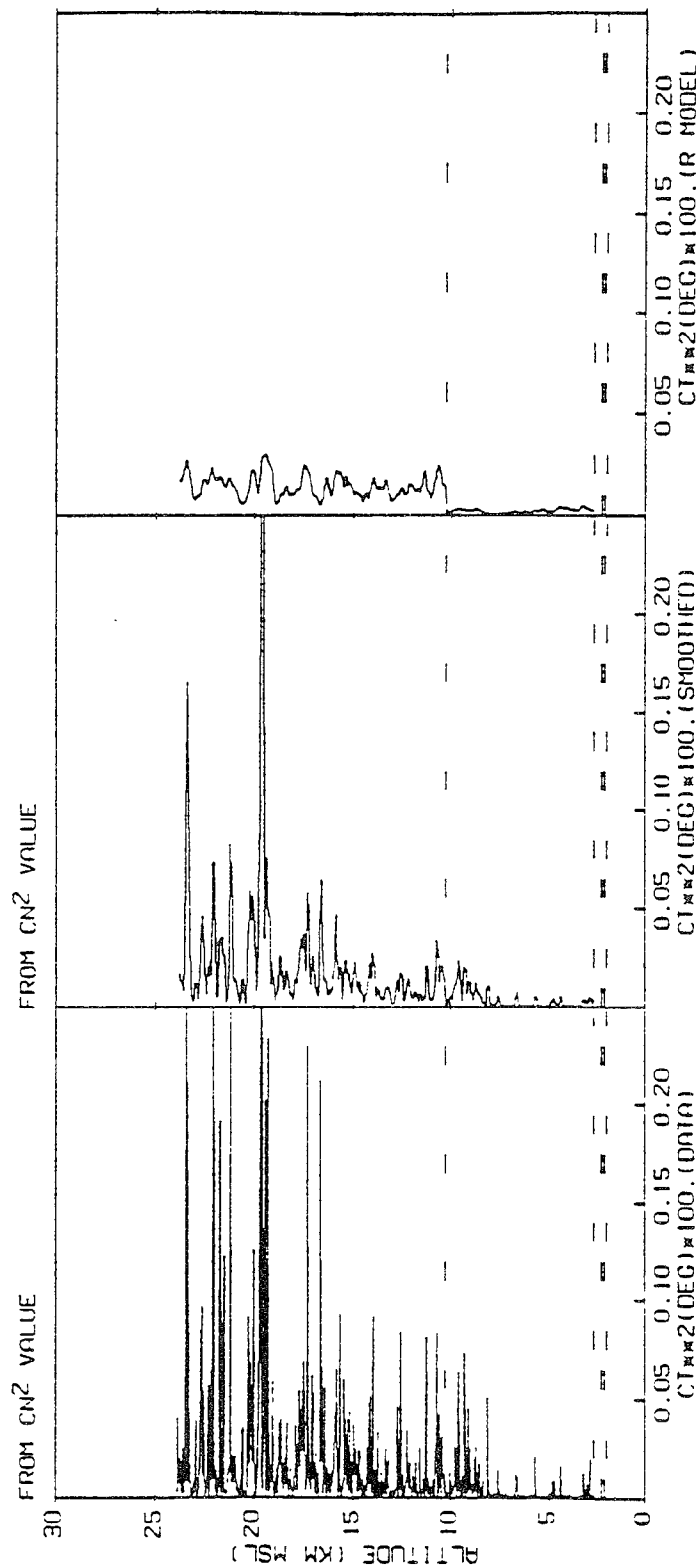


Figure 9. Thermosonde C_t^2 Measurement (Raw and Smoothed) Profiles Compared to Model (1) C_t^2 Profile, Flight L4007

INITIAL GRESS= 0.000E+00
 SUM OF SQUARES ERROR FIT= 8.17E+02
 LOG10(LOI)= -4.004E+00
 STANDARD DEVIATION= 4.566E-02

TROPOSPHERE

0.000E+00

7.597E+02

0.000E+00

0.000E+00

2.490E-05

1.729E-01

2.285E-01

0.000E+00

1.473E+00

0.000E+00

2.946E-02

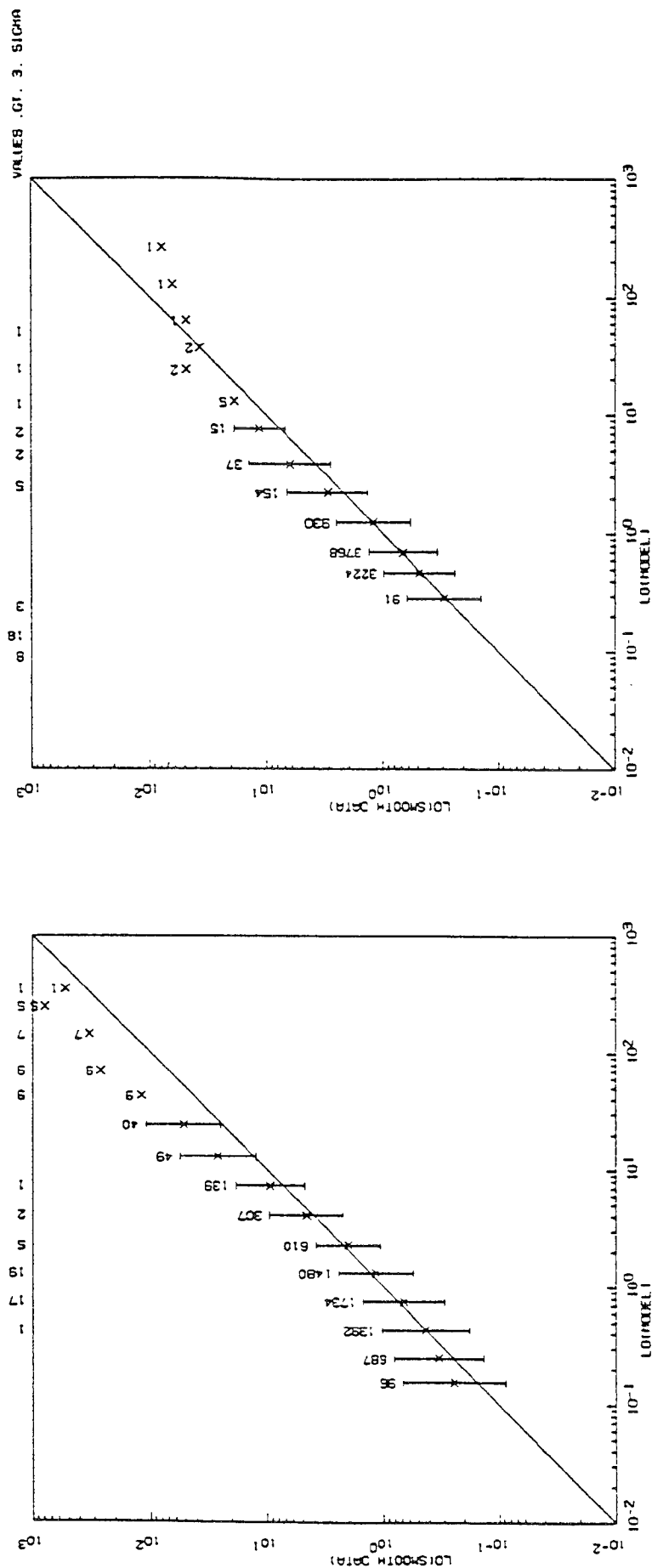
2.992E-03

3.565E-05

STRATOSPHERE

NUMBER OF VALUES LESS THAN 10**(-2)=0
 NUMBER OF VALUES GREATER THAN 10**3=4
 NUMBER ABOVE ERROR BARS IS THE ACTUAL NUMBER OF VALUES IN THE BIN

NUMBER OF VALUES LESS THAN 10**(-2)=0
 NUMBER OF VALUES GREATER THAN 10**3=0



Constants for Model (1) and Model (2)						
Model (1)			Model (2)			
a1	-4.004000	-2.680000	b1	-0.168400	-0.276000	
sa1	0.045700	0.059200	sb1	0.004890	0.005820	
a2	0.172900	0.228500	b2	0.155000	0.213600	
sa2	0.014600	0.016800	sb2	0.014800	0.017300	
a3	-2.000000	-1.473000	b3	-2.072000	-1.385000	
sa3	0.022500	0.035600	sb3	0.023600	0.033700	
a4	-0.000540	-0.002950	b4	-0.000540	-0.003070	
sa4	0.000004	0.000026	sb4	0.000004	0.000018	

FIG //

L1014 NIGHT
LAUNCH: 06-14-88 03:47:35

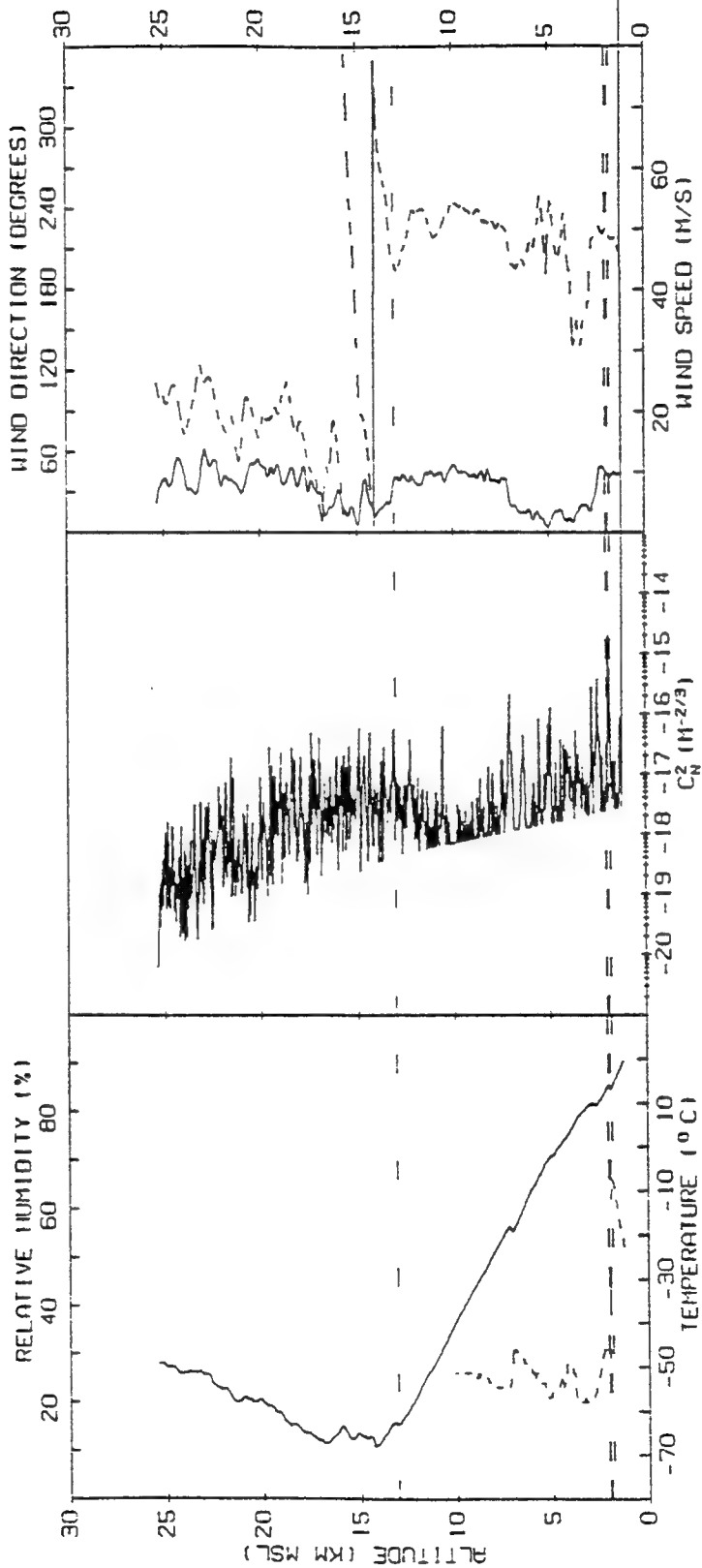


Figure 20. Same as Figure 12, but for Champaign, Illinois Flight L1014, June 1988

8

0. INT FOR ALT 2.06 THRU 25.11
 8.028E-06 DATA
 8.015E-06 SMOOTH DATA
 8.516E-06 MODEL

 MODEL FOR TROPOSPHERE LOG10(ILO-SWELL)=-4.004E+00, 1.729E-01*LOG10(IV, 0.000E+00),
 -2.001E+00*LOG10(IV)-5.391E-04
 MODEL FOR STRATOSPHERE LOG10(ILO-SWELL)=-2.580E+00, 2.285E-01*LOG10(IV, 0.000E+00),
 -1.473E+00*LOG10(IV)-2.949E-03

L1014 NIGHT
 LAUNCH: 06-14-88 03:47:35

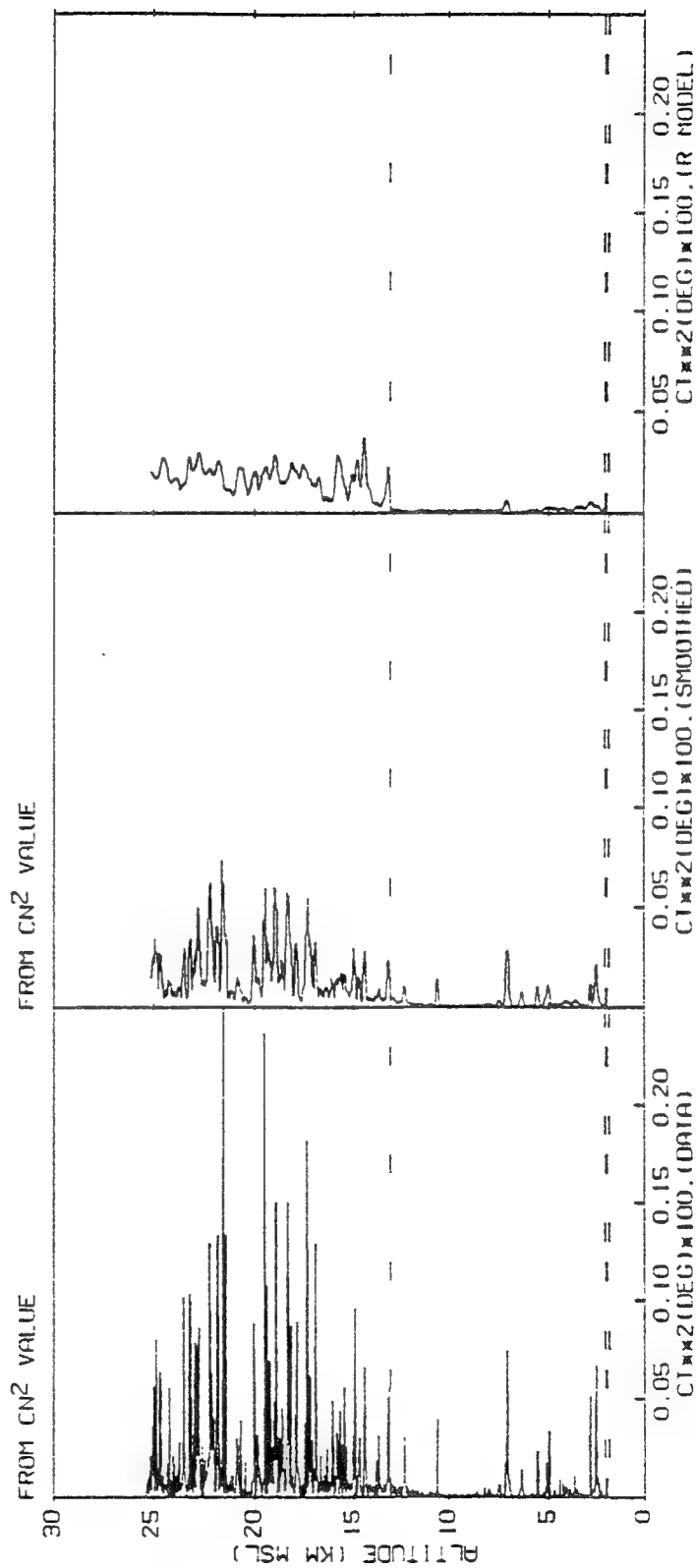


Figure 21. Same as Figure 2 but for Champaign, Illinois Flight L1014, June 1988

13, 9

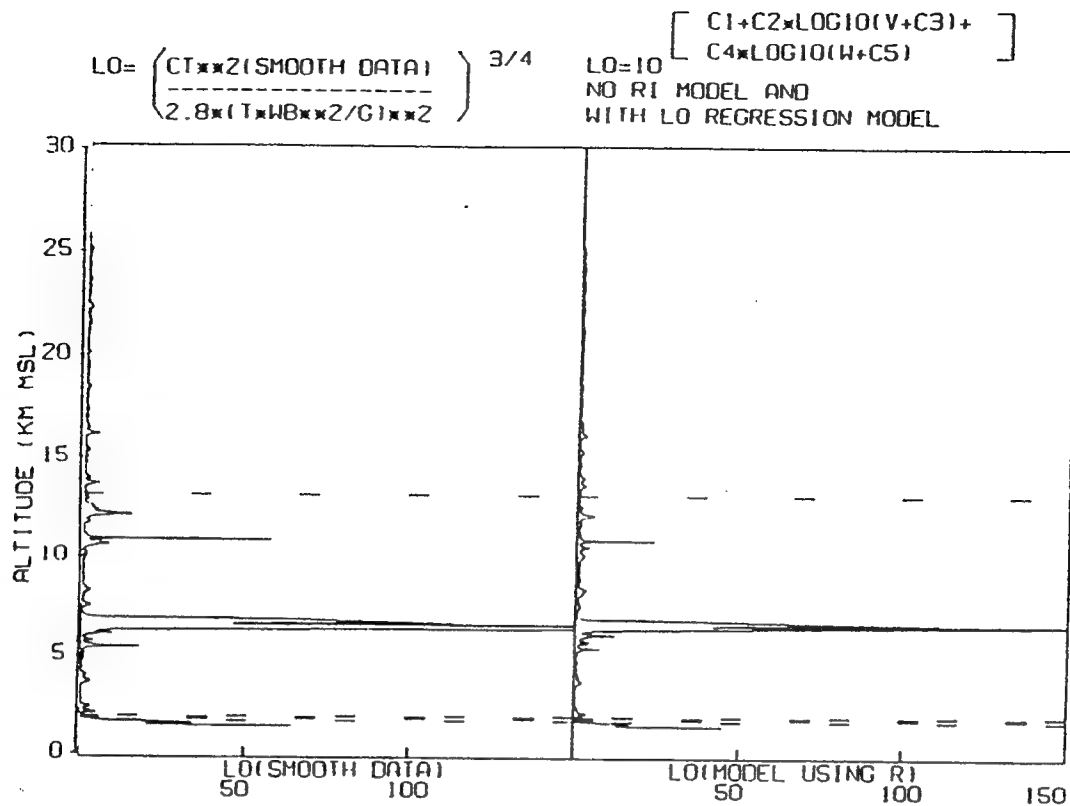


Figure 22. Same as Figure 3 but for Champaign, Illinois Flight L1014, June 1988

14

L4007 NIGHT
LAUNCH: 05-04-86 01:18:12

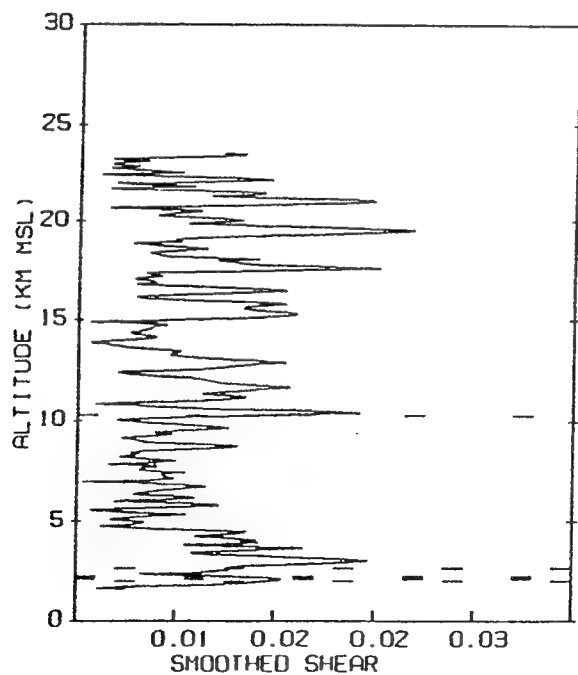


Figure 38. Smoothed 300 m Rawinsonde Shear for Pennsylvania State University Flight L4044

15.

8. INT FOR ALT 2.62 THRU 23.78
 6.598E-06 DATA
 6.550E-06 SMOOTH DATA
 4.333E-06 MODEL
 MODEL FOR TROPOSPHERE LOG10(ILO-SMALL)=1+(3/4)*(1.566E+00+2.962E+01*(S/EQR))
 VELOCITIES SMOOTHED OVER 3.000E-01 K-METERS
 MODEL FOR STRATOSPHERE LOG10(ILO-SMALL)=1+(3/4)*(5.080E-01+3.701E+01*(S/EQR))

L4007 NIGHT
 LAUNCH: 05-04-86 01:18:12

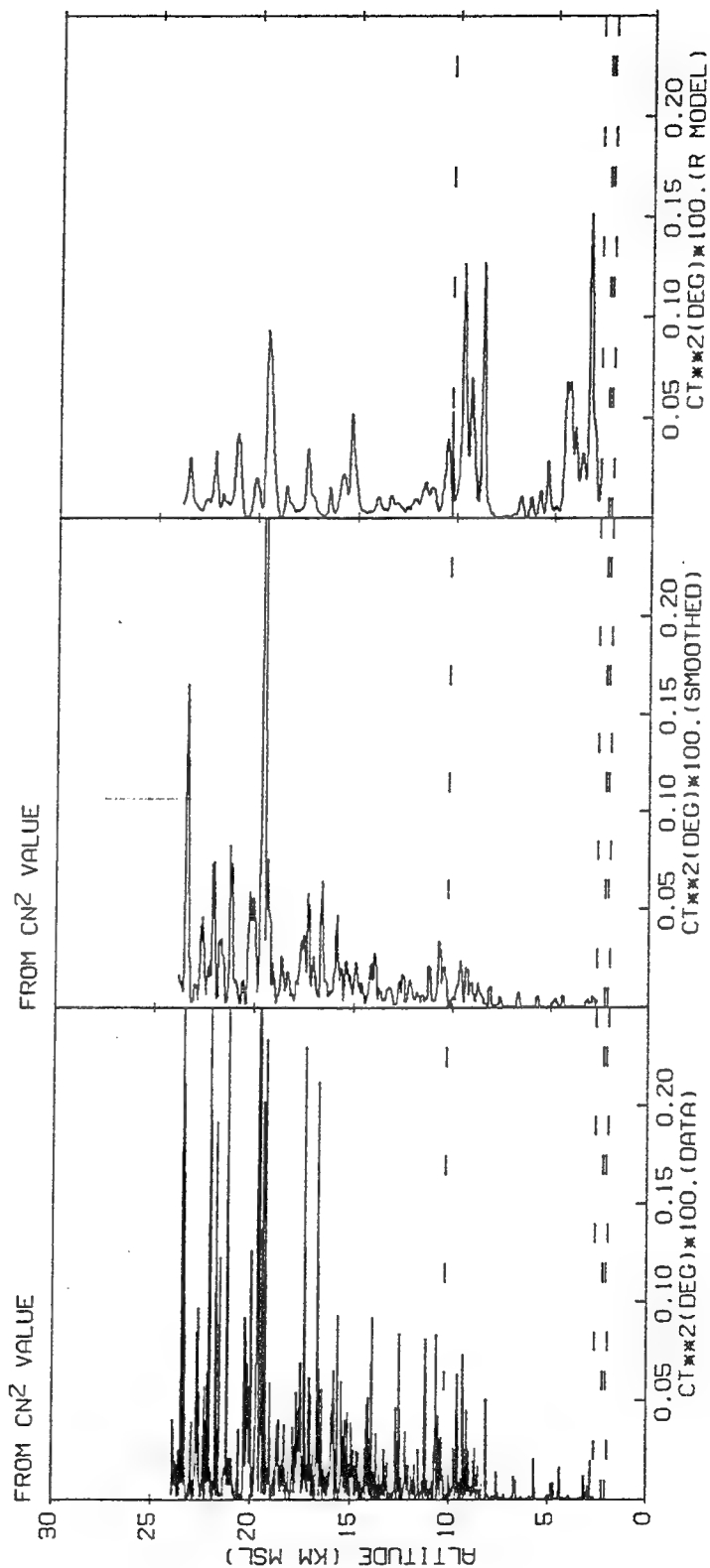


Figure 16. Thermosonde C_t^2 measurement (raw and Smoothed) Profiles Compared to Dewan, et al. C_t^2 Model Profile, Flight L4007

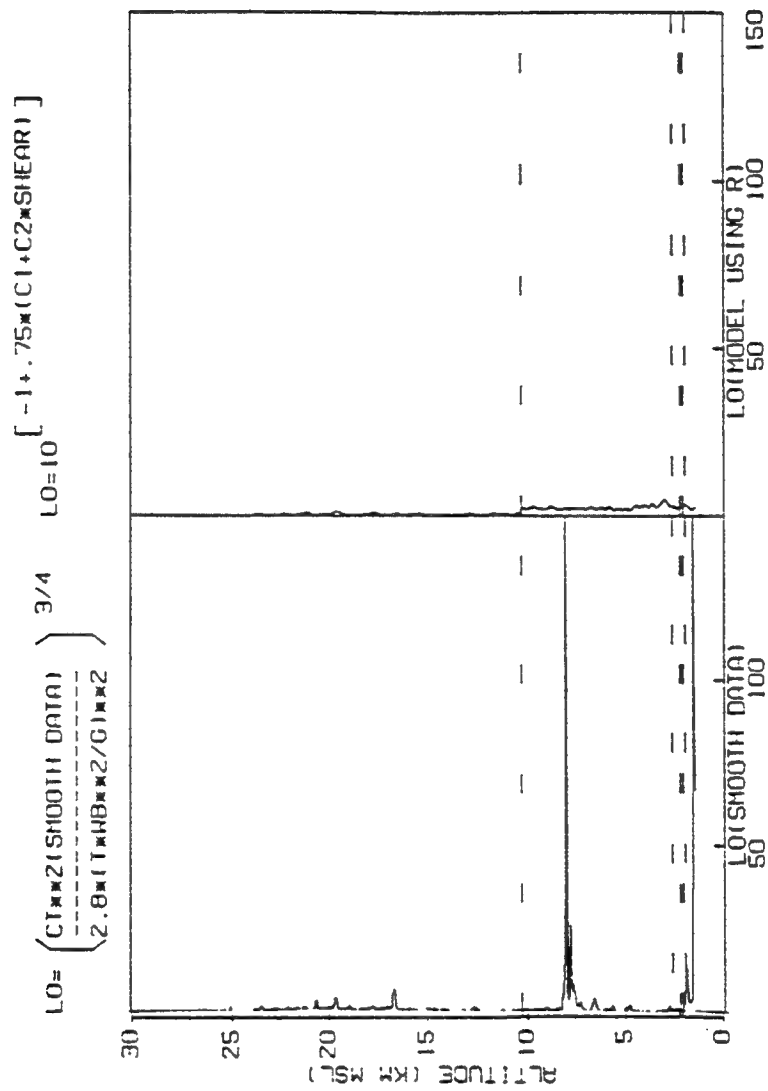


Figure 40 L(z) From Smoothed Thermosonde Data Compared to Dewan, et al. L(z) Model Profile. Flight L4007

L4007 NIGHT
LAUNCH: 05-04-86 01:18:12

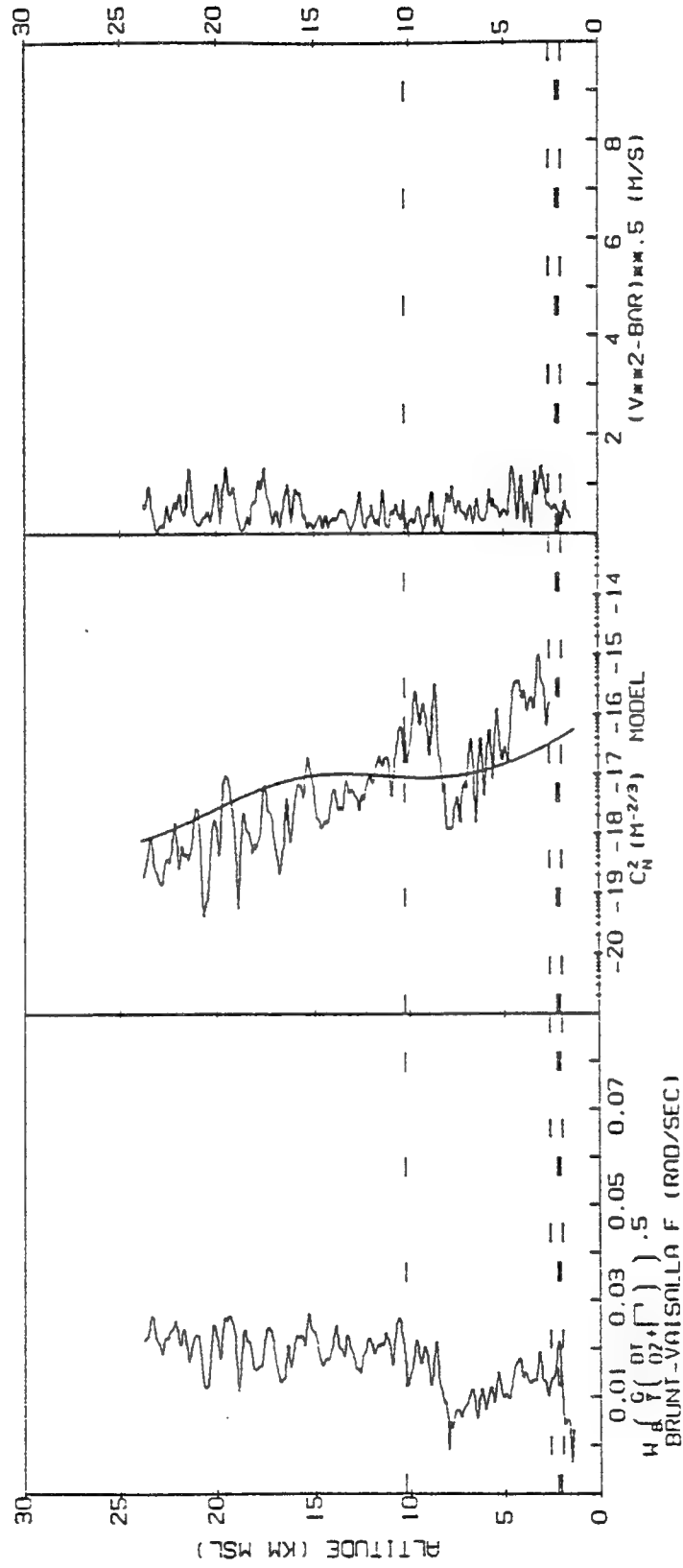
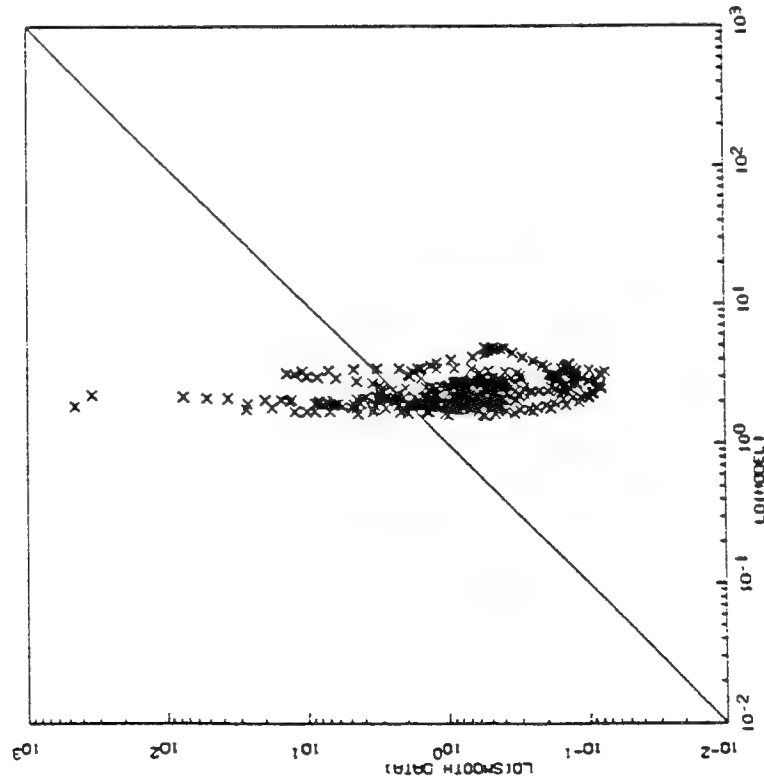


Figure 44. Brunt-Vaisala Frequency and RMS Wind Speed Profiles Derived From Smoothed Measurement Compared With Dewan et al. Model C_n^2 Profile.
Flight L4007

TROPOSPHERE

MODEL FIT CONSTANT = 1.565E+00 MULT S.E.M. = 2.962E+01
VELOCITIES SMOOTHED OVER 3.000E+01 K-METERS



STRATOSPHERE

MODEL FIT CONSTANT = 5.000E+01 MULT S.E.M. = 3.701E+01

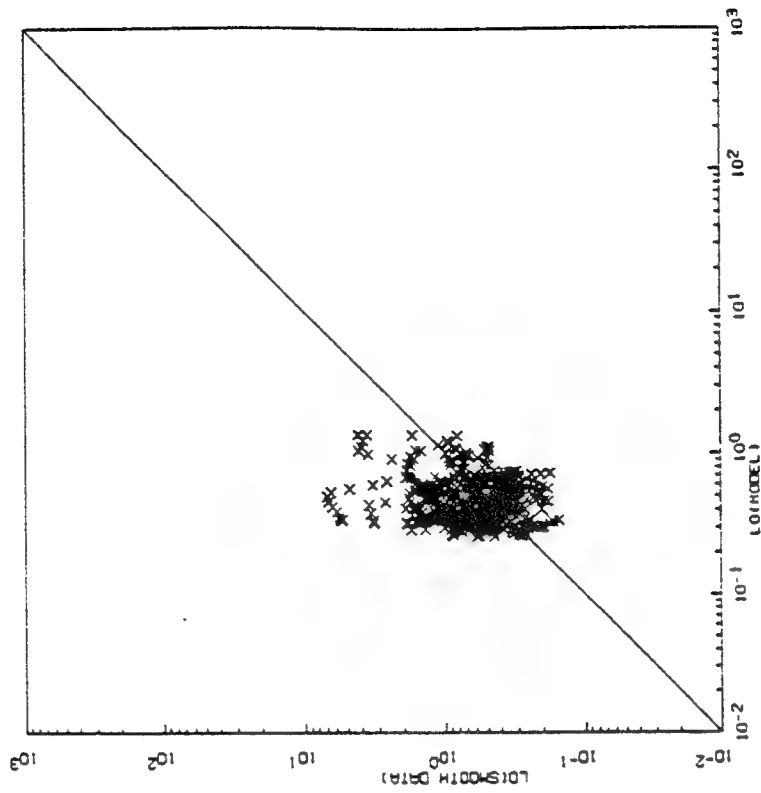


Figure 19. Scatter Plot of "L" for Smoothed Thermosonde Measurements Compared with "L" from Dewan, et al. Model. Flight L4007. Leftmost plot for troposphere. Rightmost plot for stratosphere

Quantitative Comparison Model Vs Data

$$\theta_0 = \left[2.95k^2 \int_0^\infty C_n^2(h)h^{-5/3} \right]^{-3/5}$$

Isoplanatic Angle

Pennsylvania State University Campaign

Theta x E-06

Flight #	Meas.	Mod (1)	Mod (2)
L4007	6.6	7.9	7.7
L4012	4.7	8.2	7.4
L4012	6.1	6.4	8.5
L4018	8.0	8.3	8.2
L4019	8.5	9.1	8.8
L4029	5.5	7.4	7.3
L4031	6.4	8.4	8.5
L4032	4.9	7.6	7.7
L4033	6.0	8.0	8.2
L4035	4.7	7.8	7.8
L4037	9.0	8.3	8.2
L4042	9.0	7.4	7.4
L4043	5.1	7.7	7.9
L4044	6.9	8.4	8.2
L4045	7.9	8.5	8.2
Avg.	6.6	8.0	8.0
Std. Dev.	1.5	.61	.44

Pennsylvania State University Campaign

Dewan et. al. Model Theta x E-06

Flight #	Meas.	Dewan et.al.
L4007	6.6	4.3
L4012	4.7	2.7
L4012	6.1	.25
L4018	8.0	5.6
L4019	8.5	5.4
L4029	5.5	3.2
L4031	6.4	4.8
L4032	4.9	4.8
L4033	6.0	5.4
L4035	4.7	3.9
L4037	9.0	5.4
L4042	9.0	4.7
L4043	5.1	4.1
L4044	6.9	5.6
L4045	7.9	3.2
		w/o L4014
Avg.	6.6	4.5
Std. Dev.	1.5	.97

FIG 23

Measurement Vs. Model

Theta x E-06

	Penn St.	Flatlands	WSMR 84	WSMR 85
Meas. Avg.	6.6	9.6	8.2	7.1
Meas. Std. Dev	1.5	1.9	3.1	2.5
Model Avg.	8.0/8.0	9.0/9.0	8.0/8.6	11./9.0
Model Std. Dev.	.61/.44	.62/.57	.87/1.5	1.9/2.3
Dewan Avg.	4.5			
Dewan Std. Dev.	.97			

Conclusions

- Thermosonde allows development of simple high resolution model.
- High resolution rawinsondes can take advantage of model
- Tatarski outer length parameter can be scaled by rawinsonde measurements of winds and temperature
- Competitive with NOAA model - less tuning - higher resolution
- Fidelity to structure

Wednesday 9 June 1993 p.m.

SESSION F: CLIMATOLOGIES

Chair: James H. Chetwynd, PL/GPOS

THE MOSART GLOBAL CLIMATOLOGICAL AND TERRAIN DATA BASES

Dr. William M. Cornette

Photon Research Associates, Inc.
10350 N. Torrey Pines Road, Suite 300
La Jolla, California 92037-1020

The MOSART program uses a number of global climatological and terrain data bases. These data bases include such parameters as terrain altitude, terrain scene type, surface air temperature, sea surface temperature, snow cover, amount of terrain, cloud cover (low, mid, and high etage, plus cirrus). Atmospheric data bases include the six (6) MODTRAN 2 model atmospheres, plus the additional seventeen (17) APART model atmospheres. These model atmospheres cover the Northern hemisphere (equator to pole in 15 degree increments), and include the U.S. and Israeli Standard atmospheres. These data bases are used to construct both background definition and atmospheric conditions for any location on the globe. This presentation will present the data bases and will discuss how they are used in the MOSART program. Potential growth areas for the data bases and their applications in the MOSART program will also be presented.

THE MOSART GLOBAL CLIMATOLOGICAL AND TERRAIN DATA BASES

Presented at the
Annual Review Conference on Atmospheric Models
Hanscom AFB, Massachusetts
8-9 June 1993

Presented By:
Dr. William M. Cornette



Photon Research Associates, Inc.

10350 N. Torrey Pines Court, #300
La Jolla, California 92037-1020
(619) 455-9741

Fax: (619) 455-0658
e-mail: wmc@photon.com

MOSART Data Bases: Current Status

The MOSART data bases currently consist of atmosphere, terrain, ocean, space, and molecular absorption parameters. Each of these data bases will be presented in the following section.

MOSART DATA BASES: CURRENT STATUS

- Atmosphere:
 - Pressure, Temperature, Molecular Concentrations (23)
 - Surface Air Temperature
 - Aerosol Types
 - Haze Profiles
 - Hydrometeor Types and Profiles
 - Cloud Cover (3 Etages, Cirrus, and Total)
- Terrain:
 - Altitudes
 - Terrain Scene Classification
 - Snow Cover
 - Background Materials
 - Optical Properties
 - Thermal Properties
- Ocean Temperatures
- Space (Zodiacal Light, Mean Star Radiance)
- Molecular Absorption Parameters (13 Molecules at 1 cm^{-1} Resolution)

Northern Hemisphere Model Atmospheres

The model atmospheres (i.e., pressure, temperature, and molecular concentration profiles) cover the Northern hemisphere in 15 degree Latitude increments. Each latitude increment has a summer (July) and a winter (January) variation. Several of the latitudes have other seasonal variations. Also included in the data base are the U.S. Standard (1976) and the Israeli Standard (1980) with day and night time variations.

NORTHERN HEMISPHERE MODEL ATMOSPHERES

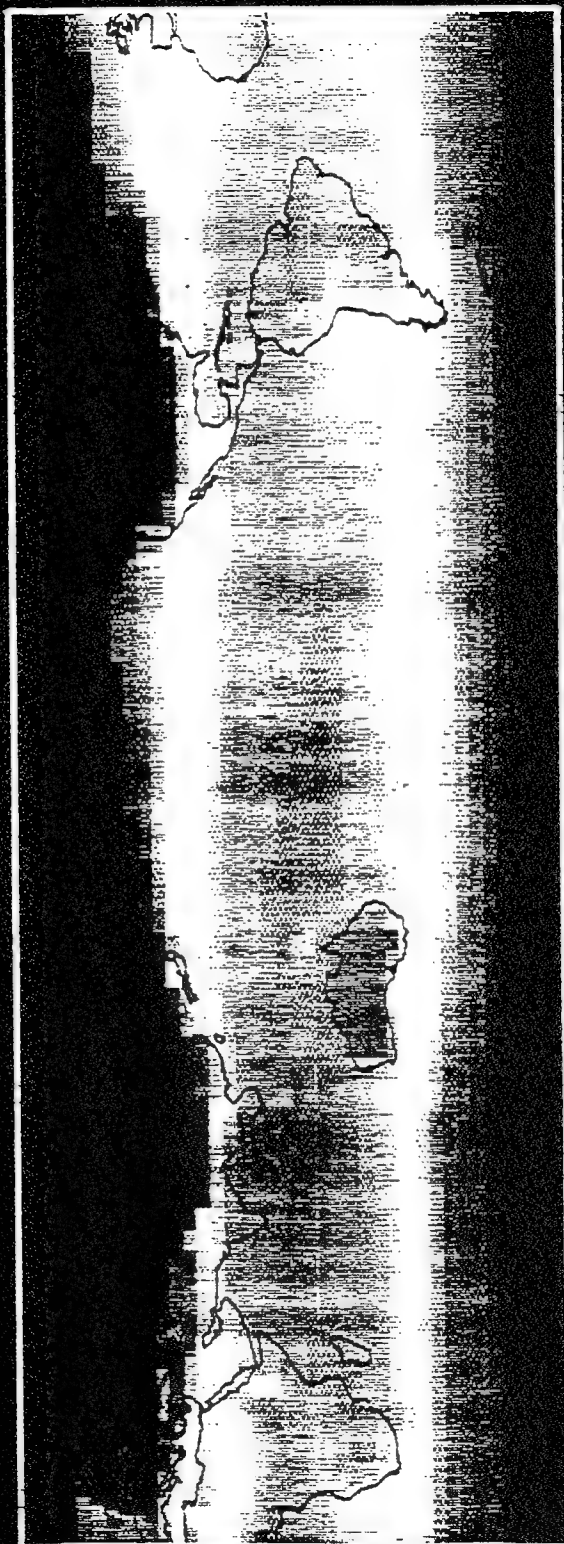
Type	Latitude	Seasons
Equatorial	0°	Summer Winter
Tropical	15°	Annual Summer Winter
Subtropical	30°	Summer Winter
Midlatitude	45°	Summer Winter Spring/Fall
Subarctic	60°	Summer Winter Winter (Cold) Winter (Warm)
Arctic	75°	Summer Winter Winter (Cold) Winter (Warm)
Polar	90°	Summer Winter
U.S. Standard	--	--
Israeli Standard	--	Day/Night

Surface Air Temperature

The NOAA Nimbus 7 data set includes a five year average of monthly surface air temperatures (mean and standard deviation) for the ascending (approximately noon) and descending (approximately midnight) passes of the satellite. The spatial resolution of the data is a constant 4.5 degrees in latitude and a varying resolution in longitude, starting at 4.5 degrees at the equator and increasing to 120 degrees at the poles. This view graph presents the mean surface air temperatures for January at noon.

SURFACE AIR TEMPERATURE

Surface Temperature (Noon)
JANUARY



COLOR SCALE

204.00

312.40

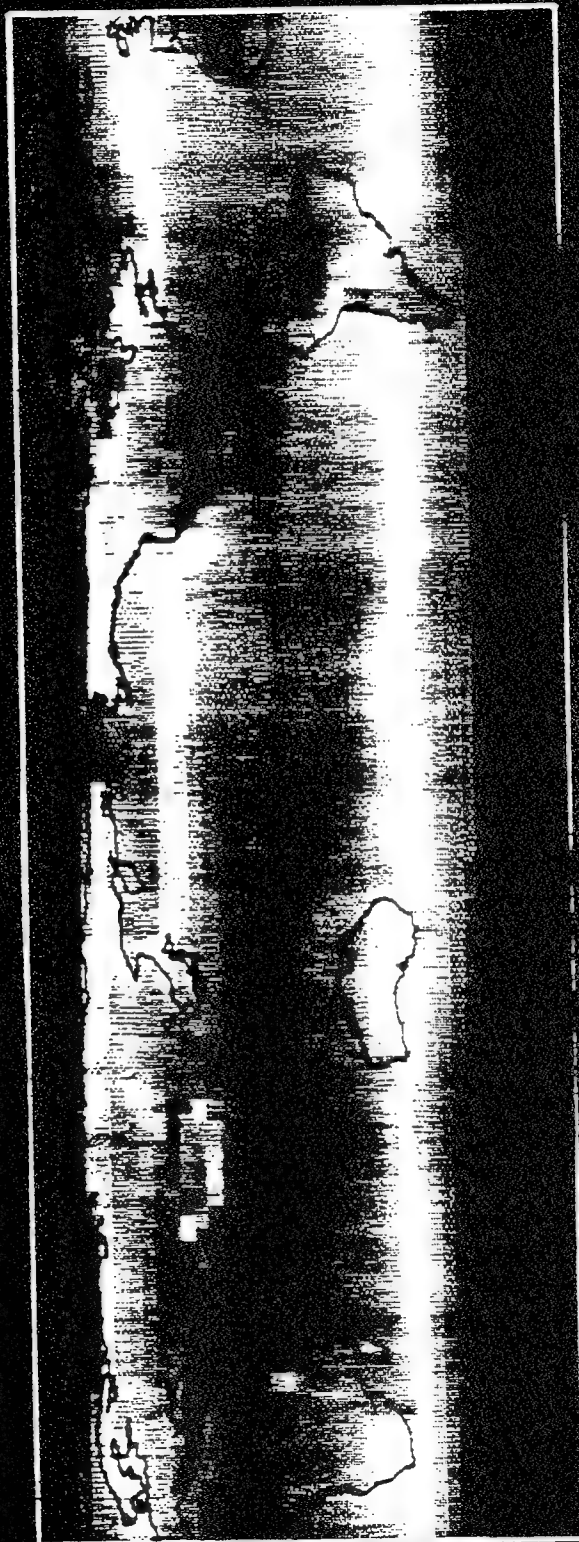


Surface Air Temperature

The NOAA Nimbus 7 data set includes a five year average of monthly surface air temperatures (mean and standard deviation) for the ascending (approximately noon) and descending (approximately midnight) passes of the satellite. The spatial resolution of the data is a constant 4.5 degrees in latitude and a varying resolution in longitude, starting at 4.5 degrees at the equator and increasing to 120 degrees at the poles. This view graph presents the mean surface air temperatures for July at noon.

SURFACE AIR TEMPERATURE

Surface Temperature (Noon)
JULY



Cloud Cover

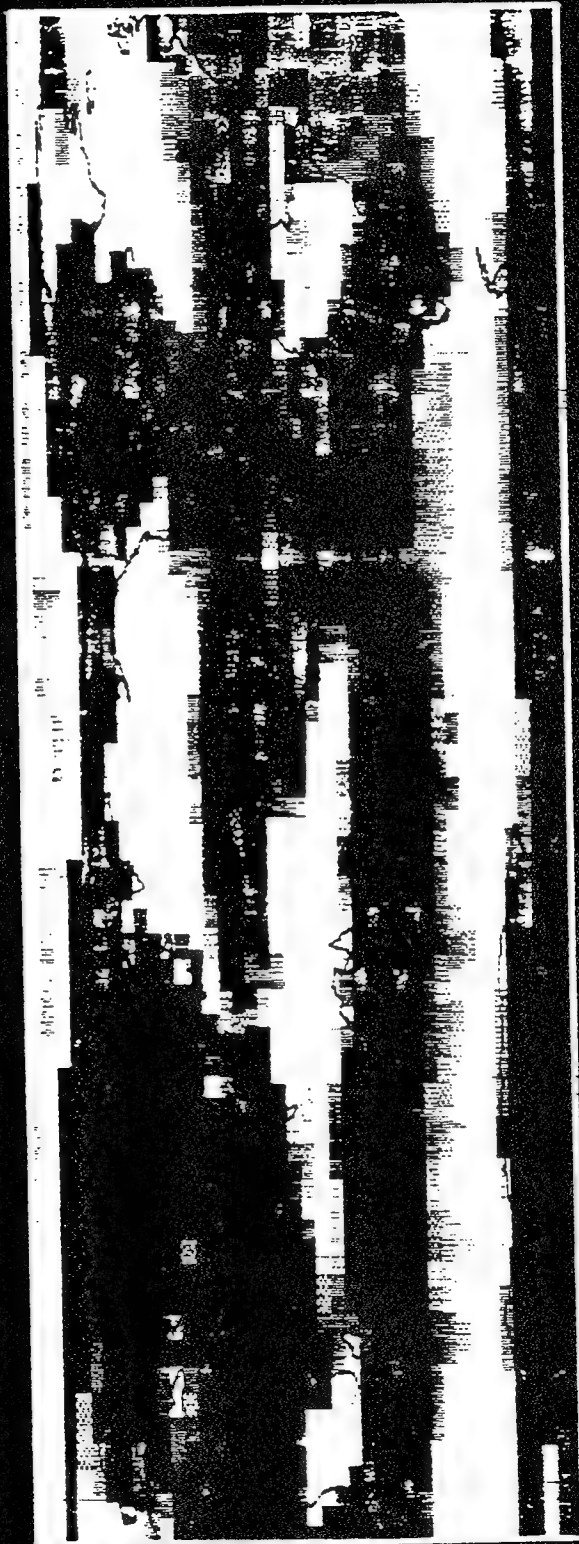
The NOAA Nimbus 7 data set includes a five year average of monthly cloud coverage for the ascending (approximately noon) and descending (approximately midnight) passes of the satellite. The spatial resolution of the data is a constant 4.5 degrees in latitude and a varying resolution in longitude, starting at 4.5 degrees at the equator and increasing to 120 degrees at the poles. The information includes:

- Total cloud cover (mean and standard deviation)
- Low etage cloud cover (mean and standard deviation)
- Middle etage cloud cover (mean and standard deviation)
- High etage cloud cover (mean and standard deviation)

This view graph presents the mean total cloud cover for January at noon.

CLOUD COVER

Cloud Cover (Noon, Total)
JANUARY



COLOR SCALE

0.00

100.00



Cloud Cover

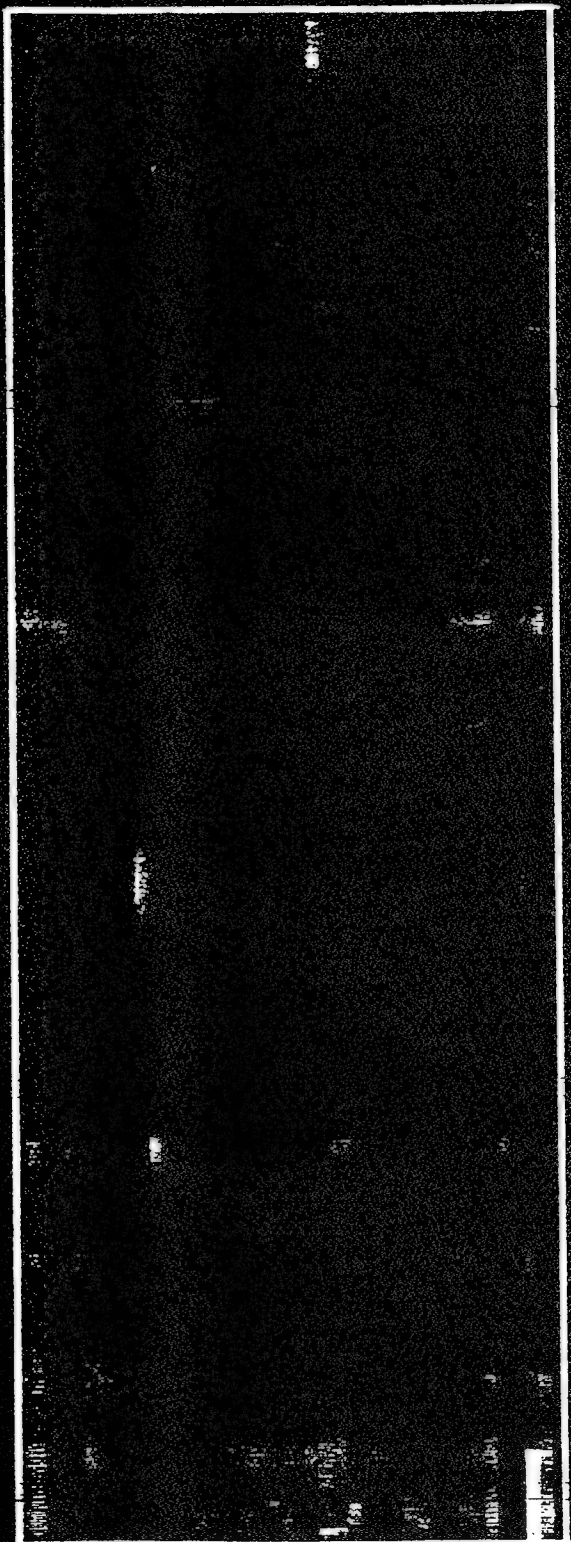
The NOAA Nimbus 7 data set includes a five year average of monthly cloud coverage for the ascending (approximately noon) and descending (approximately midnight) passes of the satellite. The spatial resolution of the data is a constant 4.5 degrees in latitude and a varying resolution in longitude, starting at 4.5 degrees at the equator and increasing to 120 degrees at the poles. The information includes:

- Total cloud cover (mean and standard deviation)
- Low etage cloud cover (mean and standard deviation)
- Middle etage cloud cover (mean and standard deviation)
- High etage cloud cover (mean and standard deviation)

This view graph presents the mean low etage cloud cover for January at noon.

CLOUD COVER

Cloud Cover (Noon, Low)
JANUARY



COLOR SCALE

0.00 100.00



Cloud Cover

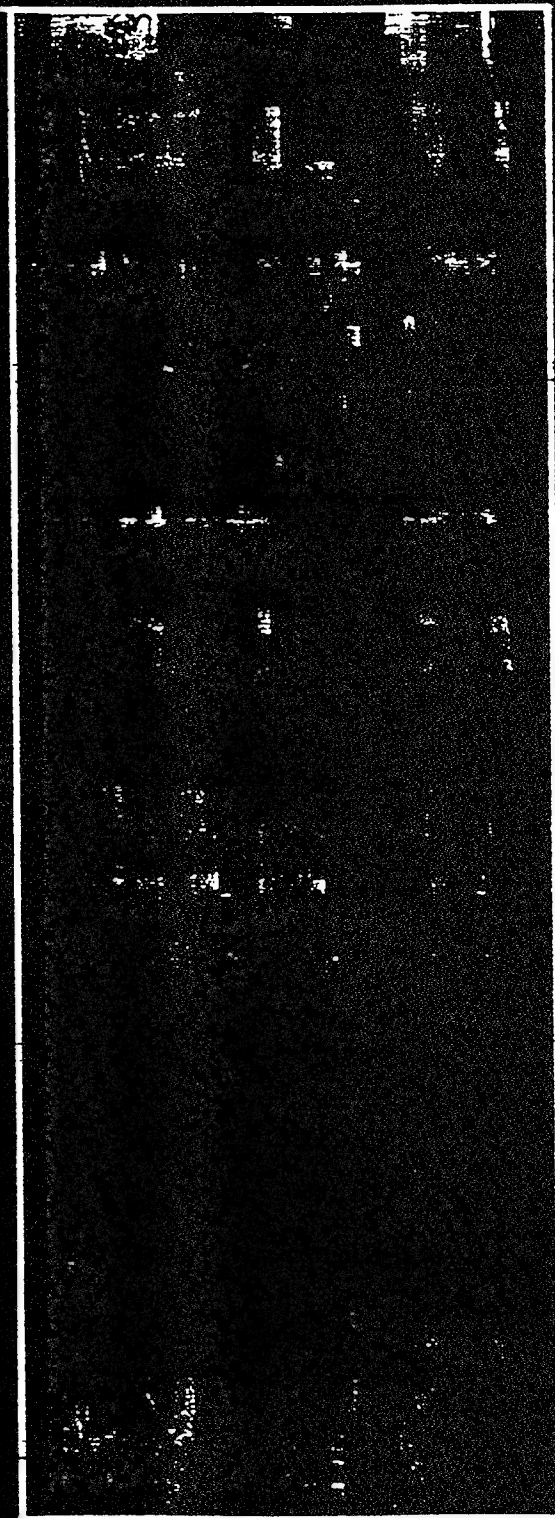
The NOAA Nimbus 7 data set includes a five year average of monthly cloud coverage for the ascending (approximately noon) and descending (approximately midnight) passes of the satellite. The spatial resolution of the data is a constant 4.5 degrees in latitude and a varying resolution in longitude, starting at 4.5 degrees at the equator and increasing to 120 degrees at the poles. The information includes:

- Total cloud cover (mean and standard deviation)
- Low etage cloud cover (mean and standard deviation)
- Middle etage cloud cover (mean and standard deviation)
- High etage cloud cover (mean and standard deviation)

This view graph presents the mean middle etage cloud cover for January at noon.

CLOUD COVER

Cloud Cover (Noon, Mid)
JANUARY



COLOR SCALE

0.00 100.00



Cloud Cover

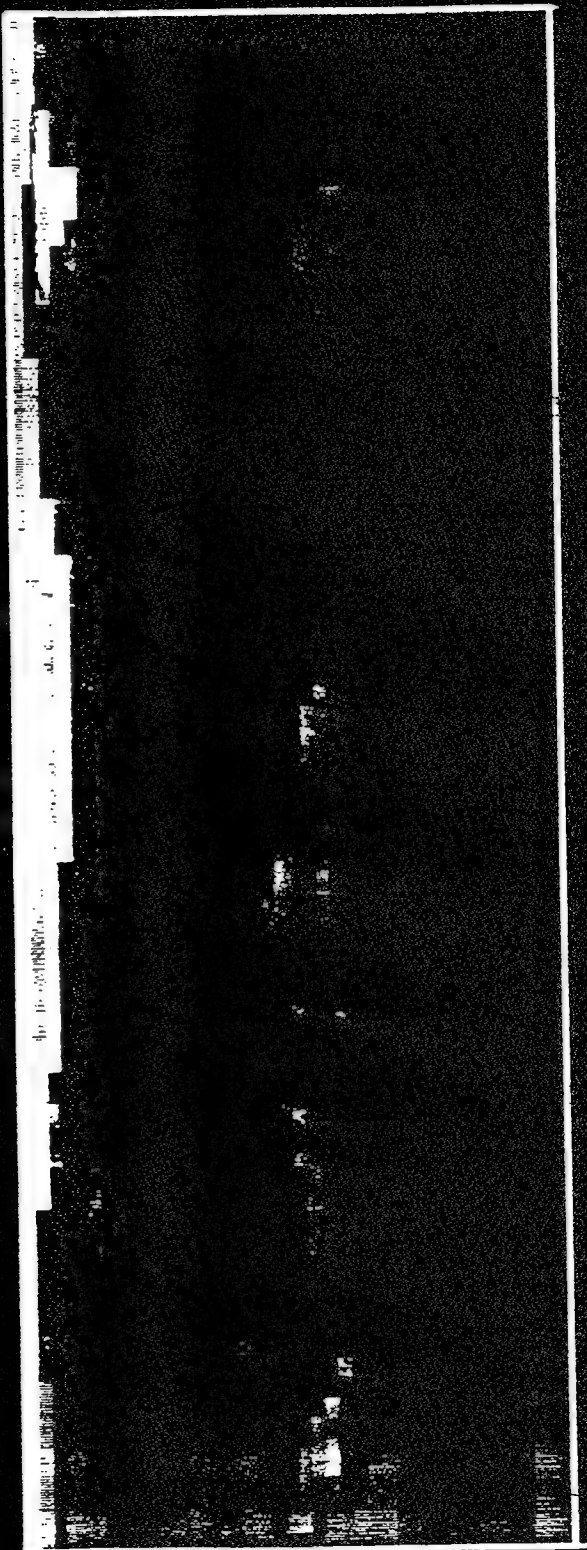
The NOAA Nimbus 7 data set includes a five year average of monthly cloud coverage for the ascending (approximately noon) and descending (approximately midnight) passes of the satellite. The spatial resolution of the data is a constant 4.5 degrees in latitude and a varying resolution in longitude, starting at 4.5 degrees at the equator and increasing to 120 degrees at the poles. The information includes:

- Total cloud cover (mean and standard deviation)
- Low etage cloud cover (mean and standard deviation)
- Middle etage cloud cover (mean and standard deviation)
- High etage cloud cover (mean and standard deviation)

This view graph presents the mean high etage cloud cover for January at noon. The data near the north pole is erroneous, since the Nimbus 7 uses solar reflectance bands to discriminate clouds. In January at the north pole, it is night for the complete 24 hours, thus leading to erroneous classification of high clouds.

CLOUD COVER

Cloud Cover (Noon, High)
JANUARY



COLOR SCALE

0.00 100.00



Cloud Cover

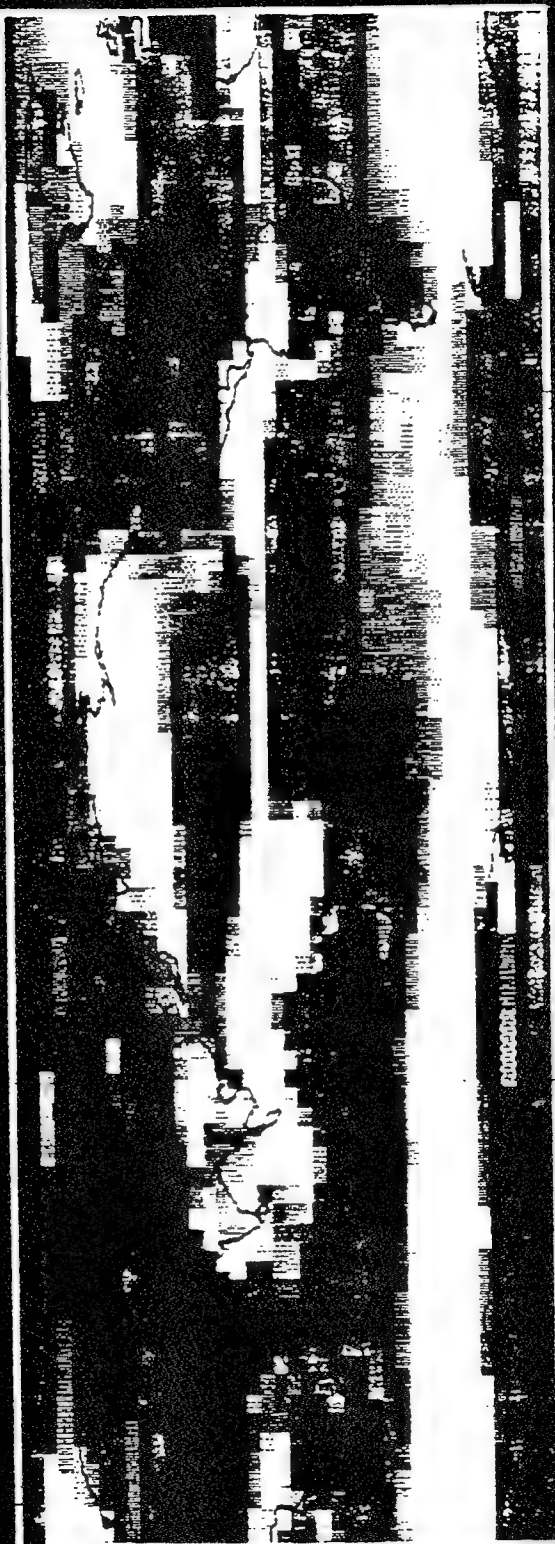
The NOAA Nimbus 7 data set includes a five year average of monthly cloud coverage for the ascending (approximately noon) and descending (approximately midnight) passes of the satellite. The spatial resolution of the data is a constant 4.5 degrees in latitude and a varying resolution in longitude, starting at 4.5 degrees at the equator and increasing to 120 degrees at the poles. The information includes:

- Total cloud cover (mean and standard deviation)
- Low etage cloud cover (mean and standard deviation)
- Middle etage cloud cover (mean and standard deviation)
- High etage cloud cover (mean and standard deviation)

This view graph presents the mean total cloud cover for July at noon.

CLOUD COVER

Cloud Cover (Noon, Total)
JULY



COLOR SCALE

0.00

100.00



Cloud Cover

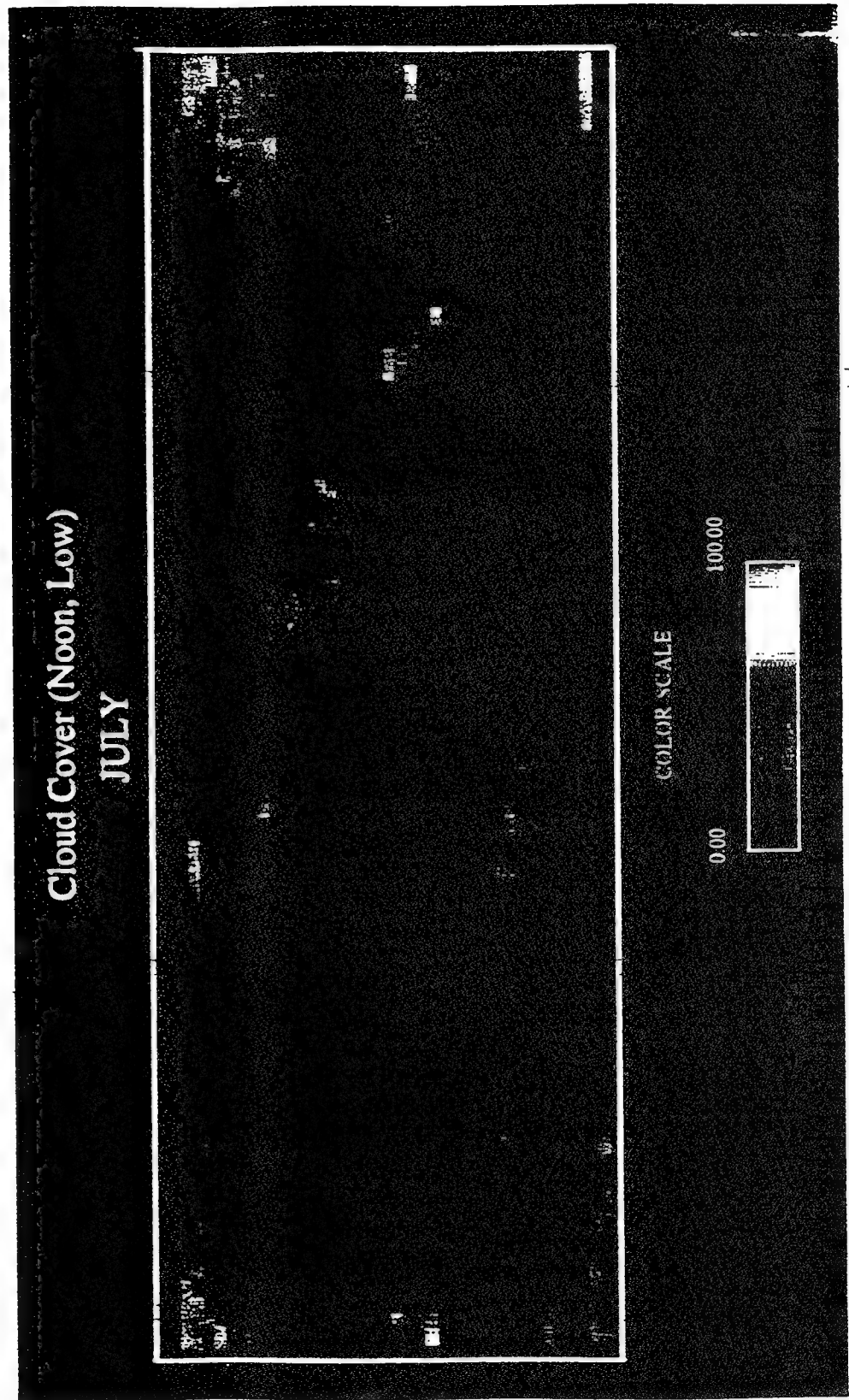
The NOAA Nimbus 7 data set includes a five year average of monthly cloud coverage for the ascending (approximately noon) and descending (approximately midnight) passes of the satellite. The spatial resolution of the data is a constant 4.5 degrees in latitude and a varying resolution in longitude, starting at 4.5 degrees at the equator and increasing to 120 degrees at the poles. The information includes:

- Total cloud cover (mean and standard deviation)
- Low etage cloud cover (mean and standard deviation)
- Middle etage cloud cover (mean and standard deviation)
- High etage cloud cover (mean and standard deviation)

This view graph presents the mean low etage cloud cover for July at noon.

CLOUD COVER

Cloud Cover (Noon, Low)
JULY



Cloud Cover

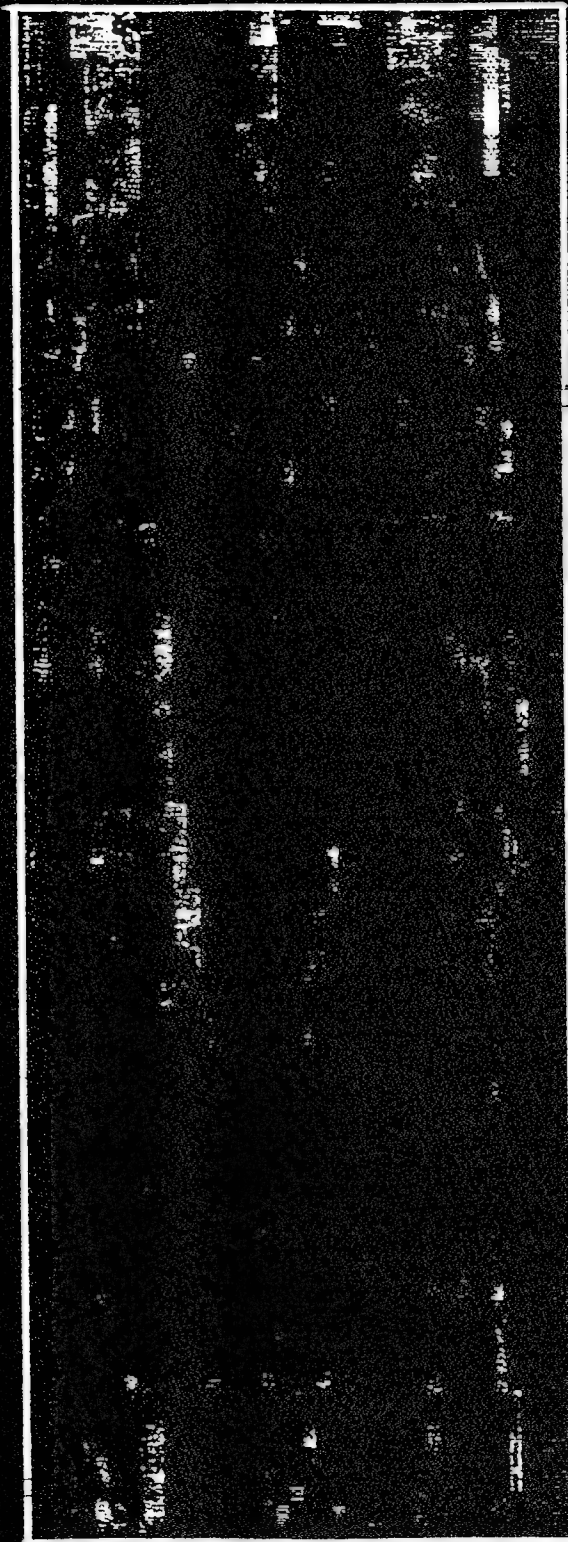
The NOAA Nimbus 7 data set includes a five year average of monthly cloud coverage for the ascending (approximately noon) and descending (approximately midnight) passes of the satellite. The spatial resolution of the data is a constant 4.5 degrees in latitude and a varying resolution in longitude, starting at 4.5 degrees at the equator and increasing to 120 degrees at the poles. The information includes:

- Total cloud cover (mean and standard deviation)
- Low etage cloud cover (mean and standard deviation)
- Middle etage cloud cover (mean and standard deviation)
- High etage cloud cover (mean and standard deviation)

This view graph presents the mean middle etage cloud cover for July at noon.

CLOUD COVER

Cloud Cover (Noon, Mid)
JULY



COLOR SCALE

0.00

1.0000



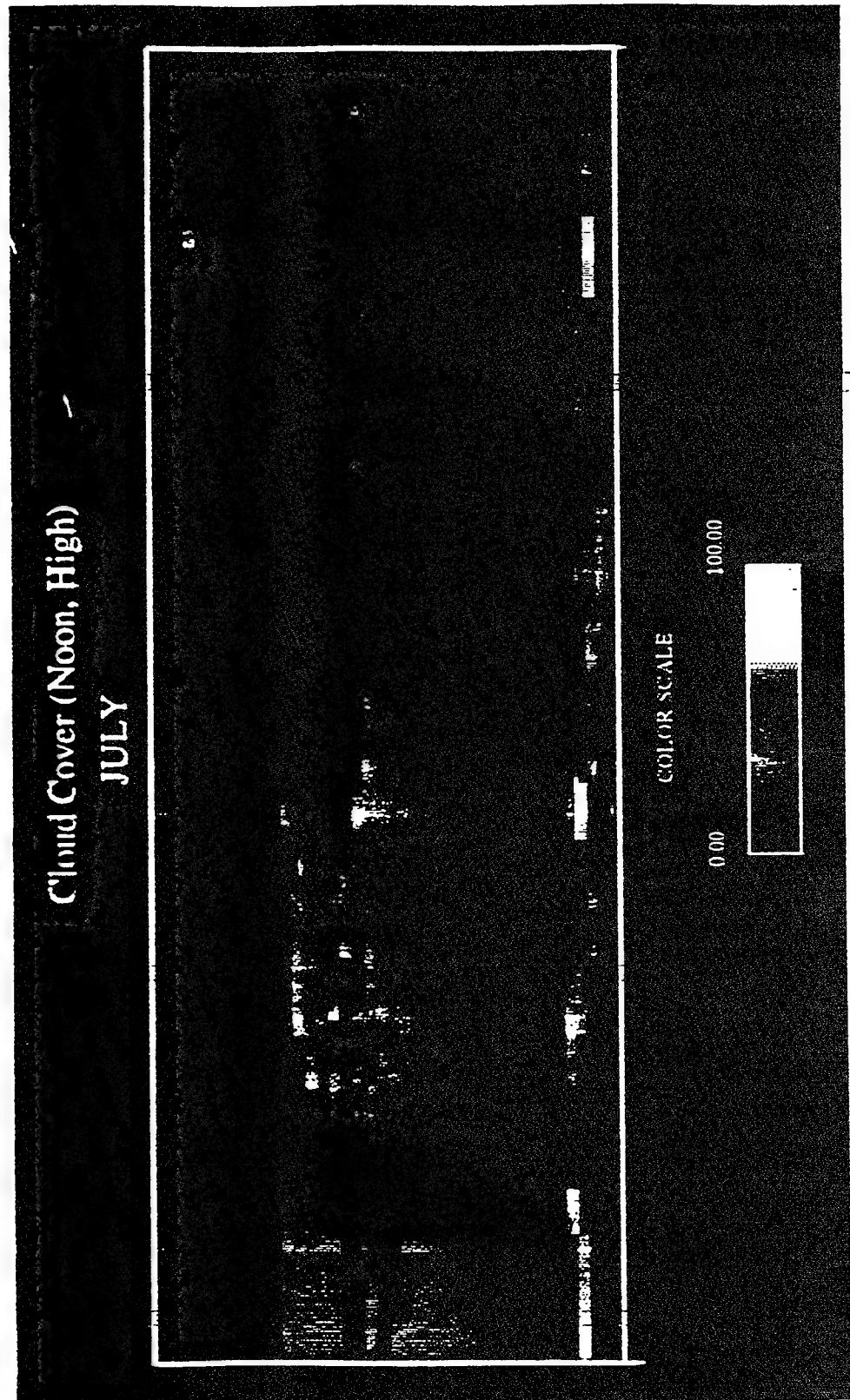
Cloud Cover

The NOAA Nimbus 7 data set includes a five year average of monthly cloud coverage for the ascending (approximately noon) and descending (approximately midnight) passes of the satellite. The spatial resolution of the data is a constant 4.5 degrees in latitude and a varying resolution in longitude, starting at 4.5 degrees at the equator and increasing to 120 degrees at the poles. The information includes:

- Total cloud cover (mean and standard deviation)
- Low etage cloud cover (mean and standard deviation)
- Middle etage cloud cover (mean and standard deviation)
- High etage cloud cover (mean and standard deviation)

This view graph presents the mean high etage cloud cover for July at noon. The data near the south pole may be erroneous, since the Nimbus 7 uses solar reflectance bands to discriminate clouds. In July at the south pole, it is night for the complete 24 hours, thus leading to erroneous classification of high clouds.

CLOUD COVER

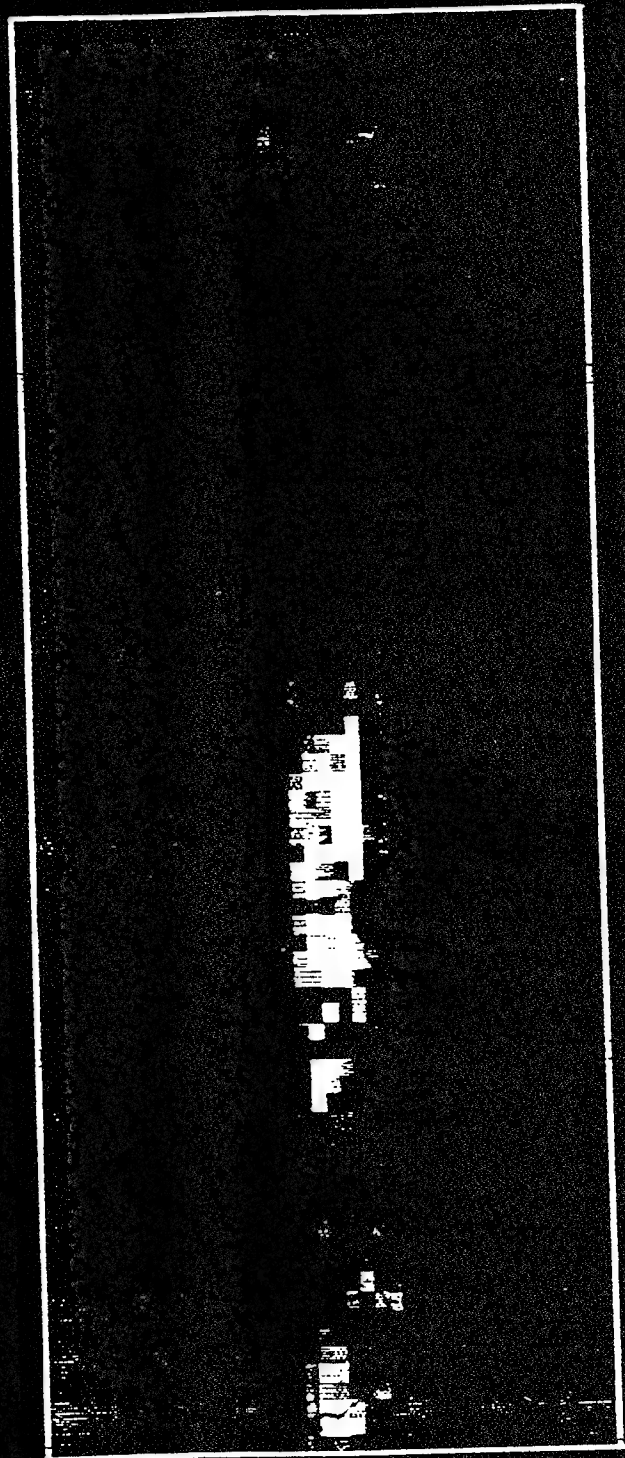


High Cirrus Clouds

The NOAA Nimbus 7 data set includes a five year average of monthly cirrus cloud coverage. The spatial resolution of the data is a constant 4.5 degrees in latitude and a varying resolution in longitude, starting at 4.5 degrees at the equator and increasing to 120 degrees at the poles. The information includes both mean and standard deviation cloud cover. It should be noted that this data applies only to cirrus cloud sufficiently opaque to be detected by satellite. Thin and subvisual cirrus clouds are not included. This view graph presents the mean cirrus cloud cover for January.

HIGH CIRRUS CLOUDS

Percentage of High Cirrus Clouds
 JANUARY



0.00 37.75

0.00



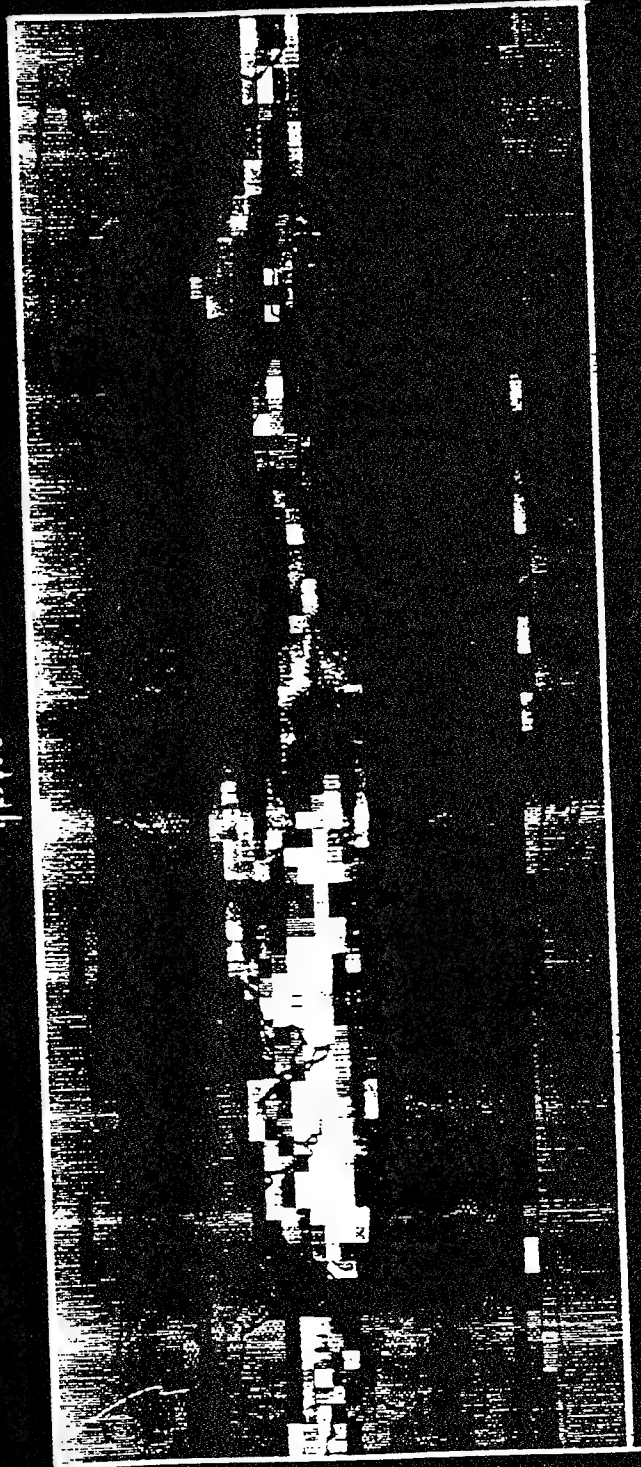
High Cirrus Clouds

The NOAA Nimbus 7 data set includes a five year average of monthly cirrus cloud coverage. The spatial resolution of the data is a constant 4.5 degrees in latitude and a varying resolution in longitude, starting at 4.5 degrees at the equator and increasing to 120 degrees at the poles. The information includes both mean and standard deviation cloud cover. It should be noted that this data applies only to cirrus cloud sufficiently opaque to be detected by satellite. Thin and subvisual cirrus clouds are not included. This view graph presents the mean cirrus cloud cover for July.

HIGH CIRRUS CLOUDS

Percentage of High Cirrus Clouds

三、



COLOR SCALE

00

38.80



Global Altitude Map

The National Geographic Data Center provides terrain altitude at a variety of resolutions. The data base used by MOSART and presented in the view graph is at 10 minute increments in both latitude and longitude.

GLOBAL ALTITUDE MAP



Global Terrain Scenes (Deterministic)

Photon Research Associates, Inc. has developed deterministic representations of various sites over the globe. The descriptions of the fifteen sites that are represented statistically in the MOSART code are shown, together with their locations.

GLOBAL TERRAIN SCENES (DETERMINISTIC)

• City/Harbor Land/Sea Interface	San Diego, CA
• Arctic Tundra Land/Sea Interface	Point Barrow, AK
• Forested Low Relief Terrain	Wa Wa, Ontario, Canada
• Subarctic Rocky Land/Sea Interface	Trondheim, Norway
• Forested Terrain/Agricultural Terrain	Fulda, Germany
• Flat Agricultural	Alberta, Canada
• Desert Pavement with Dunes	Imperial Valley, CA
• Desert Land/Sea Interface	Salton Sea, CA
• Forested Mountains/Cultural	Santa Cruz, CA
• Multi-Year Sea Ice	Beaufort Sea
• Arctic Mountains with Scrub	Brooks Range, AK
• Arctic Tundra with Melt Lakes	-
• Open Ocean	-
• Mixed Farmlands/Orchards	Camarillo, CA
• Southern California Land/Sea Interface	Southern California

GENESSIS Southern California Scene

The deterministic representation of the southern California scene, developed for the Generic Scene Simulation Software (GENESSIS), is shown. The scene is represented at a spatial representation of 400 meters and is 1024 by 1024 pixels in extent. This particular scene is a synthesis of the Landsat MSS bands 1, 2, and 4. In addition to the coast line, Cataline Island and the San Andreas fault are readily apparent.



GENESYS SOUTHERN CALIF SCENE
LANDSAT 108 EARTH 1.2. MID 4
1024 LINES 1024 SAMPLES
FILE SIZE 400 METERS

Camarillo, California GENESIS Scene

The deterministic representation of the Camarillo, California, developed for the Generic Scene Simulation Software (GENESIS), is shown. The scene is represented at a spatial representation of 30 meters and is 460 by 440 pixels in extent. This particular scene is a synthesis of a mid-wave infrared band (3.6-4.1 μm). U.S. Highway 101 is visible as a horizontal line passing from right to left in the upper portion of the image. Just below the highway in the middle of the scene is the Camarillo airport. Farmland is seen below the airport, with some coastal mountains in the lower right hand portion of the scene. Camarillo, California, is located west of Los Angeles, near Ventura, California.

CAMARILLO, CALIF GENE8818 SCENE
MUJR (3.6-4.1 UM)
460 ROW X 440 COL
DATE: 08/10/1983 2030 GMT
PIXEL SIZE: 30 METERS



Global Terrain Scenes (Modified)

It was determined that the available deterministic scenes were not adequate to provide a global scene classification. Therefore, statistical representations of the scene types shown have been developed.

GLOBAL TERRAIN SCENES (MODIFIED)

- Tundra
- Pine Forest
- Mixed Forest/Farmland
- Grass Land - Savannah
- Scrub - Chaparral
- Scrub - Desert
- Urban
- Rural Land/Sea Interface
- Tropical Forest
- Tropical Savannah
- Tropical Desert
- Tropical Land/Sea Interface

Land Cover

The NOAA Nimbus 7 data set includes fractional land cover at a spatial resolution that is a constant 4.5 degrees in latitude. The resolution in longitude varies, starting at 4.5 degrees at the equator and increasing to 120 degrees at the poles. This view graph presents this data. However, this data is not presently used by the MOSART code.

LAND COVER

Percentage of Grid that is Land
 JANUARY



COLOR SCALE

100.00

0.00



Snow Cover

The NOAA Nimbus 7 data set includes a five year average of monthly snow cover. The spatial resolution of the data is a constant 4.5 degrees in latitude and a varying resolution in longitude, starting at 4.5 degrees at the equator and increasing to 120 degrees at the poles. The information includes both mean and standard deviation snow cover. The data near the north pole is erroneous, since the Nimbus 7 uses solar reflectance bands to discriminate snow. In January at the north pole, it is night for the complete 24 hours, thus leading to erroneous classification of snow. The MOSART program assumes that the snow cover is 99% over terrain in the northern latitudes in the winter. This view graph presents the mean snow cover for January.

SNOW COVER

Percentage of Grid that is Snow
JANUARY



OFFER SCALE

100.00

0.00

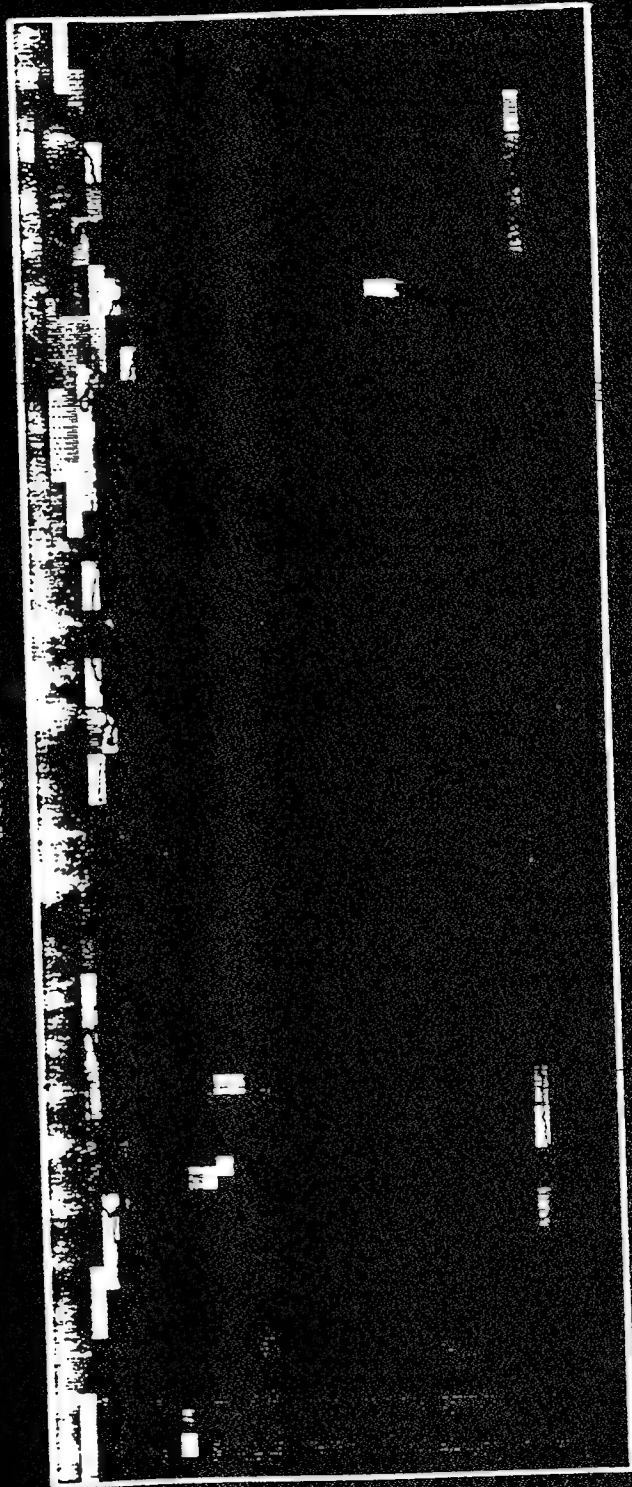


Snow Cover

The NOAA Nimbus 7 data set includes a five year average of monthly snow cover. The spatial resolution of the data is a constant 4.5 degrees in latitude and a varying resolution in longitude, starting at 4.5 degrees at the equator and increasing to 120 degrees at the poles. The information includes both mean and standard deviation snow cover. The data near the south pole is erroneous, since the Nimbus 7 uses solar reflectance bands to discriminate snow. In July at the south pole, it is night for the complete 24 hours, thus leading to erroneous classification of snow. The MOSART program assumes that the snow cover is 99% over terrain in the southern latitudes in the winter. This view graph presents the mean snow cover for July.

SNOW COVER

Percentage of Grid that is Snow
 JULY



Color Scale

0.00 100.00



Scene Type Map

Using a variety of sources (e.g., The Times World Atlas, various geography and remote sensing texts), the world has been classified on a 1 degree by 1 degree grid with regard to scene type. Seasonal variations are included where appropriate (e.g., sea ice versus open ocean). The geographical distribution of ten of the twenty-eight available scenes is shown in this view graph. The remaining scenes are grouped together as "Other."

SCENE TYPE MAP



Apr - Oct



Oct - Apr

- Blue - Ocean
- Light Blue - Sea Ice
- White - Continental Ice
- Green - Tropical Forest
- Tan - Grassland
- Brown - Scrub Desert
- Grey - Mixed Forest/Farmland
- Red - Forested Mountains
- Pink - Arctic Mountains
- Purple - Tropical Savannah
- Black - Other

Terrain Materials

Each of the terrain scenes discussed earlier consists of some combinations of the basic terrain materials shown. Each material has its own set of optical and thermal properties for use by the MOSART code.

TERRAIN MATERIALS

- | | |
|---------------------------------|-----------------------|
| • Water | • Sand |
| • Snow | • Rock |
| • Ice | • Packed Dirt |
| • Broad Leaf Trees [*] | • Tilled Soil |
| • Pine Trees | • Urban Commercial |
| • Irrigated Low Vegetation | • Urban Residential |
| • Meadow Grass | • Asphalt |
| • Tundra [*] | • Concrete |
| • Scrub | • Metal Building Roof |

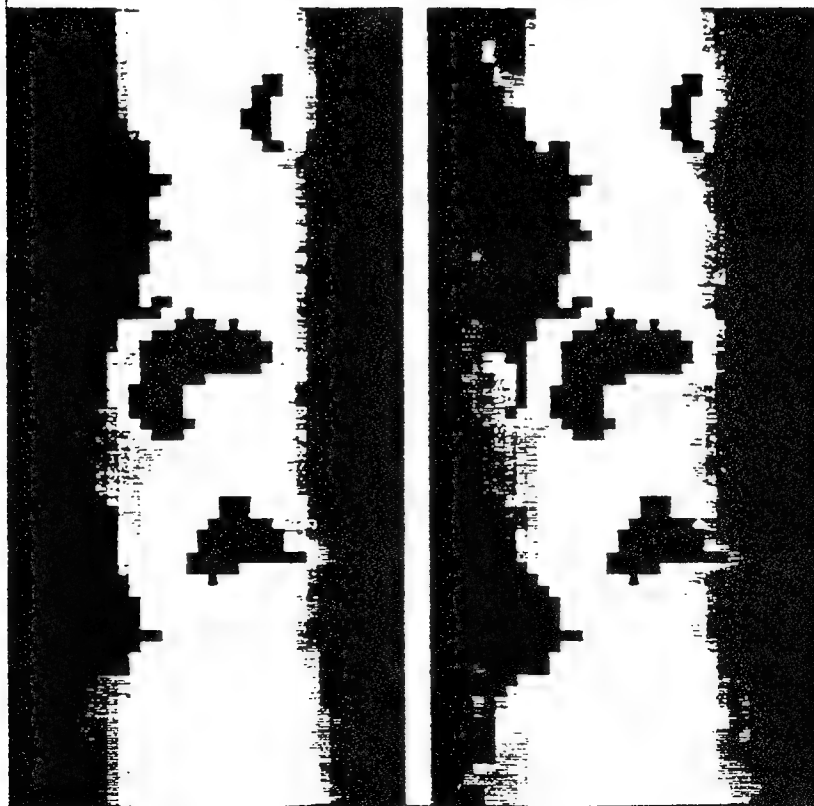
^{*} Summer and Winter Variations

Ocean Surface Temperature

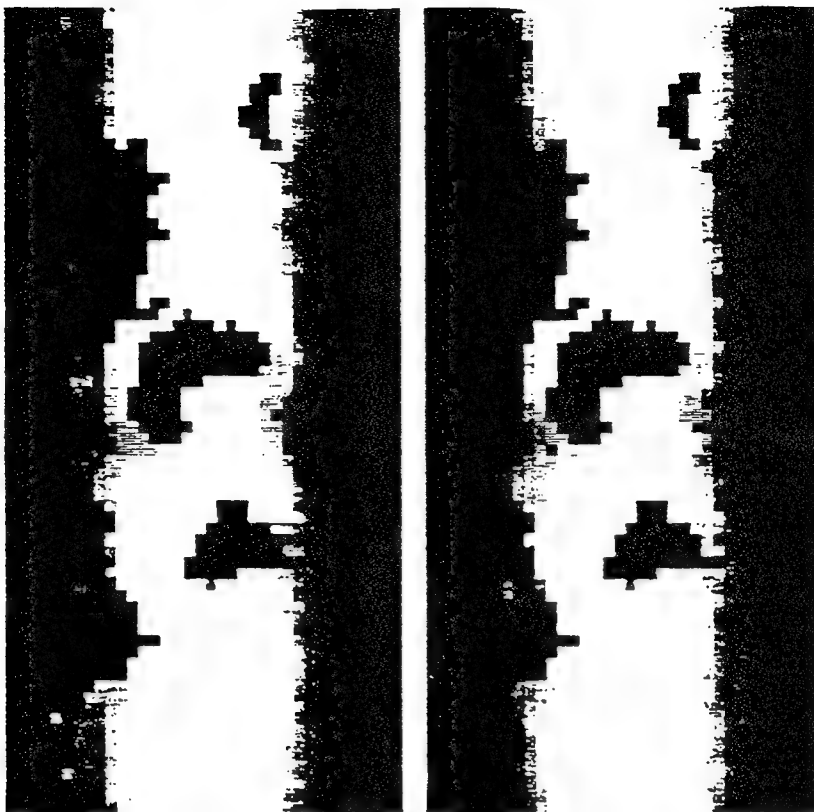
The temperature of the ocean surface is presented for four (4) seasons of the year. The spatial resolution of the data is 5 degrees by 5 degrees. In those cells where no ocean is present, a value of 0 K is used. In some regions of the globe, the data was rather sparse, so some cells were obtained by interpolating from measurements in adjacent cells.

OCEAN SURFACE TEMPERATURE

FEB - MAR - APR



MAY - JUN - JUL



AUG - SEP - OCT

NOV - DEC - JAN

Ref.: S. Levitus, Climatological Atlas of the World Ocean

Space Backgrounds

The space backgrounds used in the MOSART code are:

- Zodiacal light
- Mean star radiance (averaged over 5 degree by 5 degree cells)
- Galactic radiance
- Extragalactic radiance

The zodiacal light model is fairly sophisticated for compatibility with the Strategic Scene Generation Model. The other models are fairly simplistic models developed at Photon Research Associates, Inc. a number of years ago. The extragalactic radiance model was modified from the data in The Infrared Handbook (Zissis and Wolf) to include a 4 K uniform background.

SPACE BACKGROUND

- Zodiacal Light
- Mean Star Radiance
- Diffuse Galactic Sources
- Extra-Galactic Radiance:
 - Ref. The Infrared Handbook (3 - 30 μm)
 - 4 K Background

Molecular Absorption Parameters

The molecular absorption parameters are identical to the one used in the MODTRAN 2 code for the molecules shown. It includes values of S/d , $1/d$, and continuum due to line tails as a function of temperature and Lorentz line width. MOSART includes the capability to add additional molecules of interest. Also, the temperature dependence of the Lorentz line (i.e., the deviation from a square dependence) is also available not currently used by the data base.

MOLECULAR ABSORPTION PARAMETERS

- Taken from MODTRAN 2 (1992 Line Atlas)
- Parameters:
 - s/d (Function of Temperature)
 - 1/d (Function of Temperature)
 - Line Wing Continuum (Function of Temperature)
 - Lorentz Line Width
- Molecules:

- H ₂ O	- NO
- CO ₂	- SO ₂
- O ₃	- NO ₂
- N ₂ O	- NH ₃
- CO	- HNO ₃
- CH ₄	- N ₂
- O ₂	

MOSART Data Bases: Future Growth

The MOSART data bases, although quite extensive, still require upgrades and improvements, a few of which are presented here.

Concerning atmospheric profiles, the current data base is exclusively for the northern hemisphere. The pressure and temperature profiles for the southern hemisphere need to be added. Also, the NRL MSISE-90 molecular concentration profiles, which cover both hemispheres in 10 degree latitude increments for each month should be added.

The terrain data bases have not been updated in several years. The terrain material optical parameters need to be replaced by a set with much higher spectral resolution for compatibility with the atmospheric band parameters. More materials are needed, as are improved terrain material thermal properties. A number of additional deterministic scenes have been created since the data base was created. Statistical representations of these scenes need to be created and added to the data base.

MOSART DATA BASES: FUTURE GROWTH

- Atmospheres:
 - Southern Hemisphere
 - NRL MSISE-90 Molecular Concentrations
- Terrain:
 - Higher Spectral Resolution
 - More Materials
 - Improved Thermal Properties
 - Additional Scenes
- Ocean:
 - Bio-Matter and Salinity
 - Temperature Profile
- Suggestions?

North Korea

This North Korea scene is one example of a deterministic scene that can be added to the MOSART scene data base.

NORTH KOREA



Iraq

This Iraq scene is one example of a deterministic scene that can be added to the MOSART scene data base.

IRAQ



Iran

This Iran scene is one example of a deterministic scene that can be added to the MOSART scene data base.

IRAN



SHARC/SAMM/MODTRAN CALCULATIONS USING A CLIMATOLOGY MODEL ATMOSPHERE GENERATOR

S. Adler-Golden, J. Gruninger,
and M. Matthew

Spectral Sciences Inc.
99 S. Bedford St.
Burlington, MA 01803

Upper atmospheric IR radiances have been simulated using new input profiles that describe latitude, seasonal, solar/geomagnetic, and diurnal (including solar terminator) variabilities. The profiles, from the SHARC Atmosphere Generator, are based on a combination of semi-empirical models, including the new NRL climatology database and the MSISE-90 model, and theoretical calculations. Agreement with field experiments is greatly improved, and the terminator behaviors of O₃ and OH emissions can be simulated with SHARC for the first time. The profiles can be generated down to sea level for use with SAMM, MODTRAN, or other codes that cover the lower atmosphere.

SHARC/SAMM/MODTRAN Calculations Using a Climatology Model Atmosphere Generator

S. Adler-Golden, J. Gruninger, and M. Matthew
Spectral Sciences Inc.
99 S. Bedford St., Burlington, MA 01803

Annual Review Conference on Atmospheric
Transmission Models

Geophysics Directorate, Phillips Laboratory
Hanscom AFB, MA 01731-5000

8-9 June 1993



MOTIVATION

OVERALL OBJECTIVE:

Improve Accuracy of IR Radiance Codes (MODTRAN, SHARC, SAMM, etc.) by Using Realistic Atmospheric Temperatures and Species Densities

- Provide Access to Atmospheric Models and Databases
- Incorporate Atmospheric Variability
- Permit Terminator Modeling Capability
- Provide Common Profiles for Different Codes



OUTLINE

1. Basic Atmospheric Profile Models
MSISE-90, NRL Climatology Database
2. SHARC/SAMM Atmosphere Generator
3. Illustrative Calculations
 H_2O , CO_2 , NO , O_3 Profiles, Limb Radiances
4. Summary



CLIMATOLOGY MODELS

- NRL DATABASE (Summers et al.)
 - Month and latitude averages
 - Includes Most IR-Active Species
 - Altitude Range 0-120 km
- MSISE-90 (NASA/Hedin)
 - Extends MSIS Down to Ground
 - Provides P, T, N₂, O₂, O, H Profiles
 - Includes Solar/Geomagnetic Variability
 - Lacks IR-Active Species

NEEDED: NO, CO₂, O₃ (Upper Atmosphere)
Terminator Behavior
SAMM/MODTRAN Trace Species



SHARC/SAMM ATMOSPHERE GENERATOR

- Incorporates NRL Database, MSISE-90
- Includes Empirical Terminator/Diurnal Models
For O_3 , OH, NO, CO_2 , O
Utilizes Calculations by Rodrigo et al.
- 0-300 km Altitude Range, Arbitrary Layering
- Interactive, Menu-Driven
Inputs: lat, long, day, time, F10.7, Ap
Default Options Also Available
- Output Formats Compatible with SHARC, SAMM,
MODTRAN/LOWTRAN



SHARC/SAMM ATMOSPHERE GENERATOR

Species	PROFILE SOURCES				CODES		
	MSISE-90	NRL	AFGL	Custom	SHARC	SAMM	LOW/MOD
T	x				x	x	x
N ₂	x				x	x	
O ₂	x				x	x	x
CO ₂				x	x	x	x
NO			x	x	x	x	x
O ₃		x		x	x	x	x
H ₂ O		x			x	x	x
CO		x			x	x	x
CH ₄		x			x	x	x
N ₂ O		x			x	x	x
HNO ₃		x			x	x	x
NO ₂		x			x	x	x
SO ₂			x		x	x	x
NH ₃			x		x	x	x
O		x					
OH	x			x	x	x	
H	x			x	x	x	



IR RADIANCE CALCULATIONS

ADVANTAGES OF APPROACH:

No Two Calculations Are The Same

DISADVANTAGES OF APPROACH:

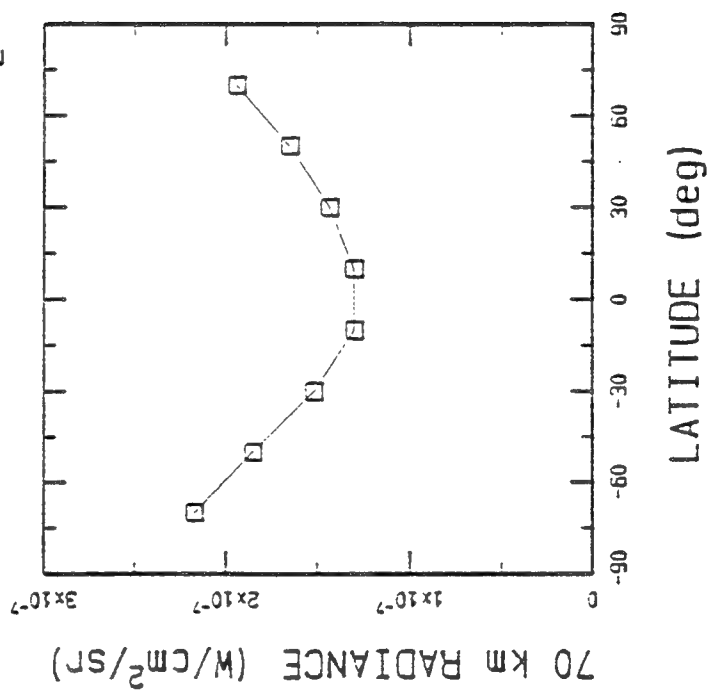
No Two Calculations Are The Same



H₂O LIMB RADIANCE

17-25 μ M ROTATIONAL EMISSION SIMULATION FOR CIRRIS-1A

MODTRAN/MSIS/NRL H₂O

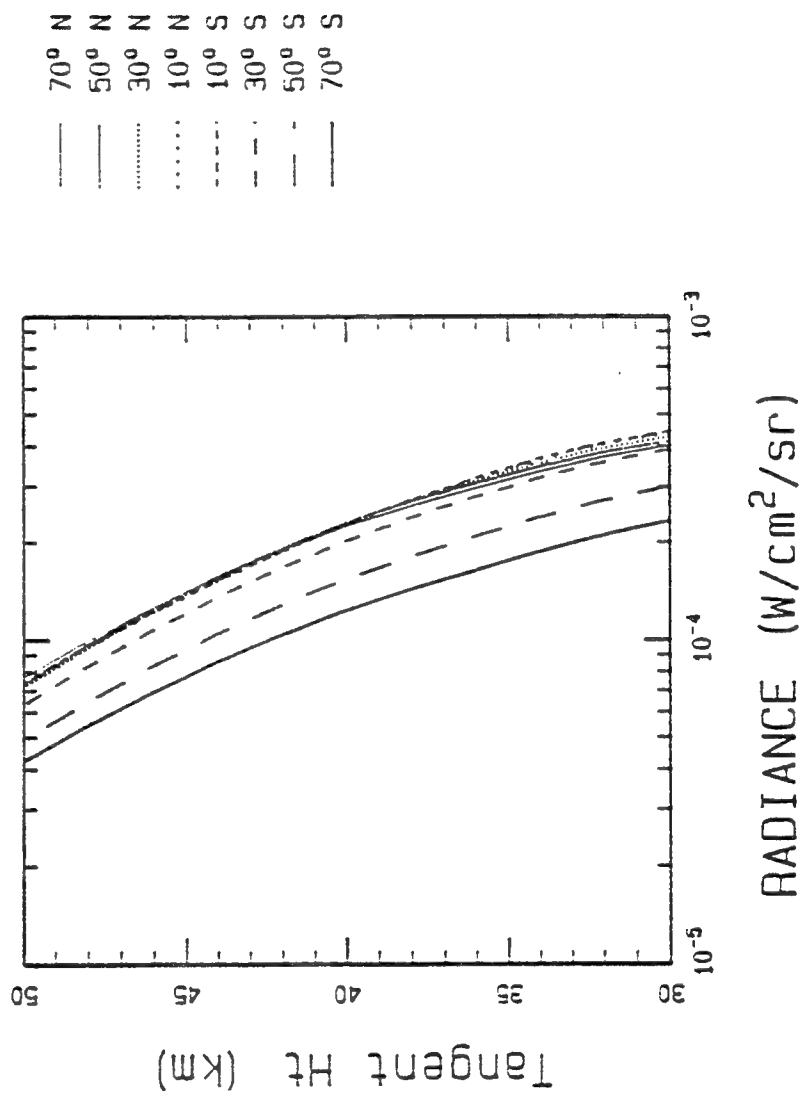




STRATOSPHERIC CO₂

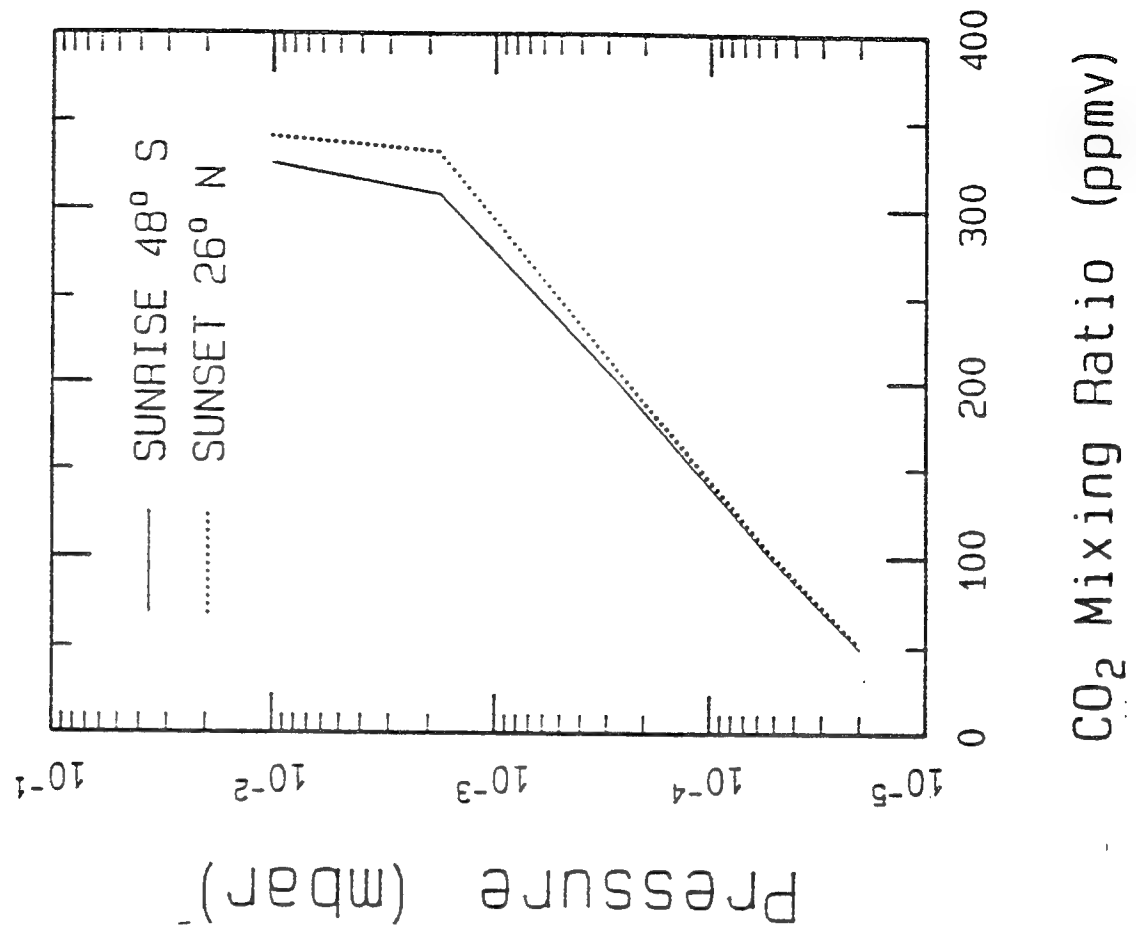
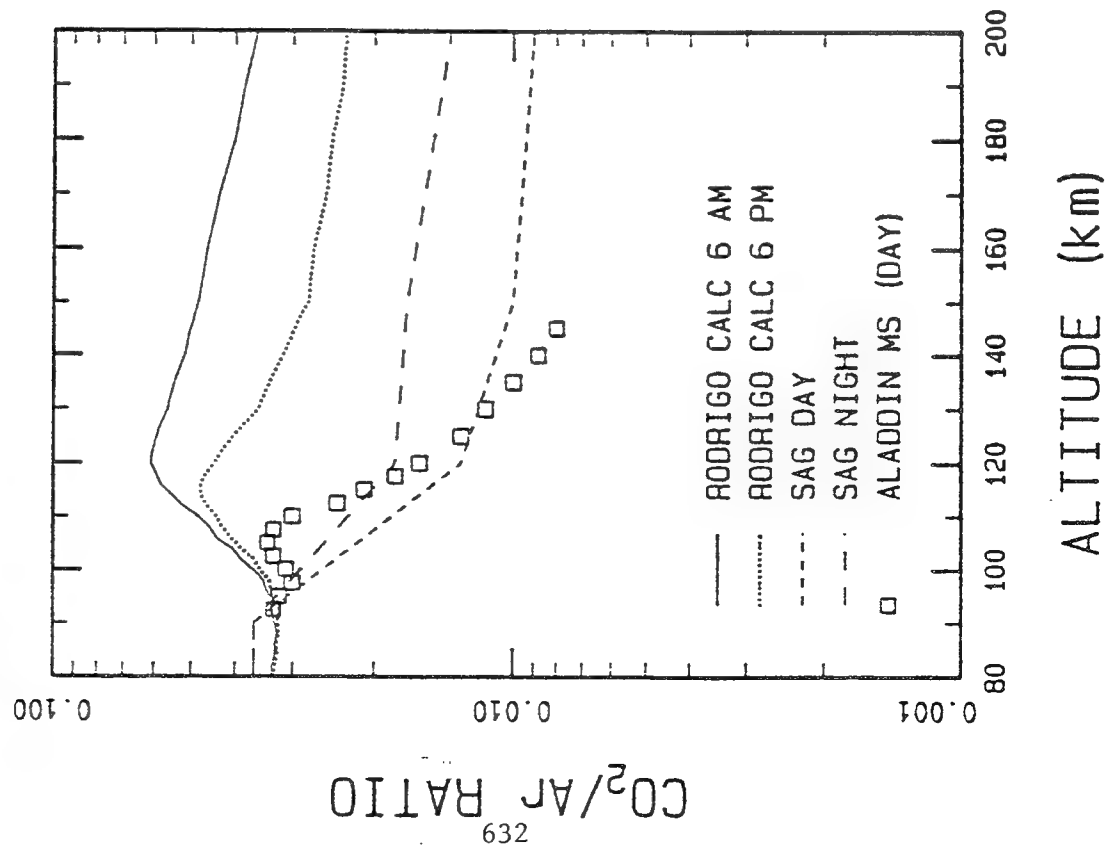
MODTRAN Calculation for Horizon Sensor Simulation

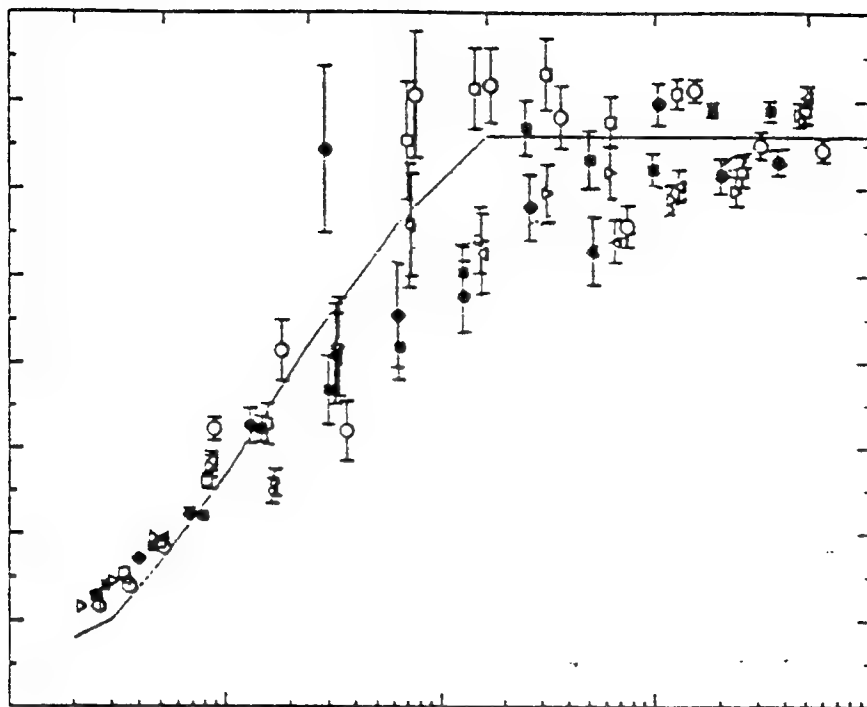
14-16 μm Radiance





UPPER ATMOSPHERIC CO₂







UPPER ATMOSPHERIC CO₂

SHARC VS. CIRRIIS-1A DATA (J. O. Wise et al.)

ν_2 Nighttime Radiance (W/cm²/sr)

100 km 120km 140 km

Avg Mlat < 60	6.2E-7	1.4E-7	1.3E-8
SHARC/SAG	3.7E-7	1.2E-7	1.7E-8

Night/Day Ratio

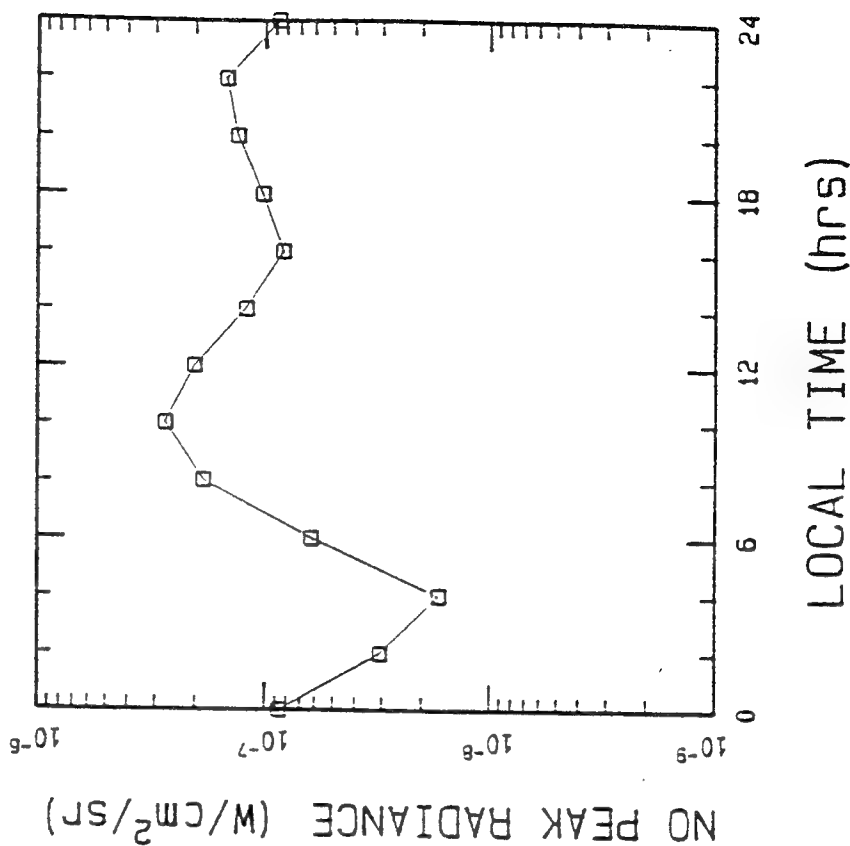
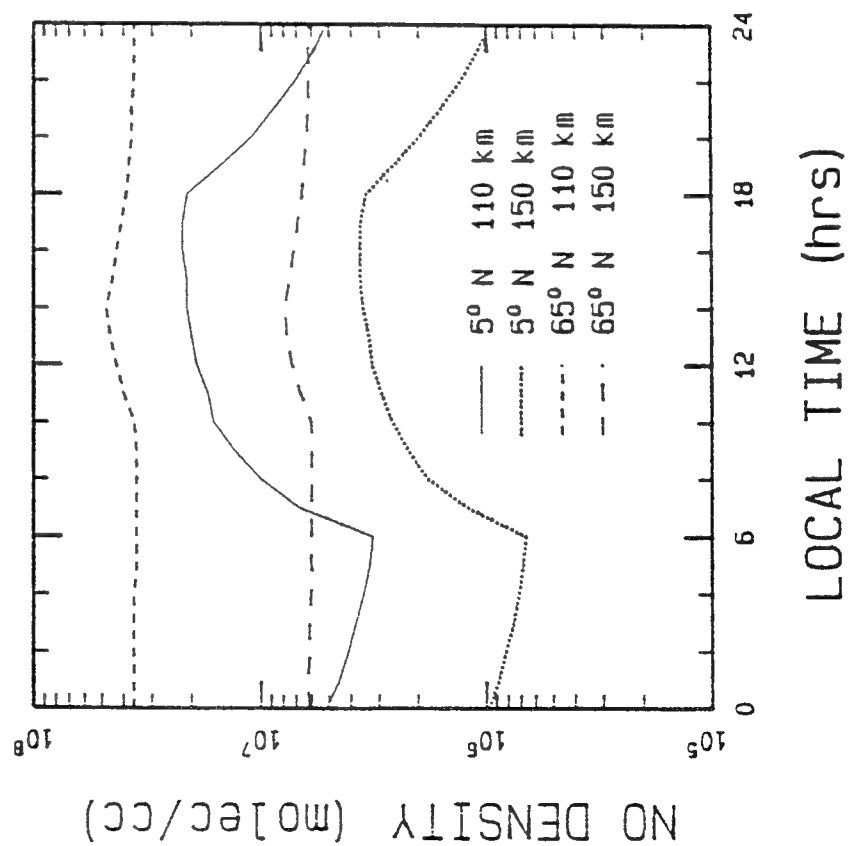
Avg Mlat < 60	0.85	0.77	0.67
SHARC/SAG	0.84	0.75	0.65



UPPER ATMOSPHERIC NO

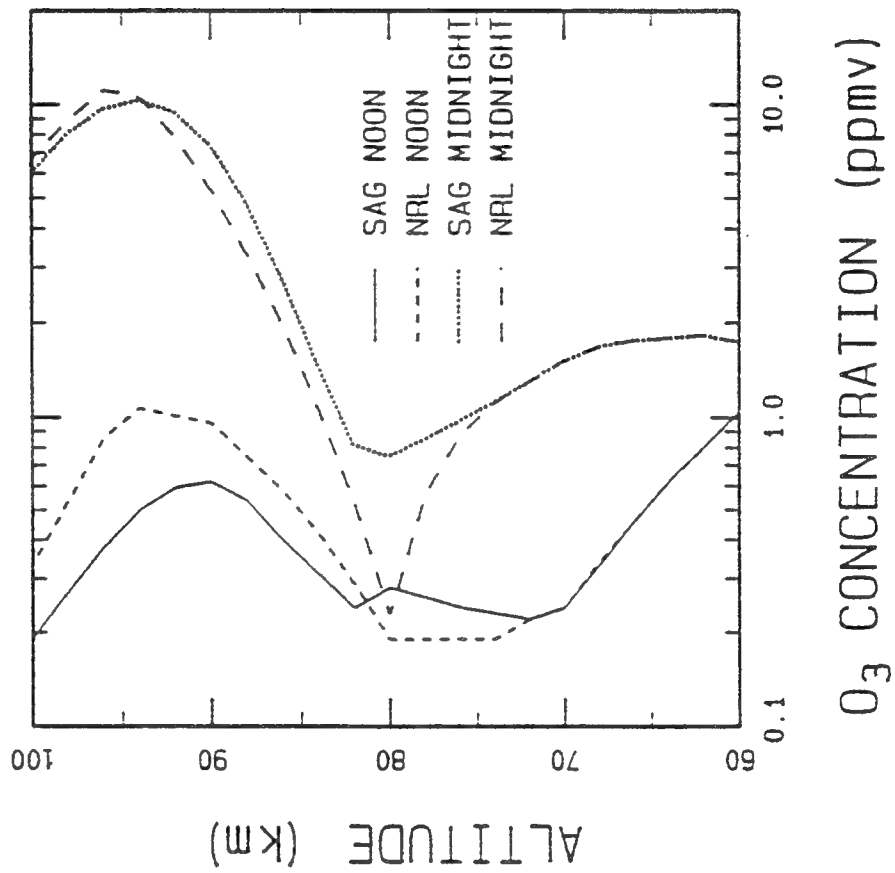
DIURNAL/LATITUDE VARIATION

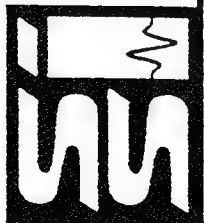
CIRRIS-1A ORBIT



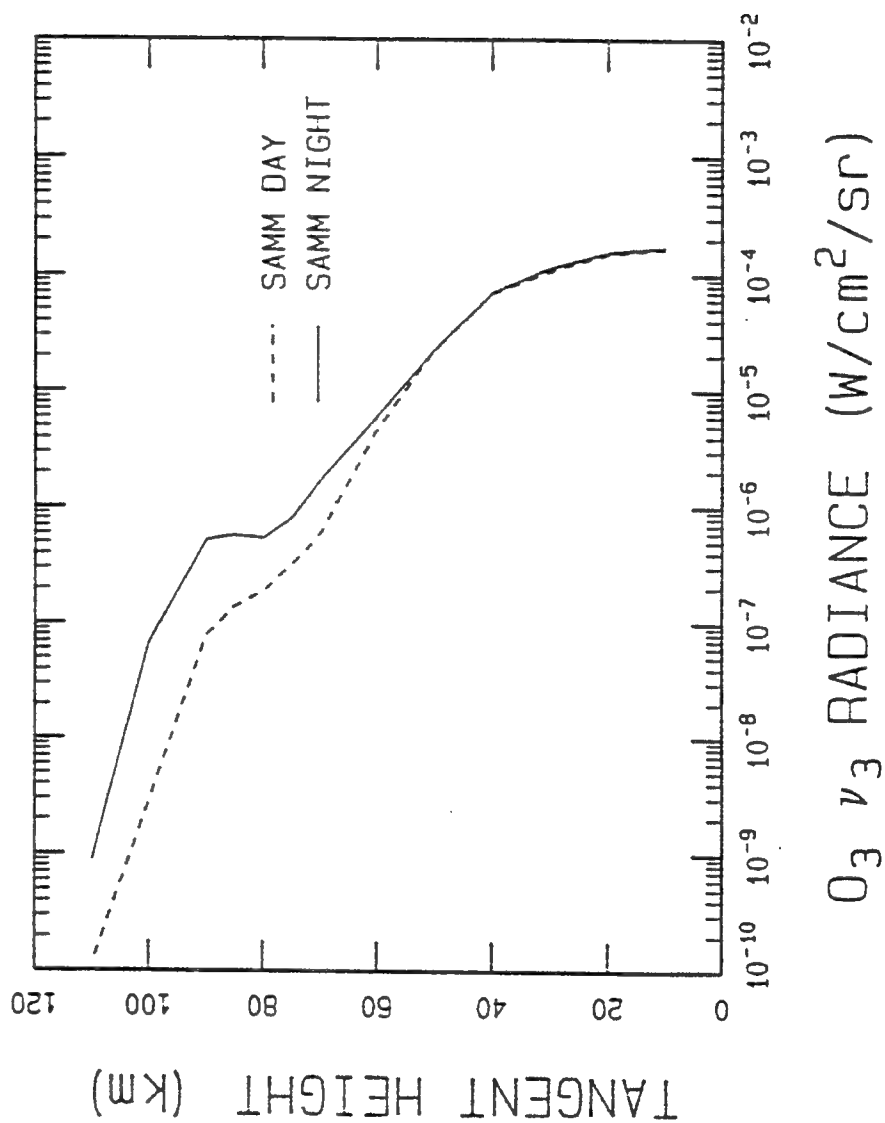


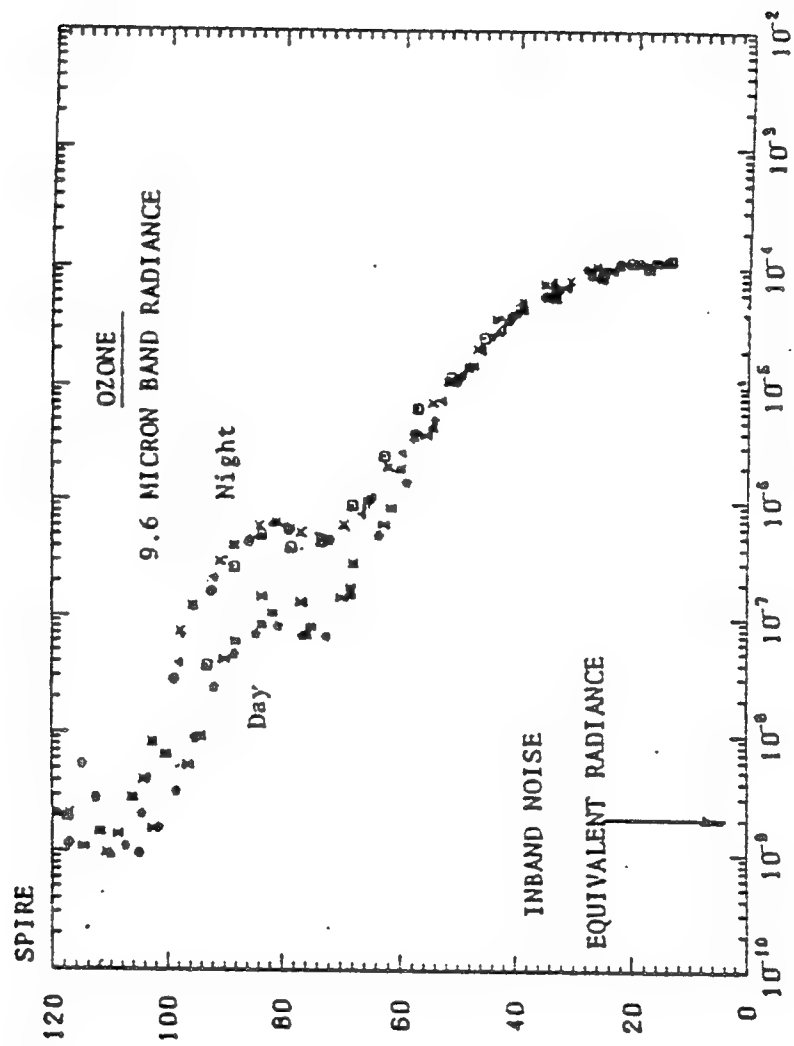
O₃ CONCENTRATION PROFILE

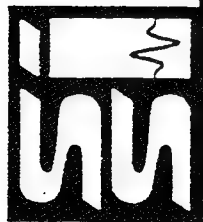




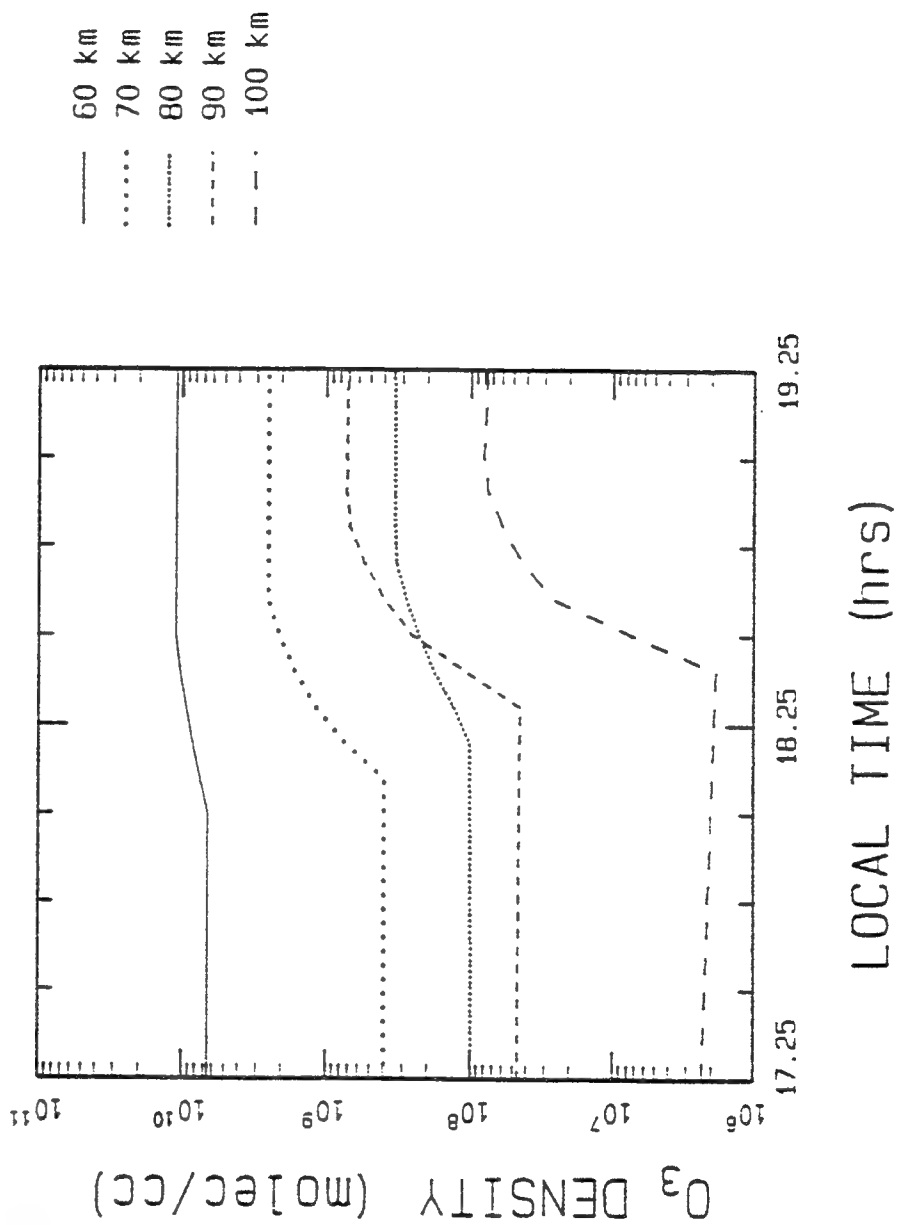
O_3 LIMB RADIANCE

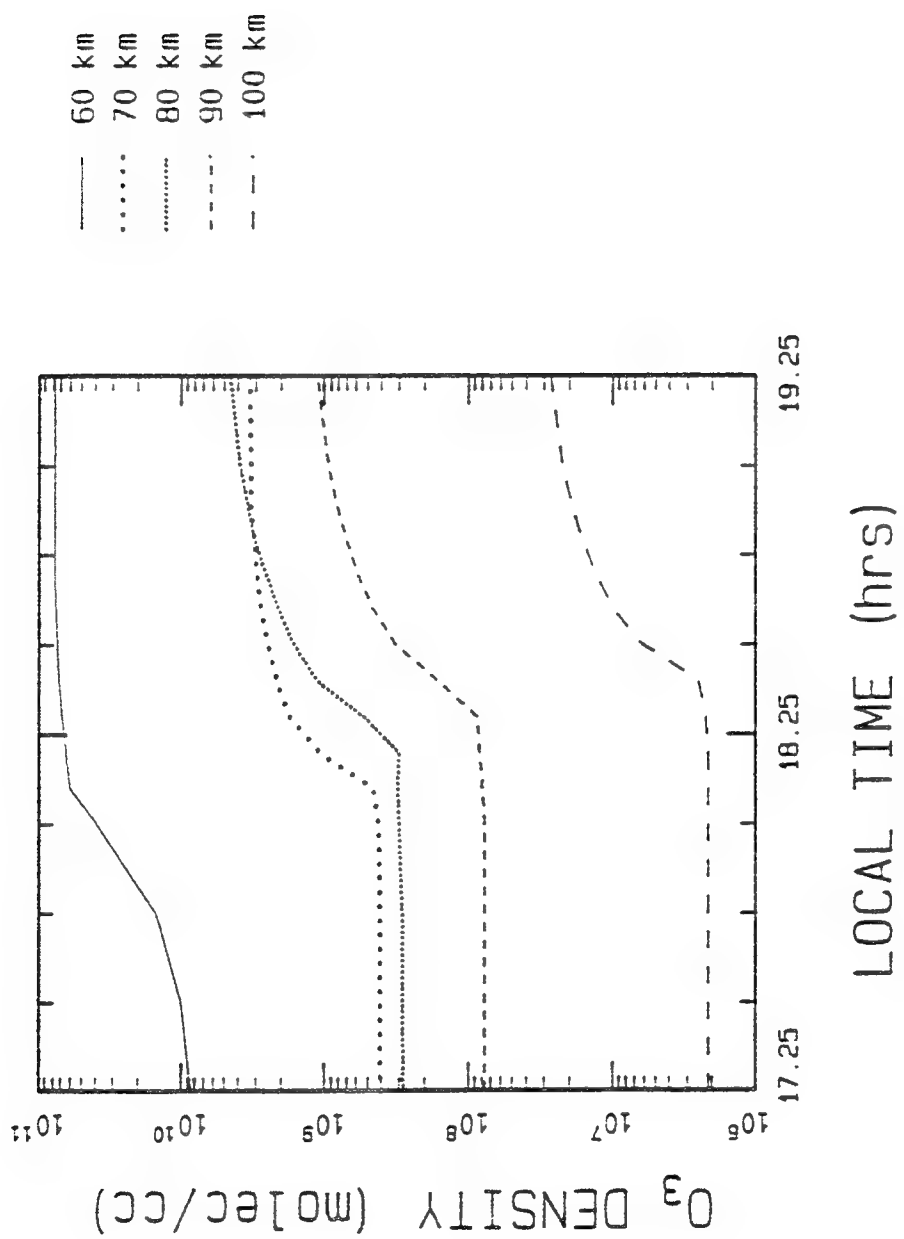






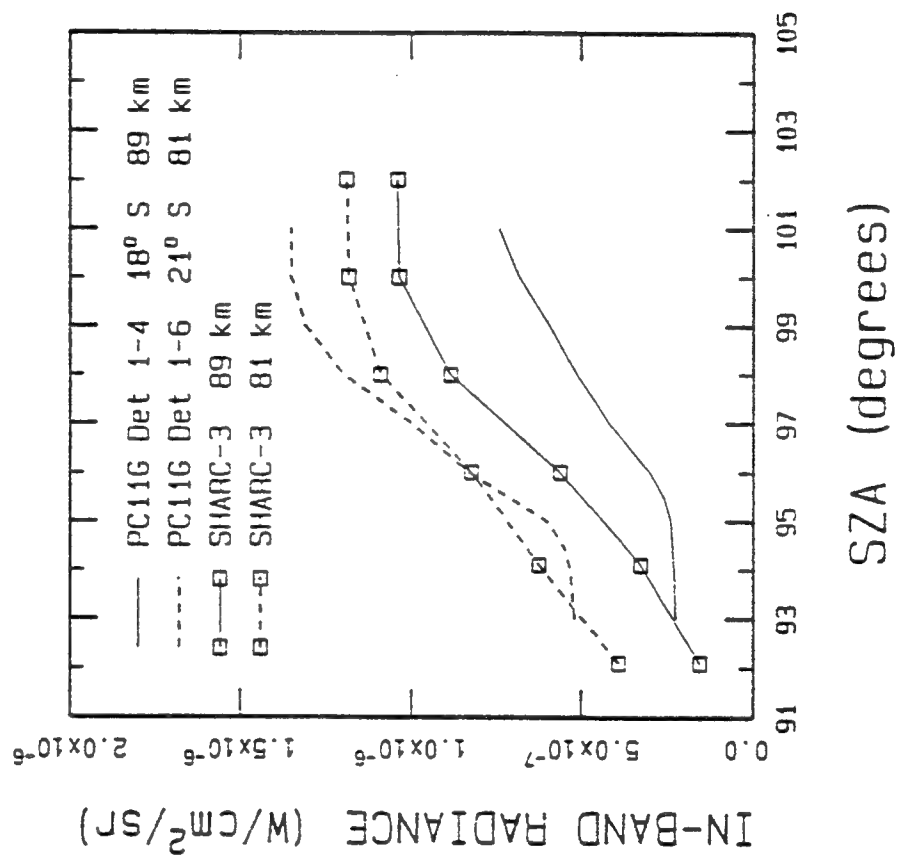
O₃ TERMINATOR BEHAVIOR







O₃ TERMINATOR: DATA/MODEL COMPARISON





SUMMARY

SHARC/SAMM ATMOSPHERE GENERATOR DEVELOPED
Integrates Empirical Climatology Models with Air Force
IR Radiation Codes

- Supports SHARC, SAMM, MODTRAN/LOWTRAN
- Interactive, Stand-Alone Program
- Diurnal, Latitude, Seasonal, Solar, Geomagnetic,
Terminator Variabilities Included
- 0-300 km Altitudes, Arbitrary Layering

EXPLORATORY RADIANCE CALCULATIONS PERFORMED

- Systematic Comparisons with Data Planned
- Initial Comparisons Show Good Agreement

IMPROVEMENTS RECOMMENDED: Odd Nitrogen, H, O Profiles

Wednesday 9 June 1993 p.m.

SESSION G: LIDAR APPLICATIONS

Chair: E.P. Shettle, Naval Research Lab

DEVELOPMENT OF A SIGNAL-TO-NOISE PERFORMANCE MODEL WITHIN BACKSCAT VERSION 4.0

M.G. Cheifetz, D.R. Longtin, and J.R. Hummel

SPARTA, Inc.
24 Hartwell Ave.
Lexington, MA 02173

The lidar backscatter simulation, BACKSCAT Version 4.0, has expanded its capabilities and now includes a comprehensive and versatile signal-to-noise performance model. This signal-to-noise (SNR) model can give performance and sensitivity estimates for both direct detection and coherent (heterodyne) lidar systems. The model contains all the important noise sources inherent in the detection process and allows various detector types to be simulated and analyzed. In this paper we will summarize the SNR model and its inputs, describe some of the built-in detectors, and give examples.

Research Supported by Phillips Laboratory, Geophysics Directorate
Contract F19628-91-C-0093

DEVELOPMENT OF A SIGNAL-TO-NOISE PERFORMANCE MODEL WITHIN BACKSCAT 4.0

By
M.G. Cheifetz, D.R. Longtin, & J.R. Hummel

At
Annual Review Conference on
Atmospheric Transmission Models
Phillips Laboratory/Geophysics Directorate
Hanscom AFB, MA

9 June 1993

SPARTA, Inc.
24 Hartwell Avenue
Lexington, MA 02173
(617) 863-1060

*** Work Performed Under Contract F19628-C-91-0093**



OUTLINE

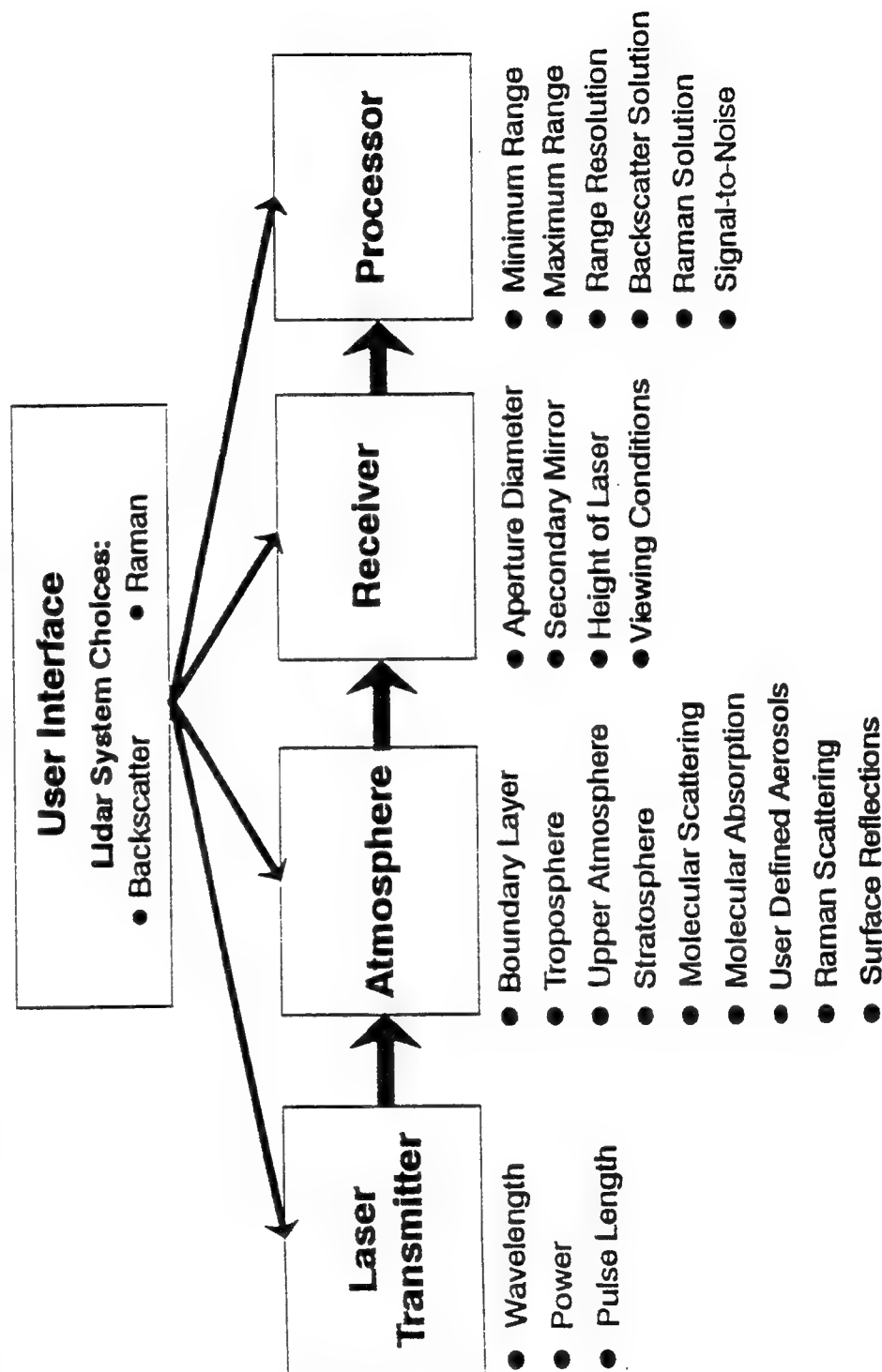
- SNR Model Description
- Example Results
- Summary



BACKSCAT VERSION 4.0

A LIDAR SIMULATION TOOL

Developed for the Geophysics Directorate of Phillips Laboratory, BACKSCAT is Used to Study the Performance of Lidars Under Different Laser System and Atmospheric Conditions





BACKSCAT SIGNAL-TO-NOISE PERFORMANCE MODEL

- SNR Performance Predictions Now Included in BACKSCAT for Both Direct Detection and Coherent Lidar Systems
 - Based on standard signal-to-noise relations
- Any Detector Type and Spectral Region may be Used
- Detection System Model Includes All Important Noise Sources



SNR PERFORMANCE MODEL

PERFORMANCE MODEL INCLUDES EFFECTS FROM:

<u>SIGNAL</u>	<u>NOISE</u>
<ul style="list-style-type: none"> • Hardware Optical Efficiencies • Atmospheric Attenuation • Aerosol Backscatter • Detector Quantum Efficiency • Aperture Size/Obscuration • Laser Output Power • Laser Beam Quality 	<ul style="list-style-type: none"> • Signal Photon Shot Noise • Background Photon Shot Noise • Thermal (Johnson) Noise • Detector Dark Current • Preamplifier Noise • Spatial/Spectral/Temporal Noise Suppression • Hardware Optical Efficiencies • Detector Quantum Efficiency • Detector NEP & Excess Noise Figure



SNR MODEL (NEW) INPUTS

- Detector Parameters
 - Quantum efficiency (responsivity)
 - Gain
 - Excess noise figure
 - Noise sources
 - Thermal (Johnson) , dark current, amplifier
 - or
 - System NEP (D^*)
- Background Spectral Radiance
- Receiver Spectral Filter Width for Background Suppression
- Transmitter and Receiver Optical Efficiencies
- Receiver Field-of-View



SNR MODEL ASSUMPTIONS

- SNR Relatively Large
 - Not in photon counting regime
- Matched Filter in Detection System ($B = 1/2t$)
- Only Pulsed Laser System Presently Included
 - No CW scanning system
- Receiver and Transmitter FOVs Matched
- Turbulence Effects Not Included
- Flicker ($1/f$) Noise Not Considered

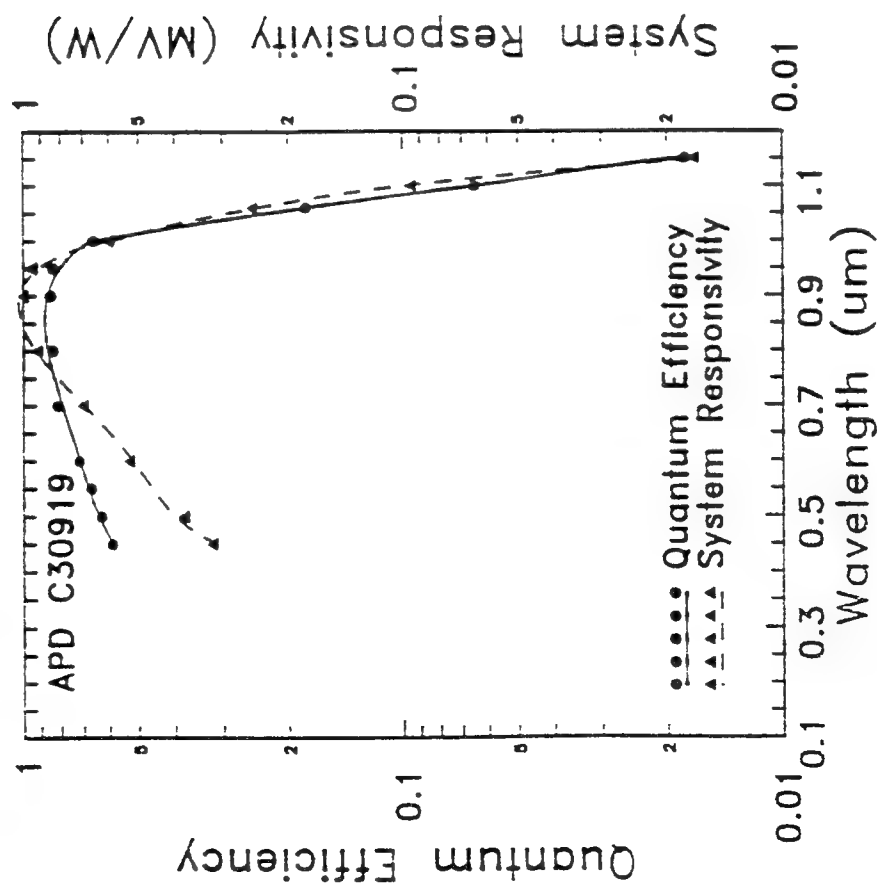


MODEL DETECTORS

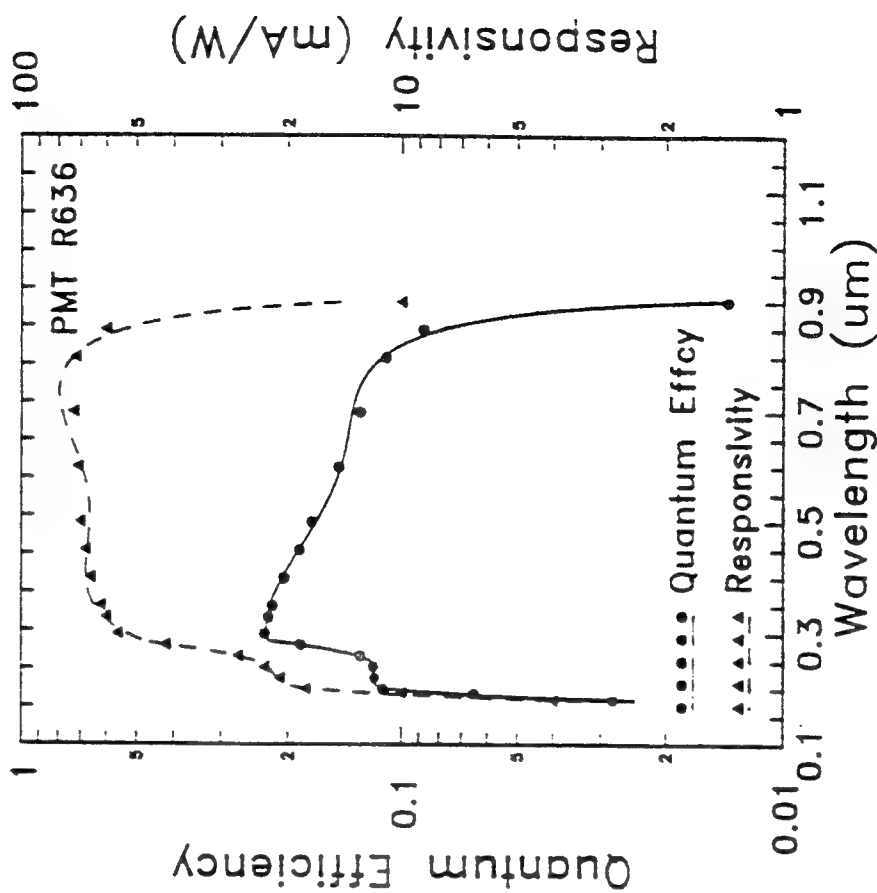
- Choice of Built-in or User Supplied Detectors
 - Five Detectors Operating Within Various Spectral Regions Built-in:
 1. APD - visible
 2. "Dimpled" APD - 1 μm optimized
 3. PMT - visible
 4. PMT - uv
 5. HgCdTe PV LWIR (10 μm)
- Quantum efficiency-gain-NEP curve fit over applicable region



MODEL DETECTOR RESPONSIVITIES



#1 Visible APD



#3 Visible PMT



TYPICAL LIDAR SYSTEM

- DIRECT DETECTION -

- Default Lidar/Atmospheric Inputs Supplied With BACKSCAT Code Were Used
- Lidar on Ground, 20° Elevation, Nighttime Operation
 - 50 cm diameter outer aperture, no obscuration
 - Receiver/detector system - visible APD (Detector #1)
 - 88% quantum efficiency
 - $2 \times 10^{-14} \text{ W/Hz}^{1/2}$ spectral NEP
 - $F = 3$, excess noise figure
 - 80% optical efficiency
 - Laser transmitter
 - 0.85 μm wavelength
 - 100 mJ per pulse with a 70 ns pulse length
 - 90% optical efficiency

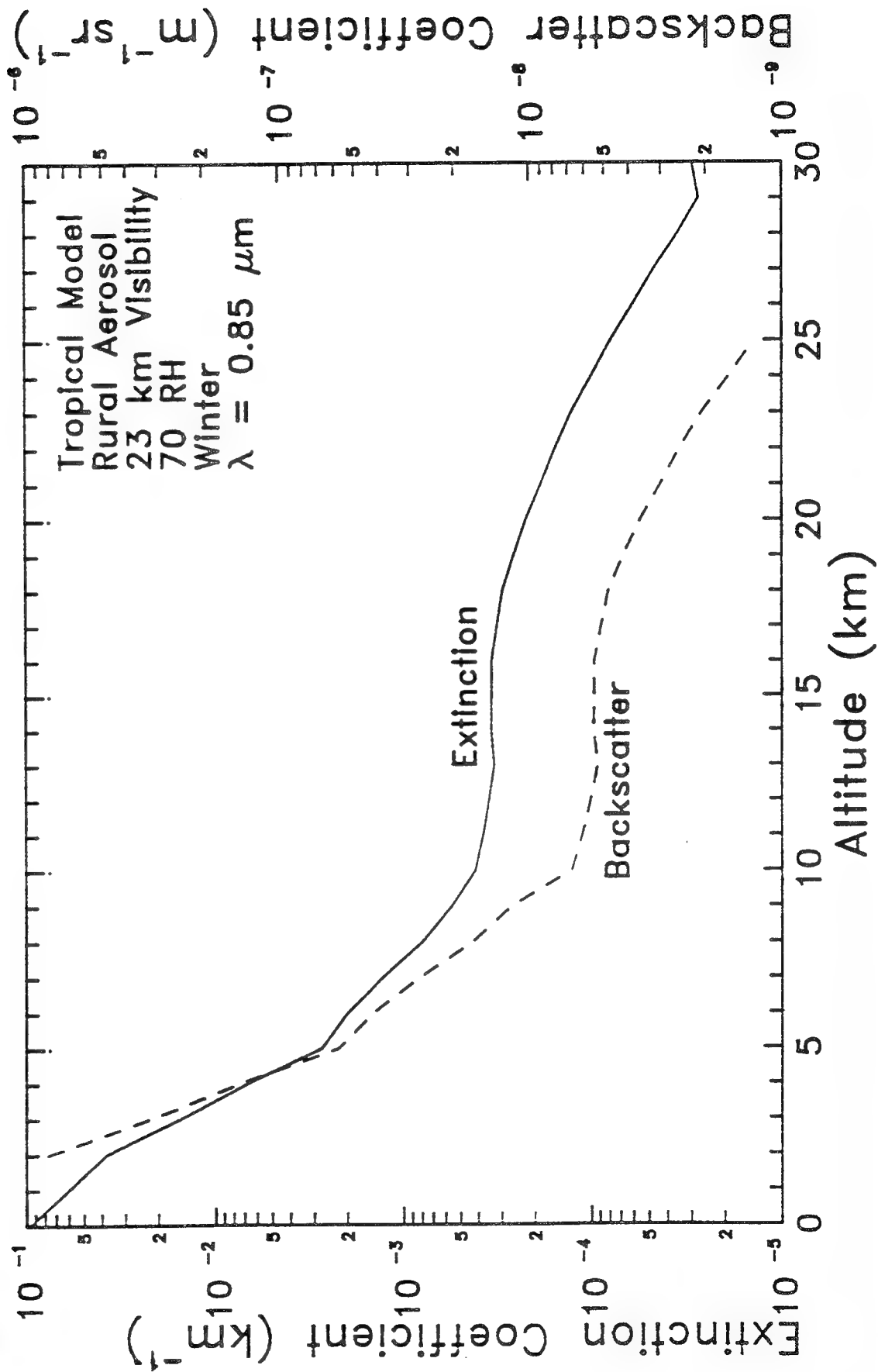


ATMOSPHERIC PARAMETERS

- Tropical Atmosphere
- Rural Aerosol Boundary Layer, 70% RH
- 23 km Visibility
- Fall/Winter Season
- Background Stratospheric Aerosol

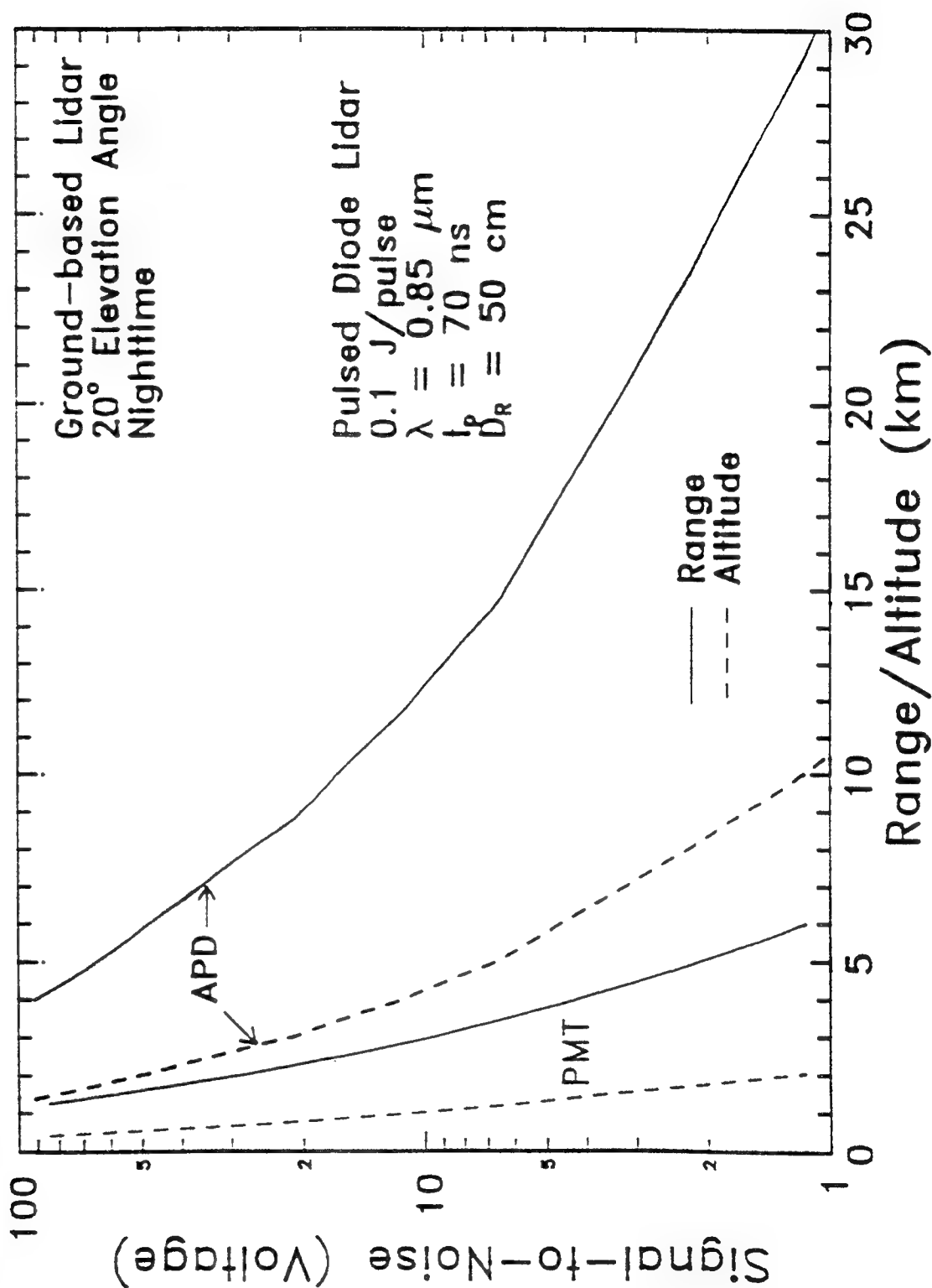


ATMOSPHERIC PROFILE





PERFORMANCE PREDICTIONS - DIRECT DETECTION -





SUMMARY

- Major Upgrade Made to BACKSCAT (Version 4)
- Allows for “Actual” System Performance Predictions
 - Direct detection and coherent systems
 - Pulse systems only, at present
- Future Upgrades to Include CW Scanning Systems and Turbulence Effects

**AN OPTICAL PROFILE FUNCTION FOR MODELING EXTINCTION AND
BACKSCATTER COEFFICIENTS IN VERY LOW STRATUS CLOUDS
AND SUBCLOUD REGIONS**

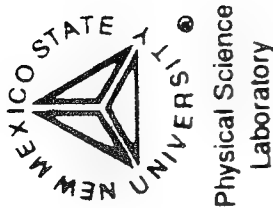
Neal Kilmer

Henry Rachele

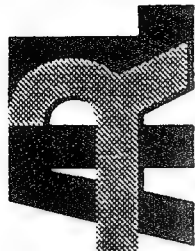
Physical Science Lab
New Mexico State Univ.
Las Cruces, NM 88003

Battlefield Envir'ment Directorate
U.S. Army Research Lab
WSMR, NM 88002

A theoretically based microphysics model developed by the authors simulated 135 vertical profiles of drop size distributions in and below very low stratus clouds. These profiles were computed as a function of air mass type, maximum liquid water content, and surface (2 m) values of temperature, relative humidity, and visibility representative of worldwide conditions. These drop size distribution profiles with Mie efficiency factors simulated vertical profiles of extinction and backscatter coefficients for eight wavelengths. The extinction and backscatter profiles were fit with the Rachele-Kilmer (RK) optical profile function to significantly simplify computation procedures. All constants required to evaluate the RK optical profile function have been placed in computer-accessible storage, and a computer program for performing the calculations has been prepared and is available to DoD users. Use of this program is described.



ARMY RESEARCH LABORATORY



AN OPTICAL PROFILE FUNCTION FOR MODELING EXTINCTION AND BACKSCATTER COEFFICIENTS IN VERY LOW STRATUS CLOUDS AND SUBCLOUD REGIONS

Neal H. Kilmer (PSL)

Henry Rachele (ARL)

SOME PRODUCTS OF RK MODEL

Vertical profiles of:

- Drop size distribution
- Relative humidity
- Temperature
- Drop concentration
- Liquid water content

PURPOSE

To present a relatively simple continuous function that can be calculated easily to simulate vertical profiles of extinction and backscatter coefficients in very low stratus clouds and subcloud regions representative of worldwide conditions.

THE RK OPTICAL PROFILE FUNCTION

$$\sigma_e = \sigma_{e1} \left(\frac{\sigma_{e2}}{\sigma_{e1}} \right)$$

$$\left(\frac{z - z_1}{z_2 - z_1} \right)^{N(z)}$$

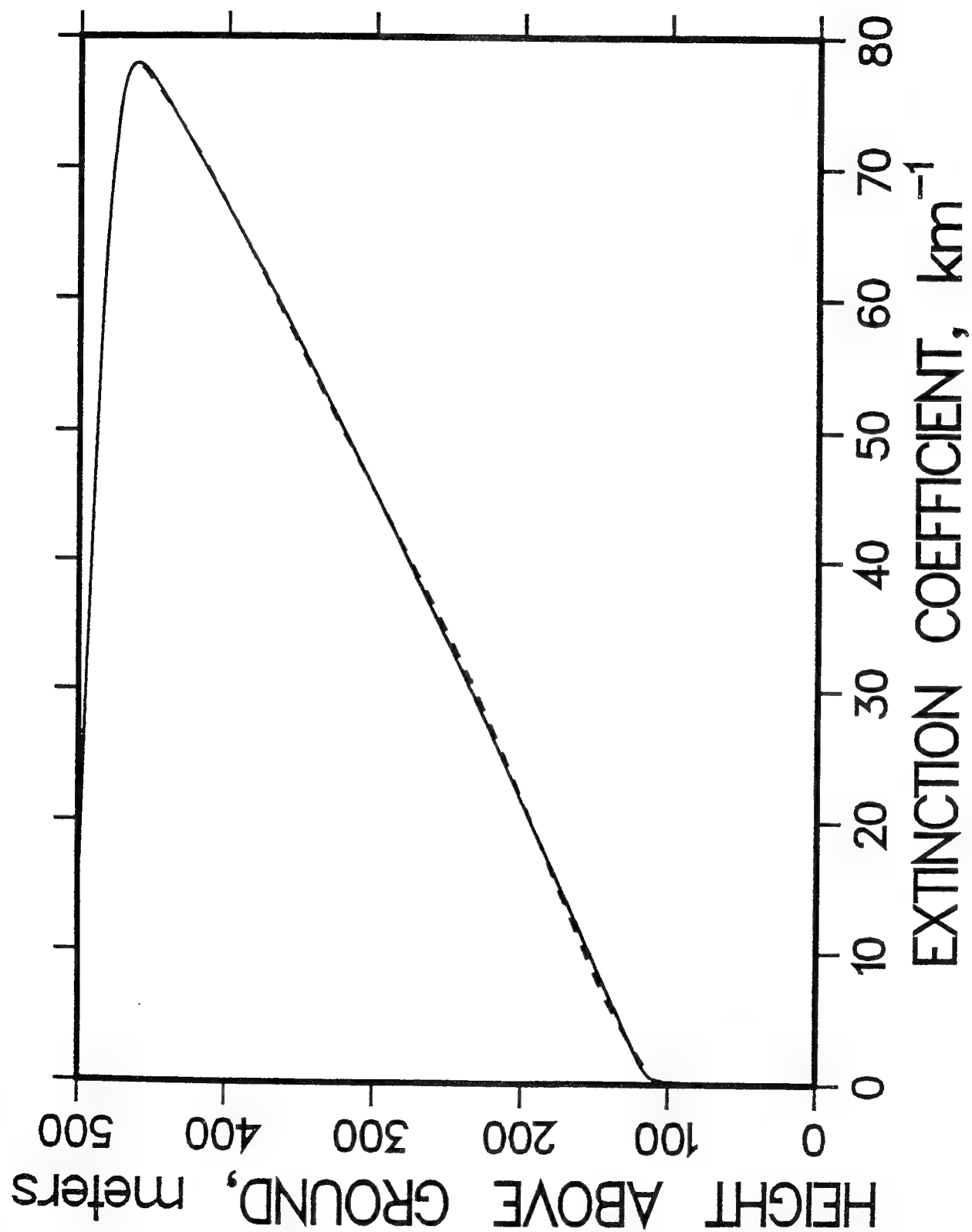
$$N(z) = \exp (c_* + d_* z + e_* z^2 + f_* z^3)$$

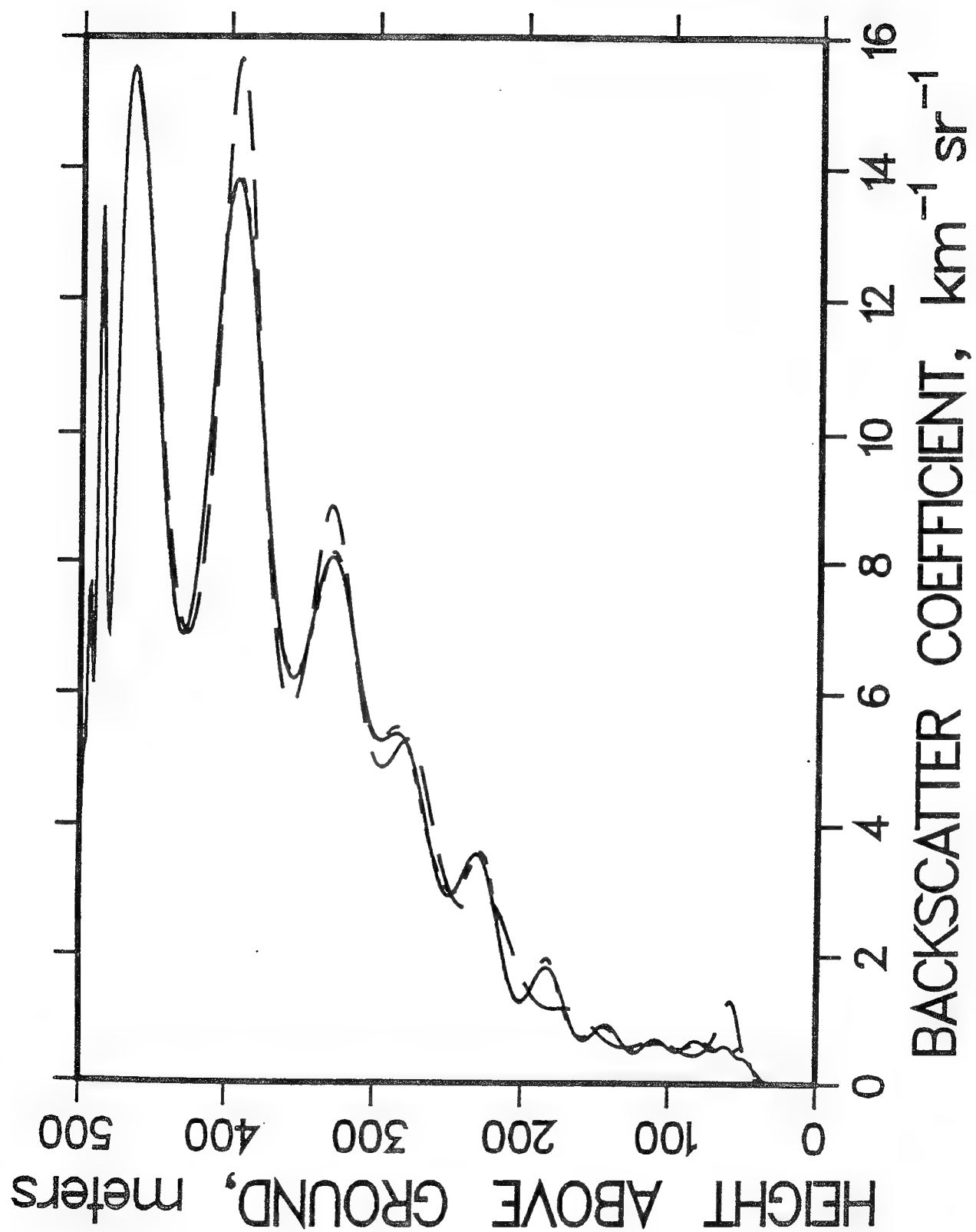
$$N(z) = A_0 + C_1 z + C_2 z^2 + 2 \sum_{n=1}^{N_A} A_n \cos \left[\frac{2\pi n(z - z_{F1})}{z_{F2} - z_{F1} + 1} \right]$$

$$- 2 \sum_{n=1}^{N_B} B_n \sin \left[\frac{2\pi n(z - z_{F1})}{z_{F2} - z_{F1} + 1} \right]$$

$$\frac{\ln \left(\frac{\ln \sigma_e - \ln \sigma_{e1}}{\ln \sigma_{e2} - \ln \sigma_{e1}} \right)}{\ln \left(\frac{z - z_1}{z_2 - z_1} \right)}$$

$$N(z) =$$





PROGRAM RKOPF - USER OPTIONS

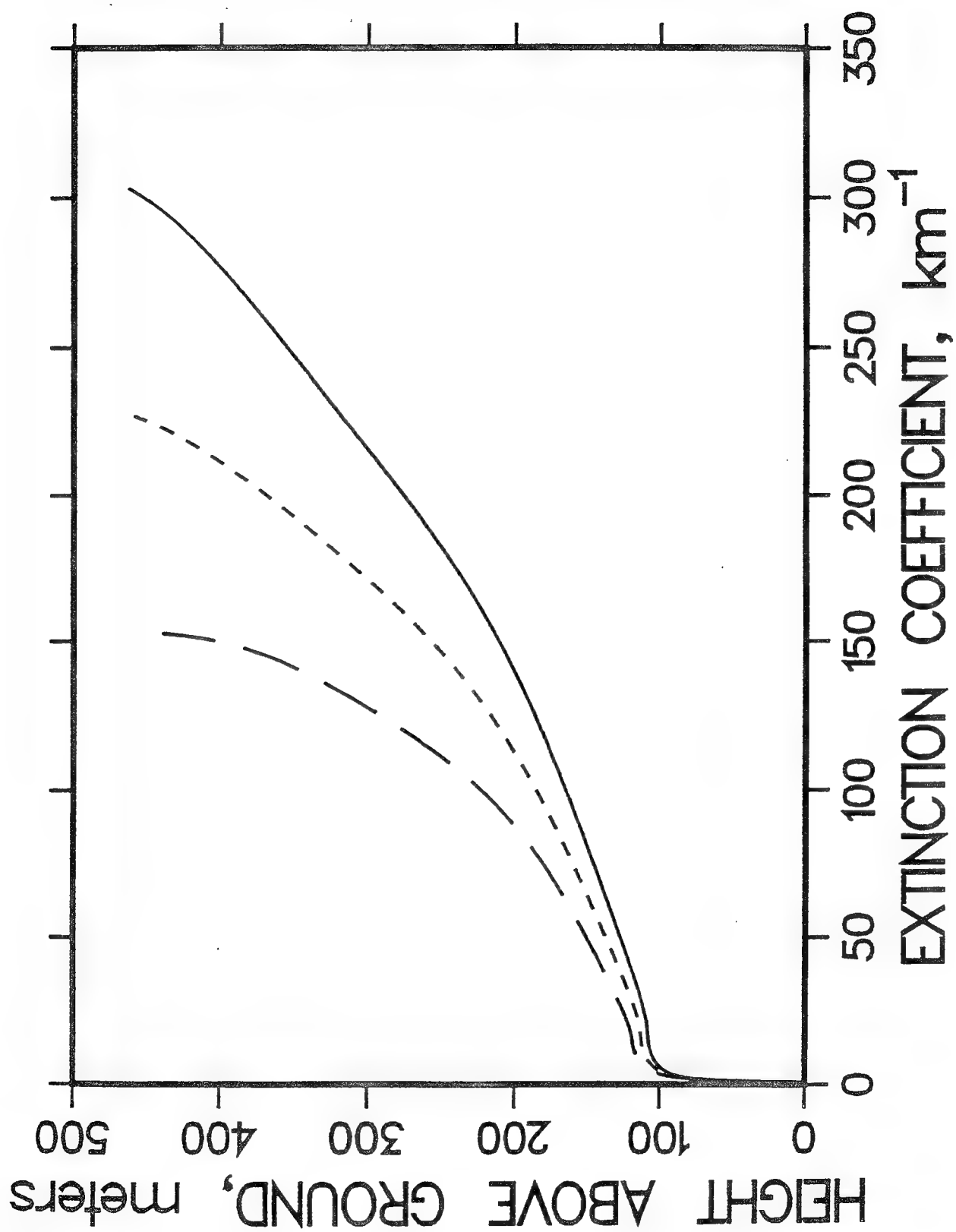
- Air mass type
- Relative humidity at reference height
- Visibility at reference height
- Ambient air temperature at reference height
- Maximum liquid water content
- Wavelength of transmission radiation
- Type of profile (extinction and/or backscatter coefficient)

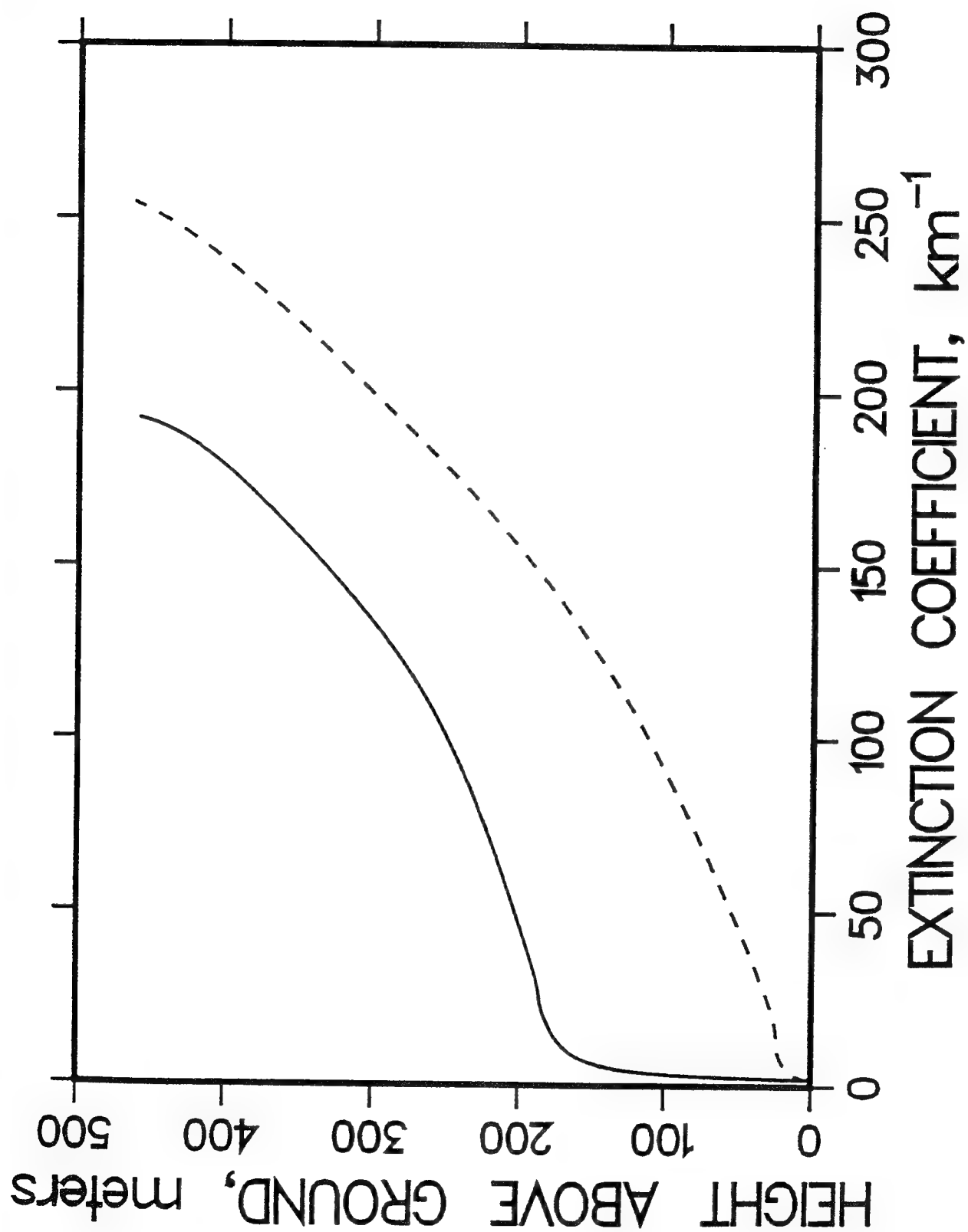
USER OPTIONS FOR OUTPUT

- Name of output file
- Lower and upper height bounds for calculated profile
- Height spacing

FORM OF OUTPUT FILE

- First line: Number of points, line type, symbol type (3i5)
- Remaining lines (one for each data point): Extinction or backscatter coefficient, height above ground level (both real using free format)





CONCLUSIONS

- Curves calculated using the appropriate form of the RK optical profile function generally appear to be very good approximations of profiles simulated using the full RK model.
- When used to approximate profiles exhibiting high-frequency fluctuations, calculated curves appear to be reasonably smoothed curves that represent the general trends well.
- Using truncated Fourier series often improves fits for upper pieces of backscatter coefficient profiles.

CONCLUSIONS

- We propose that the RK optical profile function and model-generated values of its fitting constants be considered for possible worldwide application.
- We invite anyone with network access to try this function by accessing `curie.arl.army.mil` (192.67.8.5) using telnet, logging on as `rkopf`, and then entering `rkopf` (lower-case letters).

ACKNOWLEDGMENTS

Gregory N. Whitfield (PSL)

Michael S. Paz (PSL)

Lyndal D. Frye (PSL)

Brian A. Seylar (PSL)

Robert Flanigan (ARL/BED)

Tom Crow (ARL)

TIME AND POLARIZATION DEPENDENT DOUBLE SCATTERING CALCULATIONS OF LIDAR RETURNS FROM WATER CLOUDS

Richard Garner

PhotoMetrics, Inc.
Woburn, MA 01801

We have developed a double scattering lidar program which is used to calculate lidar returns from water clouds. The program, which is implemented on a PC, is used to interpret data acquired with the Air Force Phillips Laboratory's (Geophysics Directorate/GPOA) elastic backscatter, polarization sensitive, Nd:YAG based lidar system. The program determines the four Stokes parameters of the backscatter lidar radiation, from spatially inhomogeneous media composed of spherical particles, as a function of time and as a function of telescope focal plane location. We use the program to determine particle size distributions and multiple scatter corrected extinction coefficients of water clouds. In this talk we will describe the program, compare its results to lidar data, and present and show examples of our data analysis techniques.

Work Supported by the AF Phillips Laboratory, Geophysics Directorate, Hanscom AFB, MA

37

Time, Polarization, and Focal Plane Dependent Calculations of Doubly Scattered Lidar Return Radiation from Inhomogeneous Water Clouds.

Richard Garner
PhotoMetrics, Inc.
4 Arrow Dr.
Woburn, MA 01801

Work supported by
U.S. Air Force Phillips Laboratory/Geophysics Directorate/GPOA
Hanscom AFB, MA.

Annual Review Conference on Atmospheric Transmission Models
Phillips Laboratory, Hanscom AFB, Massachusetts
8-9 June 1993

Using

- a doubled Nd:YAG elastic backscatter lidar (with capability for simultaneous polarization measurements) and
- a time, polarization, and focal plane dependent double (Mie) scattering model (implemented on a PC)

Do the following:

- Investigate regimes of validity of model,
- determine multiple scatter corrections to lidar derived extinction coefficient, and
- determine particle size distributions.

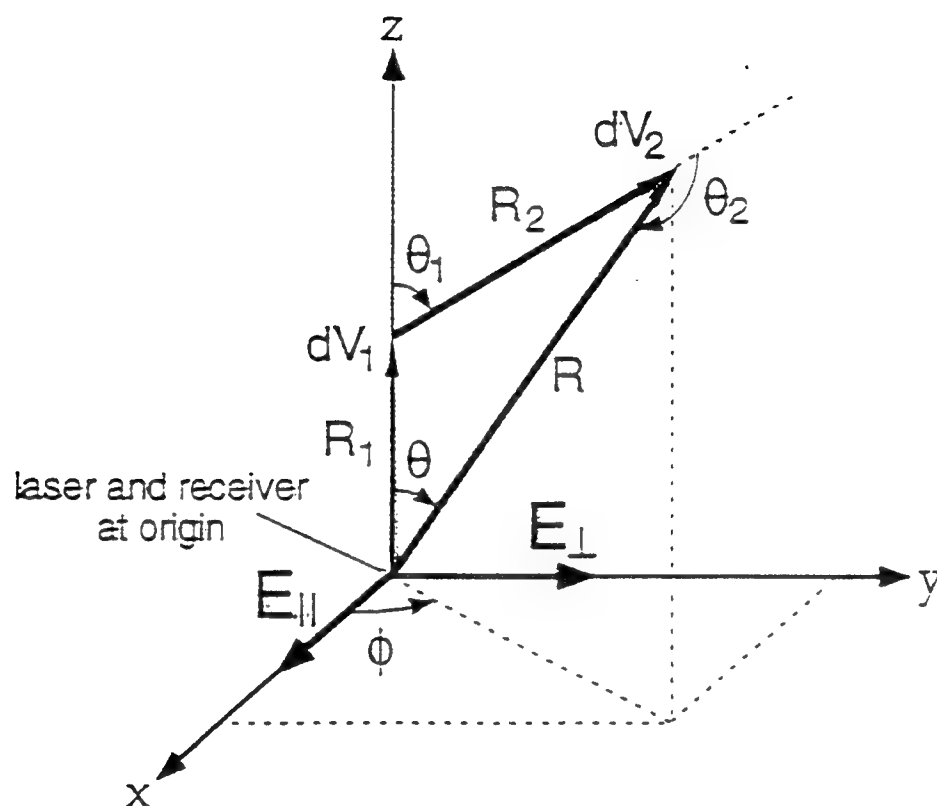
Outline of this talk:

- Describe model.
- Compare azimuthally dependent lidar returns to model calculations.
- Describe and show example of technique to determine size distribution and multiple scatter corrected extinction

Differences with Previous Models

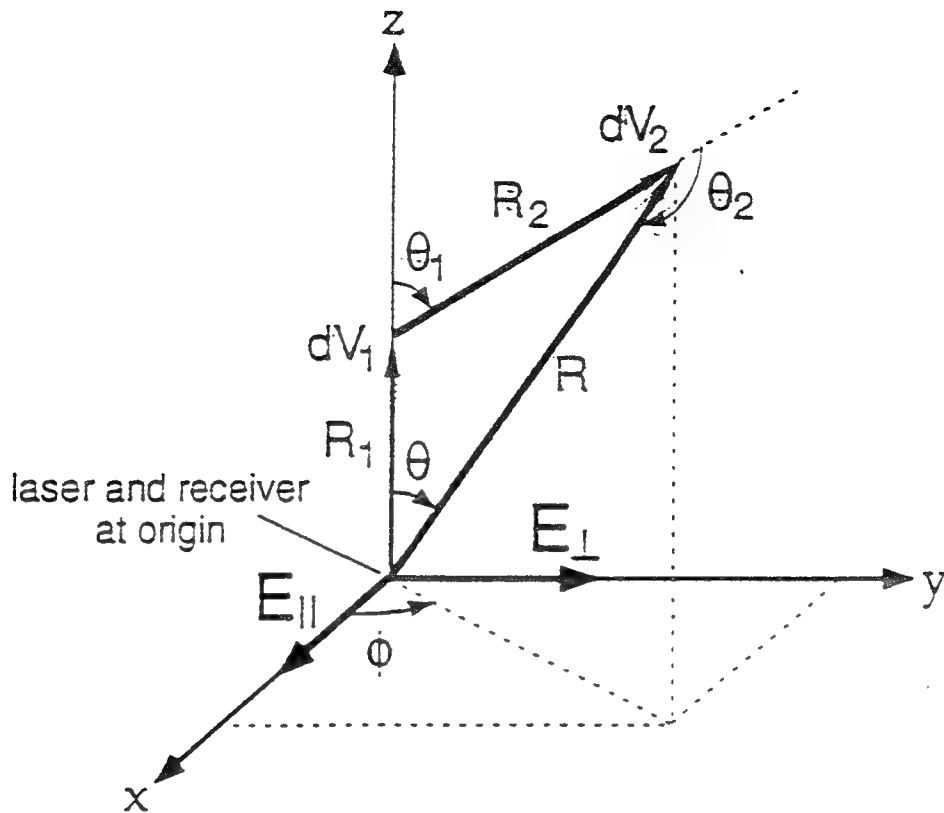
- Variable extinction along z direction
(e.g., extinction calculated from lidar data)
- Lidar return versus focal plane location
(azimuth and polar angle).
- General incident Stokes vector.
- Receiver response a function of polar angle.
- Nonintegrable singularity not encountered
(different variables of integration).
- Laser has zero divergence.

Geometry of double scattering



Two successive single scatters at volumes dV_1 and dV_2 .
First scatter constrained to lie on the z axis.

Incident Stokes vector: $\bar{P}_o = \begin{pmatrix} P_{||o} \\ P_{\perp o} \\ U_o \\ V_o \end{pmatrix} \xrightarrow[\text{typically for lidar}]{\text{}} \begin{pmatrix} P_{||o} \\ 0 \\ 0 \\ 0 \end{pmatrix}$



Received power from one set of scatters:

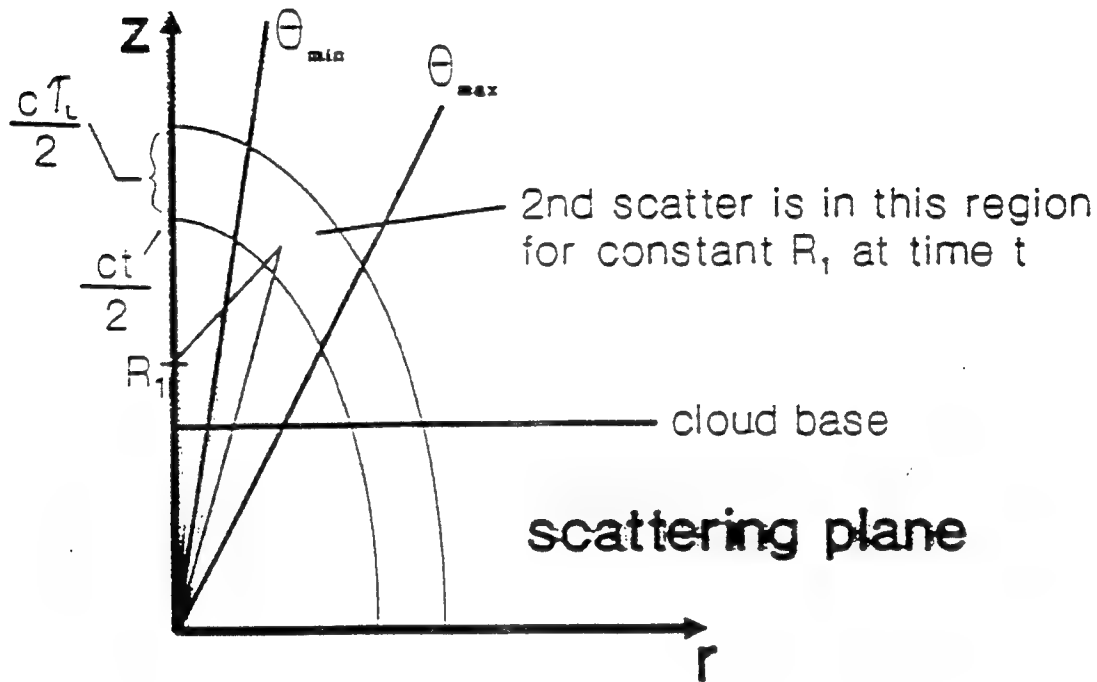
$$d\vec{P}_r = \frac{A_r(\theta) \sigma_1 \sigma_2 e^{-\tau}}{16\pi^2 R^2} \sin \theta_1 \cos \theta dR_1 dR_2 d\theta_1 d\phi \times$$

$$\vec{L}(-\phi) \vec{P}(\theta_2) \vec{P}(\theta_1) \vec{L}(-\phi) \vec{P}_o$$

- \vec{L} : rotation matrix (in space of Stokes vector)
- \vec{P} : scattering phase matrix
- σ_i : extinction coefficient at i^{th} scatter
- τ : total optical path length
- $A_r(\theta)$: receiver response (normalized to aperture area)

Integration of dP_r

- dP_r is integrated over all paths of the same length (quadruple integral).



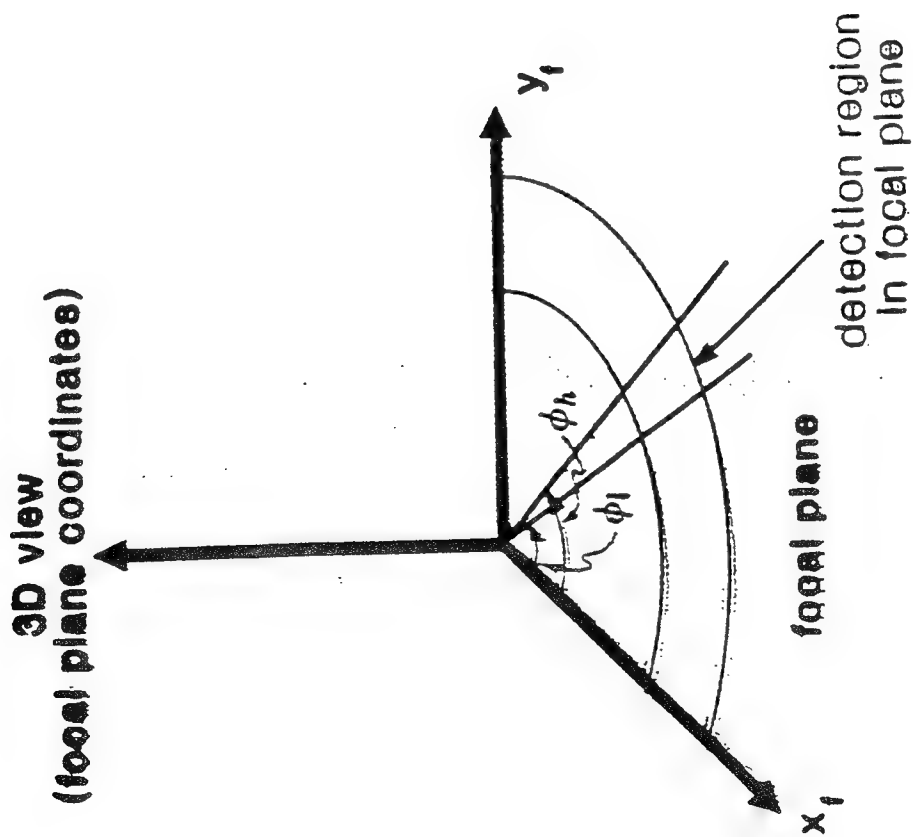
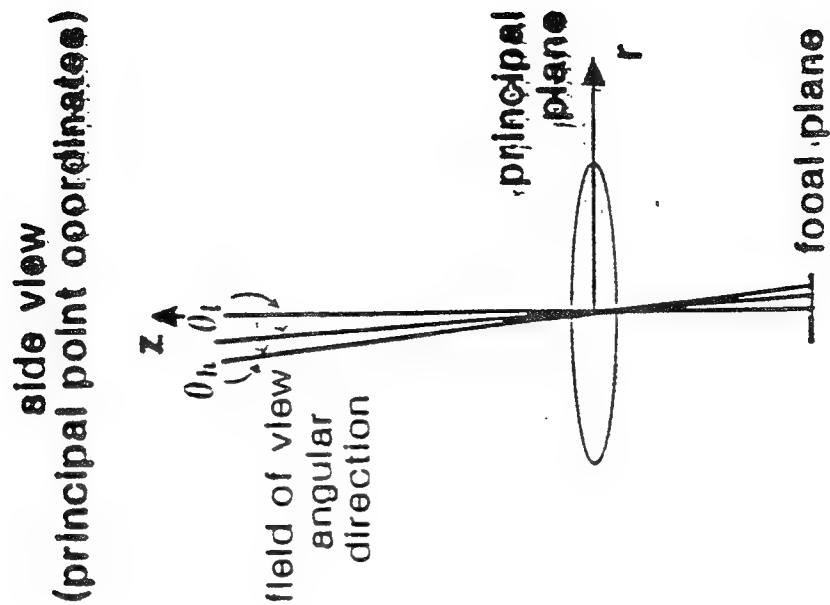
- extinction coefficient σ is a function of z ,
- $\bar{\bar{P}}$ is the Mie scatter phase matrix:

$$\bar{\bar{P}}(\theta) = \begin{pmatrix} A(\theta) & 0 & 0 & 0 \\ 0 & B(\theta) & 0 & 0 \\ 0 & 0 & C(\theta) & -D(\theta) \\ 0 & 0 & D(\theta) & C(\theta) \end{pmatrix}$$

(size distribution independent of position)

The field of view is a section of an annular region

$$\theta_l < \theta < \theta_h \quad \phi_l < \phi < \phi_h$$



$$\phi = \frac{y_f}{\sqrt{x_f^2 + y_f^2}}$$

$$\theta = \frac{\sqrt{x_f^2 + y_f^2}}{f}$$

Integration of dP_r (cont.)

- The ϕ integral can be performed analytically.
- The remaining three integrals (in R_1, θ_1, R_2) are performed numerically.
- The general expression is long and is not presented here.
- When the field of view is a complete annular region ($0 < \phi < 2\pi$):

$$\bar{P}_r(t) = \int_{z_o}^{ct/2} dR_1 \int_{\theta_{1l}(R_1)}^{\theta_{1h}(R_1)} \sin \theta_1 d\theta_1 \int_{R_{2l}(R_1, \theta_1)}^{R_{2h}(R_1, \theta_1)} dR_2 \frac{A_r \cos \theta}{16\pi^2} \frac{\sigma_1 \sigma_2}{R^2} e^{-\tau} \times$$

$$\begin{pmatrix} \frac{\pi}{4}(A_1 A_2 + B_1 B_2)(3P_{\parallel o} + P_{\perp o}) - \frac{\pi}{2}(C_1 C_2 - D_1 D_2)(P_{\parallel o} - P_{\perp o}) \\ \frac{\pi}{4}(A_1 A_2 + B_1 B_2)(P_{\parallel o} + 3P_{\perp o}) + \frac{\pi}{2}(C_1 C_2 - D_1 D_2)(P_{\parallel o} - P_{\perp o}) \\ \pi U_o(C_1 C_2 - D_1 D_2) \\ 2\pi V_o(C_1 C_2 - D_1 D_2) \end{pmatrix}$$

Parameters input to model:

- extinction as a function of range
- particle size distribution (independent of range)
- complex index of refraction
- incident Stokes vector
- field of view (polar and azimuthal angle ranges)
- aperture area and response function
- temporal pulse width

Method of Calculation:

- Mie scattering
 - Calculate phase matrix coefficients at discrete angles.
 - Store in arrays.
 - Determine values at other angles, as needed, by interpolation.
- Double scattering
 - Calculate triple integral using three nested Simpson's rule.
- Calculations are implemented on a PC.

$$x = \frac{2\pi r}{\lambda}$$

x_m : mode radius

a : spread

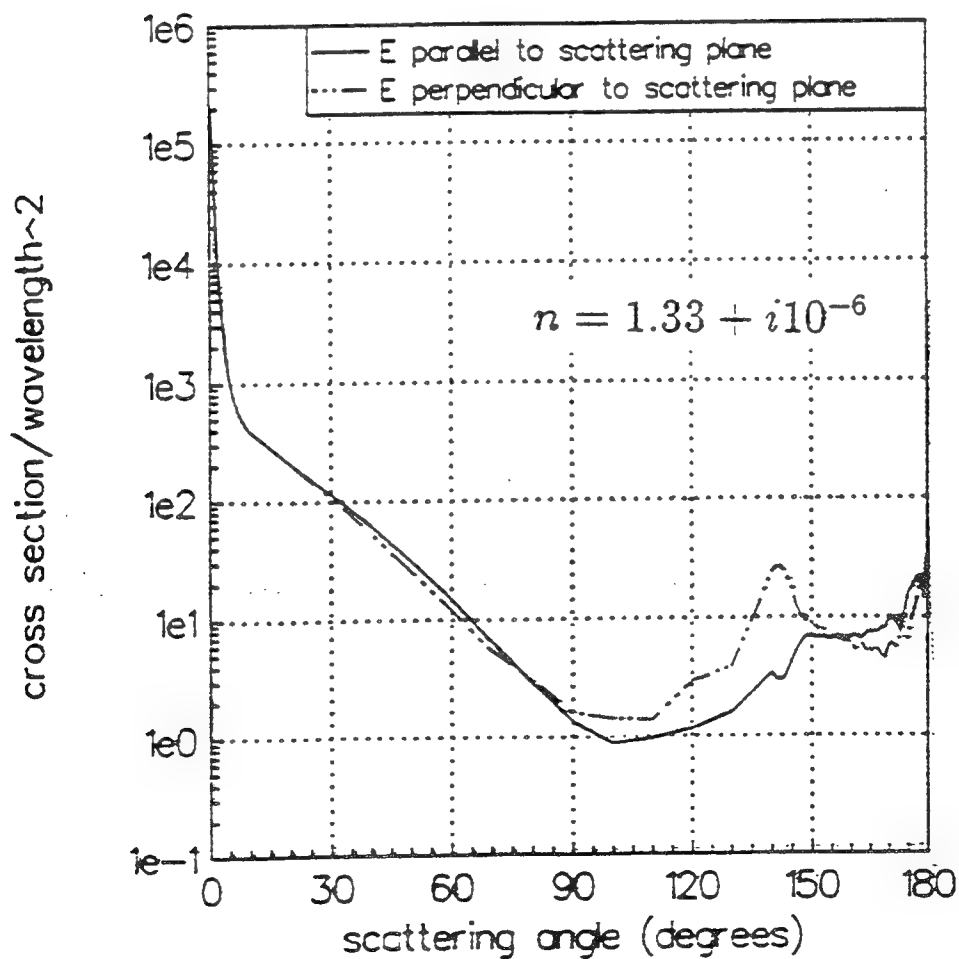
Modified gamma size distribution:

$$f(x) = \frac{a^{a+1}}{a! x_m} \left(\frac{x}{x_m} \right)^a \exp \left(-\frac{ax}{x_m} \right)$$

Mie scattering calculation ($a = 2$ $x_m = 35$)

$r_m = 3 \mu m$ for

$\lambda = 532 \text{ nm.}$

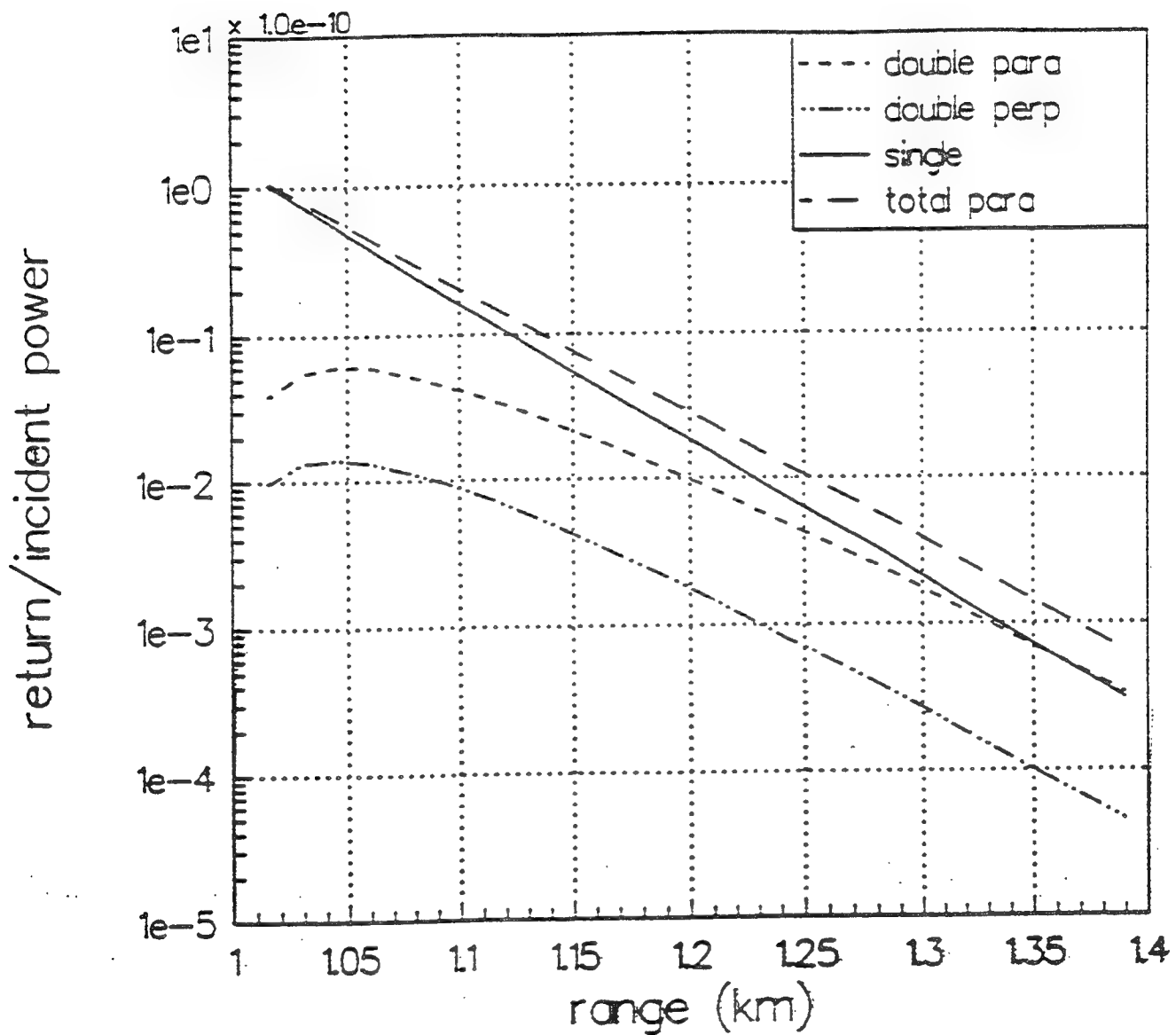


Base case:

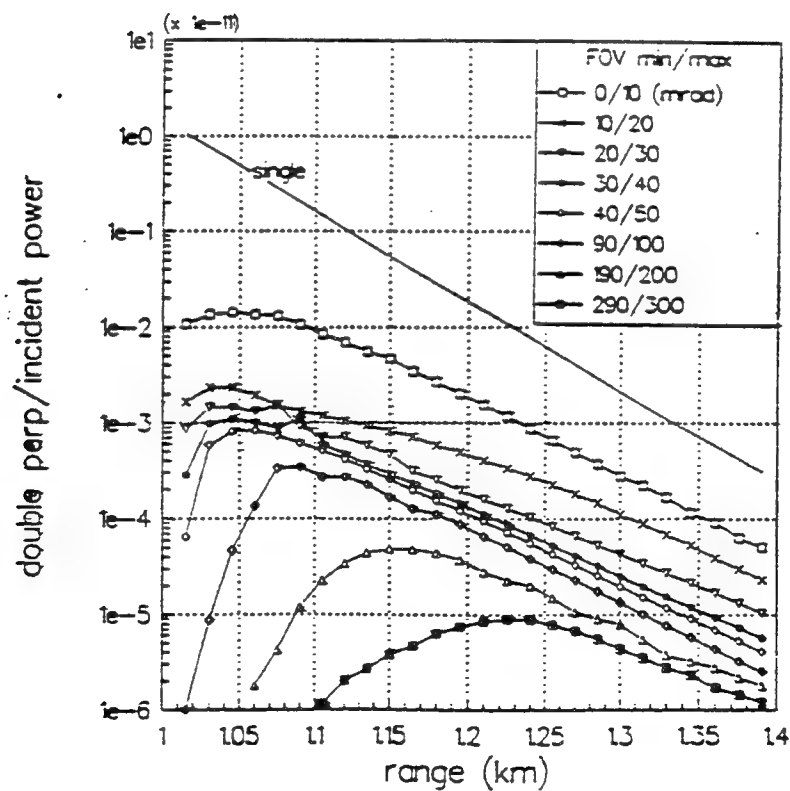
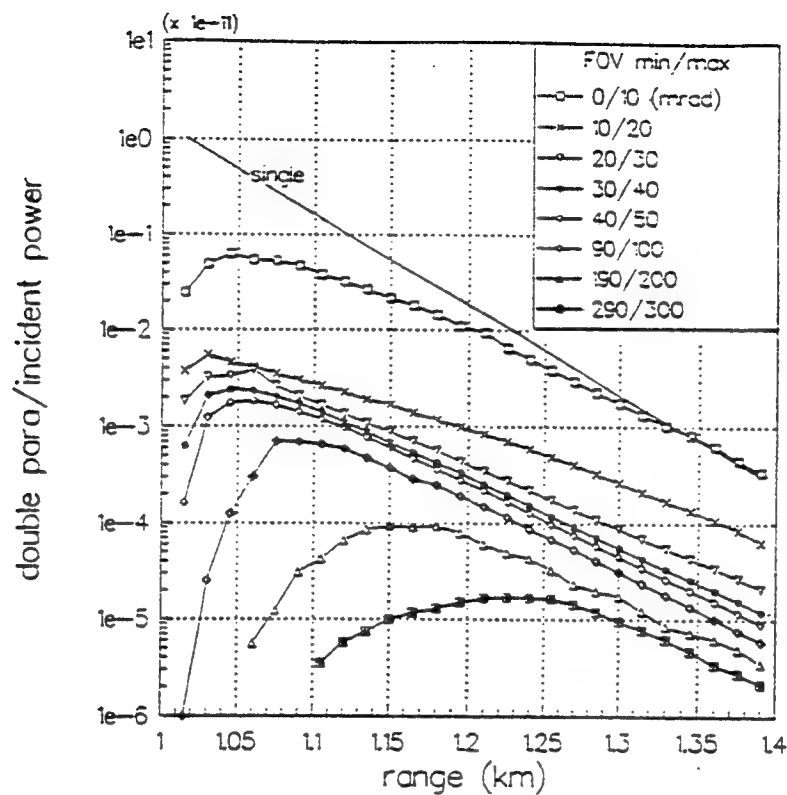
- extinction: 10 km^{-1} (constant)
- $\tau_L = 1.5 \text{ m}$
- modified gamma size distribution with
 - $x_m = 35$
 - $a = 2$
- outer boundary of field of view: 10 mrad.
(full angle)
- inner boundary of field of view: 0 mrad.
- index of refraction: $1.33 + i10^{-6}$
- cloud base: 1 km

All results shown are for variations of one or two parameters from the base case.

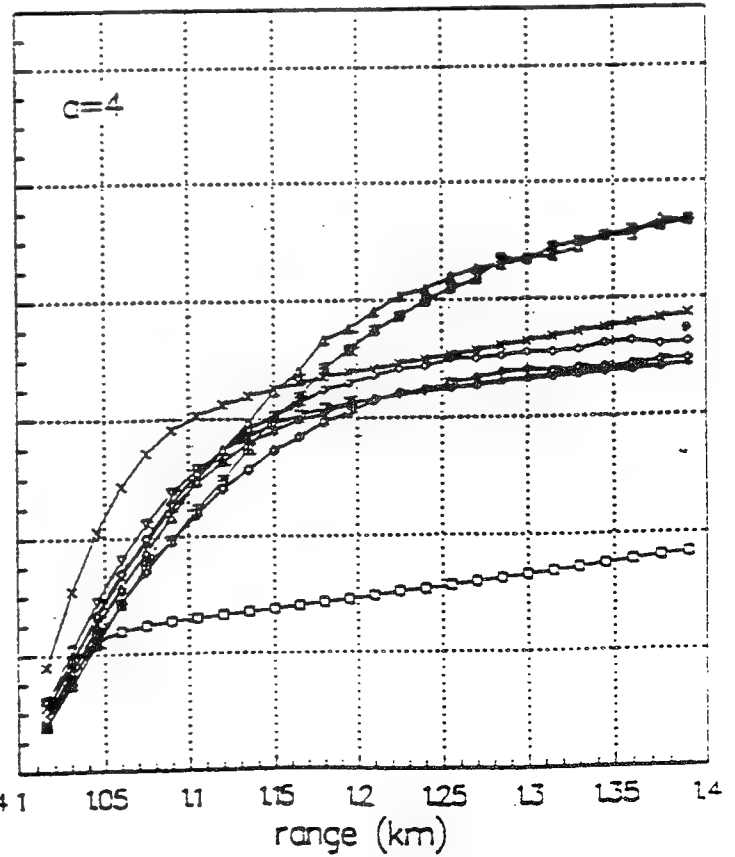
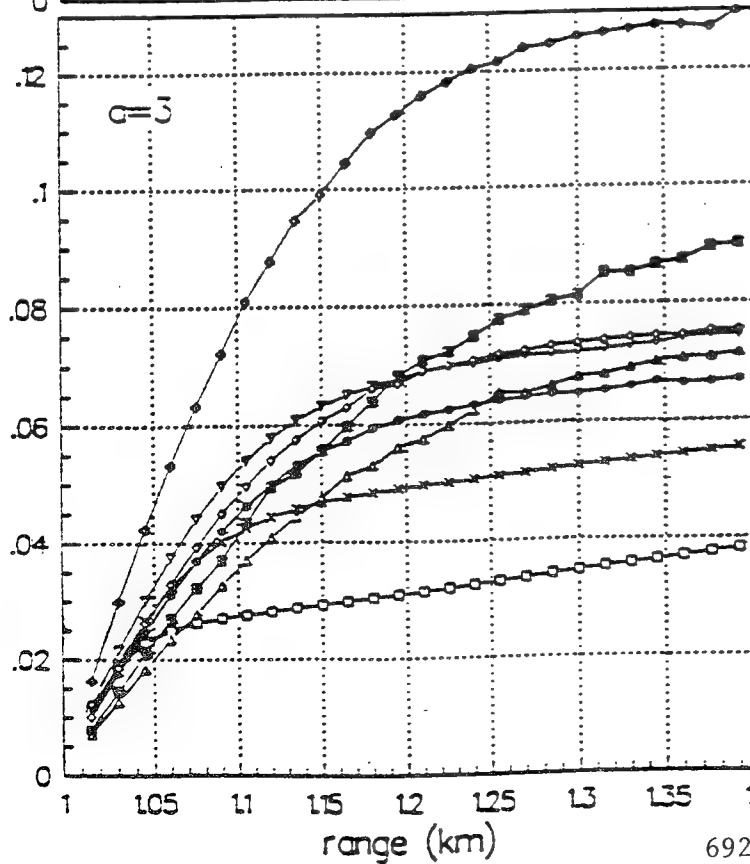
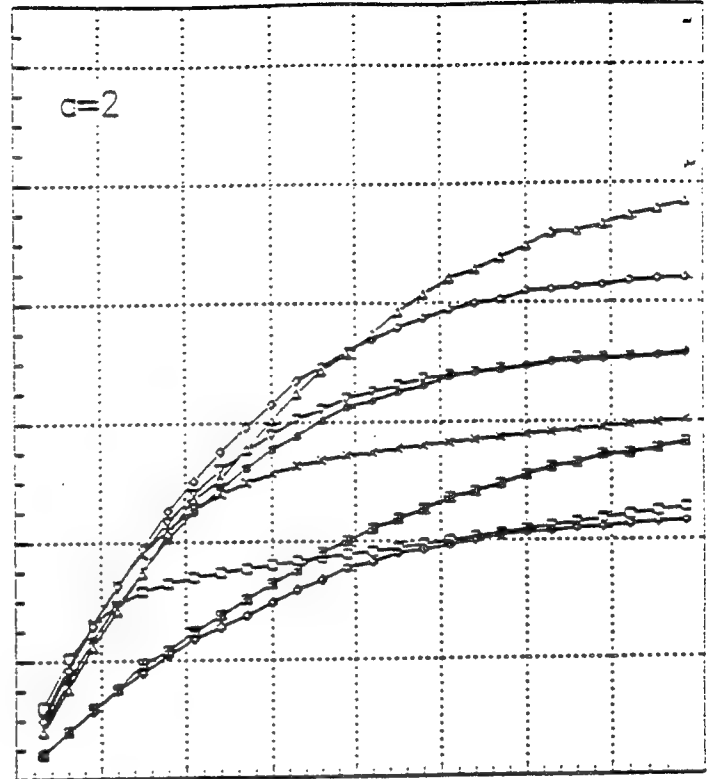
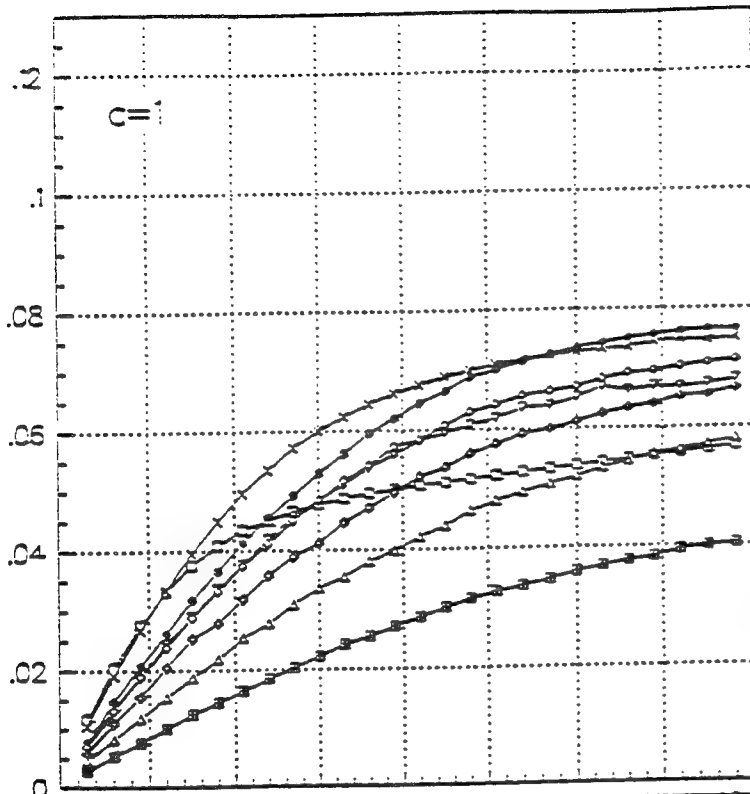
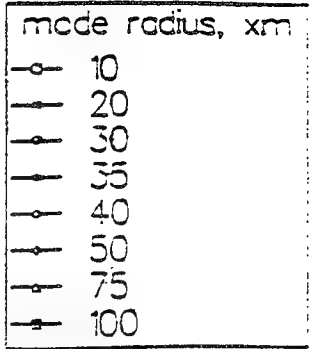
Double Scattering Model
 modified gamma ($\alpha=2, x_m=35$)
 extinction=10 1/km



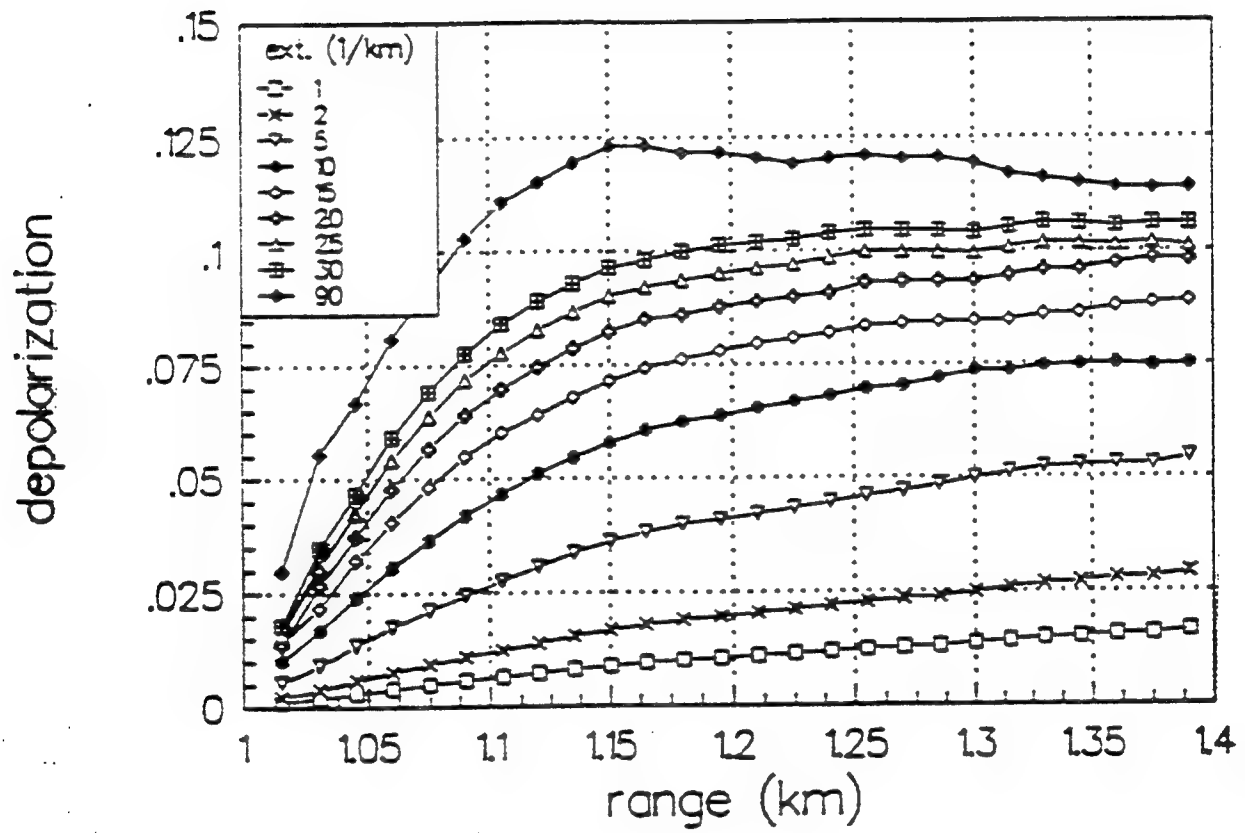
Field of view (inner and outer boundaries) scan

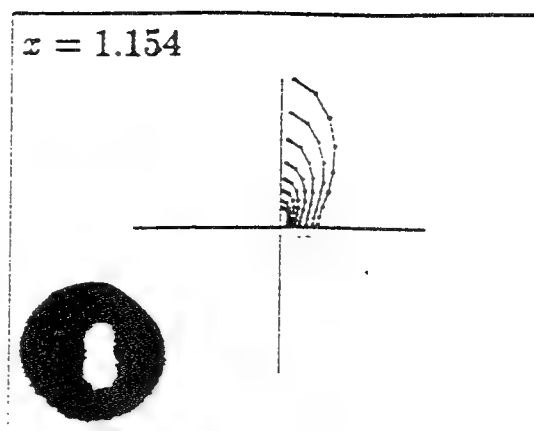
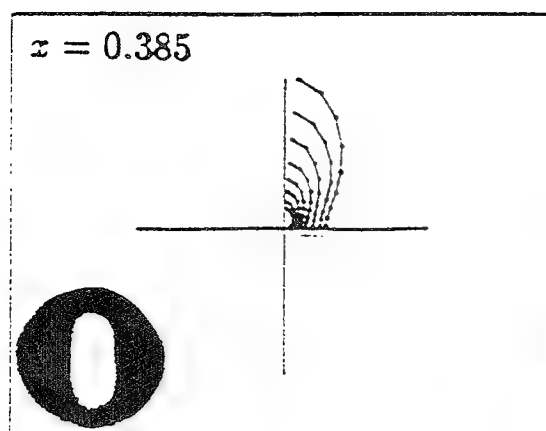


Size distribution scan (1)

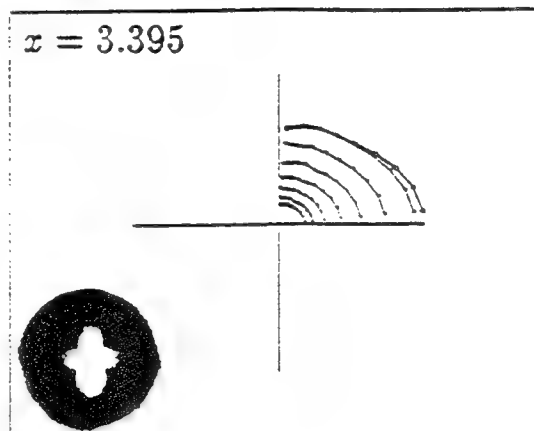
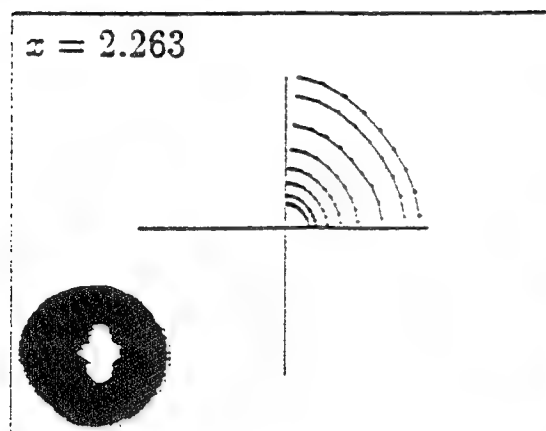


Extinction scan

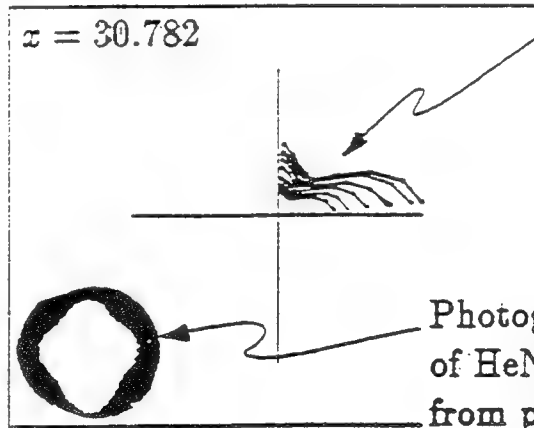
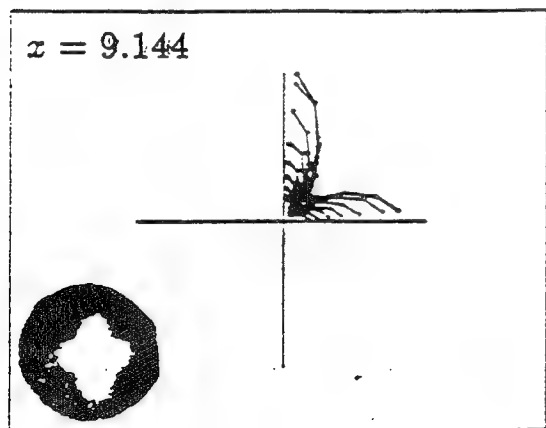




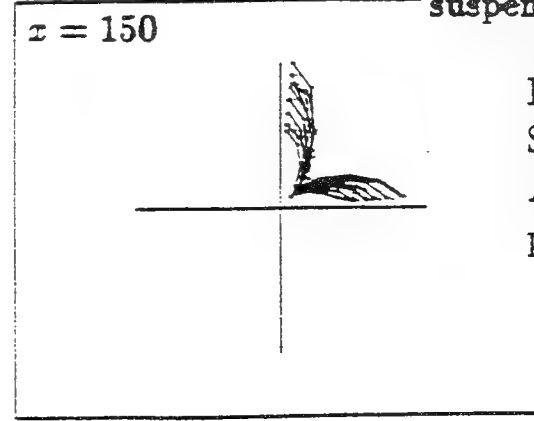
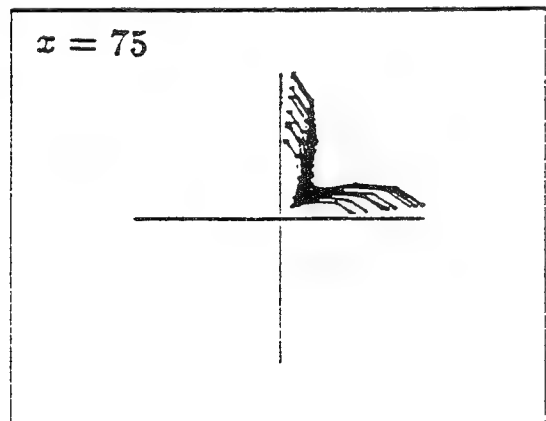
$$x = 2\pi r/\lambda$$



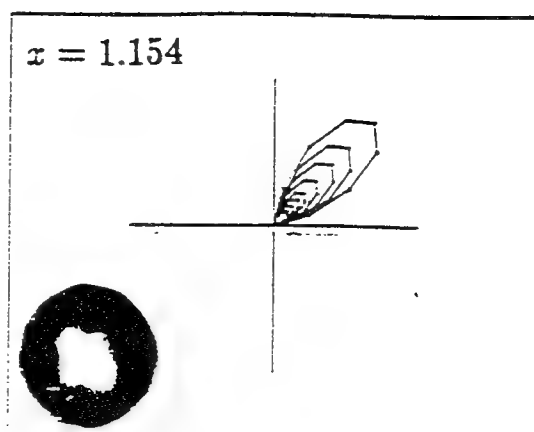
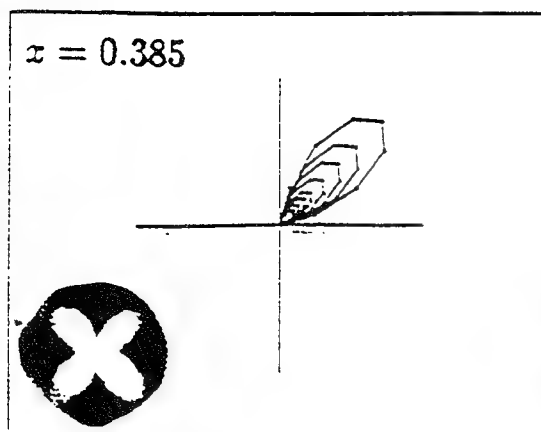
Double scatter
program results.
Returns from 1 km
to 1.2 km in
15 m steps.



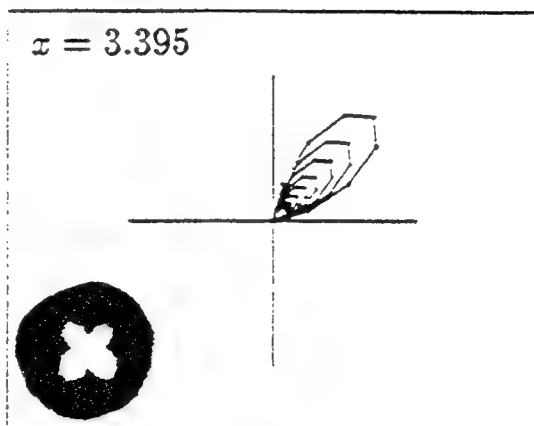
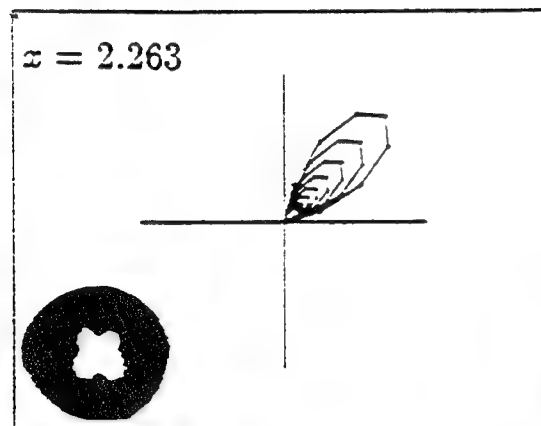
Photographs in focal plane
of HeNe laser backscatter
from polystyrene spheres
suspended in a cloud chamber



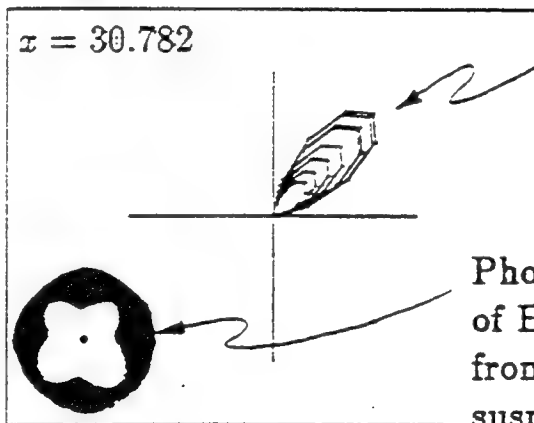
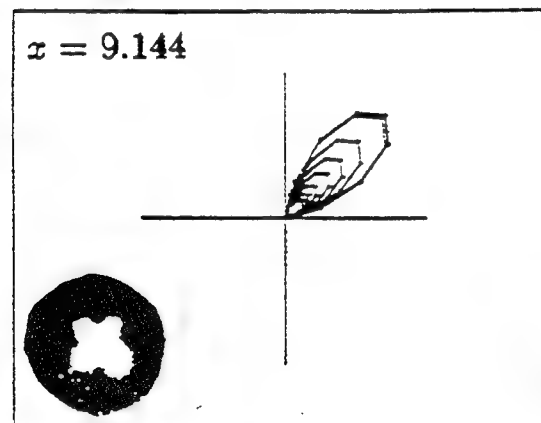
From:
S.R. Pal & A.I. Carswell
Appl. Opt. 24,
pp. 3464-3471 (1985).



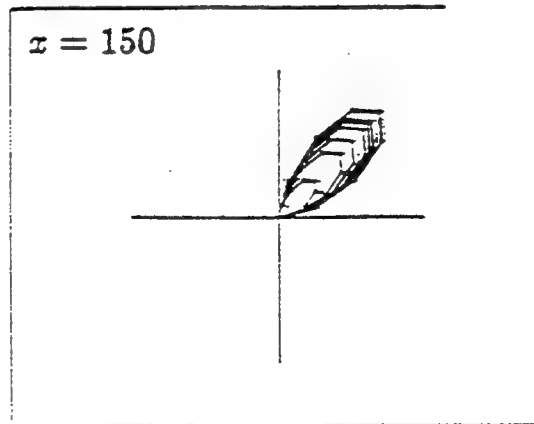
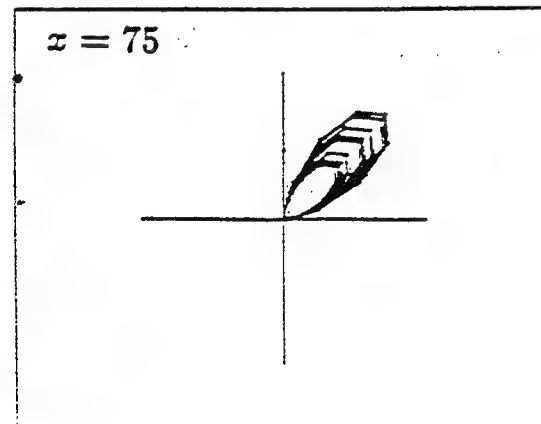
$$x = 2\pi r/\lambda$$



Double scatter
program results.
Returns from 1 km
to 1.2 km in
15 m steps.

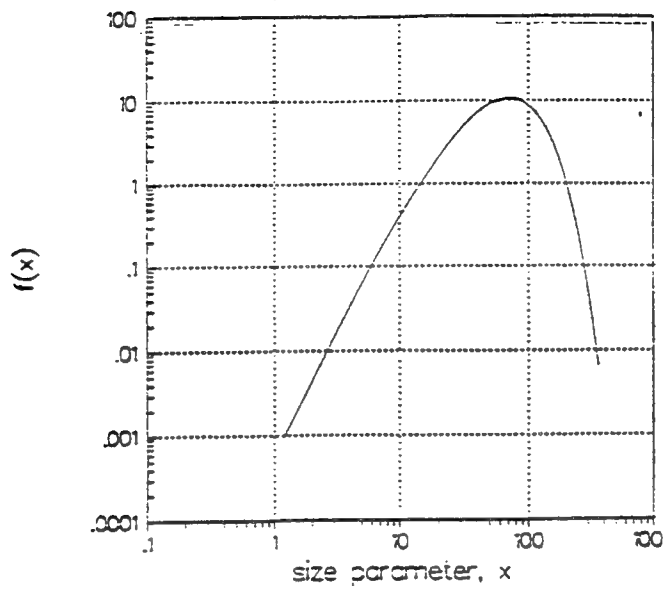


Photographs in focal plane
of HeNe laser backscatter
from polystyrene spheres
suspended in a cloud chamber

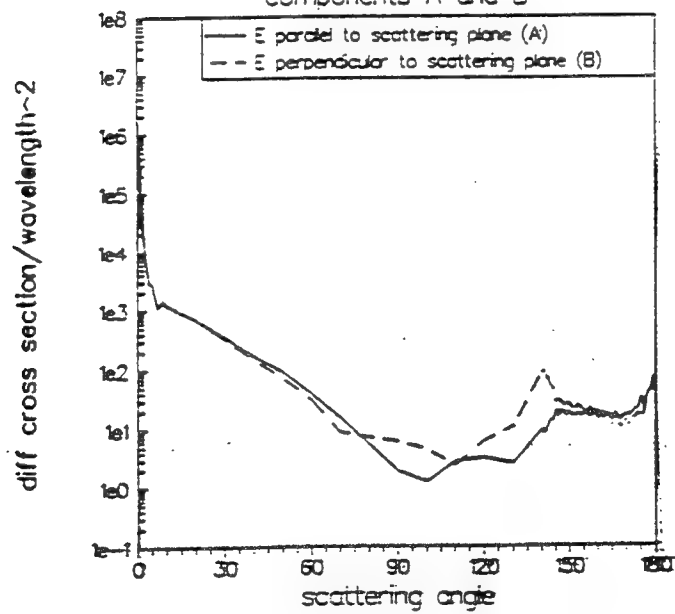


From:
S.R. Pal & A.I. Carswell
Appl. Opt. **24**,
pp. 3464-3471 (1985).

Cumulus cloud size distribution model
(Handbook of Geophysics and
the Space Environment, p. 18-29)

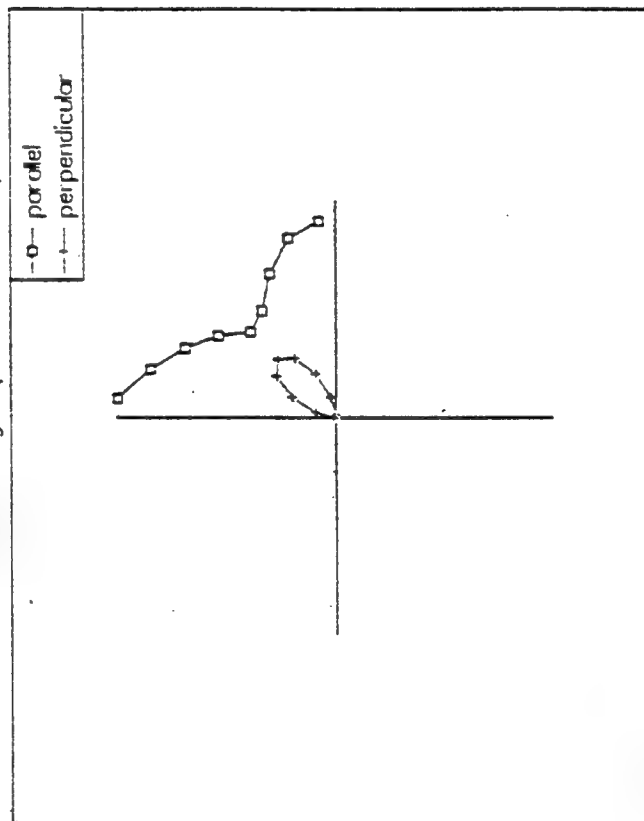


Mie scattering phase matrix
components A and B



Double Mie scatter program results

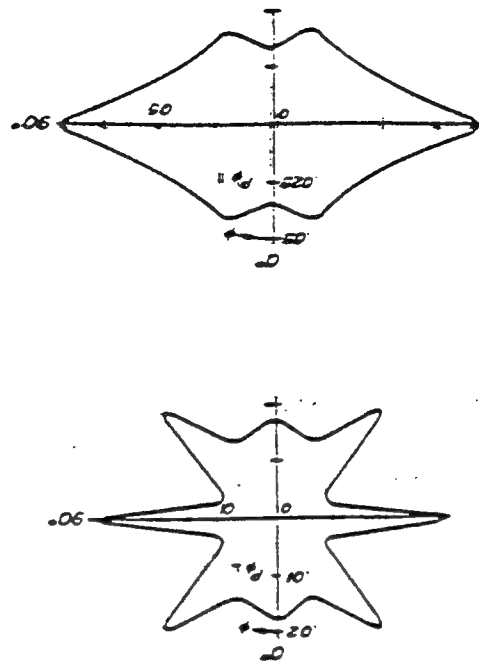
Double scattered return from cumulus cloud (1-1.2 km)
vs. azimuth angle (FOV=10 mrad)



cumulus cloud model from:
Handbook of Geophysics and
the Space Environment, p. 18-29

Multiple scatter dependence of
Lidar returns from cumulus
cloud (averaged over 1-1.2 km)
vs. azimuth angle

from:
S.R. Pal & A.I. Ourswell
Appl. Opt. **24**,
pp. 3464-3471 (1985).



Determining size distribution and multiple scatter corrected extinction

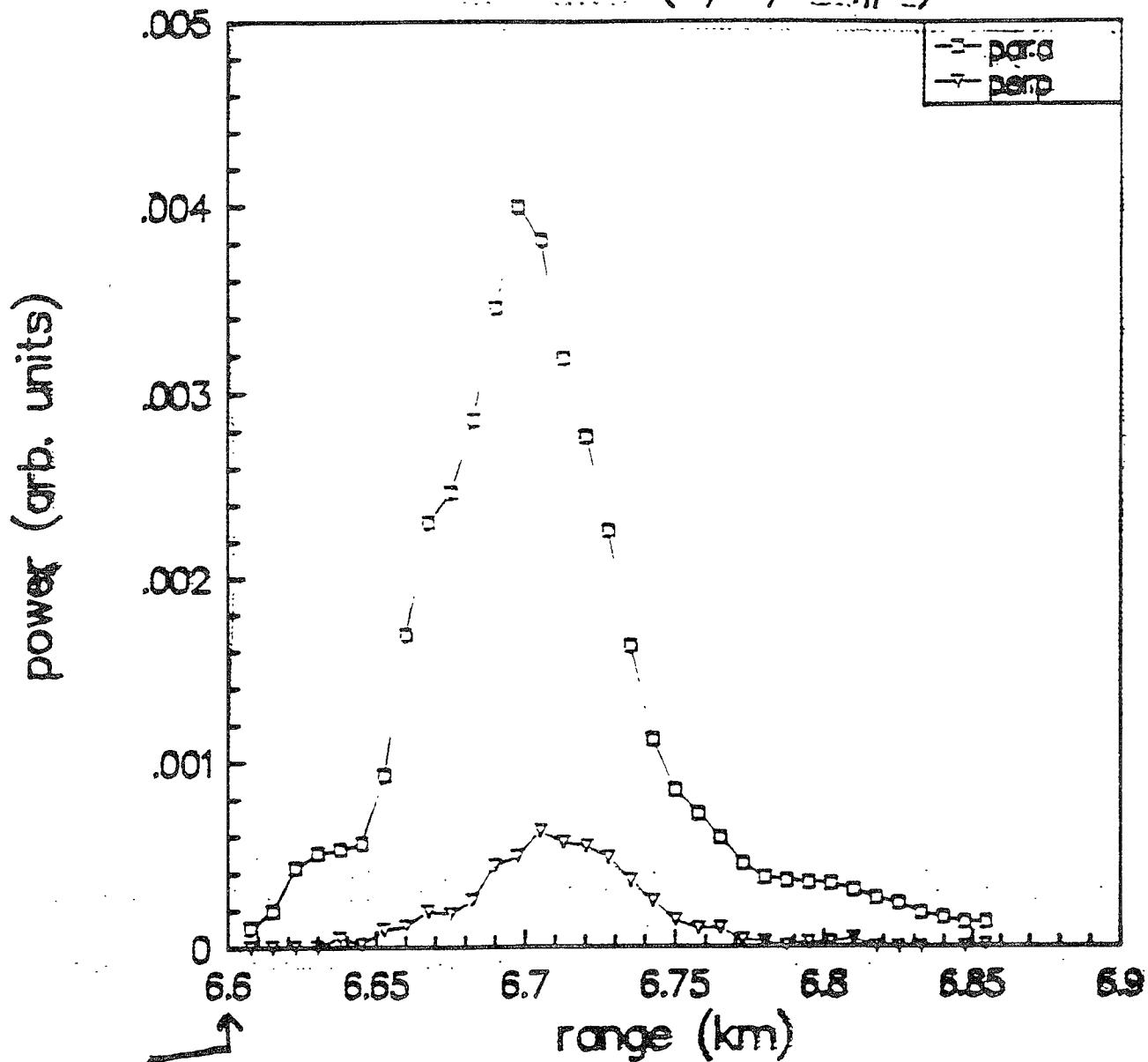
1. Acquire lidar data (parallel and perpendicular polarization components of backscattered radiation from water cloud). Calculate depolarization versus range in cloud.
2. Relatively calibrate the two channels using background data (assumed to have depolarization of unity).
3. Calculate the extinction coefficient as a function of range with the Klett technique using the parallel polarization component.
4. Use the calculated extinction profile in the double scatter model. Run the model many times for a variety of size distributions. Assume a particular size distribution (e.g., modified gamma) with free parameters that can be varied.
5. Choose the best size distribution by matching predicted depolarization to measured depolarization.
6. Calculate correction to Klett extinction above using model results.
7. Go to step 4.

Description of Lidar[†]

- primary and doubled Nd:YAG
- 25 mJ/pulse @ 532 nm
- 20 Hz pulse repetition rate
- 15 cm aperture diameter
- 10 mrad field of view
- 20 MHz (7.5 m) ~~maximum~~ data rate
- steerable (upper hemisphere)
- two simultaneous linear polarization measurements (532 nm only)
(parallel and perpendicular to laser polarization)

[†]PL/GD/GPOA Transportable Optical Atmospheric Data System (TOADS)

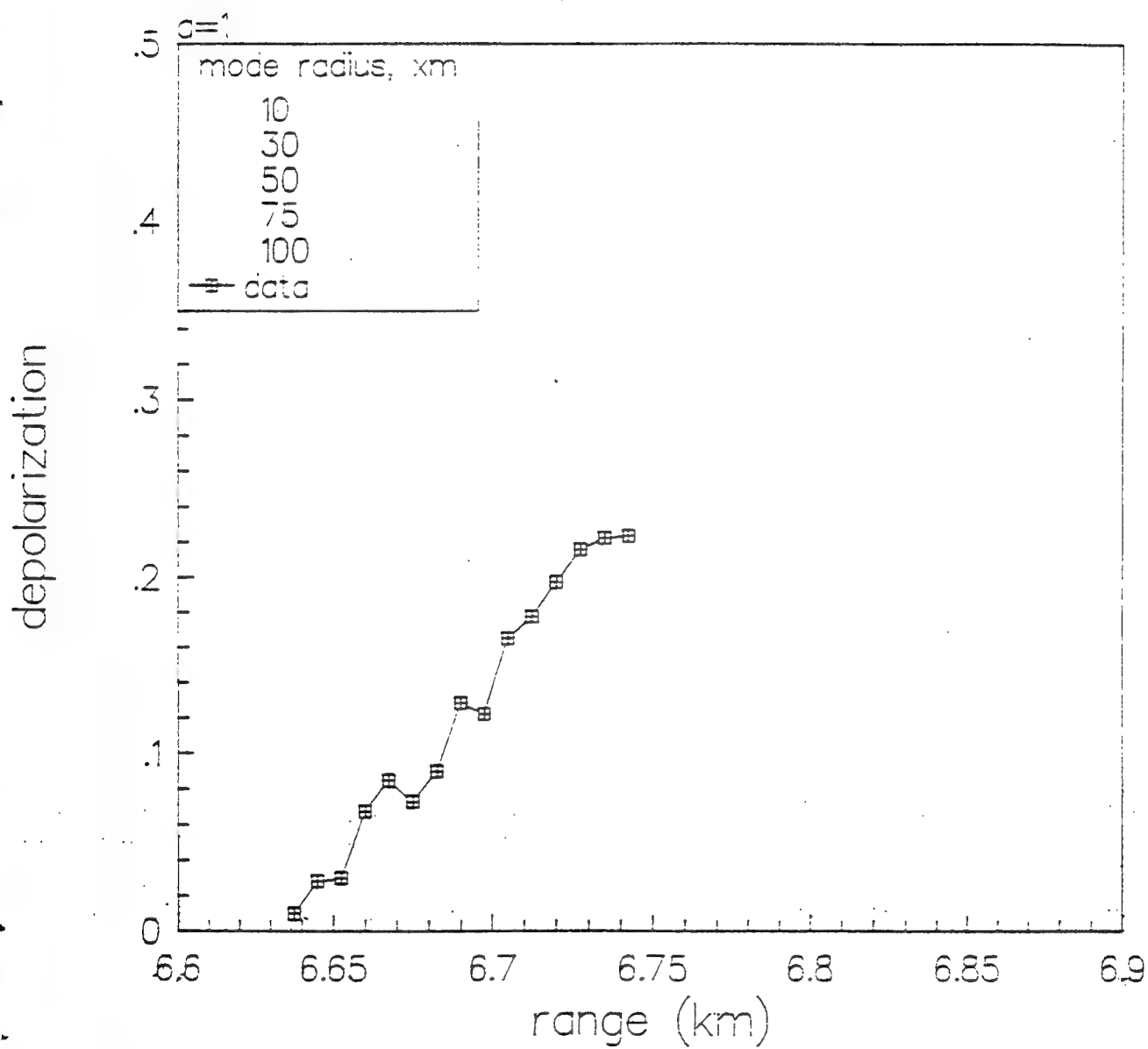
Lidar data (7/7/92, #2)



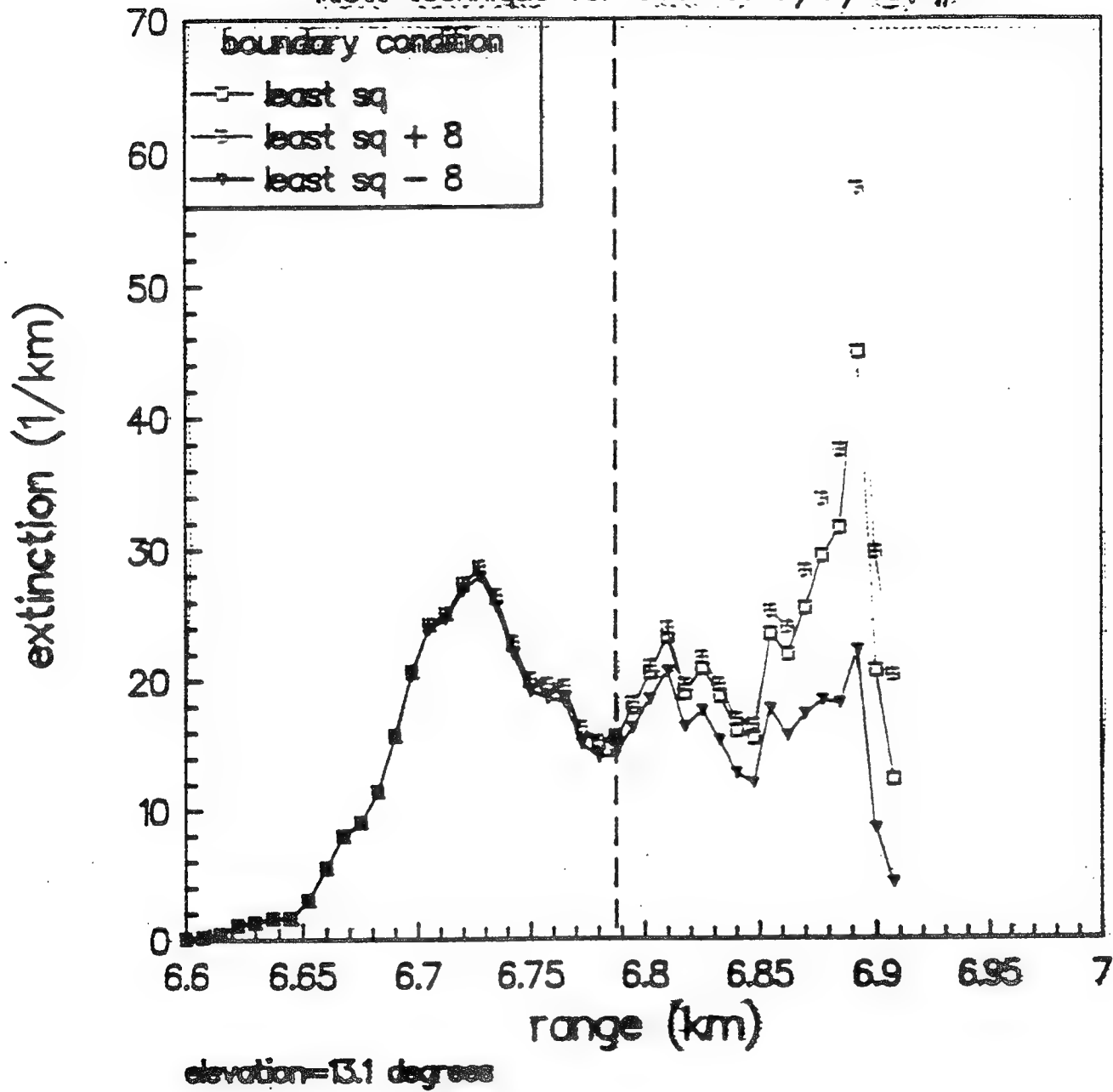
elevation = 13.1 degrees

1.5 km
altitude

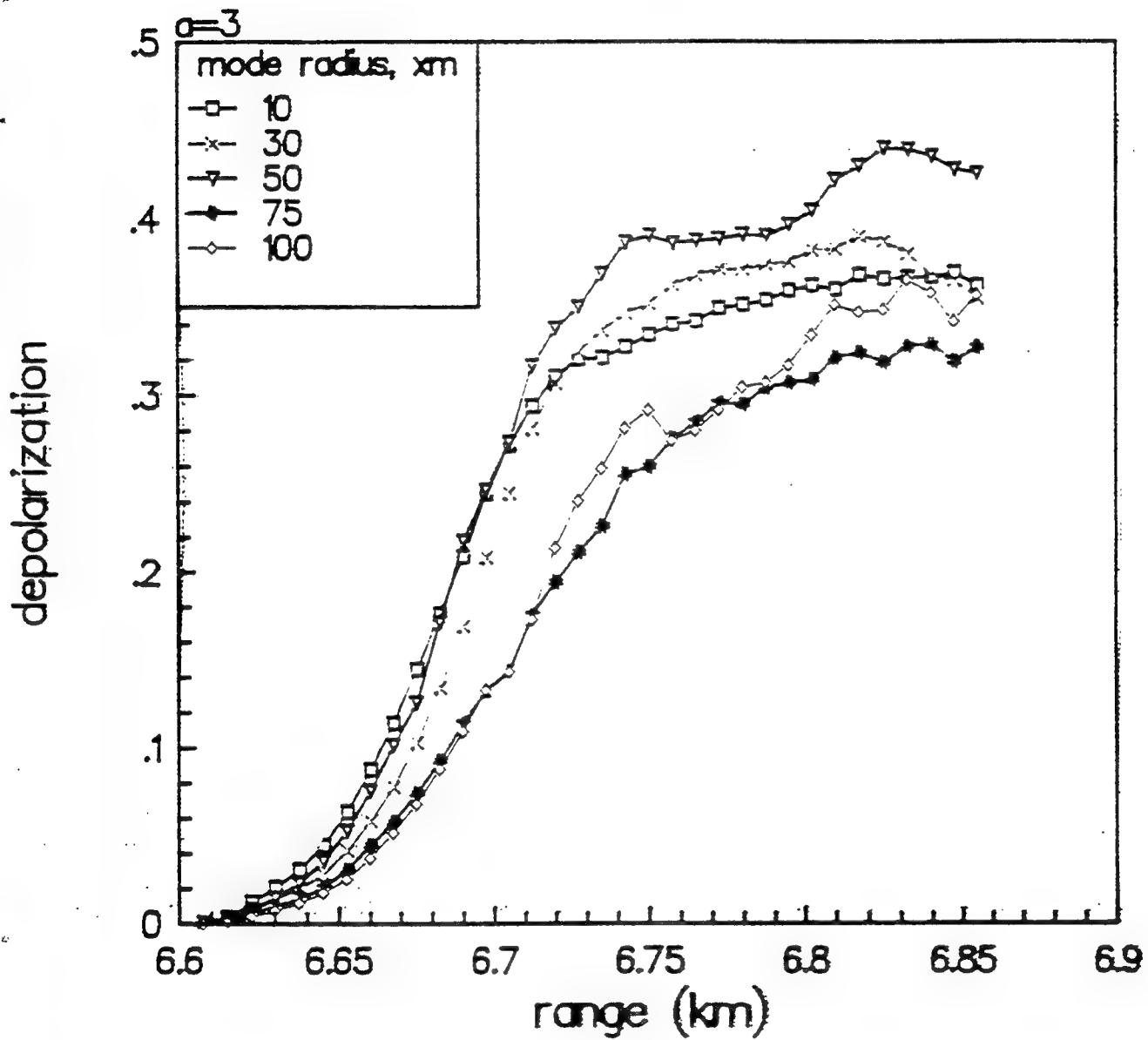
model/data comparison
7/7/92, #2



Klett technique for data of 7/7/92, #2



model/data comparison
7/7/92, #2



Technique to determine multiple scatter
correction to extinction:

Utilize ideas presented by

S.R. Pal and A.I. Carswell,
Appl. Opt 8, 1990-1995, (1976)

$$P_{\parallel s} = \frac{A}{R^2} \beta \exp(-2\tau)$$
$$P_{\parallel t} = \frac{A}{R^2} \beta \exp[-2(\tau - \tau_m)]$$

Say

$$P_{\parallel m} = P_{\parallel t} - P_{\parallel s} = \alpha P_{\perp}$$

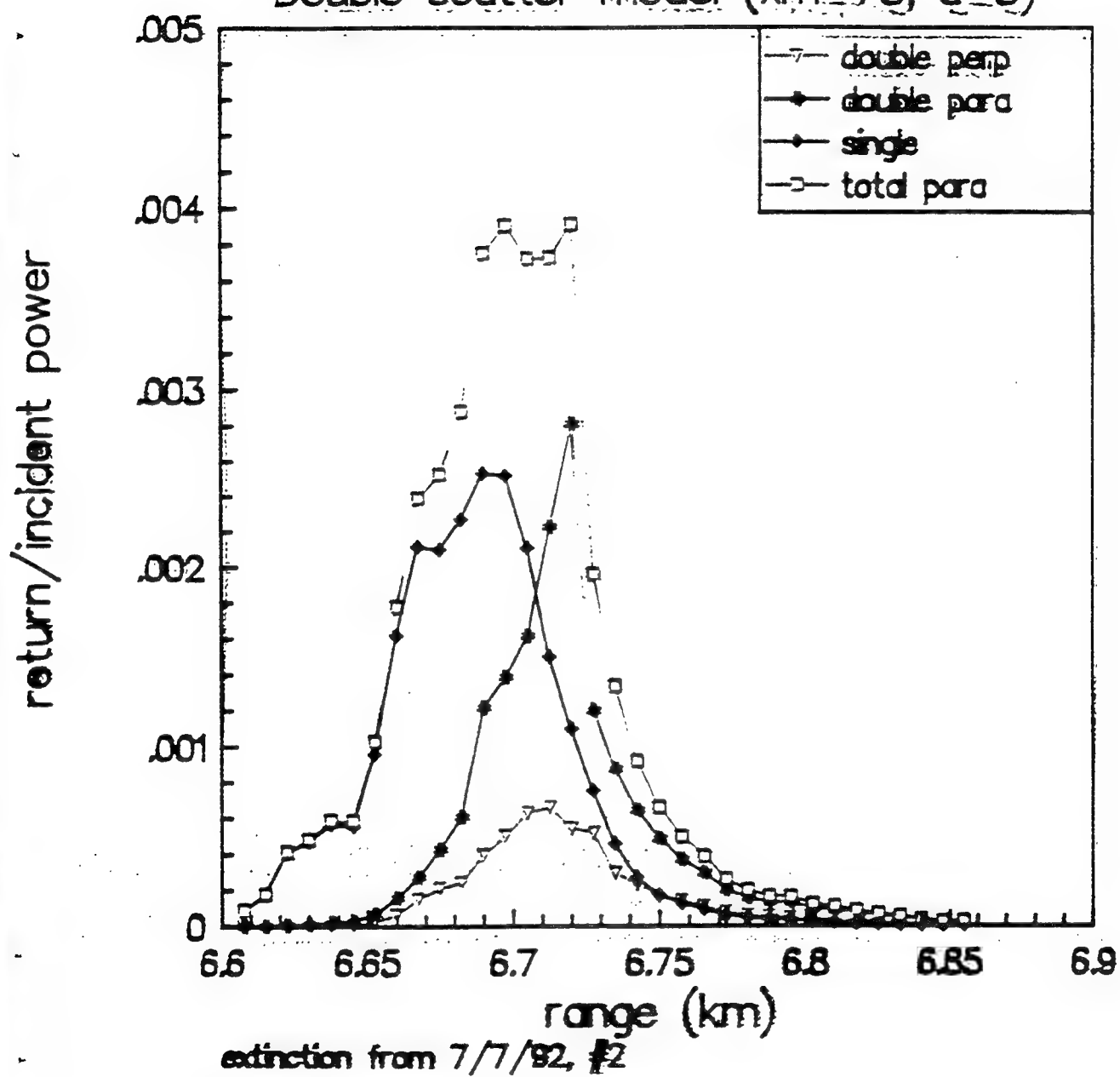
Then

$$\tau_m = \frac{1}{2} \ln \left[\frac{P_{\parallel t}}{P_{\parallel t} - \alpha P_{\perp}} \right]$$

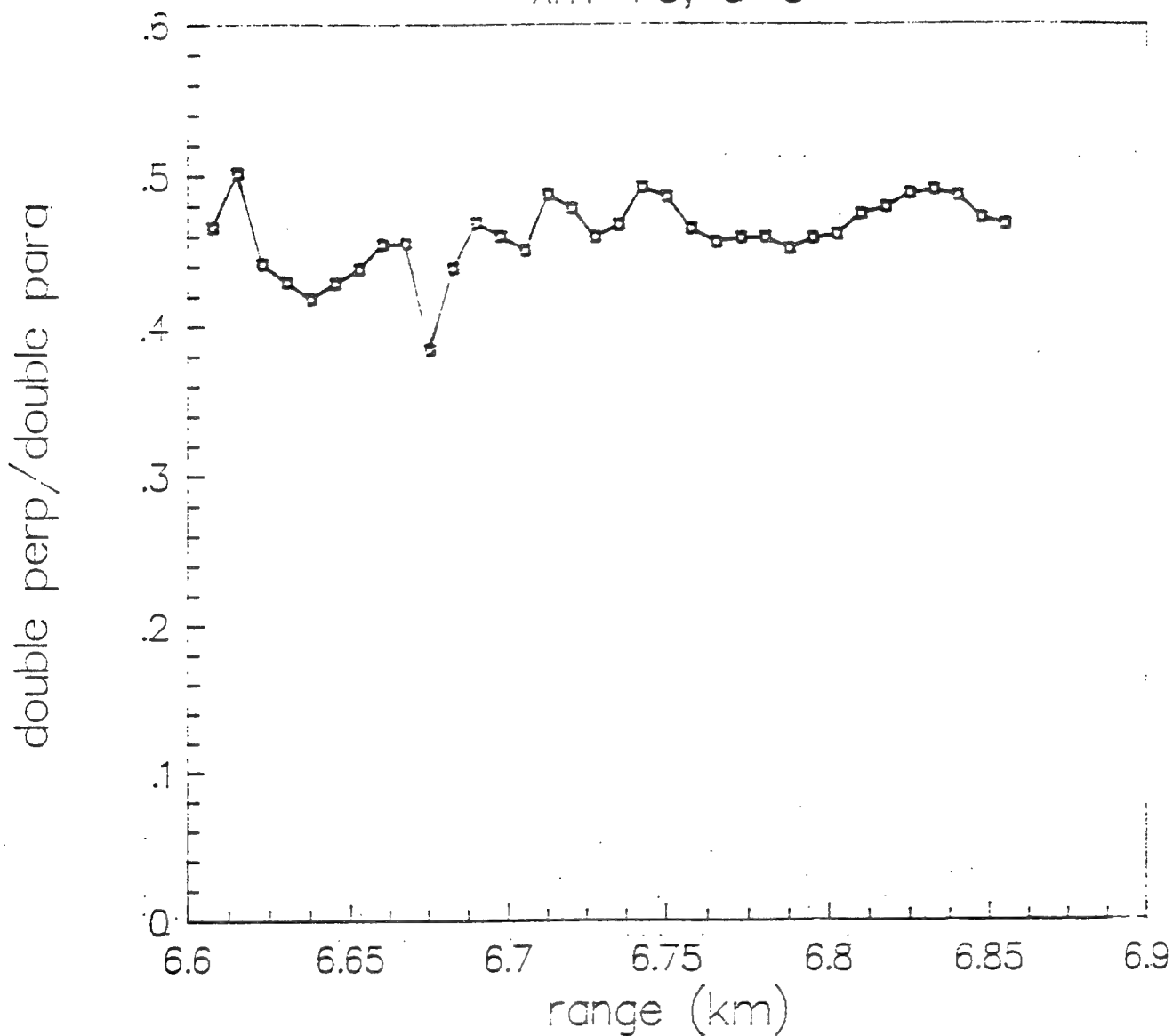
$$\sigma_m = \frac{d\tau_m}{dR} \quad \sigma \longrightarrow \sigma + \sigma_m$$

- Measure $P_{\parallel t}$ and P_{\perp} with lidar.
- Determine α with model.
- Calculate σ_m .

Double scatter model ($x_m=75$, $a=3$)

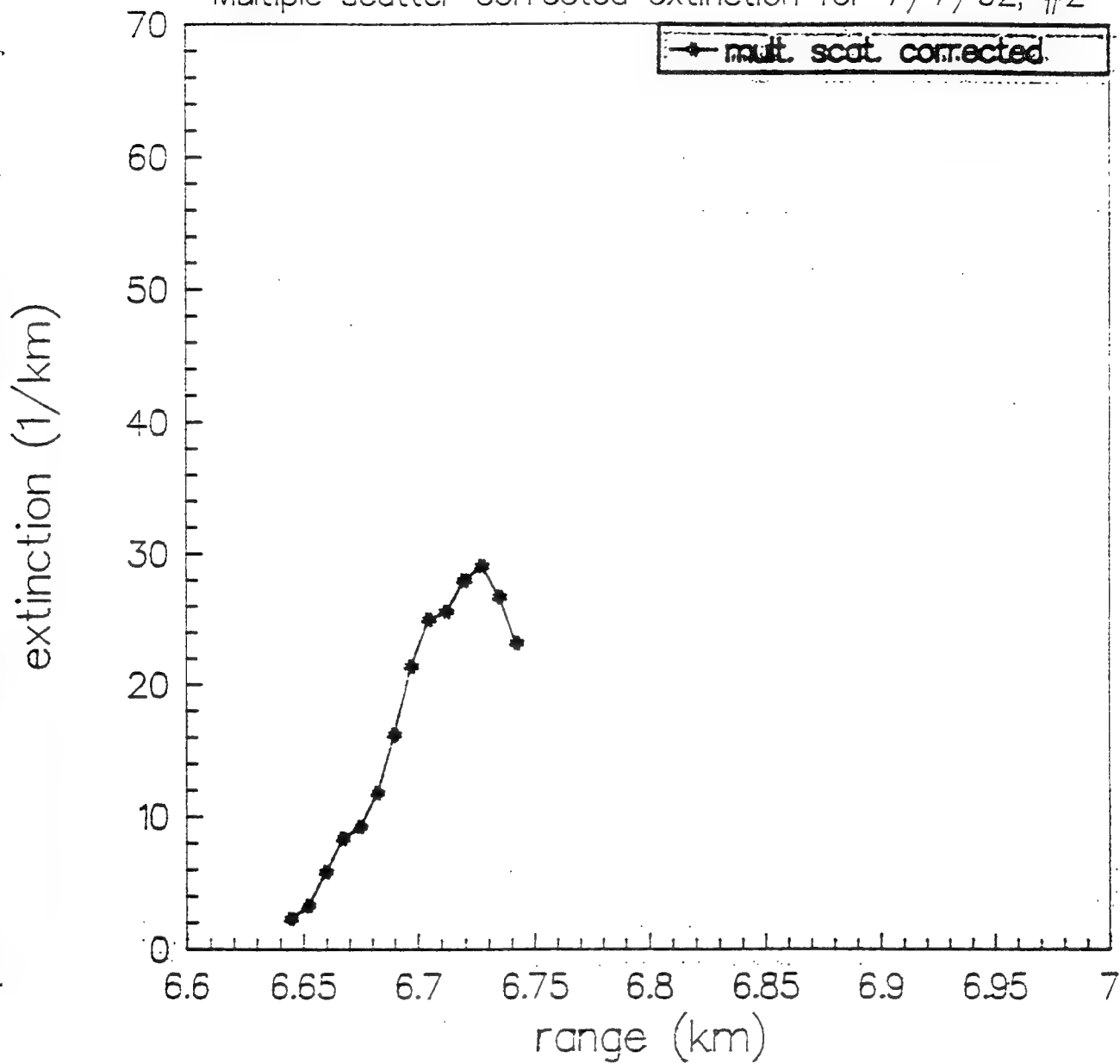


modified gamma distribution
 $x_m=75, a=3$



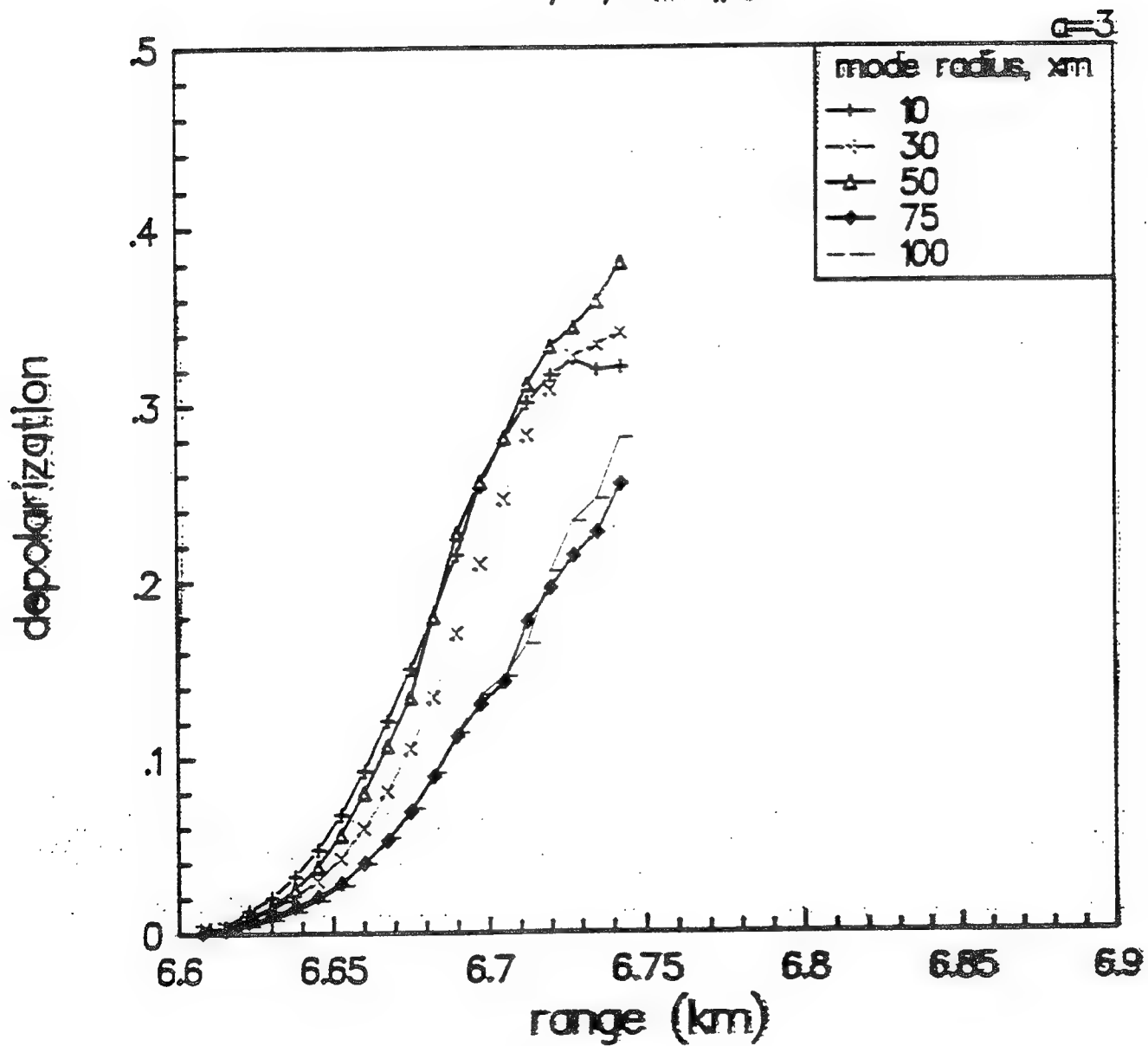
extinction from 7/7/92, #2

Multiple scatter corrected extinction for 7/7/92, #2

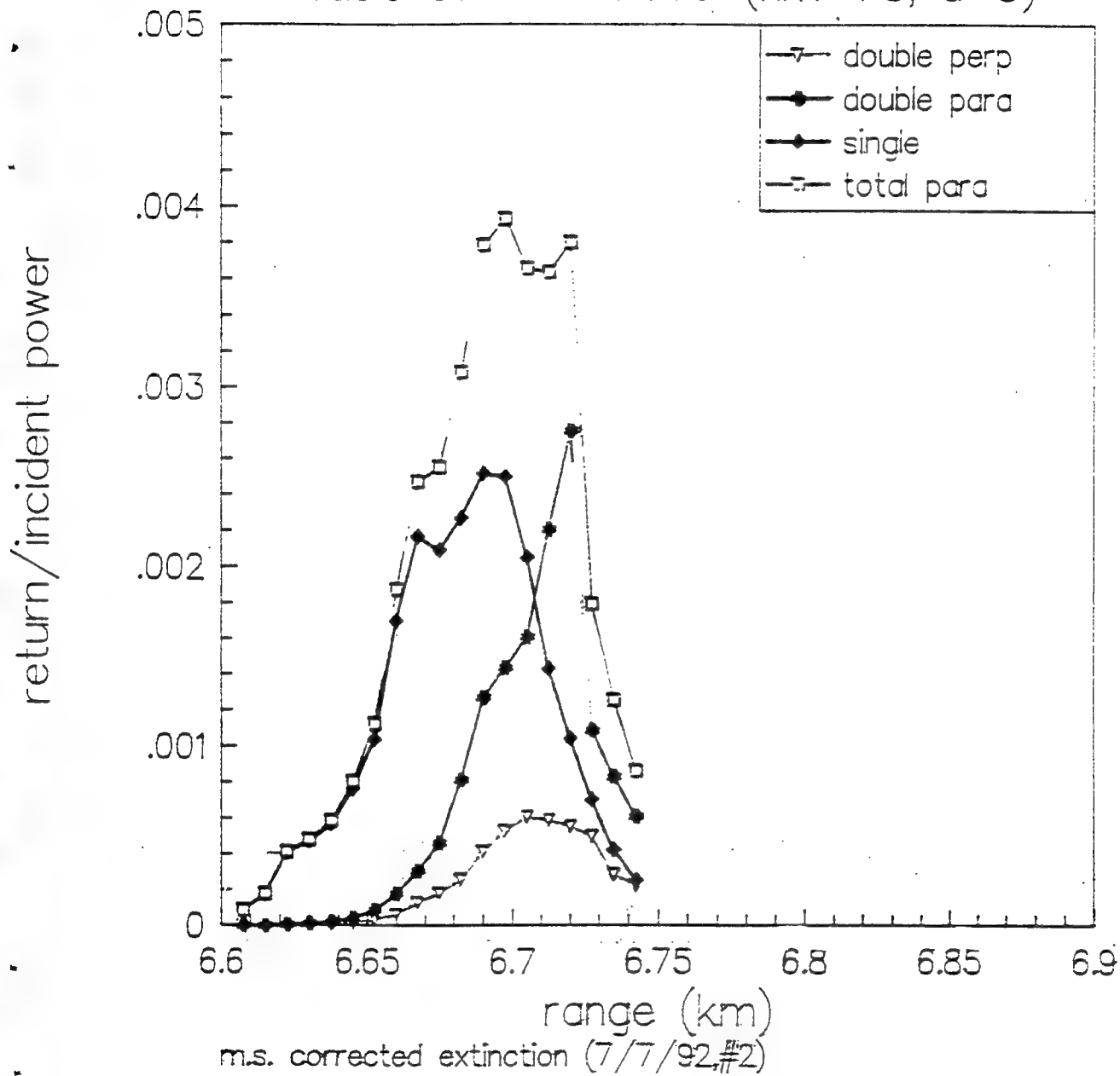


elevation=13.1 degrees

model/data comparison (m.s. corrected)
7/7/92, #2



double scatter model ($x_m=75$, $a=3$)



Conclusions

- For constant extinction the depolarization of the received radiation (single and double scattered) increases from zero to some roughly steady state value. The value is relatively low (typically in the range of 0.1 to 0.2), even for large extinctions or large fields of view.
- The steady state depolarization increases with increasing
 - extinction
 - field of view
 - cloud base
- Most double scattered power is from near the axis where much of it is polarized parallel to the incident radiation. This is the reason for the relatively low steady state depolarization.
- Relatively high steady state depolarizations are achieved for clouds that are farther away from the lidar (because regions farther from the axis then contribute more to the returned double scattered power).
- For real clouds it is important to consider the varying extinction as a function distance into the cloud. We see agreement between the model and lidar data from clouds using the extinction calculated from the data (using single scattering assumptions).
- We see agreement between model and data (lidar and cloud chamber) as a function of azimuth angle.
- The parallel component of the backscattered radiation versus azimuthal angle is sensitive to size parameter.

SKY RADIANCE AND RAY BENDING CALCULATION

Gertrude H. Kornfeld

Modeling and Simulation Branch
Army Research Laboratory

An interface of MODTRAN results with computer generation of thermal imagery is planned. The misuse of MODTRAN information might lead to dangerous conclusions.

A closed form solution for altitude dependent sky radiance that considers the curvature of the earth and ray bending, was originated in-house by the S3I Branch at ARL, and tested for the special case of a Boltzmann distribution of particle densities in the atmosphere.

Ray bending is very important because it potentially invalidates laser designators and also is an indication of unstable potentially dangerous atmospheres. A flat earth approximation would imply erroneous total reflections. The method can be amended for any analytically described atmosphere.

Sky Radiance and Ray Bending Calculation

By:

Gertrude H. Kornfeld

**Modeling and Simulation Branch
Sensors, Signatures, Signal, and Image Processing Directorate
Army Research Laboratory**





Outline



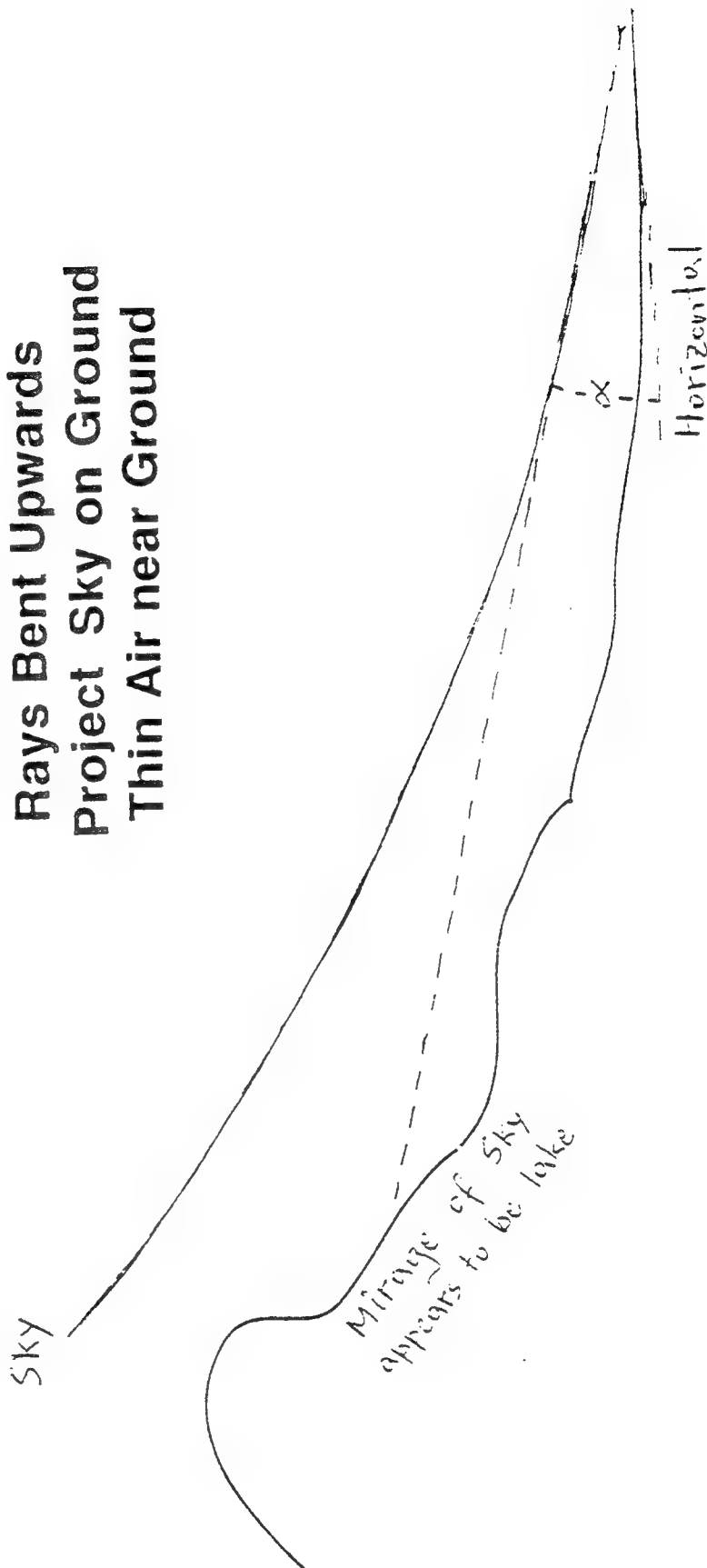
- Optical Illusions Due to Ray Bending
 - ▶ The Mirage
 - ▶ The Flying Dutchman
- Strategic Importance
 - ▶ Realistic Sky Radiance for Thermal Signature Validation
 - ▶ Orientation difficulties caused by Ray Bending
 - ▶ Misleading Laser Designator
- Closed Form Solution of Sky Radiance
 - ▶ Solution by Law of Cosines
 - ▶ Layering with Bent Rays
 - ▶ Broad Band Transmission Calculation
- Conclusions



The Mirage



Rays Bent Upwards
Project Sky on Ground
Thin Air near Ground

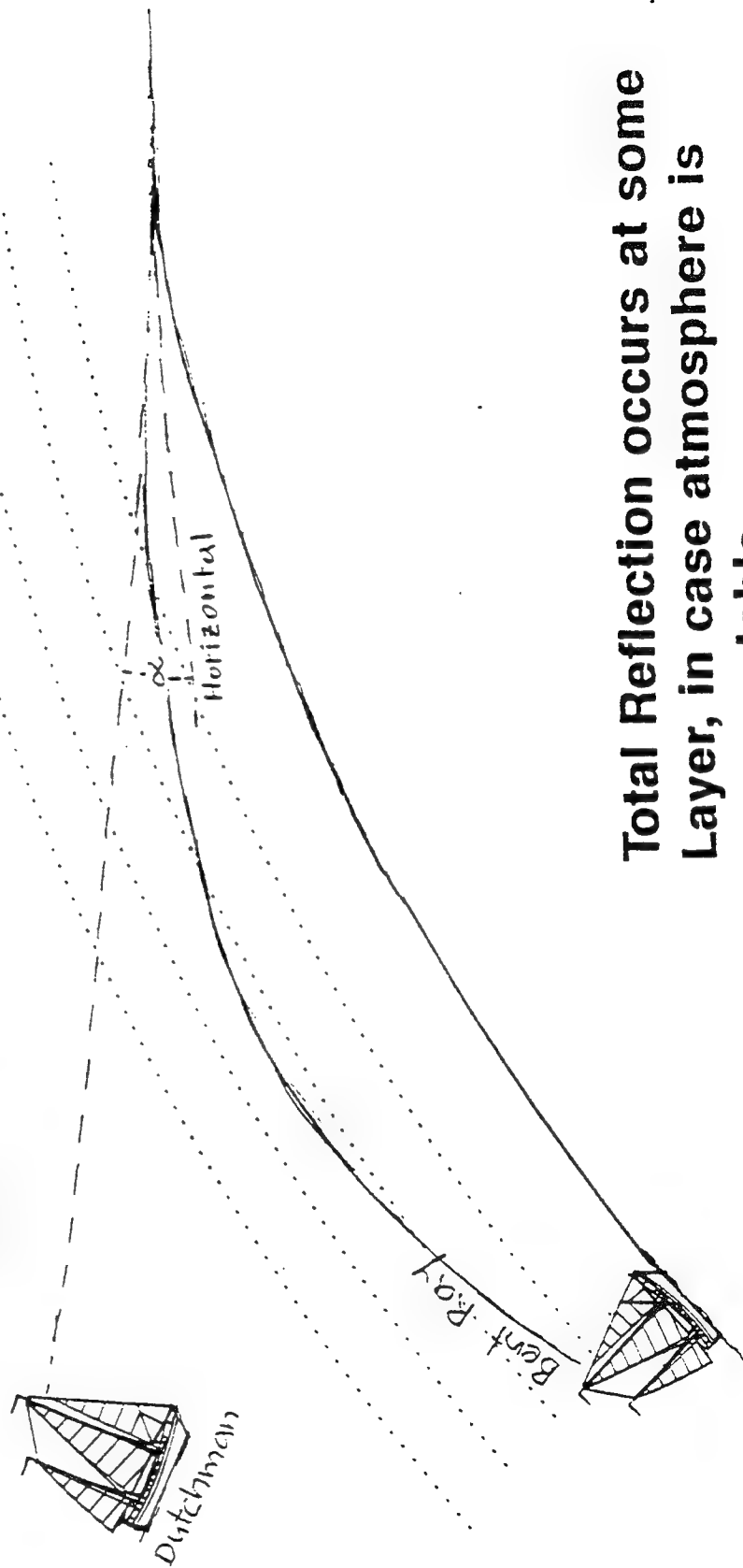




The Flying Dutchman



Rays Bent Downwards
Ship behind Horizon; Project on Sky
Dense Air near Ground



Total Reflection occurs at some
Layer, in case atmosphere is
very unstable



Snell's Law



$$n_{12} = \sin \alpha_1 / \sin \alpha_2$$

n_{12} = index of refraction of medium 2 with respect to medium 1.

In the atmosphere the index of refraction changes with pressure and temperature

Total reflection occurs in case Snell's Law would imply a sine that exceeds unity



Closed Form Solution of a Slant Pathlength



Draw triangle with sides

$R_E, R_E + H_A, R_\alpha$

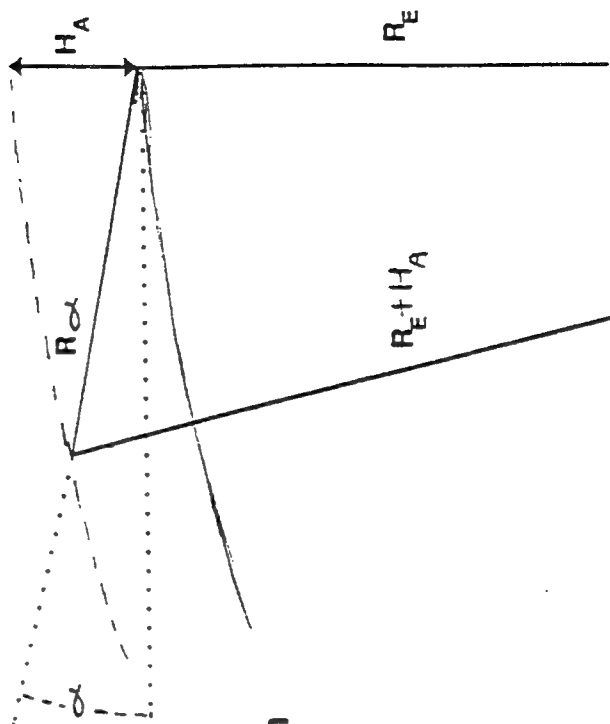
R_E = Earth Radius $\approx 6,300$ km

H_A = Altitude where atmospheric attenuation is negligible ≈ 6 to 9 km

R_α = Slant pathlength from surface to altitude H_A

α = Angle R_α makes with the horizontal

Corners at Earth Center, Earth Surface on H_A



Closed Form Solution of a Slant Pathlength

By Law of Cosines

$$(R_E + H_A)^2 = R_E^2 + R_\alpha^2 - 2R_E R_\alpha \cos(\frac{1}{2}\pi + \alpha)$$

$$\cos(\frac{1}{2}\pi + \alpha) = -\sin \alpha$$

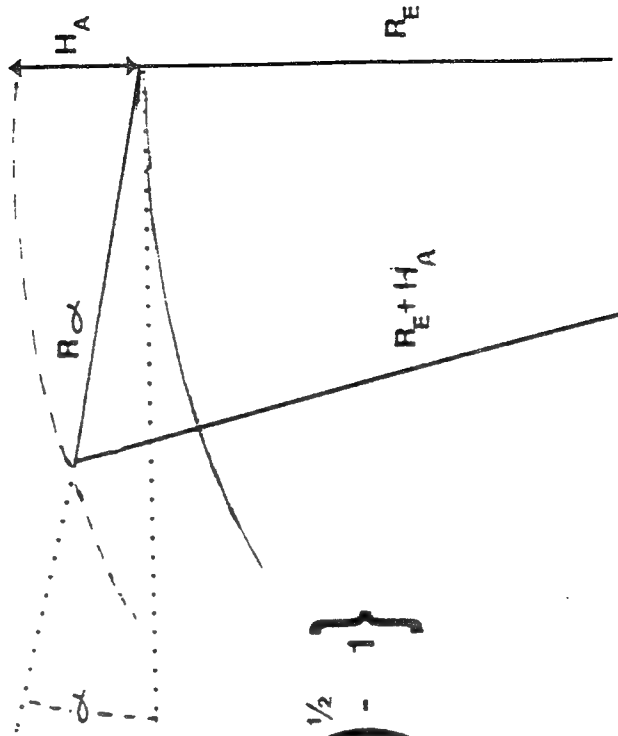
Solve Quadratic Equation for R

$$R_\alpha = R_E \sin \alpha \left\{ \left(1 + \frac{2(H_A/R_E) + (H_A/R_E)^2}{(\sin \alpha)^2} \right)^{1/2} - 1 \right\}$$

$$R_\alpha \approx \sqrt{2H_A R_E} \text{ when } (\sin \alpha)^2 \ll H_A/R_E$$

$$R_\alpha \approx H_A / \sin \alpha \text{ when } (\sin \alpha) \gg H_A/R_E$$

$$\text{At } \alpha \approx 9^\circ \text{ the terms } 2H_A/R_E \approx (\sin \alpha)^2$$





Atmospheric Layers



Divide H into M layers

Each has its broad band attenuation coefficient and index of refraction (established by Inturb)

Use Snell's law to gradually vary α

Solve quadratic Equation for individual layers

Replace R_E by $R_E + H_{(M-1)}$ and H_A by $H_M - H_{(M-1)}$

Now $(H_n - H_{(M-1)}) / (R_E + H_M)$ is infinitesimal except when $\sin \alpha$ crosses zero

$$R_\alpha \approx (H_n - H_{(n-1)}) / \sin \alpha \text{ curves gradually}$$



Sky Radiance



$R_{\alpha,m}$ is calculated for m intervals

$\tau_{\alpha,m}$ is derived by MODTRAN (broad band)

Total transmission to any range

$$\tau_{TOT} = \prod_{m=1}^M \tau_{\alpha,m}$$

For any PIXEL including the sky

$$P_{OUT}(I_x, I_y) = P_{AIR} + (P_{In}(I_x, I_y) - P_{AIR}) \tau_{TOT}$$

P_{OUT} , P_{In} are radiant powers at (I_x, I_y) location; special case the sky has $P_{In}(I_x, I_y)$ according to 3°K

CURVE FIT EXPRESSION

WEIGHTED TRANSMISSIONS

$$\mathcal{T} = \int_{\lambda_1}^{\lambda_2} d\lambda E_{\lambda} \xi_{\lambda} \prod_{m=1}^M \tau_{\lambda,m} / \int_{\lambda_1}^{\lambda_2} d\lambda E_{\lambda} \xi_{\lambda}$$

E_{λ} = INPUT ENERGY DISTRIBUTION

ξ_{λ} = DETECTOR SENSITIVITY



ENERGY BALANCE OF WATER

- PHASE CHANGE ENERGY CAL/GRAM

ICE → WATER 90

WATER → VAPOR 560

- SATURATION

- RELATIVE HUMIDITY

- EXPLANATION OF BOLTZMANN STATISTICS

ATMOSPHERIC INPUTS AT OTHER ALTITUDES

POSSIBILITIES

- STANDARD ATMOSPHERES
- DATA SET INPUTS
- CALCULATION FROM BOLTZMANN STATISTICS

$$\rho_A = \rho_0 \exp(-\epsilon_g / \epsilon_{TH})$$

ρ_0 = ATTENUATOR DENSITY AT GROUND
LEVEL

ϵ_g = GRAVITATIONAL POTENTIAL ENERGY

ϵ_{TH} = THERMAL ENERGY



Conclusions

-
- Scope of Applicability
 - ▶ Long Range Detection of Missiles
 - ▶ Possible two color Laser Designators
 - ▶ Turbulence Distortions
 - Status
 - ▶ Tested for Static Atmosphere
 - ▶ Simplified LOWTRAN 6 validated
 - Planned Improvements
 - ▶ Research Realistic Conditions
 - ▶ Interface with Turbulence Research
 - ▶ Prepare Standard Atmospheres
Ray Bending

**INTEGRATION OF LOWTRAN INTO GLOBAL
CIRCULATION MODELS FOR OBSERVING SYSTEM SIMULATION
EXPERIMENTS**

S.A. Wood and G.D. Emmitt

Simpson Weather Associates, Inc.
809 E. Jefferson St.
Charlottesville, VA 22902

The LAWS Simulation Model (LSM) simulates observations from a space-based Doppler lidar wind sounder. A main component of LSM is its atmosphere generator model that produces global estimates of aerosol optical properties, opaque clouds and subgrid scale turbulence using output from the European Center Medium Range Weather Forecast (ECMWF) global circulation model. A major issue that will be discussed is the reasonableness of the β backscatter fields resulting from the integration of LOWTRAN into the Global Circulation Models (GCMs).

INTEGRATION OF LOWTRAN INTO GLOBAL CIRCULATION MODELS FOR OBSERVING SYSTEM SIMULATION EXPERIMENTS

**S.A. Wood
G.D. Emmitt**

**Simpson Weather Associates, Inc.
Charlottesville, VA 22902**

FIGURE 1

Figure 1. Introduction slide for presentation "Integration of Lowtran Into Global Circulation Models for Observing System Simulation Experiments" by S. A. Wood and G. D. Emmitt.

Figure 2. Overview slide for "Integration of Lowtran Into Global Circulation Models for Observing System Simulation Experiments" by S. A. Wood and G. D. Emmitt.

Figure 3. Block diagram for the LAWS Simulation Model - Global Version.

Figure 4. Overview slide for the Observing System Simulation Experiments for LAWS.

Figure 5. Overview slide for the 1° X 1° Global LOWTRAN Input Data Base.

Figure 6. Flow diagram for the LSM's optical property model.

Figure 7. LAWS baseline signal to noise equation.

Figure 8. Global 9.11 μm relative aerosol backscatter ($\mu\text{m}^2 \text{ m}^{-1} \text{ sr}^{-1}$) at the earth's surface for 1/16/79 0600Z. The aerosol backscatter has been multiplied by the lidar wavelength squared.

Figure 9. Global 2.1 μm relative aerosol backscatter ($\mu\text{m}^2 \text{ m}^{-1} \text{ sr}^{-1}$) at the earth's surface for 1/16/79 0600Z. The aerosol backscatter has been multiplied by the lidar wavelength squared.

Figure 10. Global relative humidity field at the earth's surface for 1/16/79 0600Z.

Figure 11. Attenuated global 9.11 μm relative aerosol backscatter ($\mu\text{m}^2 \text{ m}^{-1} \text{ sr}^{-1}$) at the earth's surface for 1/16/79 0600Z. The aerosol backscatter has been multiplied by the lidar wavelength squared.

Figure 12. Attenuated global 2.1 μm relative aerosol backscatter ($\mu\text{m}^2 \text{ m}^{-1} \text{ sr}^{-1}$) at the earth's surface for 1/16/79 0600Z. The aerosol backscatter has been multiplied by the lidar wavelength squared.

Figure 13. Global 9.11 μm relative aerosol backscatter ($\mu\text{m}^2 \text{ m}^{-1} \text{ sr}^{-1}$) greater than 2.5×10^{-6} with integrated cloud cover less than 90% for 1/16/79 0600Z. The aerosol backscatter has been multiplied by the lidar wavelength squared.

Figure 14. Global integrated cloud cover from the top of the atmosphere to the earth's surface for 1/16/79 0600Z.

- DESCRIPTION OF OSSEs FOR SPACE-BASED DOPPLER LIDAR WIND SOUNDER
- GLOBAL LOWTRAN DATA BASE
(1° X 1°)
- GCM INPUTS (WINDS, RH, CLOUDS)
- OPTICAL PROPERTIES FOR SNR EQUATION

FIGURE 2

LAWS SIMULATION MODEL (Global Version)

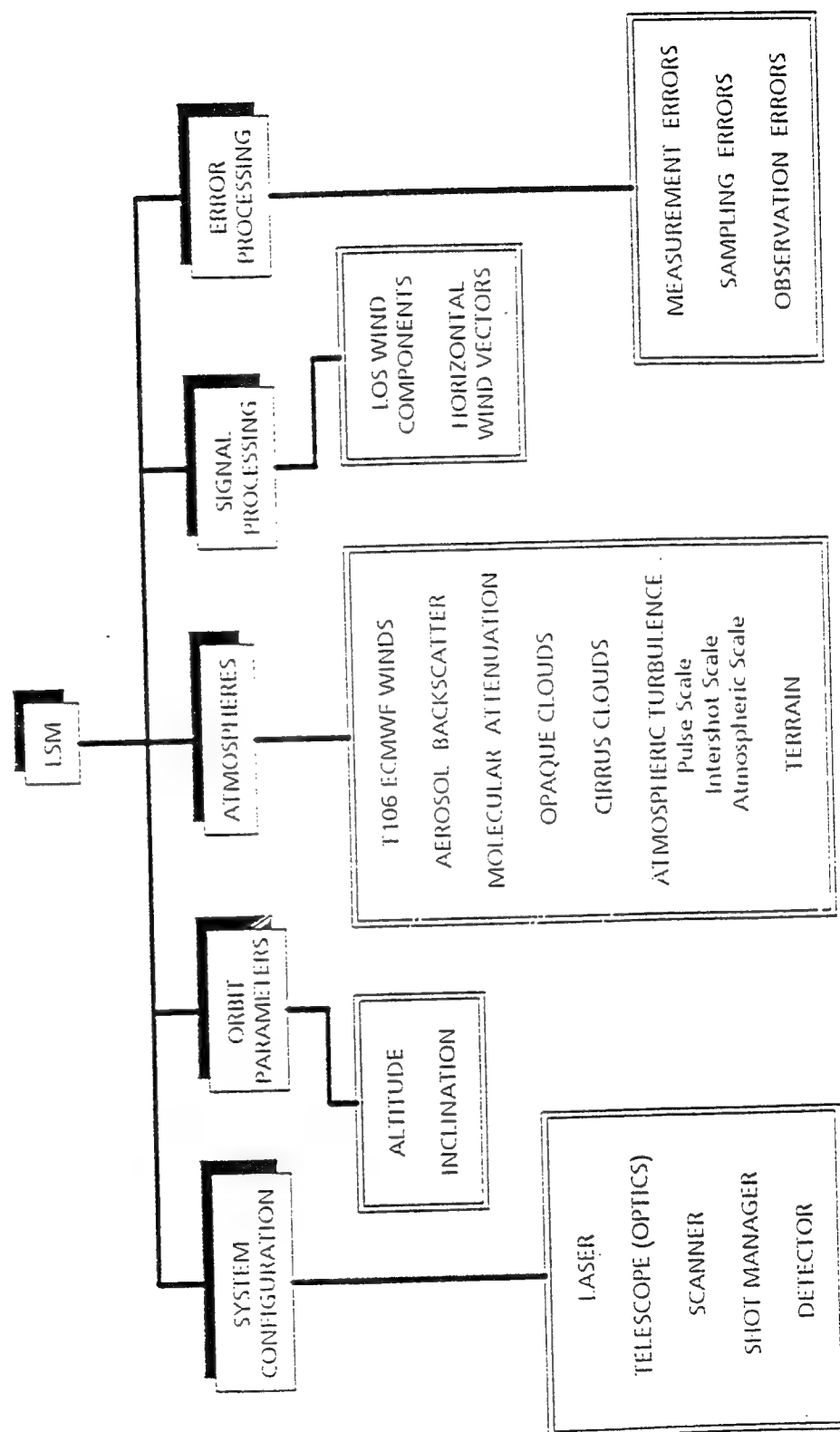
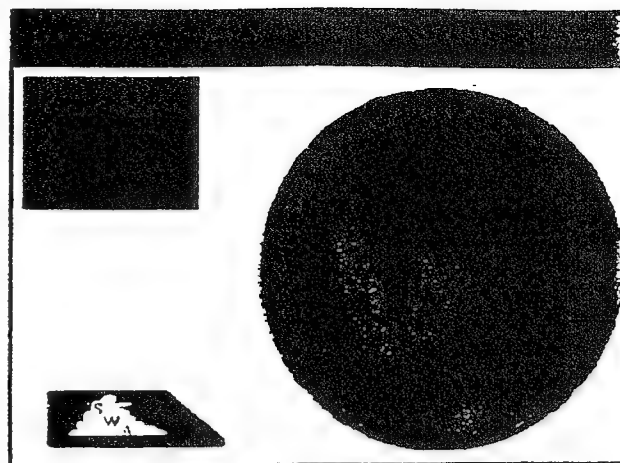
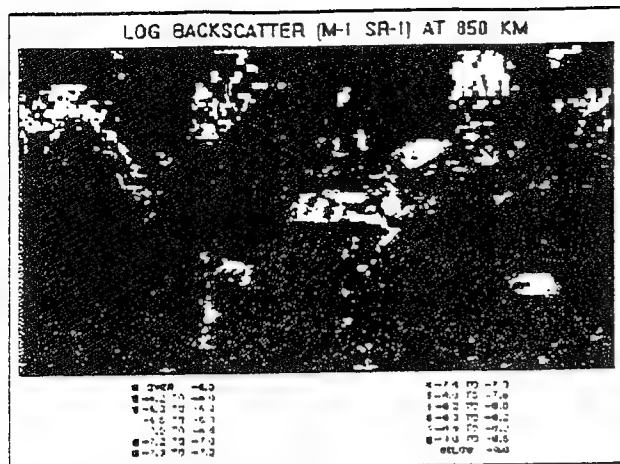
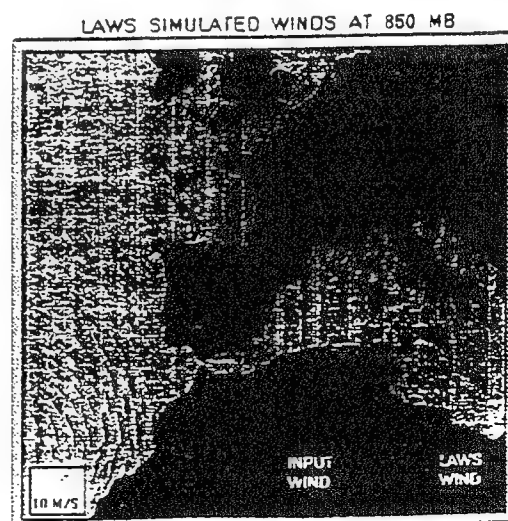
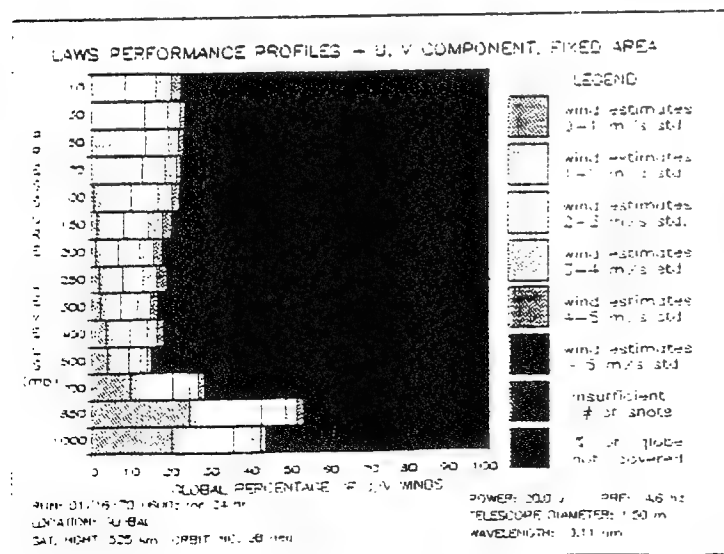
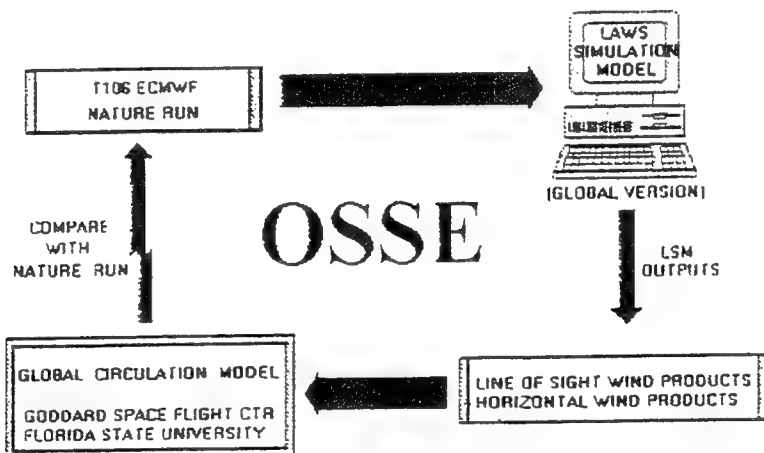


FIGURE 3

FIGURE 4



THE OBSERVING SYSTEM SIMULATION EXPERIMENTS FOR LAWS



1° x 1° GLOBAL LOWTRAN INPUT DATA BASE

- **LOCATION PROFILE**

- Tropical
- Subtropical
- Midlatitude
- Sub-Artic

- **HAZE MODEL**

- Rural
- Navy Maritime
- Ocean
- Urban
- Tropospheric
- Desert

- **COASTAL INFLUENCE**

- Open Ocean
- Weak Continental Influence
- Strong Continental Influence

FIGURE 5a

- **STRATOSPHERIC MODEL**

- Background
- Moderate Aged Aerosol
- Moderate Fresh Aerosol
- High Aged Aerosol
- High Fresh Aerosol

- **Upper Atmosphere Model**

- Normal Upper Atmosphere
- Extreme Upper Atmosphere
- Transition Volcanic to Normal
- Transition Normal to Volcanic

FIGURE 5b

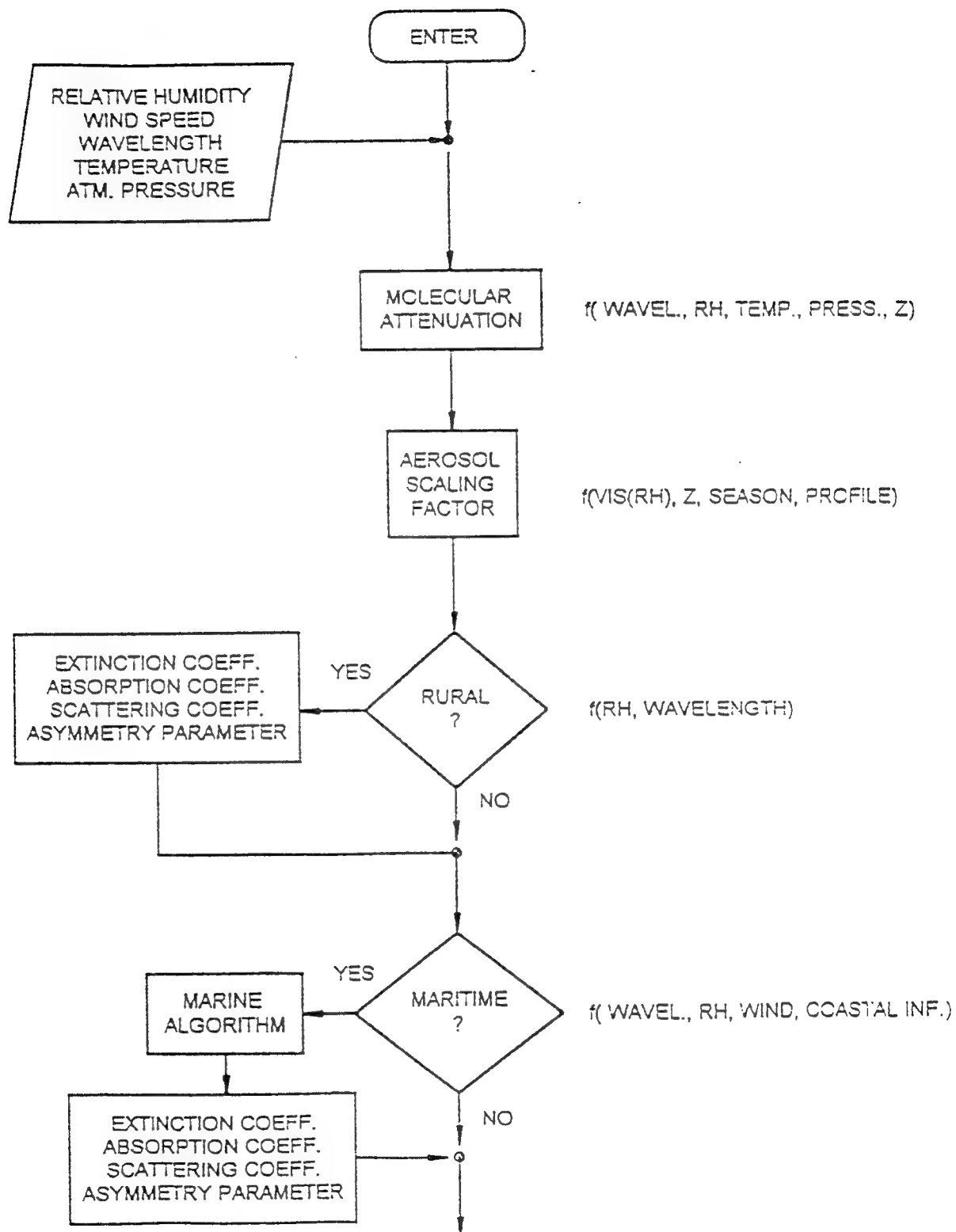


FIGURE 6a

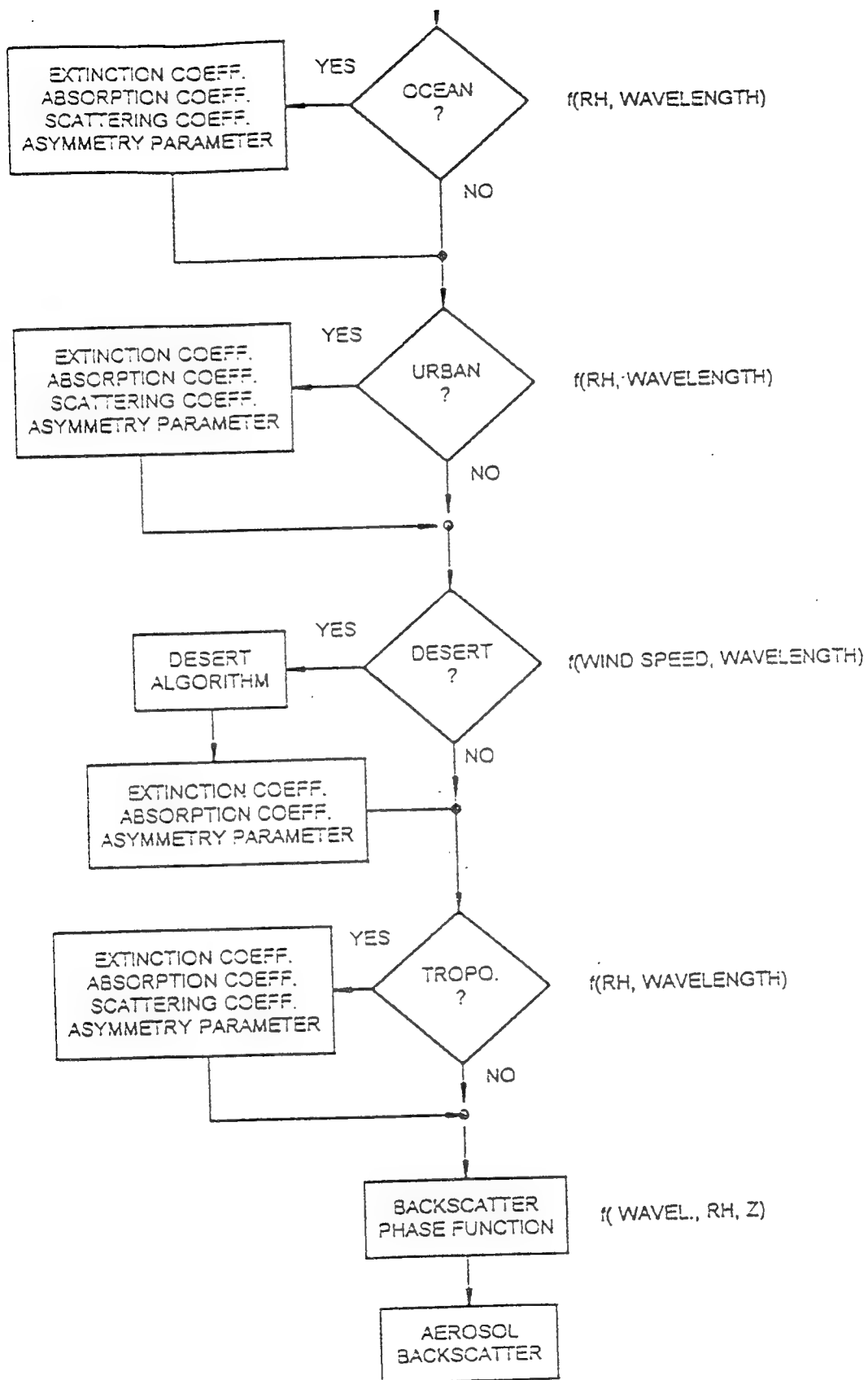


FIGURE 6b

Baseline LAWS SNR Equation

$$\text{SNR}_w = \frac{\pi \cdot n_1 \cdot n_2 \cdot n_3 \cdot n_4 \cdot J \cdot D^2 \cdot \lambda \cdot \beta \cdot e^{-2 \int \alpha(r) dr}}{8 \cdot h \cdot B \cdot R^2} = \text{wideband SNR}$$

n_1 = quantum efficiency = .40

n_2 = optical efficiency = .65

n_3 = system efficiency factor = .32

n_4 = other losses = .5

J = laser energy (Joules)

D = mirror diameter (m)

λ = laser wavelength (m)

β = backscatter ($\text{m}^{-1} \text{sr}^{-1}$)

α = attenuation as a function of distance r from telescope

h = Planck's constant = 6.63×10^{-34} joule-sec

B = processing bandwidth = $2 V_s / \lambda$ (mhz)

V_s = search window (m s^{-1}) = 50 = ($\pm 25 \text{ m s}^{-1}$)

R = slant range (m)

FIGURE 7

LOG AEROSOL BACKSCATTER ($\mu\text{m}^2 \text{ m}^{-1} \text{ sr}^{-1}$)



OVER -4.0
-4.2 TO -4.0
-4.3 TO -4.2
-4.6 TO -4.3
-5.0 TO -4.6
-5.2 TO -5.0
-5.3 TO -5.2

WAVELENGTH: 9.11 μm

-5.6 TO -5.3
-6.0 TO -5.6
-6.2 TO -6.0
-6.3 TO -6.2
-6.6 TO -6.3
-7.0 TO -6.6
BELOW -7.0

SURFACE

FIGURE 8

LOG AEROSOL BACKSCATTER ($\mu\text{m}^2 \text{ m}^{-1} \text{ sr}^{-1}$)



OVER -4.0
 -4.2 TO -4.0
 -4.3 TO -4.2
 -4.6 TO -4.3
 -5.0 TO -4.6
 -5.2 TO -5.0
 -5.3 TO -5.2

WAVELENGTH: 2.1 μm

SURFACE

-5.6 TO -5.3
 -6.0 TO -5.6
 -6.2 TO -6.0
 -6.3 TO -6.2
 -6.6 TO -6.3
 -7.0 TO -6.6
 BELOW -7.0

FIGURE 9

RELATIVE HUMIDITY AT THE SURFACE



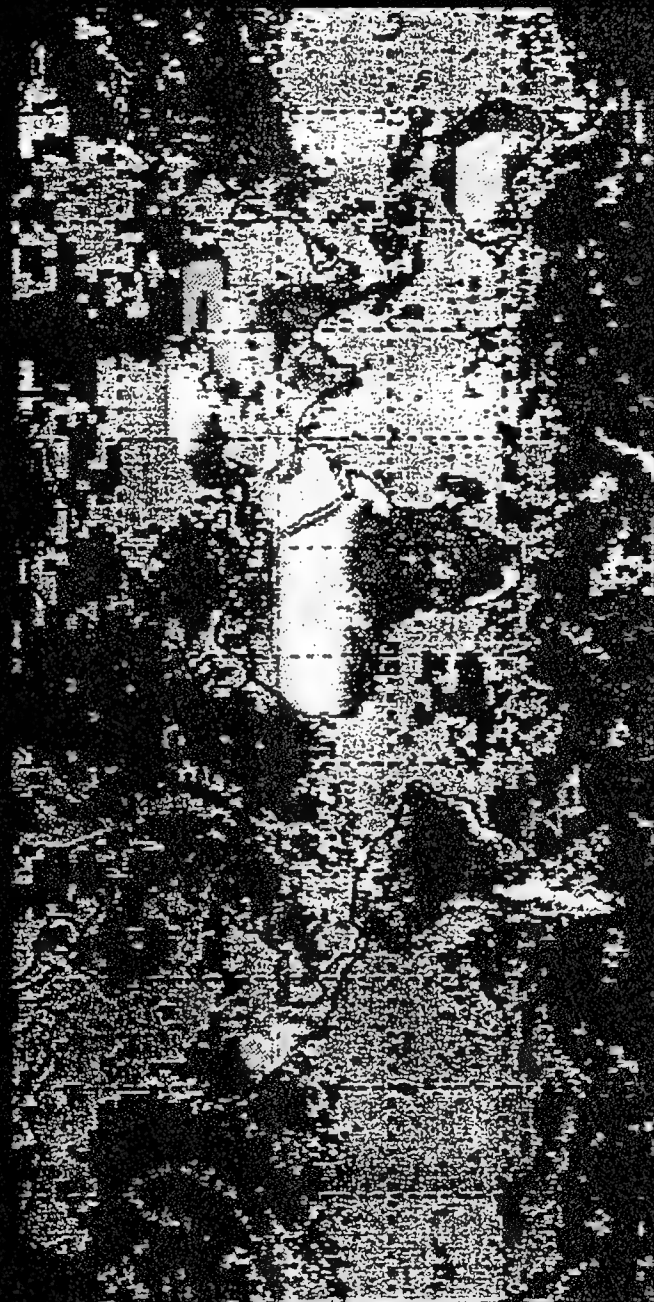
21 -	< 28	56 -	< 63	91 -	< 100
14 -	< 21	49 -	< 56	84 -	< 91
07 -	< 14	42 -	< 49	77 -	< 84
00 -	< 07	35 -	< 42	70 -	< 77
00 -		28 -	< 35	63 -	< 70

0600Z

1/16/79

FIGURE 10

LOG ATTENUATED BACKSCATTER ($\mu\text{m}^2 \text{ m}^{-1} \text{ sr}^{-1}$)



OVER -4.0
-4.2 TO -4.0
-4.3 TO -4.2
-4.6 TO -4.3
-5.0 TO -4.6
-5.2 TO -5.0
-5.3 TO -5.2

WAVELENGTH: 2.1 μm

SAT. ALT. - 525 KM

NADIR ANG. - 45°

SURFACE

-5.6 TO -5.3
-6.0 TO -5.6
-6.2 TO -6.0
-6.3 TO -6.2
-6.6 TO -6.3
-7.0 TO -6.6
BELOW -7.0

FIGURE 11

LOG ATTENUATED BACKSCATTER ($\text{m}^2 \text{ m}^{-1} \text{ sr}^{-1}$)



OVER -4.0
-4.2 TO -4.0
-4.3 TO -4.2
-4.6 TO -4.3
-5.0 TO -4.6
-5.2 TO -5.0
-5.3 TO -5.2

WAVELENGTH: 9.11 μm

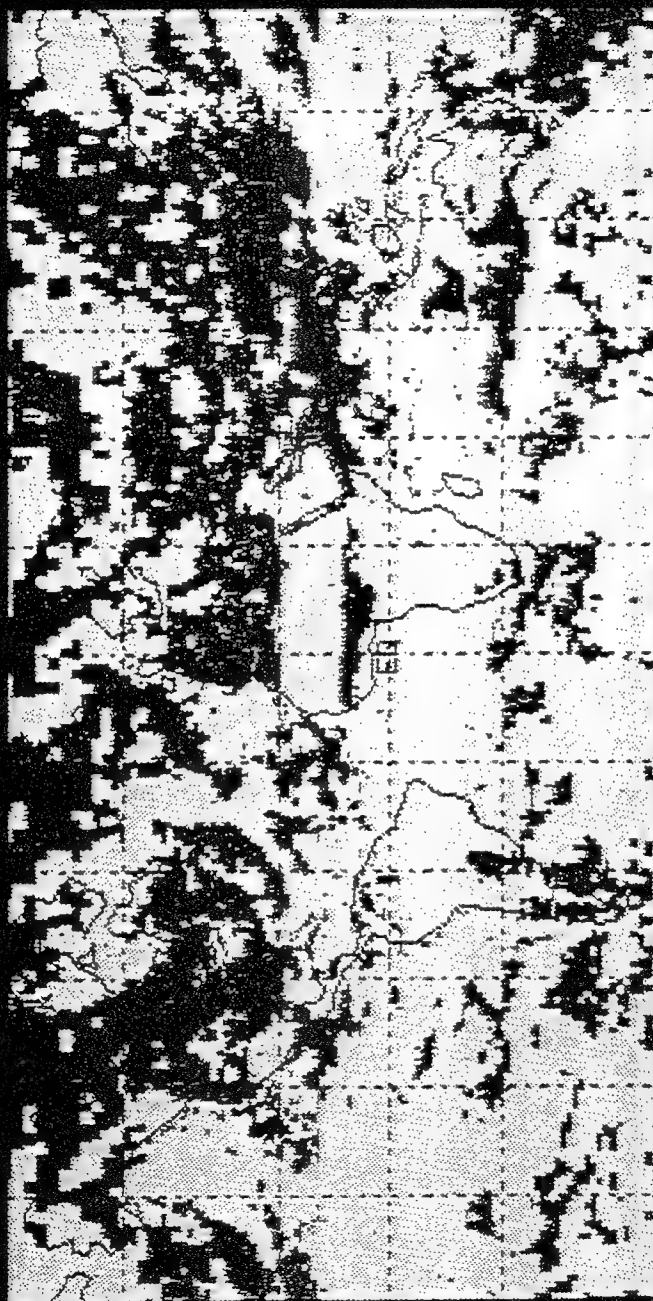
SAT. ALT. 525 KM
NADIR ANG. 45°

SURFACE

-5.6 TO -5.3
-6.0 TO -5.6
-6.2 TO -6.0
-6.3 TO -6.2
-6.6 TO -6.3
-7.0 TO -6.6
BELOW -7.0

FIGURE 12

LOG ATTENUATED BACKSCATTER ($\text{dm}^2 \text{ m}^{-1} \text{ sr}^{-1}$)



OVER -4.0
-4.2 TO -4.0
-4.3 TO -4.2
-4.6 TO -4.3

WAVELENGTH: 9.11 DM

SAT. ALT. - 525 KM
NADIR ANG. - 45°

-5.0 TO -4.6
-5.2 TO -5.0
-5.3 TO -5.2
-5.6 TO -5.3

ATM. TOP TO EARTH'S SURFACE
INTEGRATED CLOUD COVER THRESHOLD: 80 %

FIGURE 13

INTEGRATED CLOUD COVER FROM THE TOP OF THE ATMOSPHERE TO THE SURFACE OF THE EARTH



91 - ■ - 100	56 - < 63	21 - < 28
84 - ■ - 91	49 - < 56	14 - ■ - < 21
77 - ■ - 84	42 - ■ - < 49	07 - ■ - < 14
70 - ■ - 77	35 - ■ - < 42	00 - ■ - < 07
63 - ■ - 70	28 - ■ - < 35	00 - ■

FIGURE 14

AEROSOL DISTRIBUTION AND IR BROADBAND TRANSMITTANCE IN THE MARINE BOUNDARY LAYER IN THE MEDITERRANEAN ENVIRONMENT

Mireille Tanguy, Michel Autric, and Bernard Salles

DCN/CESDA Mourillon/GR. OPT
BP 77
83800 Toulon Naval FRANCE

An IR broadband transmissometer has been settled near the Toulon's coast in the Mediterranean Sea. The atmospheric transmittance has been measured along a horizontal path of 8 km at about 30 m above the sea surface. Meteorological parameters, aerosol density distribution and visibility have been recorded too. Partial results have been presented during the SPIE meeting in Orlando (April 1991). So further conclusions will be presented on:

- Aerosol density behavior
- Atmospheric transmittance behavior
- Systematic comparison between measures and LOWTRAN 7
using Navy maritime model and Maritime model.

**AEROSOL DISTRIBUTION AND IR BROADBAND
TRANSMITTANCE IN THE MARINE
MEDITERRANEAN BOUNDARY LAYER**

DCN TOULON (FRANCE)

Directorate for Naval Construction working for the French Navy

CTSN / LSA / GR. OPTRONIQUE

Technical Center of Naval Systems

I.M.F. of MARSEILLE (FRANCE)

Fluids Mechanisms Institute

author : Miss Mireille TANGUY

co-authors : M. Herve BONHOMMET (DCN)
M. Bernard SALLES (DCN)
M. Michel AUTRIC (IMF)

OUTLINE

INTRODUCTION

THE GEOGRAPHIC SITE AND THE TECHNICAL MEANS

THE AEROSOL DENSITY MEASUREMENTS

THE ATMOSPHERIC TRANSMITTANCE MEASUREMENTS AND
THE LOWTRAN 7 CODE

CONCLUSION

INTRODUCTION

FINAL GOAL :

- Improvement of the software : PREDIR used for the prediction of the range of the Navy's IR optronics passive systems
- LOWTRAN code : subroutine of PREDIR for radiance and transmittance calculations

OUR PRESENT STUDY :

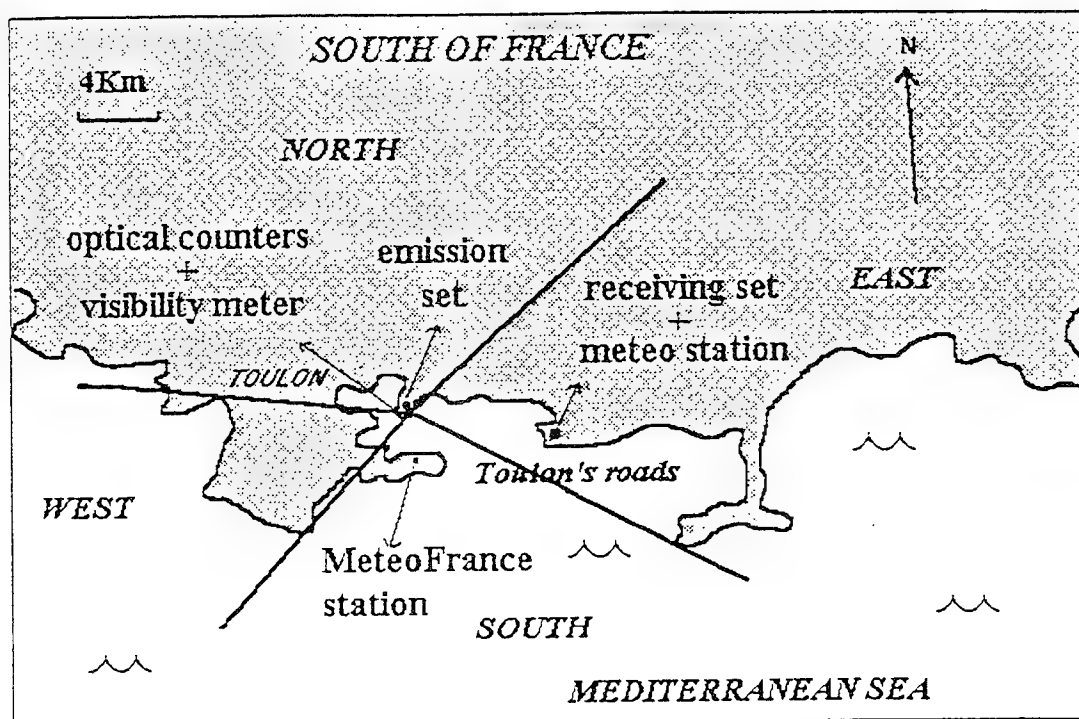
- Validation of the LOWTRAN version 7 in a marine mediterranean environment for the following conditions :

Atmospheric Transmittance

aerosol contribution at 14 meters high

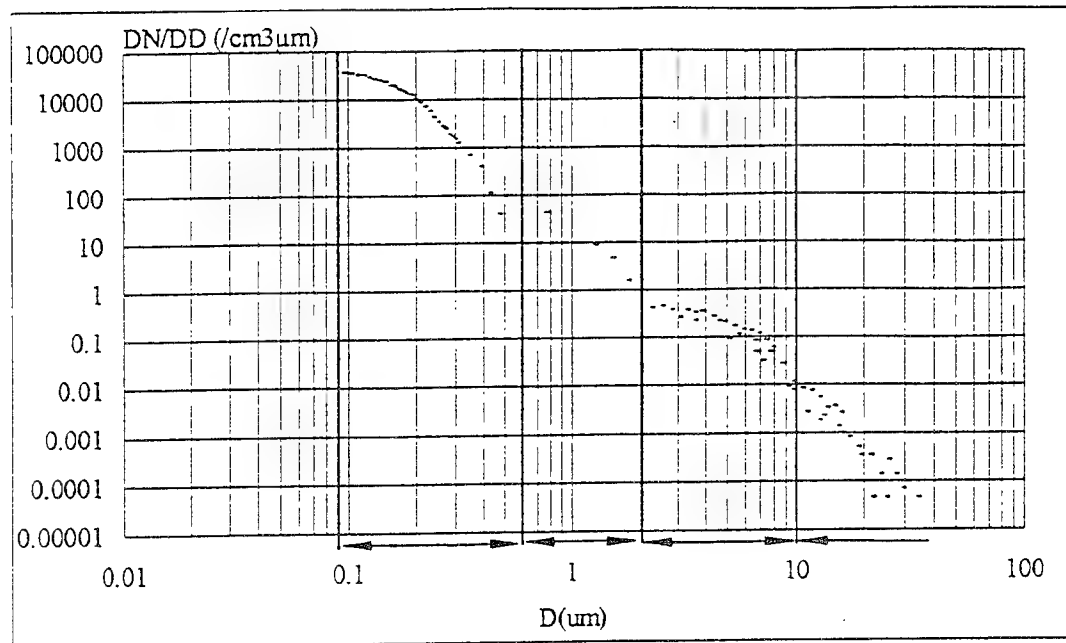
horizontal path at 30 meters high in a coastal zone

GEOGRAPHIC SITE AND THE TECHNICAL MEANS



	AEROSOLS	TRANSMITTANCE
period	Août-September	Oct-Nov-Dec
CSASP 100 HV	14 m (building)	
ASASP-X	14 m (building)	14m(building) - 7m(ship)
TRANSMISSOMETER		3-5 / 8-12 μ m - 30m - 8km
METEOFRANCE	125 m (2km to South)	
VISIBILITY METER	17 m (building)	17m(building) - 8m (ship)
AUTOMATIC METEO		40m (receiving set)

AEROSOL DENSITY MEASUREMENTS



3 kinds of exploitation :

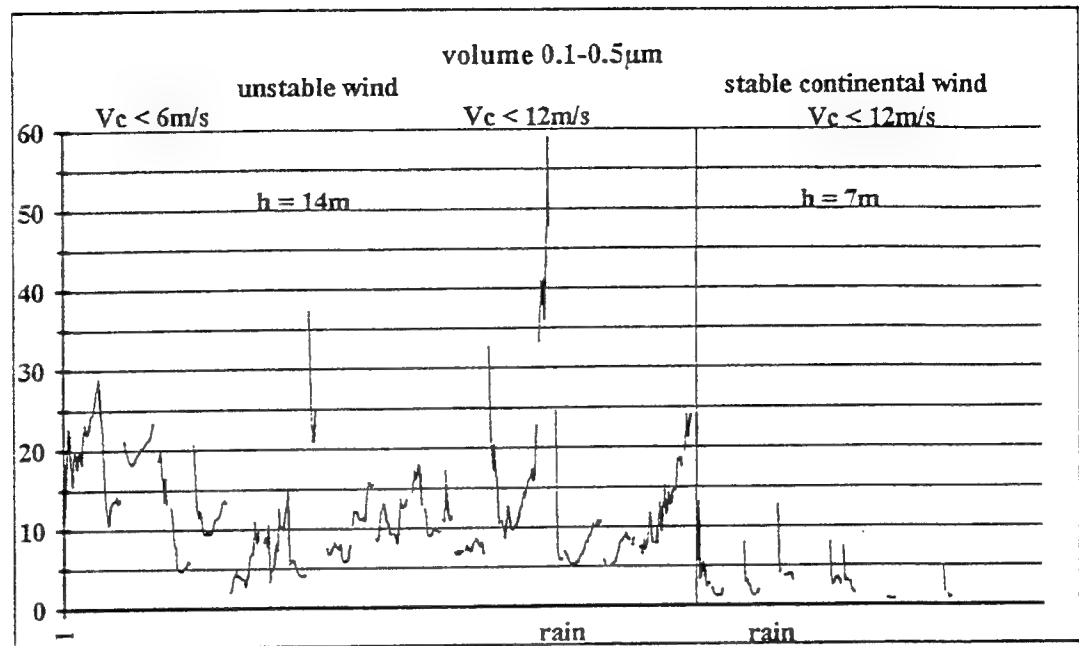
- average volume over 4 diameters ranges :
 0.09µm-0.5µm 0.5µm-2µm 2µm-10µm 10µm-47µm

$$\text{volume } d_1 - d_2 = \frac{1}{(d_2 - d_1)} \times \int_{d_1}^{d_2} \frac{4}{3} \times \pi \times r^3 \times \frac{dN}{dr} \times dr$$

- extinction coefficients K_{aer} calculated from measured aerosols distributions (Mie theory)
- total transmittance by introducing extinction coefficients into "user defined card" of Lowtran code

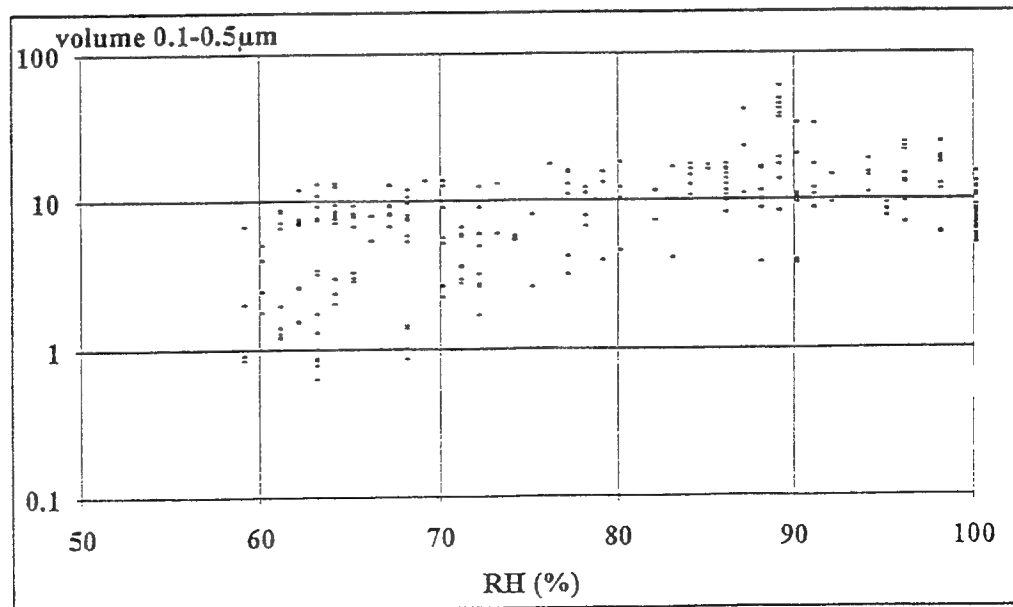
AEROSOLS DENSITY MEASUREMENTS

The average volumes and the meteorological conditions



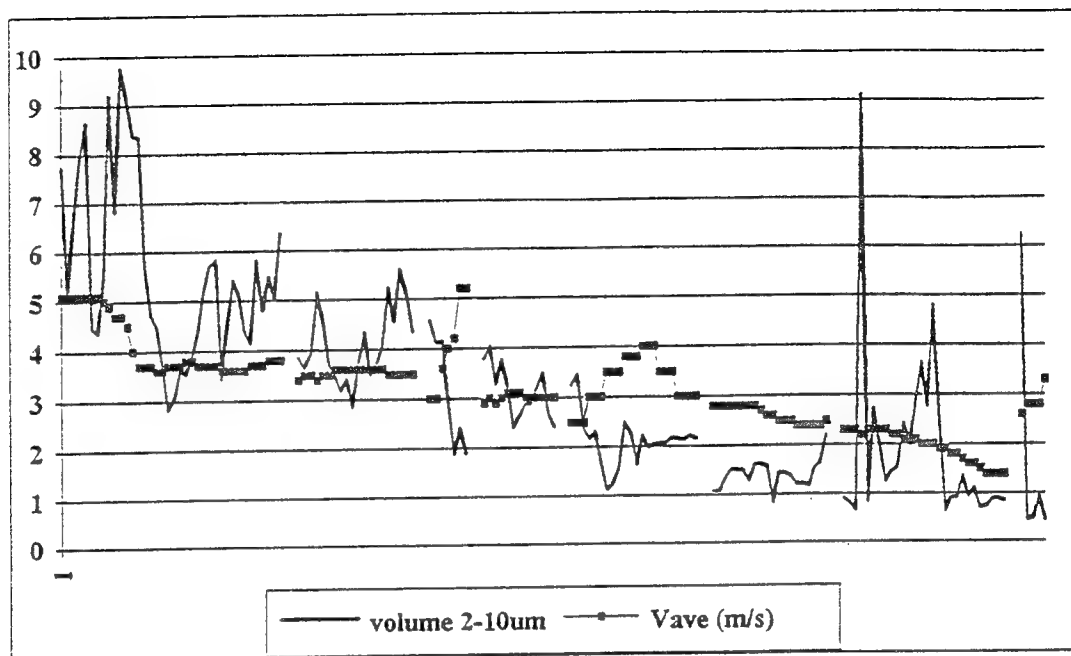
bad relation between air mass and $[0.1\mu\text{m}-0.5\mu\text{m}]$ aerosol density :

- proximity of coast
- likeness of the trajectory of depression and anticyclone air mass

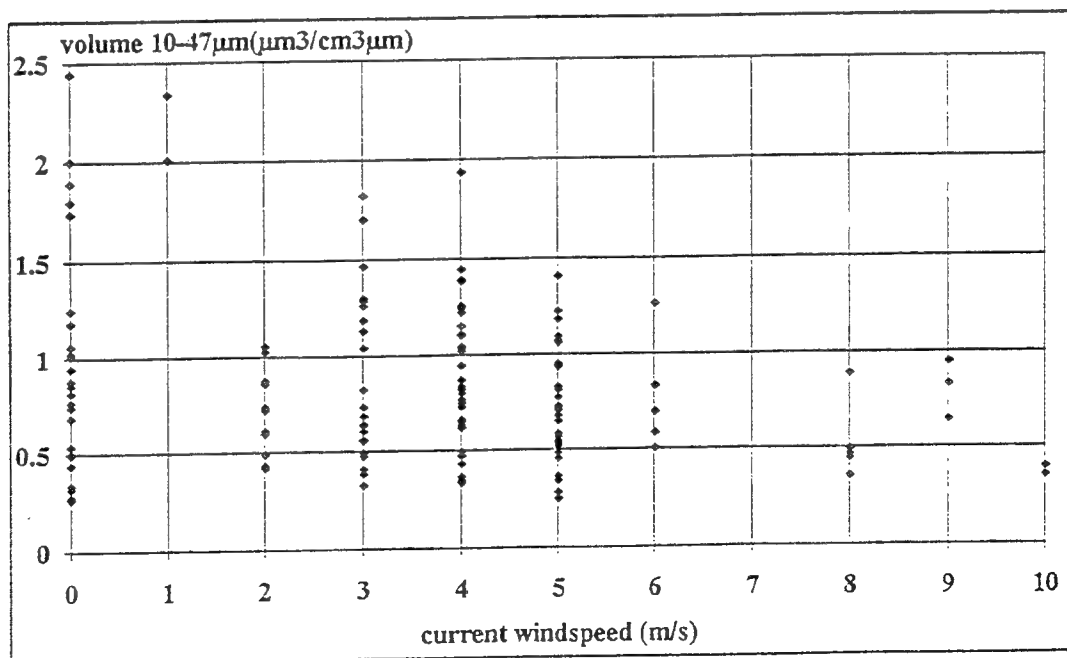


AEROSOLS DENSITY MEASUREMENTS

The average volumes and the meteorological conditions

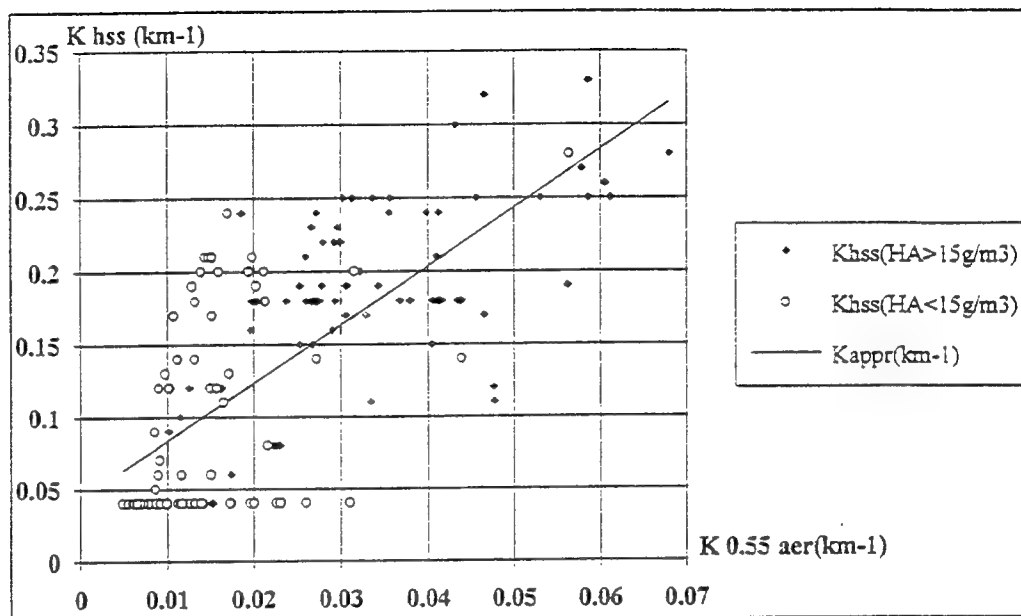


volume 0.5-2 μm = volume 2-10 μm Vave : 24hours average windspeed

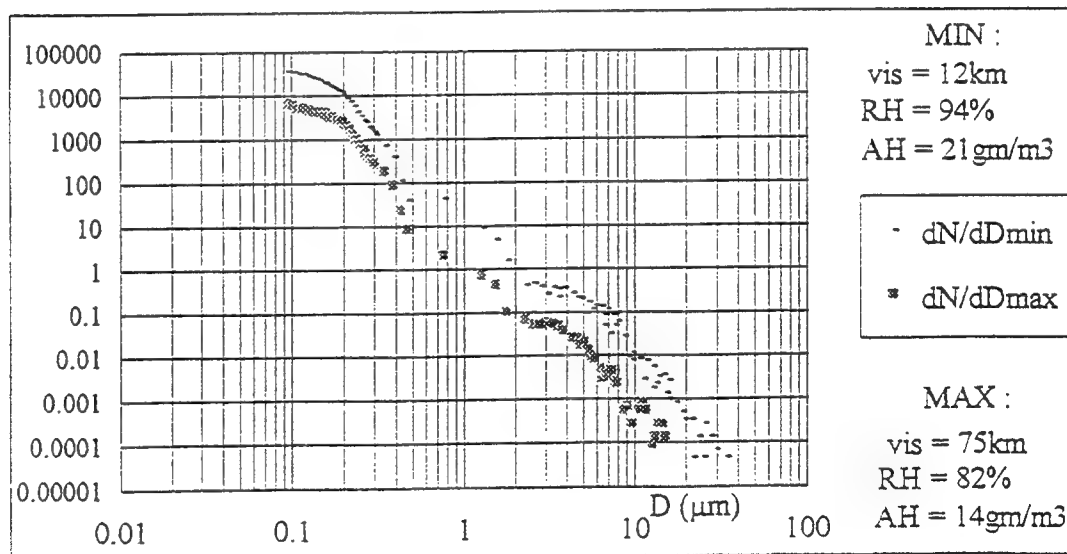


AEROSOL DENSITY MEASUREMENTS

aerosols extinction coefficients

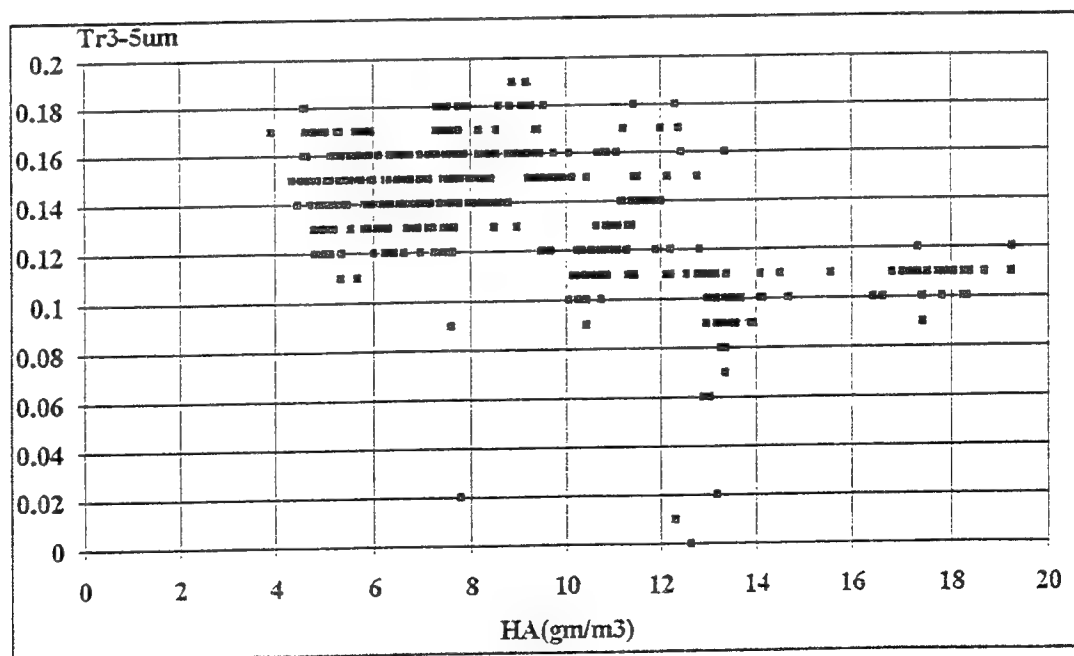
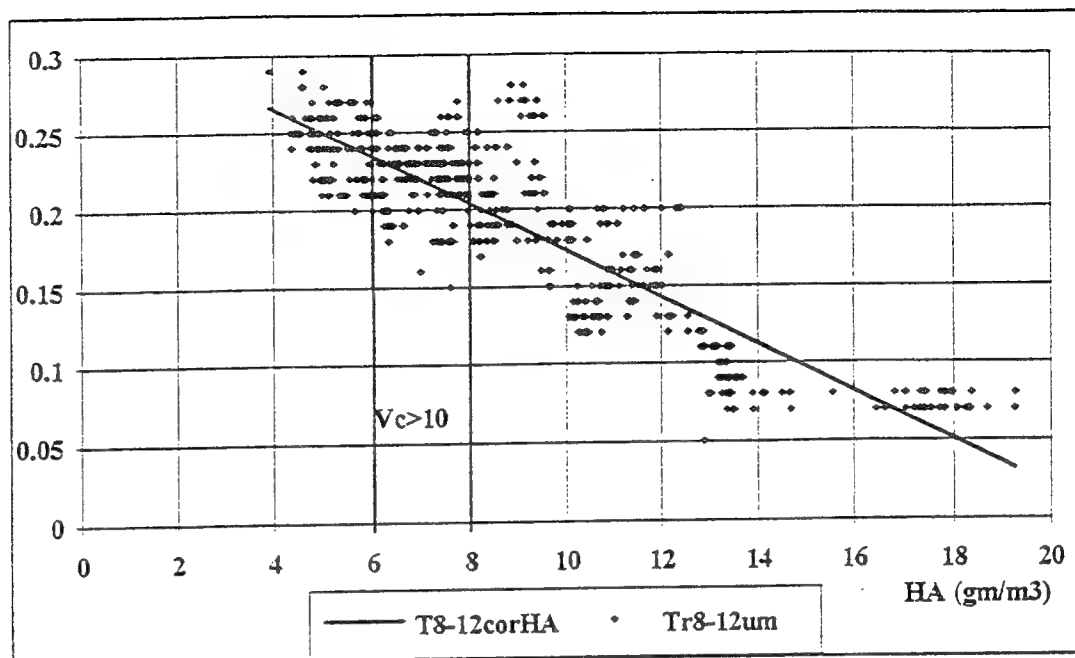


$$K(0.55\mu\text{m}) \text{ appr} = 4 \times K \text{ aer}(0.55\mu\text{m}) + 0.04$$



LOWTRAN7	3-5 μm	8-12 μm	$\Delta T/T_{3-5\mu\text{m}}$	$\Delta T/T_{8-12}$
Tmin	27.7%	16.6%		
Tmax	17.7%	3.7%		
AH _{max} =AH _{min}	20%	14.3%	28%	15%

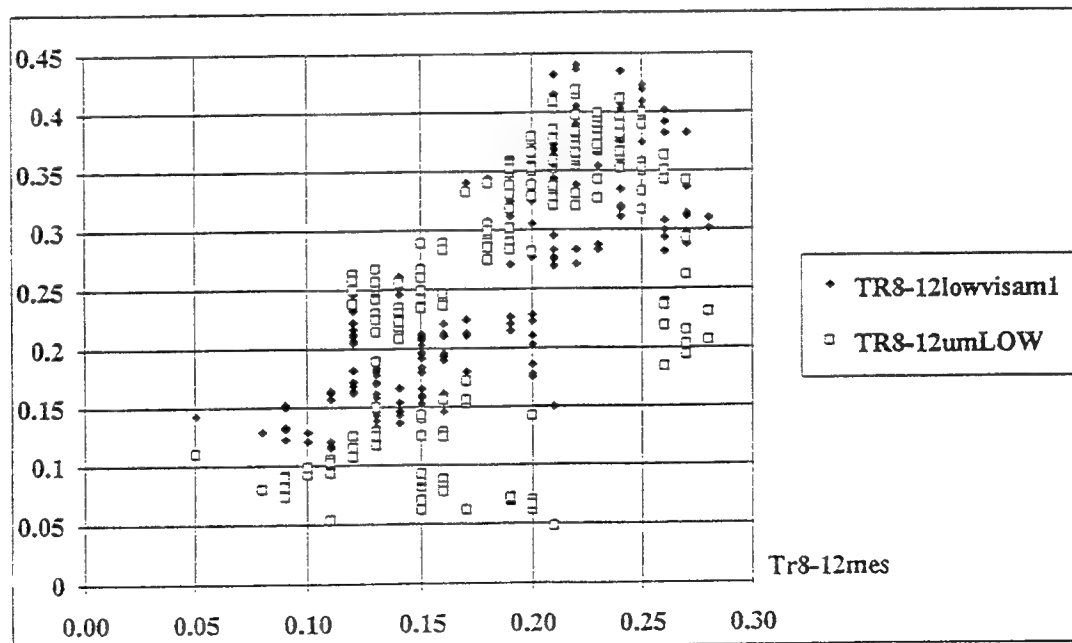
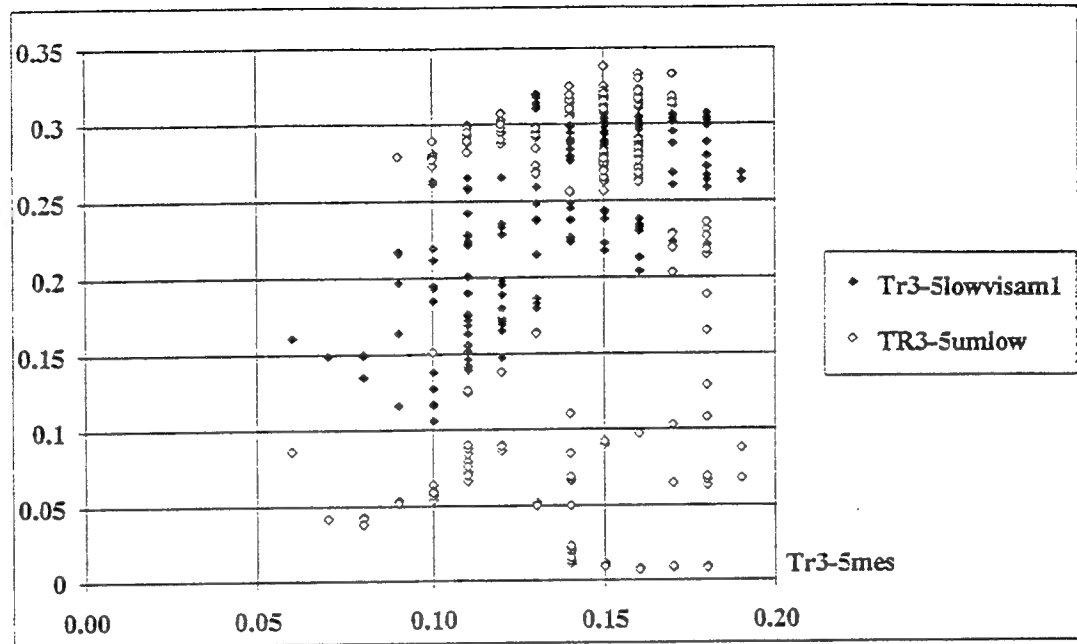
ATMOSPHERIC TRANSMITTANCE MEASUREMENTS



- accuracy of temperature measurements
- feature of thermometer's location
- aerosols density's variations are not preponderant

ATMOSPHERIC TRANSMITTANCE MEASUREMENTS

LOWTRAN 7 CODE NAVY AEROSOL MODEL

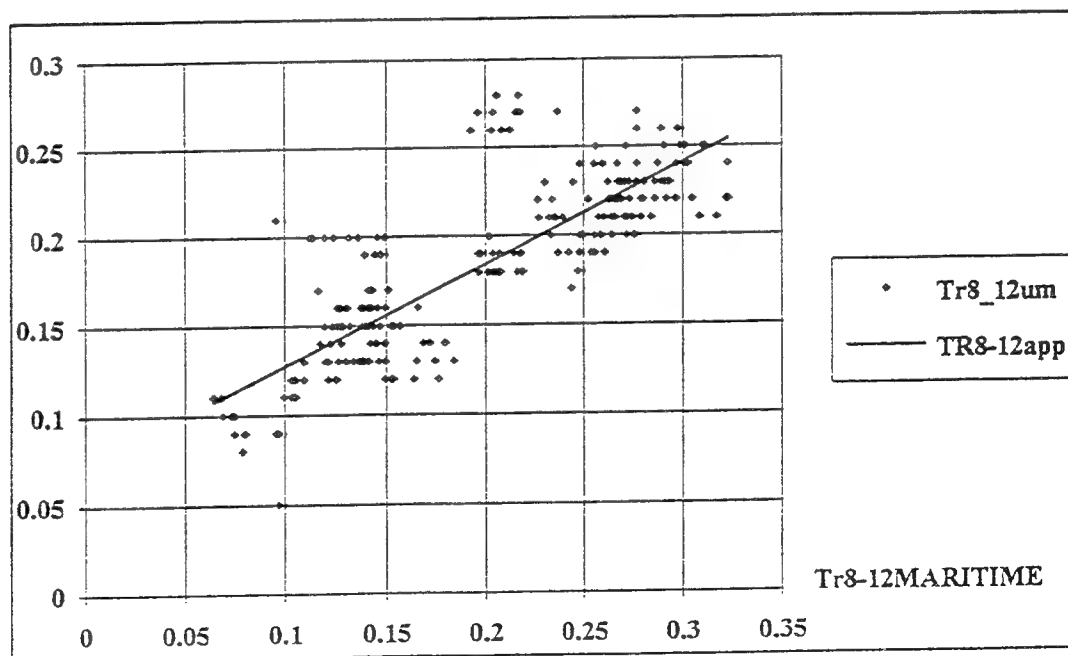
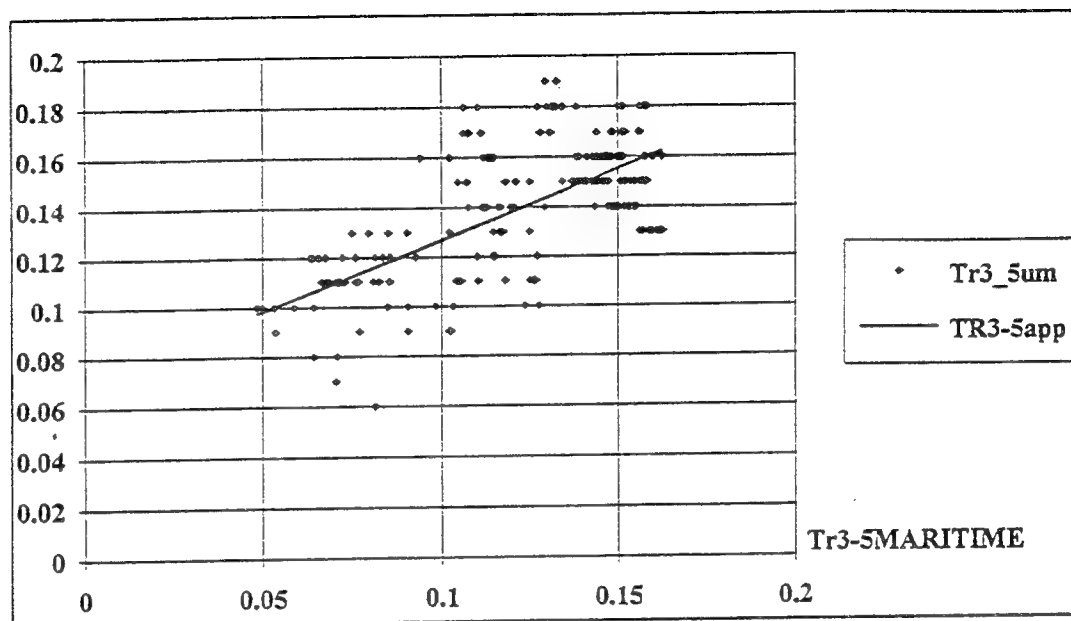


black points : using visibility
white points : without visibility

ATMOSPHERIC TRANSMITTANCE MEASUREMENTS

LOWTRAN 7 CODE

MARITIME MODEL



CONCLUSION

COASTAL MEDITERRANEAN ZONE

- Navy Aerosol Model unadapted at 14 meters high

- reference aerosol distribution

+

surface range

+

absolute humidity

⇓

estimation of atmospheric transmittance at 30 meters high

MARITIME MODIFICATIONS TO LOWTRAN RADIANCE

C.R. Zeisse

NCCOSC RDTE DIV 543
53170 Woodward Road
San Diego, CA 92152

LOWTRAN 6 has been modified for shipboard observation ($H_1 \approx 10$ m) of the marine horizon ($\text{ANGLE} \approx 90 \pm 1^\circ$) in the long wave band (830 to 1250 cm^{-1}). For paths to the sky an anomalous dip originally occurred in the radiance calculated just above the horizon. This dip disagreed with low altitude observations of the maritime sky and was removed by increasing the atmospheric layering. For paths to the earth, the earth has been reinterpreted as the sea. Using Cox-Munk wave slope statistics for the sea surface, the following sea radiance contributions have been introduced in addition to the path radiance already provided by LOWTRAN 6: (1) thermal emission from the sea, (2) reflection of sky radiance by the sea, and (3) solar glints. These modifications increase the calculated radiance by as much as a factor of two and bring calculations to within a few $^\circ\text{C}$ of marine observations. They are being considered for introduction into future LOWTRAN versions. Finally, it will be proven that the Ben-Shalom radiance formula does not respond to aerosol content, making it inappropriate for use in the marine environment.

Maritime Modifications to LOWTRAN Radiance

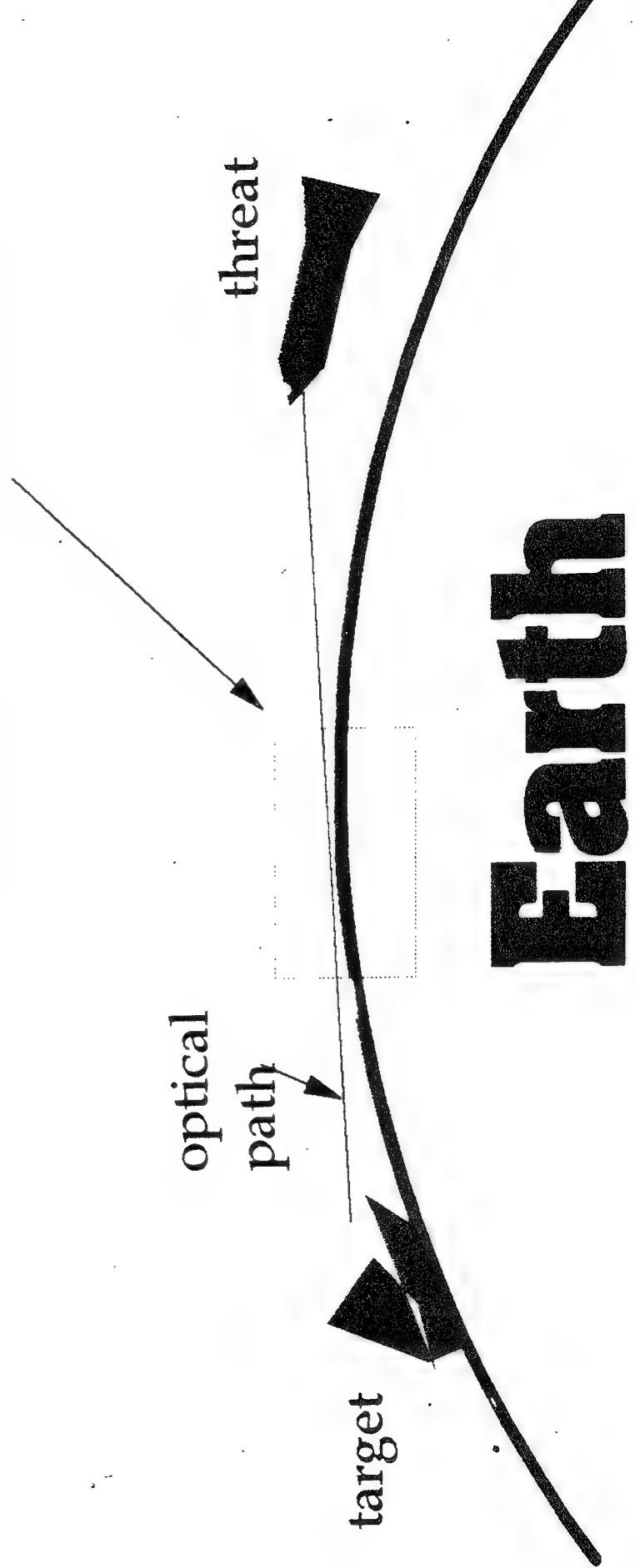
C. R. Zeisse

Tropospheric Branch
Naval Command Control and Ocean Surveillance Center
Research, Development, Test, and Evaluation Division
San Diego, CA

Advanced Navy Aerosol Model

ANAM

region of ANAM importance



Maritime Modifications to LOWTRAN 6 at NRaD

Layer the Dip away (Wollenweber & Hughes, 1988).

Reflect the Sky in the Sea (Wollenweber & Hughes, 1988).

Allow the Sea to Radiate (Wollenweber & Hughes, 1988).

Reflect the Sun in the Sea (Zeisse & Hughes, 1993).

MODIFICATIONS ASSOCIATED ENTIRELY WITH THE ATMOSPHERE

**Remove the dip at the horizon
by adding layers.**

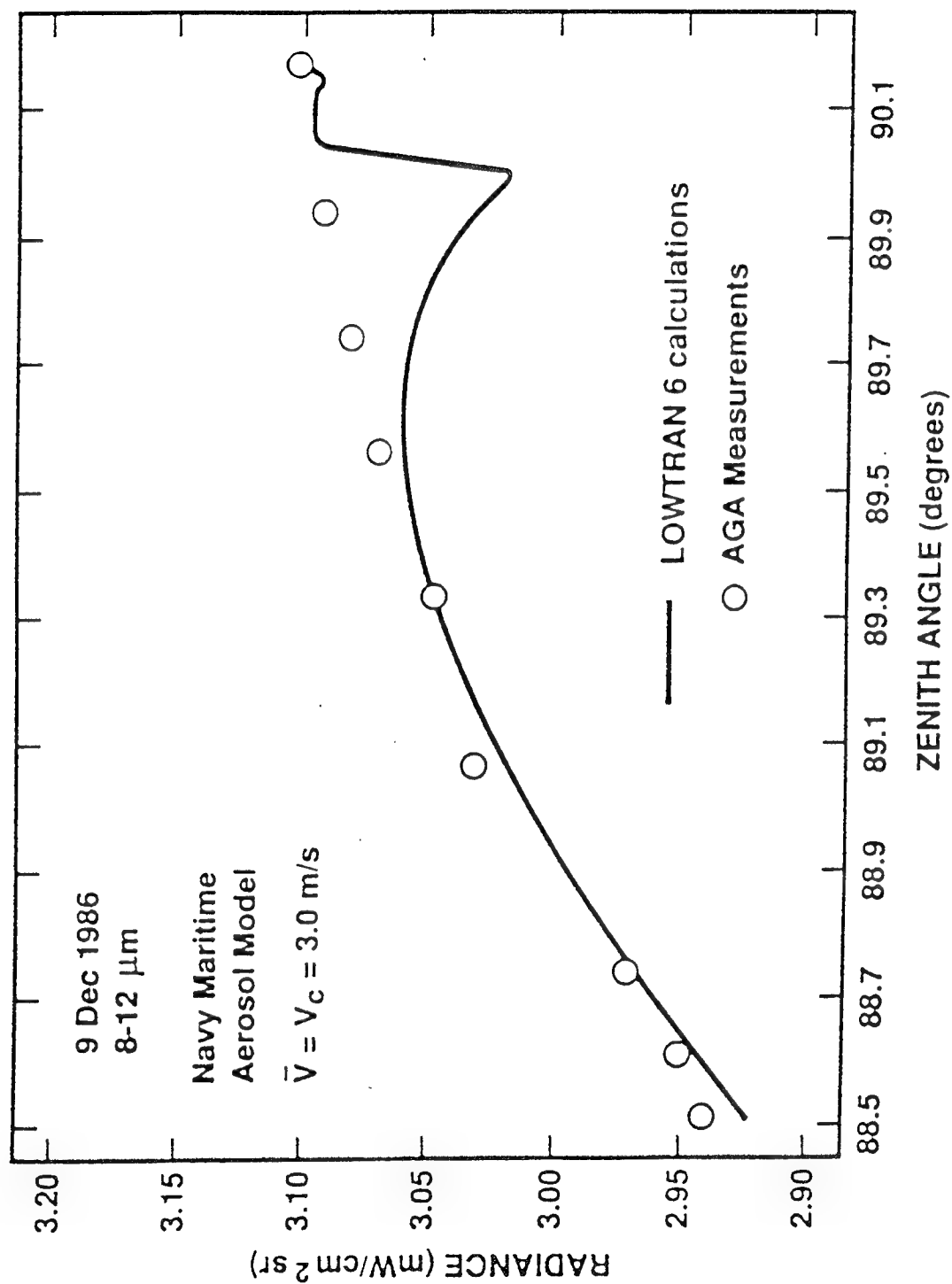
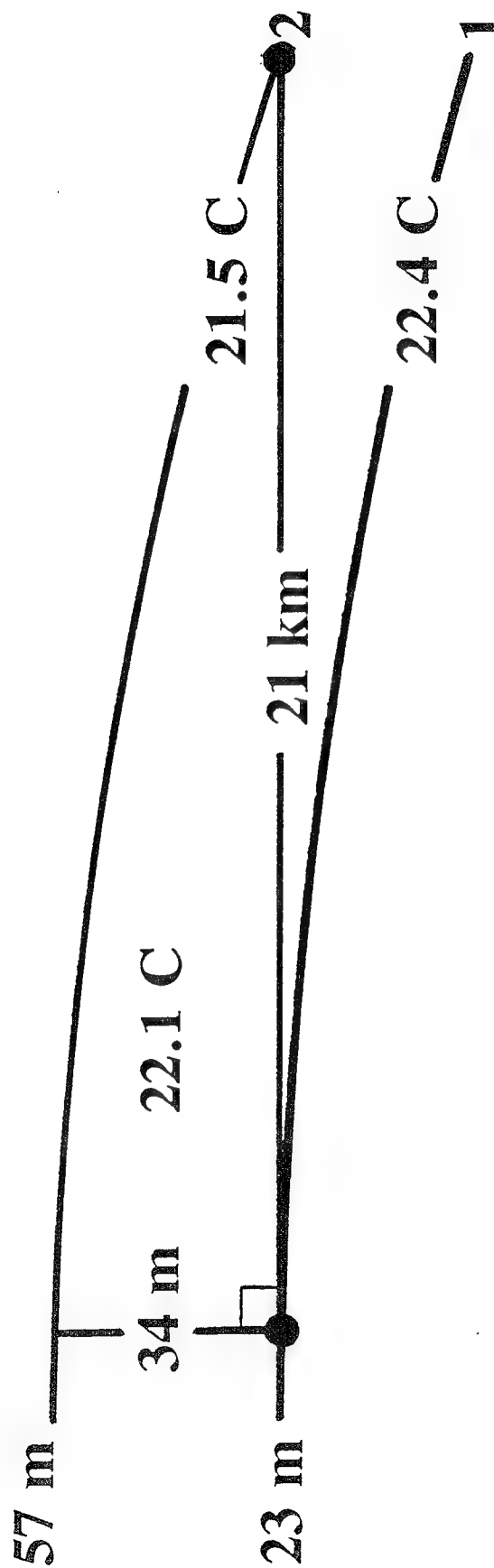


Fig. 1. Comparison of measured sky radiances and those calculated by LOWTRAN 6 vs zenith angle.

HORIZONTAL GEOMETRY WITHIN LAYER 1

October 10, 1991



Note: Range/Height ≈ 600

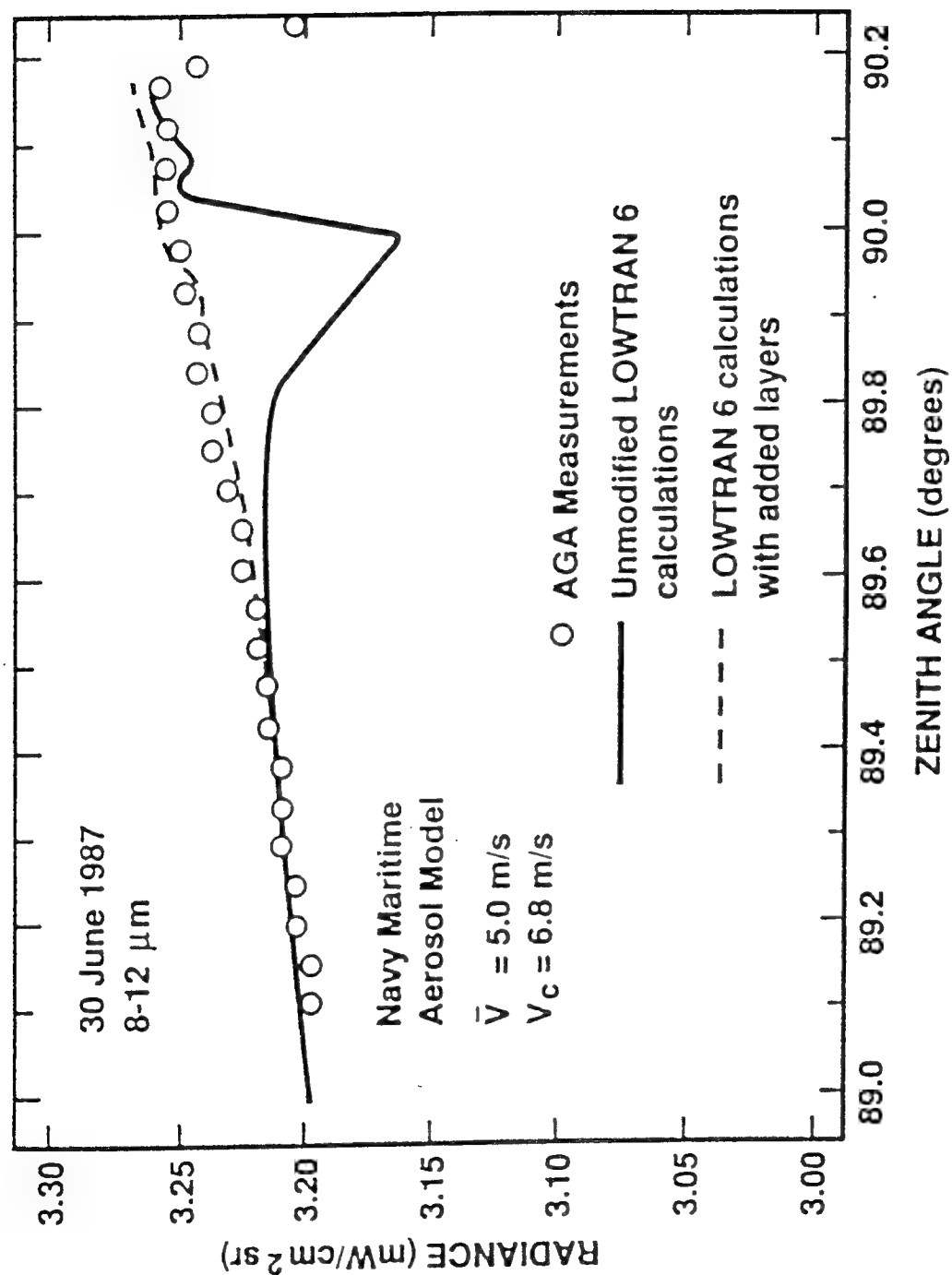
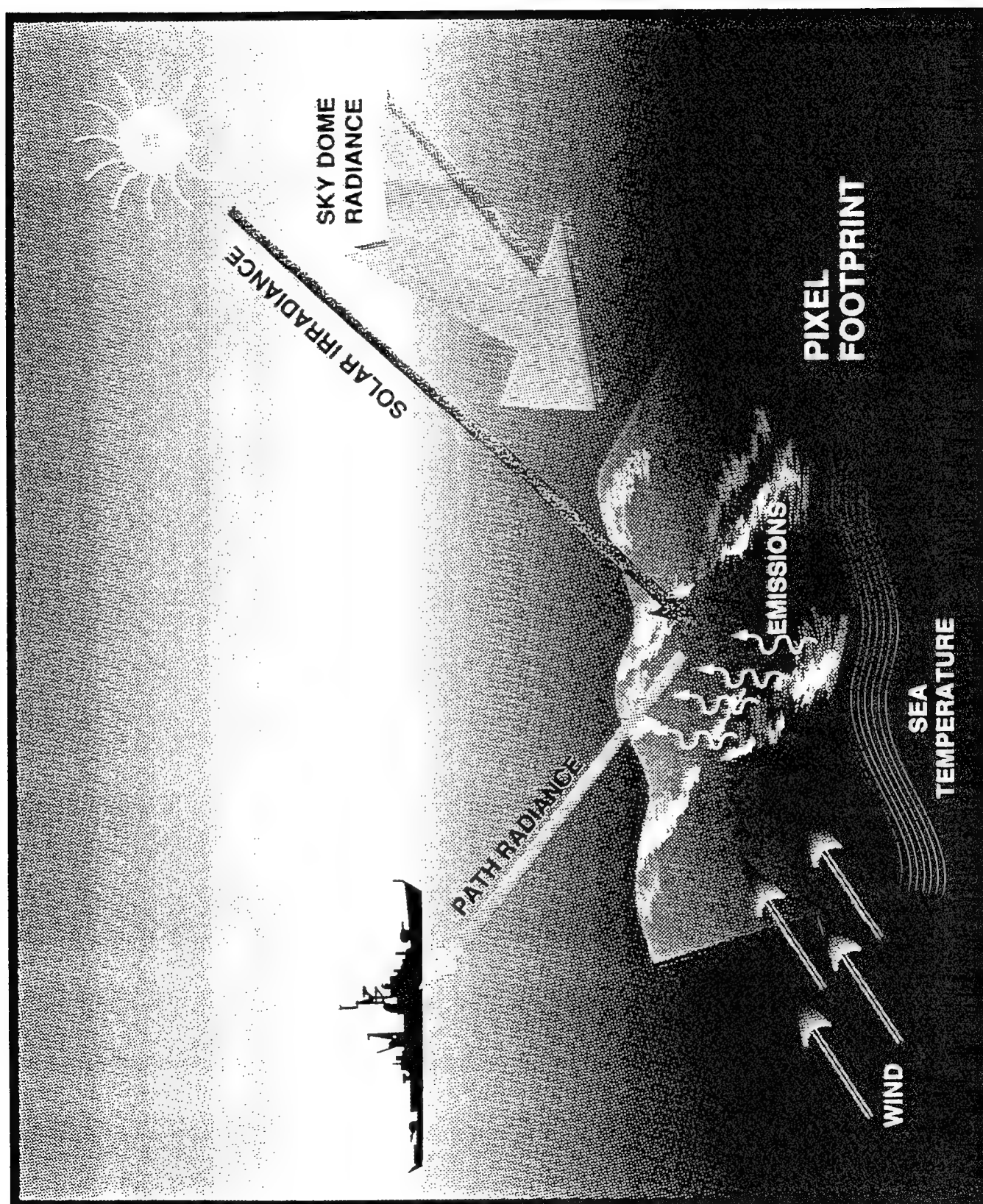


Fig. 4. Comparison of sky radiances measured with the AGA system on 30 June 1987 with radiances calculated with LOWTRAN 6 with and without layers added.

**MODIFICATIONS ASSOCIATED PRIMARILY WITH
THE SEA**

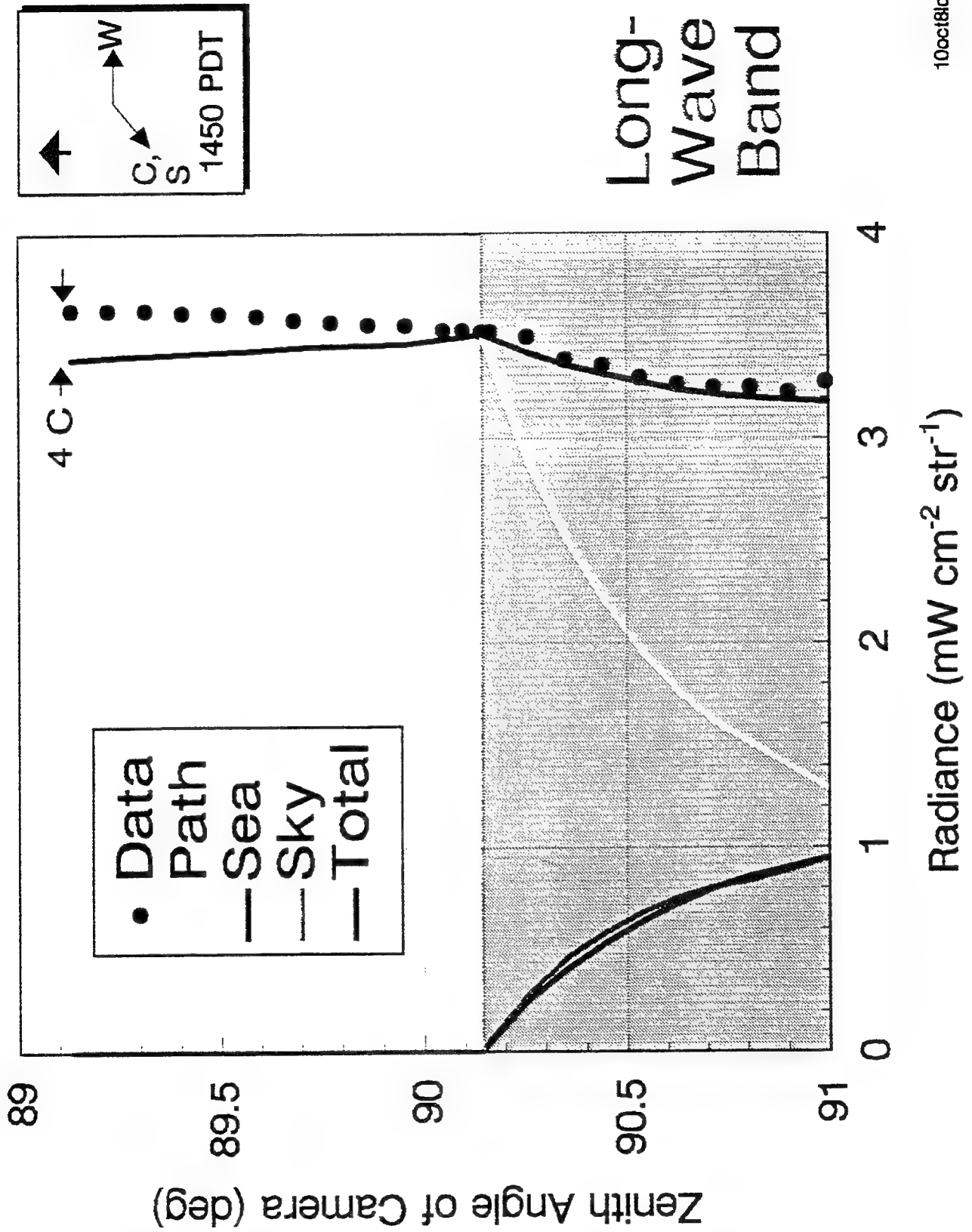
Sky Dome Reflections, Sea Emissions, and Solar Glints



OUTLINE OF COX-MUNK APPROACH

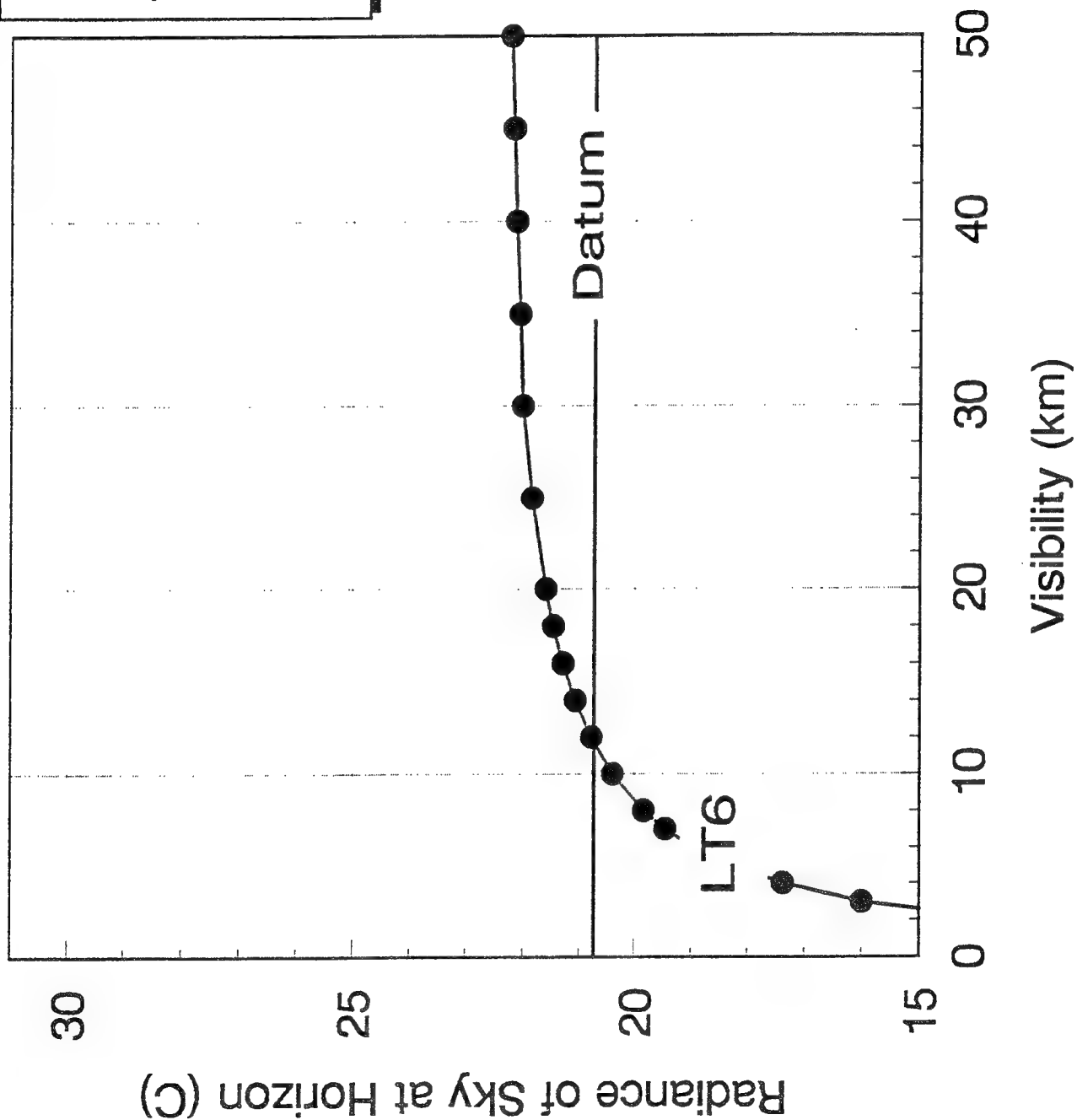
- (1) Select a slope for a small facet within the pixel footprint.**
- (2) Weight it with the Cox-Munk probability.**
- (3) Reflect sky radiance into the camera ("SKY").**
- (4) Add thermal emission from the facet ("SEA").**
- (5) Reflect solar irradiance into the camera ("SUN").**
- (6) Repeat for a new slope.**

VERTICAL RADIANCE SLICE: 10 OCTOBER 1991

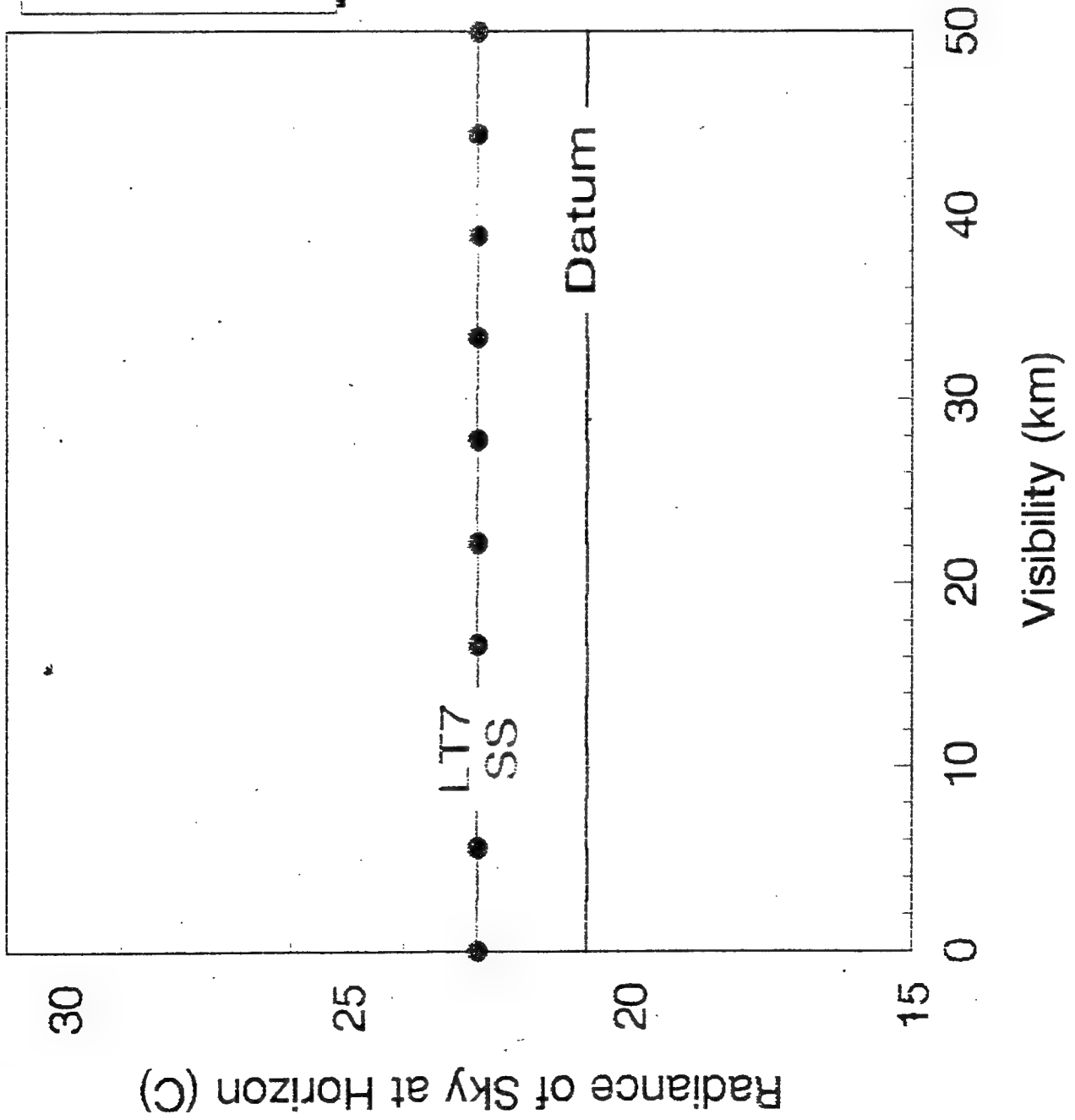


10 OCTOBER 1991 HORIZON RADIANCE

ICSTL = 5
V = 4.6 m/s
<V> = 3.2 m/s
H1 = 23 m
A = 90.141°
1450 PDT



10 OCTOBER 1991 HORIZON RADIANCE (6 to 12 μm)



Definitions

$N^*(T)$	Planck blackbody radiance (Planck function / π)
T	absolute temperature
e	extinction
a	absorption
s	scattering
τ	transmittance from a given point on the optical path to the observer

LOWTRAN 6 Radiance (Lowtran 4 manual, p. 9)

$$N = - \int_1^{\tau_a^{edge}} N^*(T) \tau_s d\tau_a$$

If the atmosphere is optically thick [$\tau_a^{edge} = 0$] and
if T changes slowly during extinction [$N^*(T) \approx \text{constant}$]

$$N \approx N^*(T) \int_0^1 \tau_s d\tau_a$$

Ben-Shalom Radiance

$$N = - \int_1^{\tau_e^{edge}} N^*(T) d\tau_e$$

If the atmosphere is optically thick [$\tau_e^{edge} = 0$] and
if T changes slowly during extinction [$N^*(T) \approx \text{constant}$]

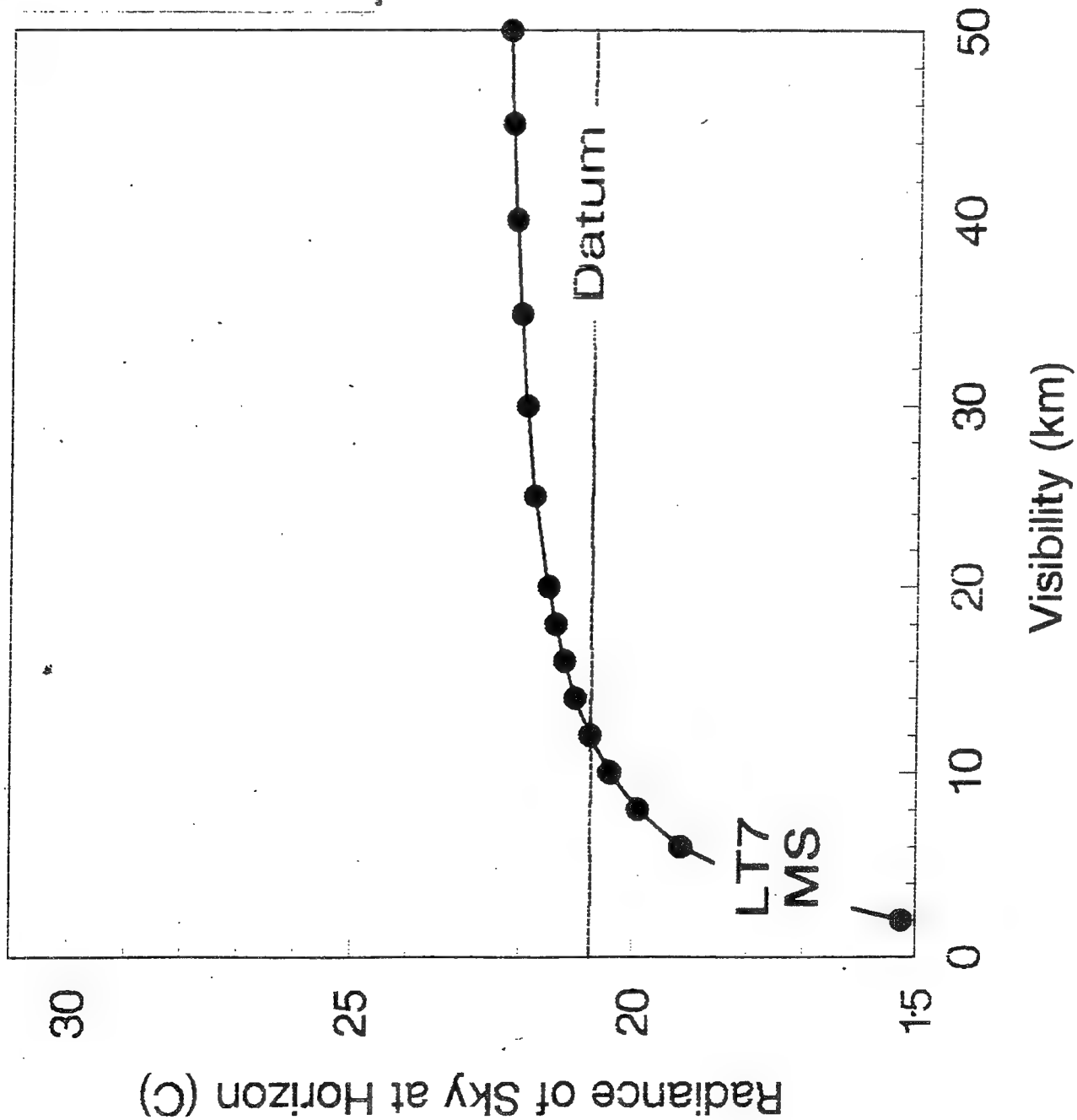
$$\begin{aligned} N &\approx N^*(T) \int_0^1 d\tau_e \\ &= N^*(T) \tau_e \Big|_0^1 = N^*(T) \end{aligned}$$

For horizontal paths Ben-Shalom gives $N^*(T)$, the blackbody radiance for the atmosphere near the observer.

Large changes in scattering and absorption will not alter this result provided that T stays constant during extinction.

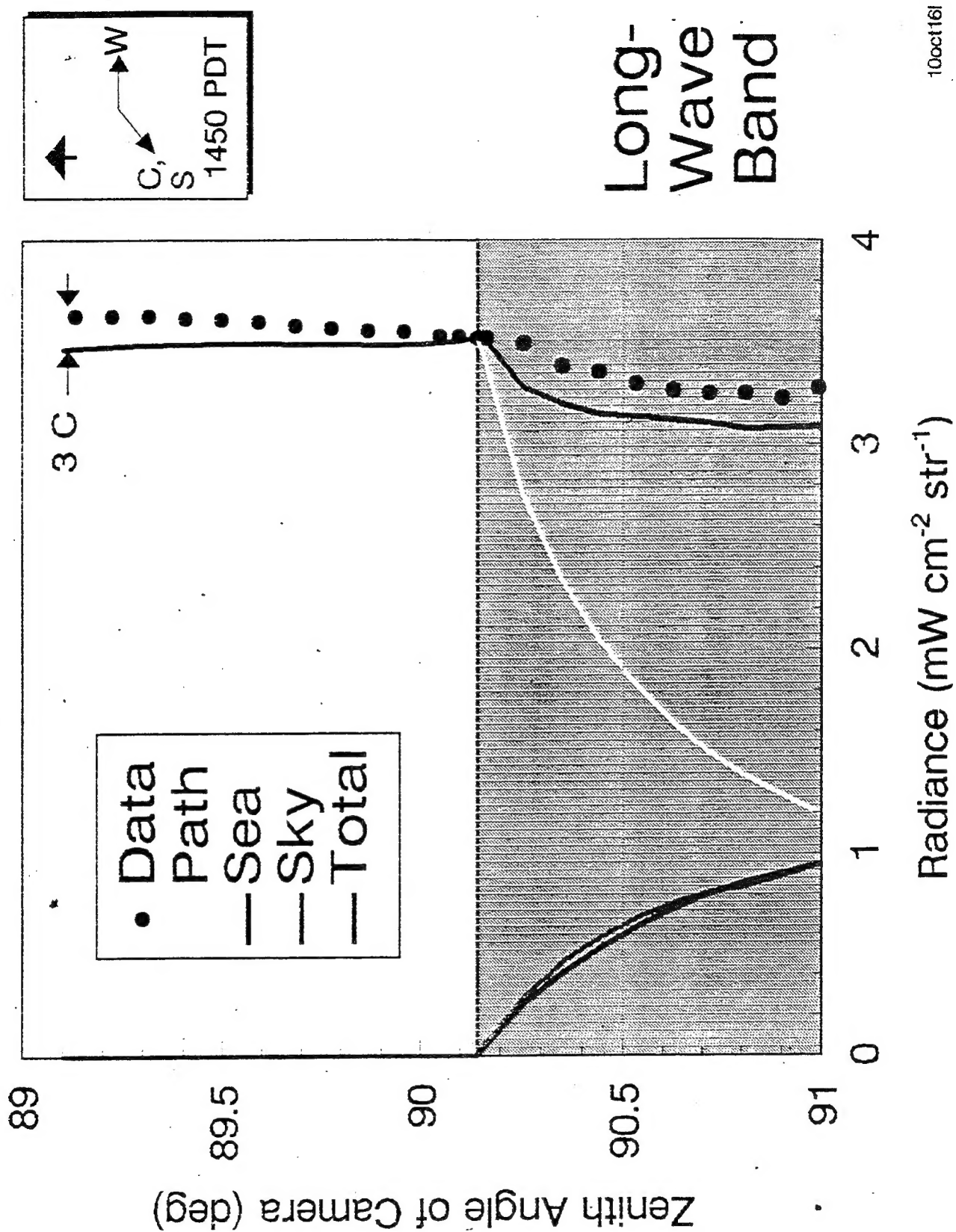
10 OCTOBER 1991 HORIZON RADIANCE

ICSTL = 5
 $V = 4.6 \text{ m/s}$
 $\langle V \rangle = 3.2 \text{ m/s}$
 $H1 = 23 \text{ m}$
 $A = 90.141^\circ$
 1450 PDT



Long-
Wave
Band

VERTICAL RADIANCE SLICE: 10 OCTOBER 1991



The following

CONCLUSIONS

can be drawn for horizontal paths in the ocean environment where aerosols are important:

1. Maritime modifications to LOWTRAN 6 improve the agreement with marine observations.
2. Multiple scattering LOWTRAN 7 (IMULT = 1) responds to aerosols.
3. Single scattering LOWTRAN 7 (IMULT = 0) does not respond to aerosols.
4. Ben-Shalom radiance violates Kirchhoff's Law, does not respond to scattering or absorption, and is inappropriate for marine use.

Relationships

$$\tau_e = \tau_a \tau_s$$

$$\tau_s \equiv 1 \text{ if no scattering}$$